Pan-Arctic Perspective of Soil Temperature, Fresh Water Temperature, and River Ice Thickness and their Impacts in a Changing Climate

By

Marie Wrede Broesky

A Thesis submitted to the Faculty of Graduate Studies of

The University of Manitoba

in partial fulfillment of the requirements of the degree of

MASTER OF SCIENCE

Department of Civil Engineering

The University of Manitoba

Winnipeg, Manitoba, Canada

Abstract

The pan-Arctic is disproportionately affected by global temperature increases due to climate change. Polar amplification and local climate feedback cycles, cause air temperature to rise around 2.4 times faster in the Arctic. The pan-Arctic covers approximately 26 million km^2 of subbasins which contribute freshwater to the Arctic Ocean. Large-scale studies of climate warming impacts on terrestrial systems are rare because gathering observed data is expensive, difficult, and dangerous, and what is available is difficult to compile and lacks consistency. Modeled data are required for comprehensive long-term studies. This study analyses the pre-whitened annual trends of modeled soil temperature, water temperature, and river ice thickness for the historical period (1979-2019) and future projections (2020-2100) across the pan-Arctic domain using the AHYPEv4 model. These terrestrial hydrological components directly impact pan-Arctic ecology, and communities through permafrost thaw, increases in water temperature and decreases in river ice thickness. Analysis is done for the entire pan-Arctic domain, at the continental scale by comparing North America and Eurasia, and at the watershed scale for the 12 largest rivers (by historical volumes). Future climate projections come from the sixth phase of the Coupled Model Intercomparison Project, CMIP6. To capture uncertainty of future climate projections and socioeconomic response, an ensemble of climate models (CanESM5, MIROC6, and MRI-ESM2-0) and future warming scenarios (ssp1-2.6 and ssp5-8.5) capture the extreme ends of future change. This study shows increasing trends for future periods. Soil temperature increases from 0.032°C/year to 0.054°C/year, water temperature increases from 0.014°C/year to 0.031°C/year and losses in maximum ice thickness increase from 0.062 cm/year to 0.111 cm/year. Change point analysis shows that socio-economic pathways which result in

lower future warming have mitigating effects on future trends mid-century, but higher warming scenarios yield more severe trends towards the end of the century. The changes analyzed in this study have global and regional impacts. Results from this study are vital for further modelling of ocean processes, and regional ecological shifts and inform policy makers, who are concerned about current impacts from historical changes, of the influence todays actions (socio-economic pathways) have on future trends.

Acknowledgements

Funding for this research was provided by the Natural Sciences and Engineering Research Council of Canada and the University of Manitoba. I would also like to express my gratitude for the funding received through the scholarship provided by the family of Duncan Norrie.

I want to thank my advisors, and all those who have mentored me throughout my academic journey. A special thank you to Dr. Tricia Stadnyk, who first inspired my passion for hydrology. As I describe it, the first day in her class was the first day that I understood why I was in engineering. Trish, without your optimism, guidance, and understanding I would still be trying to write this thesis. I want to thank the team at UC-HAL who have lent their expertise and encouragement throughout this process. To those who came before me in the “AHYPE journey”, I hope I make you proud.

I have had the privilege of being surrounded by endless support. Thank you to my husband for never letting me quit, even though I don’t believe it would have been entirely unreasonable to do so. Thank you to my daughter for seeing the first plots generated for this document and shouting, “Mommy you did it! I am so proud of you!” Without my parents, family, and friends this just wouldn’t have been possible. Thank you to the friends who gave me endless advice and kept me company. A special thank you to Jenna, who fits into both the academic and friend column of acknowledgments. Everyone needs another graduate student to pull them through, and your support and opinions helped map out the journey.

Table of Contents

List of Figures

List of Tables

1. Introduction

The current state of science is in overwhelming agreement that we 1) have sufficient observations and evidence, and 2) can conclude that the Arctic is undergoing rapid, accelerating changes due to climate change. Increases in temperatures are detectable on a global scale, and current deviations from historic records have reached peak interest in the scientific community. Temperature changes often reported as global means, do not occur equally across the globe. And changes are exasperated by polar amplification (D. M. Smith et al., 2019), a phenomenon causing the Arctic to warm at much higher rates than the global average. The arctic has warmed on average 2.7°C from 1971 to 2017, with a warming of 3.1°C in the cold season and 1.8°C in the warm season. Approximately 2.4 times more than what is being observed in the Northern Hemisphere alone (Box et al., 2019). Therefore, the arctic is not just the canary in the coalmine, but it is under a critical lens as an important example of how to successfully adapt as our environment continues to change.

Although observations have contributed to the consensus that change has already occurred, monitoring practices and observation gauge distributions across the pan-Arctic basins are insufficient to successfully study the Arctic at a large scale and over long time periods. Small, dense research networks are successful in studying portions and differing landscapes, which are typically extrapolated to describe Arctic climate change impacts (McClelland et al., 2004; S. L. Smith et al., 2010; Vincent et al., 2015; Yang et al., 2021). But large-scale studies encompassing the entire domain currently rely on model predictions, requiring improvements in modelling practices and technological

advancements in computing that allow for the handling and simulation of such large datasets.

Defining features of the Arctic are the various aspects of its frozen landscape, soil and water are found in a state of being temporarily or permanently frozen due to the consistently cool climate. The ecosystem and people living there have developed in congruence with the frozen landscape. They have adapted to, and often depend on, this frozen state, which under continued warming creates a need to adapt to the impacts of rapidly rising temperatures. What may appear to be small increases in temperatures on a global scale can cause thaw events in the Arctic where the loss of previously frozen soil and water drastically changes the interaction of people and the environment, and in some cases create dangerous conditions.

This study aims to investigate the impacts of future climate change on river temperatures, ice thickness, and soil temperatures on a large scale through the management of large forcing data sets and hydrologic modelling. Water being the medium that touches all aspects of the Arctic environment through its freeze thaw cycles and movements that are being reviewed in this study.

1.1. Pan-Arctic Domain

This study encompasses the pan-Arctic domain in a single continental scale hydrological model. The pan-Arctic domain refers to all watersheds contributing freshwater to the Arctic Ocean, and includes watersheds which contribute to the Arctic Ocean freshwater budget indirectly such as those that drain into the Hudson Bay, sometimes also referred to as “all arctic regions” (T. Prowse et al., 2015). The Arctic HYPE version 4 (AHYPEv4) model covers an area of approximately 26 million km^2. Figure 1 shows the study domain

which is included in the current configuration of the AHYPEv4 model. It in part covers all continents in the Northern Hemisphere, and includes portions of Canada, the United States, the United Kingdom (Shetland Islands), Faroe Islands, Iceland, Greenland, China, Mongolia, Kazakhstan, Russia, Finland, Sweden and Norway. The model extends from its southern most point near 45°N all the way up to 84°N in the northern hemisphere and wraps around the globe.

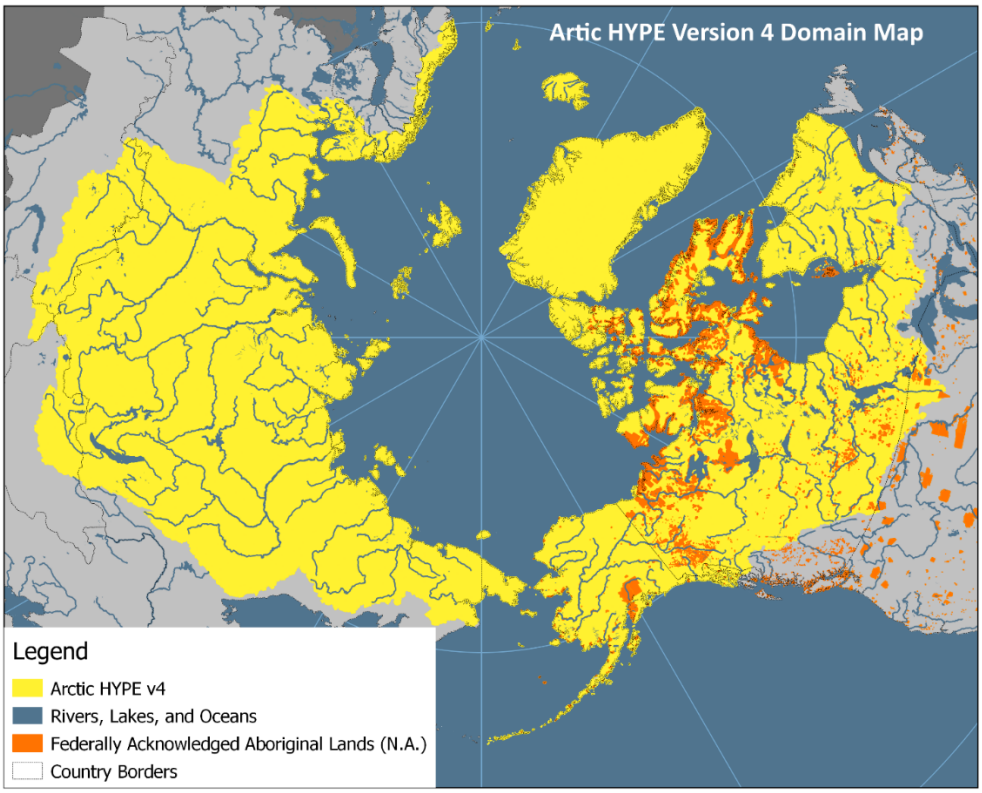

Figure 1 View of the AHYPEv4 model domain centered around the North Pole. The model domain is highlighted in yellow, and federally acknowledged aboriginal lands are shown in orange for the North American continent.

The pan-Arctic domain covers a wide variety of landscapes that creates a complex network of rivers and water bodies, making it a difficult to model domain. It includes urban centers, mountains, prairie, forests, glaciers, ice, grass and shrubland, wetlands, and

tundra. According to Václavík et al. (2013) the majority of land is made up of boreal systems such as boreal forests and tundra, and extensive cropping systems.

Much of the hydrology is significantly impacted by changes to soil temperature which impact permafrost extent. Permafrost thaw releases previously stored water and alters connectivity near the surface and in deep groundwater. In Eurasia, major river basins include the Yenisey, Lena and Ob and contribute approximately 31% of pan-Arctic discharge, in North America the Mackenzie, Yukon and Nelson river basins contribute approximately another 11% of pan-Arctic discharge (Stadnyk et al., 2021). The modeling of major river outlets is impactful for modelling of ocean processes and circulation. In this study, changes in the 12 largest rivers by volume are included as well as large scale continental changes.

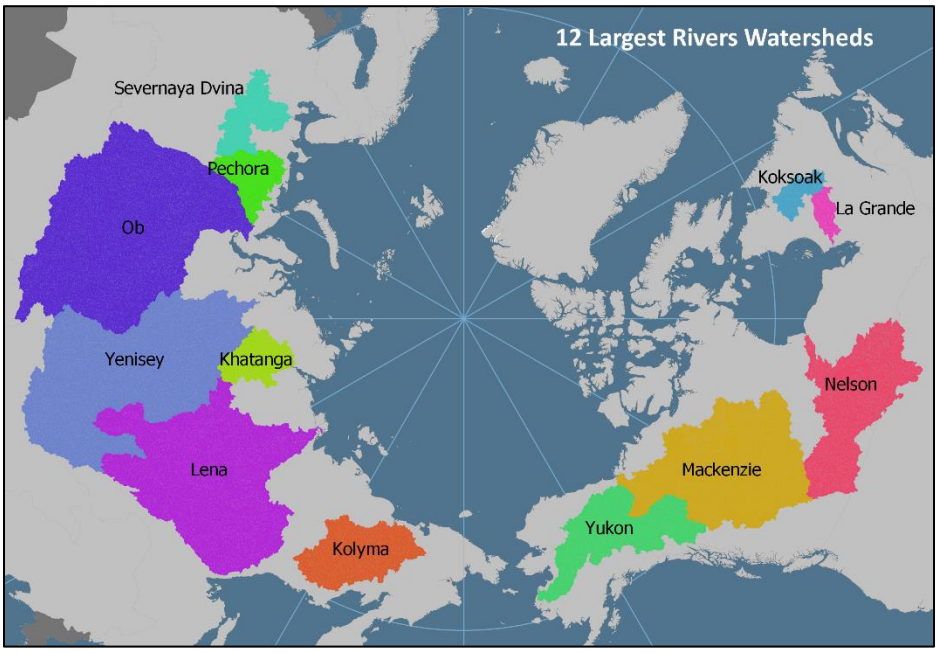

Figure 2 Map of the 12 largest rivers in the Pan-Arctic domain which count as the highest contributors of freshwater to the Arctic Ocean.

The pan-Arctic climate ranges from an average temperature of 9.6° to -28.5°C, calculated for the recent period of 1991-2019 using HydroGFDv3 forcing. Below is a map showing the climate distribution for each subbasin within the AHYPEv4 model. Climate is largely correlated with latitude and shows strong latitudinal temperature bands for different climatic zones. Other influences are altitude, with mountain ranges being highlighted with lower temperatures than their latitudinal bands. Examples of this are seen in the Rocky and Alaskan Mountains in North America, and Stanovoy Range in Eastern Russia. The range of average climatic temperatures covers approximately 30°C, and this does not include the extreme variations around these. This speaks to the complexity of the domain and the variety of natural processes and ecosystems it supports.

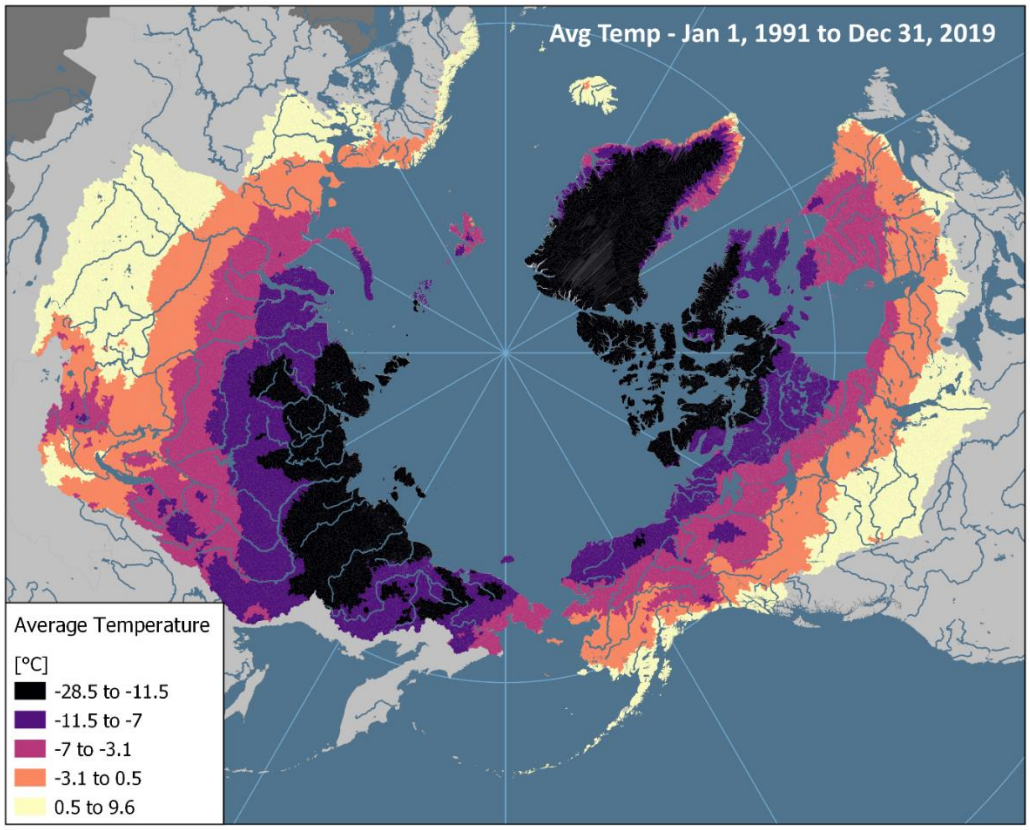

Figure 3 Climate average temperatures (1991-2019) for each subbasin, used to present the pan-Arctic domain separated into five climate bands demonstrating the wide range in average air temperatures spread across the domain.

1.2. Climate Change in the Arctic

Arctic climate change is occurring more rapidly in recent decades due to polar amplification (D. M. Smith et al., 2019). Not only does rapid climate change leave affected communities scrambling to adapt and understand how these changes will impact their daily lives, it is likely that areas that experience the most extreme climate changes are also those which have notable gaps in observed data (Arvid Bring & Destouni, 2011). Historically we have recorded an annual temperature increase that is 2.4 times faster in the Arctic when compared to the northern hemisphere average annual temperature (Box et al., 2019). Bring et. al (2016) summarized changes to arctic terrestrial hydrology and emphasizes the interconnectedness of hydrological processes and increases in soil temperatures. Melting of previously frozen soil ice alters the movement of water, changes storages, and hydrological cycles. This introduces new temperature sources to streams and dynamic connectivity within watersheds which can no longer be delineated based on historical elevation observations. Additionally, permafrost temperatures have been observed to be increasing similarly to air temperature (Box et al., 2019). Even with a stabilization of global temperatures, permafrost is estimated to continue degrading, making a loss of permafrost extent inevitable regardless of climate scenario (Chadburn et al., 2017).

Compared to future climate scenarios reflecting global warmings of +1.5°C and +2.0°C in accordance to the Paris Agreement targets, the Arctic is projected to increases by +3.6°C and +4.5°C in the same respective periods (Casagrande et al., 2021). These projections are in agreement with the historically observed ration of arctic air temperatures to global means and correspond to warmings of 2.4 times and 2.25 times faster warmings

respectively. Other reviews of CMIP6 air temperature projections agree that the Arctic shows a higher increases in temperature and a more significant spread between model projections (Hu et al., 2021).

1.3. Observed Data in the Arctic

A topic which will frequently surface in this thesis is the lack of available data observations in the Arctic. The remoteness of points of interest, high cost associated with the installation and maintenance of specialty instrumentation which can be used in cold climates, and the sheer vastness of the domain create significant barriers to a large-scale study. It is most likely that observations are only available for specific research study sites that have been dedicated to maintaining consistent observations. Options for spatial coverage then fall to satellite observations which are still developing, and modeling of the environment with little information to train or validate model performance for the entirety of the domain. However, some observations of interest such as soil temperatures below the surface cannot be measured by satellites, and therefore the gathering of observed data is limited to in-situ methods (Sharon L. Smith et al., 2022). Additionally, snow processes often hinder the applicability of satellite measurements. Capabilities of satellite observations are limited when it comes to determining snow and ice thicknesses and satellites are unable to take measurements below snow, which impacts our ability to understand cold season processes at a large observational scale (Park et al., 2016). When data are available, datasets for the same variables tend to be inhomogeneous over longer periods of time. Improvements in technology, changes in instrumentation, and data recording create discontinuities in observation methods, making analysis difficult (Vincent et al., 2015). Data discontinuities impact the accessibility of data, making processing time

and resource intensive. Some coding tools have been developed to attempt to address this problem but often data are processed on a case by case basis with in house methods which vary across institutions (N. Brown, 2022).

1.4. Previous Research

Computational cost requirements, a lack of observational data coverage, and system complexity in the Arctic have largely left the pan-Arctic domain unexplored at a large scale. Research is more commonly focused on specific portions of the Arctic at smaller research sites, limited to a historical analysis, or grouped in with global scale studies. Arvid, Bring and Destouni (2011) called specifically for process-based hydrological modelling in the Arctic to help more accurately interpret changes in climate and their impacts on the hydrological cycle.

The HYPE model has been used for modelling applications within this domain for multiple previous hydrologic studies. Stadnyk et al. (2021) studied historically and future modelled flows for the same pan-Arctic domain, using previous forcing data sets and future climate projections as this study. Stadnyk & Déry completed a continental study using AHYPE for historical flows in Canada (Stadnyk & Déry, 2021). A project by Stadnyk et al. (2020) produced an adaptation of the AHYPE model to all subbasins which drain directly into the Hudson Bay, this being named the HHYPE model. Braun et al. (2021) assessed future model ensembles across the same domain. Bajracharya et al. (2020) studied the individual subbasins within just the Nelson-Churchill watershed which are two of the rivers flowing into the Hudson Bay domain in order to assess modelling parameters in cold region flow, and incorporated soil moisture and finer vertical soil discretization into the

AHYPE model to better represent cold temperature soil processes (A. R. Bajracharya et al., 2023).

Van Vliet et al. (2013) studied water temperature at a global scale and concluded that rivers at high northern latitudes showed slower increases in water temperature on an annual scale as they were still frozen for most of the year, however summer months show the highest increases in water temperature as thermal capacity increases with increases in river discharges. Wanders et al. (2019) studied water temperature at a global scale and modeled it using a dynamic 1D water routing model at high resolution for the historical period. Park et al. (2017) studied water temperature in the pan-Arctic for major river outlets. Their work utilized the CHANGE model in seven arctic watersheds but only for historical time series. Yang et al. (2002) studied the hydrologic changes due to temperature warming in the Lena River watershed. This is one of the largest watersheds in the pan-Arctic domain, and although the study mentions the impact of hydrologic changes on water temperature and ice thickness only changes in water volume are examined. Yang et al. (2021) studied heat fluxes entering the Arctic Ocean and Hudson Bay from Canadian Rivers from available observational records at 15 rivers, records lengths of water temperature measurements vary from 16 to 529 point observations which were then statistically analyzed to understand the seasonality of the heat flux within the record.

Studies of river ice have been more likely to look at the timing of observed river ice break up and freeze up, and their changes. Vincent et al. (2015) reported observed historical trends in earlier river ice break up for a limited number of stations which had observations for sufficient and consistent time periods. Arp et al. (2019) studied ice thickness in

connection to Arctic lakes who's water is withdrawn for the construction of ice roads, in order to provide future management plans to protect freshwater habitat. Beltaos and Bonsal (2021) studied river ice thickness and ice-jam floods in the Peace-Athabasca Delta, modelling ice thickness from 1950 to 2100, and studying how thermal river regime and ice thickness changes could impact ice break up processes in the future.

Schneider et al. (2021) utilized a 1D heat conduction model to study the thaw of frozen soil in the Arctic and its impact on infrastructure such as gravel roads, however their method is only applied with a single observational site. But the work stresses the very real threat that permafrost thaw presents to infrastructure, as stable frozen soils can thaw within the infrastructure life cycle under current high warming scenarios. Oelke and Zhang (2004) modelled circum-Arctic soil temperatures using a 1D heat transfer model incorporating satellite observations of snow as in their forcing data for the historical period of 1980-2001 at various depths. Hirota et al. (2002) modeled soil temperatures for frozen soils for sites located in Canada. Mohammadi and Hayley (2023) completed a qualitative assessment of regions which are vulnerable to the settlement that occurs when permafrost thaw impacts soils structural strength. On a global scale, soil moisture has been modeled using satellite data by Martens et al. (2017) over a historical period. Lembrechts et al. (2022) produced global soil temperature maps based on bias adjustments to global modeled air temperature.

While previous work addresses some of the localized gaps in climate change impact studies for the Arctic, this will address the gaps in Arctic-wide studies by providing a spatially complete modeled water temperatures, river ice thicknesses, and soil temperature for a historical period and projected into the future using multiple future

warming scenarios. To the best of our knowledge, this will among one of the first serially complete pan-Arctic climate change datasets produced. While the dataset produced will be spatially congruent and serially complete, significant uncertainties are noted due to the lack of observations for comprehensive model evaluation. Analyses will focus on major river basins and seasonal time scales to reduce the model error effect.

1.5. Scope and Objectives

The research objective is to present an updated continental scale investigation of changes projected to occur in pan-Arctic River temperature regimes, including ice thickness, and soil temperature. This is done by assessing the modeled changes in the three mentioned secondary hydrological model outputs over a period spanning from 1979 to 2100. The unique perspective of this study is to use a new iteration of a large-scale continental hydrological model to address the above objective, incorporate current best practices for climatic studies, and utilize recently produced CMIP6 global climate forcings. The following questions will be addressed in this research in order to be able to draw conclusions about its objective:

1. What trends do we see in water temperature and ice thickness in rivers at a continental scale and in major pan-Arctic basins?
2. What trends do we see in soil temperature at a continental scale and in major pan-Arctic basins?
3. Are there hotspots of change? Among the major pan-Arctic basins, are any warming more rapidly, and if so, are those basins home to communities or known ice roads?
4. Are there any significant agreements/disagreements among different climate projections in the above trends and change points.

In addition to trends, change point analysis will be used to identify if there are significant change points or decades of significant change in water temperature, ice thickness, and

soil temperature. Finally, this work will also produce updated future modeled hydrological data at freshwater outlets to the Arctic Ocean to contribute to further study of the Arctic domain. All work is aimed to be efficiently reproduceable using transparent practices and openly available coding tools.

2. Literature Review

This section provides background information relevant to this study. First it includes a review of climate change impacts on freshwater temperature (2.1.1), river ice thickness (2.1.2), followed by the definition of permafrost, a description of current permafrost cover in the pan-Arctic, and climate change impacts on soil temperature and permafrost (2.1.3). Then information on modelling methods for water temperature (2.2) and soil temperature (2.3) are discussed. This section concludes with an overview of Arctic communities and their relationship to and dependency on water temperature, river ice, and permafrost (2.4).

2.1. Climate Change Impacts

In the IPCC's sixth assessment report they state that there is a high confidence that changes in lake and river ice, and permafrost are harmful to the livelihoods and cultural identity of communities in the Arctic (Calvin et al., 2023). The following sections summarize the current state of knowledge on climate change in arctic regions, and on how climate change has already impacted the model outputs being examined in this thesis.

2.1.1. Fresh Water Temperature

Fresh water temperature in the pan-Arctic rivers has been overall increasing due to climate change, which is expected due to the close correlation between air temperature

and water temperature (Bolduc & Lamoureux, 2018; Zhu et al., 2018). Study of Arctic climate change commonly focuses on ocean warming, and the impacts this has on sea ice and larger scale ocean circulation (Casagrande et al., 2021; Greenan et al., 2019; Rosenzweig et al., 2017). However, freshwater inflows into the Arctic Ocean can have a profound impact on coastal ecosystems, and overall ocean processes by freshening the saline ocean (K. A. Brown et al., 2020; McClelland et al., 2004). Ocean models rely on freshwater inflow data to set boundary conditions (Lammers et al., 2007). Changes in freshwater temperature alter timing and quantities of freshwater ocean inflows. Impacts to the freshwater ecosystem themselves are also profound under climate change, with specific concerns around fish species and ecosystem stability (Bolduc & Lamoureux, 2018; Kangur et al., 2016; Kotowych et al., 2023).

There have been few studies of water temperature observations on the pan-Arctic scale. One, by Lammers et al. (2007) studied archived Arctic river water temperature for 17 watersheds in the Russian pan-Arctic. Only five stations showed statistically meaningful Mann-Kendall warming trends for the decadal maximum temperatures, and none for the mean temperature. Park et. al (2017) modeled water temperature at pan-Arctic river outlets only, but not throughout the watersheds. Freshwater temperature was simulated for the period of 1979-2013 using the CHANGE model, a coupled hydrological and biogeochemical model, and is one of the only available large-scale studies of water temperature in the pan-Arctic. The results indicate a modeled warming trend of around 0.16°C/decade at the outlets. Wanders et al. (2019) modeled a global average increase of 0.16°C/decade for 1960-2014 in water temperatures, and an increase of 0.62°C/decade in daily maximum temperatures for the Northern Hemisphere. Changes in

water temperature due to climate change are of concern for watershed biology, aquatic species, riverbank stability, and river navigability (Yang & Peterson, 2017).

2.1.2. River Ice Thickness

Studies in river ice thickness are isolated mainly to studies of observed records, and therefore the spatial distribution of studies is significantly limited. More likely, studies are dedicated to analyzing ice freeze up and break up timing which is more easily detectable remotely through various techniques such as satellite data and has greater long term records of observations which have served as simple climate indicators (Podkowa et al., 2023; Walsh et al., 2005). Studies of river ice timing can still be helpful in assessing river ice thickness, as it can be inferred that shorter ice-on periods produce thinner river ice cover.

In the 2005 Arctic Climate Impact Assessment, Walsh et al. (2005) note that the greatest economic impact from changes to river ice are likely to come from decreases in ice thickness that in turn decrease the load carrying capacity of ice for vehicles. Changes in ice thickness also impact river ecology, however winter river ecology is not as well as studied and currently it is hypothesized that changes mainly influence space within rivers available for habitat, flow velocities, river temperatures, and light availability (Thellman et al., 2021).

A study compiling trends in the most available river ice records for the Canadian Arctic by Prowse et al. (2011) report that there were no obvious trends in river ice thickness for Canadian ice thickness records (De Rham et al., 2020), but in Russia a reduction in maximum ice thickness of 2-14 cm from 1990-2010 were observed when compared to maximum ice thicknesses in the 30-year period prior to these observations. Siberian

Rivers, the Ob, Yenisey and Lena had the greatest decreases of 5-10cm, 6-14cm and 11-15 cm respectively. Yang et al. (2002) studied the historical hydrologic response up until 1999 due to climate change in the Lena watershed alone, including measurements in river ice thickness. The study found significant thinning in river ice thickness during the winter and spring months, particularly in northern regions. It also explored the relationship between river ice thickness and air temperature, reporting that the decrease in ice thickness is closely related to increases in air temperature, and that increases in snow cover also correlate with decreasing ice thickness due to the insulation it provides. Ice thickness was observed to have a 20-36 cm thinner multi-decadal average due to warming. One modelling effort by Park et al. (2016) using the same CHANGE model as for water temperature, estimates a decrease of 0.3 cm/yr in maximum river ice thickness for Siberian Rivers from 1979-2009, and an increasing trend of 0.5 cm/yr in North American rivers for the same period.

2.1.3. Permafrost and Soil Temperature

Warming of soil temperature in permafrost areas is synonymous with the warming of air and soil temperatures across the pan-Arctic domain, which is mostly underlain by some type of permafrost. Dobinski (2011) provides a succinct summary of different definitions and the current state of permafrost. Permafrost refers to a thermal state beneath the ground surface. The ground is in a state of permafrost when it is below 0°C for at least 2 years. Although water is often present and frozen within the soil, permafrost is solely the descriptor of a thermal state, the presence of water is not a required factor in order for an area to be considered to be permafrost. Permafrost is also defined by how much of an area it covers, ranging from continuous permafrost which has 90-100% coverage,

discontinuous which has a coverage of 50-90%, to isolated patches with <10% coverage(Chadburn et al., 2017).

Approximately 24% of the Northern hemisphere is covered by permafrost when excluding glaciers and land ice (Dobinski, 2011). Approximately 65% of Russia is considered permafrost, most of it being continuous. North America contains patches of continuous and discontinuous permafrost in western Arctic however more sporadic and isolated permafrost areas are becoming dominant in the eastern Arctic and internal Alaska (Westerveld et al., 2023).

It is much more difficult to describe permafrost as it changes temporally, as some areas may experience permafrost accumulation and degradation. Another way to categorize permafrost is as either latitudinal or altitudinal. Latitudinal permafrost is dependent on decreases in energy input from the sun due to climatic zones. Altitudinal permafrost is an increased likelihood of permafrost occurrence with altitude due to decreasing temperatures, this can also be referred to as alpine permafrost. However, it should be noted that particularly in the case of the Ural Mountains (Russia), the Scandes (Norway), Rocky Mountains (Canada/U.S.) latitudinal and altitudinal permafrost overlap(Dobinski, 2011).

Due to irregularities of permafrost's spatial distribution, and varying rates in thaw there is an appreciation for the difficulty of predicting future changes in permafrost and there are significant amounts of uncertainty in future estimates of permafrost cover (Walvoord & Kurylyk, 2016).

Changes in soil temperature leading to the degradation of permafrost is one of the major components of climate warming consequences, with serious implications for the climate change feedback cycle. Box et al. (2019) summarizes some of the key indicators on climate change and notes permafrost thaw alters ecosystems and hydrology. Ecosystems can change from forests to fens and bogs, ground water source connections can be altered along with surface water storage, and the release of soil carbon could be enormous since it is estimated that around 50% of the global soil carbon is stored within the Arctic. As carbon is released from permafrost thaw, it contributes to the acceleration of climate change (Zimov et al., 2006). Permafrost thaw increases groundwater connectivity, and an increase in its contribution to stream flows will alter river nutrient export downstream and into the ocean (Walvoord & Striegl, 2007), and overall alters the runoff configuration in Arctic watersheds (A. Bring et al., 2016). Ecological impacts of soil temperature should not be underestimated, as temperature in the soil governs the "performance of terrestrial species" much more than air temperature (Lembrechts et al., 2022).

Although large region studies of soil temperatures are uncommon, one recent study compiled observations of soil temperature warming in permafrost areas for available station data from 1980-2020. Smith et al. (2022) found that there is a divide in trends for warmer permafrost, which is closer to average temperature of 0°C and colder permafrost which is below -2°C. Warmer soils on average showed warming at less than 0.3°C/decade and colder soils had warming up to 1°C/decade. Oelke and Zhang (2004) modeled soil temperatures for the circum-Arctic, using satellite observations of snow cover to improve performance and incorporate the insulative effect of snow on soil

temperature. Concluding that areas with increasing air temperatures and decreasing precipitation in the form of snow are most likely to increase in soil temperature. Strong warming trends were modeled in the Canadian Arctic Archipelago at 0.05 to 0.20 °C/year for 1980-2001, an area which also experienced the greatest temperate increases and snow depth decreases over this period. East of the Lena River also had similar warming soil temperature trends of 0.05 to 0.15°C/year. The same study reveals that areas of continuous permafrost show stronger warming trends compared to areas with discontinuous, sporadic permafrost and even seasonally frozen ground regions. A more detailed look at regional warming rates revealed that in colder soils in Alaska and the Mackenzie River watershed historical warming is between 0.4-0.8°C/decade, in Northern Quebec and Baffin Island it is up to 0.7°C/decade, in high latitude Arctic stations it is between 0.4-0.6°C/decade, and in Russia warming is up to 0.5°C/decade. In warmer permafrost in Alaska and the Mackenzie River watershed warming is less than 0.1-0.3°C/decade.

The study by Smith et al. (2022) clearly shows the separation in warming rates for colder and warmer soils, H. Henry (2008) also commented on the difference between cooler and warmer soils. This study also used weather station data to assess soil freezing dynamics and projected them into the near future, concluding that sites which are just below freezing temperature would experience the greatest change in the number of soil freezing days observed annually.

2.2. Modelling Water Temperature

Modelling water temperature is not just important for predicting future water temperatures, but also for a wide range of applications as water temperature monitoring is still

uncommon and records are inconsistent (Yang & Peterson, 2017). Ecohydrological applications of water temperature modelling for understanding the impacts of long term warming, for example on fish species sensitive to higher water temperatures, is still emerging but highly important in colder regions where hydrological systems can have higher interannual variability (Bolduc & Lamoureux, 2018; Null et al., 2013). Modelled water temperature is also impactful for ocean modelling studies, since the pairing of increases in freshwater streamflow and temperature to the Arctic Ocean impact stratification, circulation, sea ice cover, and marine permafrost (Yang et al., 2021).

Water Temperature can be modelled using data-driven methods or process-based methods. Data-driven methods either take a statistical approach or they utilize observable relationships between water temperature and other stream features or meteorological factors to predict water temperature (Yang & Peterson, 2017). Data-driven methods are attractive and have been utilized heavily for a long time already, in the study of the ecological impacts of water temperature and its relationship to biological processes (Sahoo et al., 2009), but are less common in hydrological applications which tend to champion the process based approach which better represent the state of the environment. Computational requirements are relatively low for data-driven methods as modelling can be done using simple relationships, algorithms, and statistical methods. Under the umbrella of data-driven methods fall statistical models such as stochastic or regression approaches as well as machine learning techniques which sometimes are paired with other methods or utilize algorithms of varying complexities which learn from available data sources to then be able to predict water temperature (M. T.H. Van Vliet et al., 2011; Zhu & Piotrowski, 2020). Beyond lower computational budgets, data-driven

methods are also often seen as favorable as fewer parameters are necessary for model set up. The requirements for model inputs can be as simple as using air temperature as the only predictor of water temperature (Zhu et al., 2018). Overtime complexity of these models has increased as more sophisticated methods are put into practice and tested, but comparatively to process-based methods the data-driven methods are championed as lower effort modelling still maintaining good model performance (Jiang et al., 2022). However, data-driven methods rely on observed data to be present, making it unreliable in the pan-Arctic (Yang & Peterson, 2017), and are also likely underestimating future changes in stream temperature compared to process-based methods (Leach & Moore, 2019). There are also concerns about data-driven model transparency, ethics, and their tendency to reduce mechanic insights into model functioning. It is instead recommended that these data-driven methods to be used in addition to process-based models, as a way to explore data management and the internal structures of process-based models (Muñoz-Carpena et al., 2023).

Process-based models are the more complex method of the two. As our understanding of the physical world expands, so does the complexity with which environmental processes are represented in process-based models, making these models have the highest computational requirements (Razavi et al., 2012). They calculate water temperature by solving the energy balance equation within the river system and require model inputs including meteorology, channel morphology, basin characteristics etc. (Yearsley, 2012). The basic energy balance considers the exchange of heat fluxes at the riverbed-water interface and at the air-water interface. As can be expected this method is more computationally intensive and requires the description of multiple input parameters

which may be determined through channel/basin characteristics or model calibration methods (Yang & Peterson, 2017). It is often suggested that this method is most appropriate when assessing water temperature responses to changes in climate. As it best represents the reality of stream heat exchange processes and is not solely reliant on historical stream data (Leach & Moore, 2019).

Both modelling approaches are limited by data availability. Water temperature measurements are becoming more available as interest around this stream characteristic has increased and measuring technology has become cheaper and easier to install and operate. However, historical records tend to be short, intermittent, and spatially sparse (Yang & Peterson, 2017). As data-driven methods need to be trained with available data there is a significant disadvantage when records are short and do not cover multiple points within the area of interest. This has been attempted to be addressed by methods which pair water temperature with other variables in order to utilize more readily available data such as streamflow (Sadler et al., 2022), a secondary method is to use a regional approach, by using a model set up for a similar area and applying it to a data sparce or ungauged region (Souaissi et al., 2023). Process-based approaches are also affected by data limitations, as the large number of parameters which drive these models need information in order to be described properly (Yearsley, 2012). Short records of observed water temperature hinder the ability to validate models and assess their performance.

There have been few applications of water temperature models on a continental scale in the pan-Arctic (Park et al., 2016). Best model performance can usually be expected in small scale applications of models where data rich basins have been chosen. Some modelling efforts occur on a regional scale using stations with data to represent ungauged

but hydrologically similar basins (LeBlanc et al., 1997). Statistical methods and process-based methods vary depending on the scale of application as relationships can vary at different spatial scales similarly to the concept often experienced in modeling streamflow. Water temperature is most commonly modeled at daily time scales as this is also the temporal scale at which it has been frequently recorded but more and less detailed studies also occur, some looking at water temperature on an hourly scale (requiring this application to occur at smaller spatial scales)(Null et al., 2013), and larger scales such as weekly, monthly or seasonally averaged water temperatures (Weierbach et al., 2022).

2.3. Modelling Soil Temperature

Soil temperature models fall into similar categories as water temperature. Models are either based on data or based on modelling the mechanics of soil temperature fluxes. Models based on data rely on statistics or correlations drawn between observable parameters and soil temperature. Just as with water temperature, soil temperature is closely related to air temperature. Early modeling efforts by Zheng et al. (1993) solely rely on this relationship and successfully predict soil temperatures based on a moving window average of air temperature. Other hydrological and meteorological factors also impact soil temperature, such as humidity, precipitation, net radiation and windspeeds and their inclusion can greatly improve model performance (Bayatvarkeshi et al., 2021).

Other important properties for modelling soil temperature are the properties of the soil themselves, which increase in importance when snow isolates the soil from the direct impacts of air temperature. These properties can be difficult to obtain for large scale modelling, and simplifying assumptions often need to be made. Oelke and Zhang (2004) used remote sensed snow cover information to improve models of soil temperature, and

found that mean annual air temperatures tend to be 2-4°C cooler than soil temperatures which are insulated by snow cover for significant portions of the year in the Arctic. Models which are process based attempt to emulate the mechanics of heat transport within the soil but require a variety of input parameters to describe the heat transfer properties of the soil. Physically based or mechanistic models tend to have a better model performance, however they also have much higher data requirements (Sándor & Fodor, 2012). High data intensive modelling efforts are hampered by challenges to consistently measure soil temperature, as it is only possible to do so at stations and then at specifically chosen depths (Alizamir et al., 2021).

One of the challenges with modelling soil temperature is the variability in the soil column, and where within the soil the temperature is being modeled or observed for can vary from study to study. Mehdizadeh (2020) states that shallower soil depths show greater variation in soil temperature on various time scales.

With the rise of more advanced and sophisticated computing capabilities data-driven methods which utilize machine learning have risen to popularity. These, however, have the drawback that they require frequently and consistently available data in order to train their models. Recent work has mainly focused on improving soil temperature modelling by pairing machine learning techniques with more traditional modelling methods (Alizamir et al., 2021; Bayatvarkeshi et al., 2021; Mehdizadeh et al., 2020). A lot of effort has also gone into modelling soil temperature in areas where snow cover insulates the soil over the winter months (Royer et al., 2021). Once the snow is insulated, the relationship to air temperature becomes less important and thermal properties of the soil dictate

temperature fluxes. Hirota et al. (2002) improved on soil temperature modelling in cold climates by taking the effects of snow cover into consideration.

The modelling of soil temperature is closely related to the modelling of permafrost, as the definition of permafrost is solely reliant on the soil's temperature. One of the simplest ways of modelling soil temperature, but more specifically permafrost cover is by using its relationship to long term temperature trends. Permafrost is closely related to air temperature, and the southern border of permafrost occurrence is correlated to the -1°C average annual temperature (Dobinski, 2011). Chadburn et al. (2017) modelled changes in permafrost cover by using a relationship between the mean annual average temperature (MAAT) and inferring changes in permafrost based on change in the MAAT.

2.4. Pan-Arctic Communities

Ramage et al. (2021), only two years ago, published the first estimate of the population that lives within the Arctic Circumpolar Permafrost Region, and how many will be impacted by permafrost thaw. Around 42% of permafrost settlements will experience permafrost thaw by 2050 which affects a total of 3.3 million people. Settlements are directly impacted by permafrost thaw due to the structural degradation of soil and infrastructure, a decrease in in traditional and commercial food accessibility, and an overall decline in health conditions. Furthermore, this study stresses that adaptation capacity varies largely between settlements, depending on their size and accessibility to resources. Westerveld et al. (2023) also provides a summary of the population which lives in the permafrost region in a recently released permafrost atlas. There are few large cities in the pan-Arctic domain, therefore it is difficult to understand and quantify the true impacts and magnitude of climate change in this region, and the people affected. Aside

from the study by Ramage et al. (2021) and the permafrost atlas comprehensive numbers have not been published in literature. The atlas reports that it is approximated that around 5 million people live in the Arctic permafrost area, an area contained within the pan-Arctic. 3.77 million of this population reside in Russia, and another 248,000 reside in North America. Settlements are mainly on sporadic permafrost, and changes in soil temperature are not immediately evident, however those settlements on continuous and discontinuous permafrost are more likely to feel the immediate effects of soil warming. The largest permafrost settlement is Surgut located near the Ob River in Russia and on sporadic permafrost, home to 361,000 people. The largest settlement on continuous permafrost is Yakutsk on the banks of the Lena River, home to 308,000 people.

On a community level, several studies have been done to compile the evidence of climate change impacts and vulnerabilities. Ford and Pearce (2010) reviewed the vulnerability of communities in the Inuvialuit Settlement Region of Canada (High Arctic). Frequently described during interviews of community members is the change in ice dynamics, and increased erosion. Also frequently mentioned is the melting of permafrost. Communities worry about food security, transportation, and an inability to practice traditional cultural activities. Tam et al. (2013) interviewed community members in the western James Bay, studying vulnerabilities to climate change at a local level. Community members once again brought up ice dynamics, and they are concerned about ice thickness. Ice is observed to not freeze thick enough to travel on safely and is freezing much later in the season. This impacts their ability for traditional subsistence hunting, fishing, trapping, and gathering. Winter roads are noticeable operable for shorter periods of time. Limiting local community access, and transportation of commercial goods. Cold et al. (2020) reviewed

the vulnerability of transportation methods to climate change, for communities in the Yukon River basin. This study further identified highly influential changes in ice, increased erosion, and changes in water levels. Communities which are not connected to the traditional road network of seasonal roads, but reliant on the construction of ice roads or natural corridors, were more vulnerable to changes in the environment, particularly changes in the environment. Not only does climate change alter the structure of the environment, but it also creates additional unpredictability which makes travel more dangerous. Overall, this study concludes that remote communities are highly vulnerable to changes in ice conditions and ice thickness on rivers which are used for local travel and for the transportation of goods.

The design and construction of arctic infrastructure has always considered the impacts of snow and ice which create a challenging and exciting environment for innovation and exploration (T. D. Prowse et al., 2009). However, increasingly a challenge is the adaptation to the loss of a consistently frozen subsurface or surface (lake and river) ice and the uncertainty of where and when. Winter roads are often used for local travel for social and cultural practices between communities (T. D. Prowse et al., 2009). Winter roads and ice bridges are usually built seasonally on lakes and rivers to provide connectivity for communities which otherwise are not connected to the road network to replenish supplies in an affordable manner, or to move supplies and aid in exploration for different industries. One alternative method for winter road construction which tends to be used by the mining industry utilizes the extraction of freshwater from nearby lakes and using it to create thick layers of ice, this method is highly reliant on freshwater available and has significant impacts on local ecology especially in drought scenarios (Arp et al.,

2019). In the case for northern Canada, the winter roads double the of the road system in the Northwest Territories (T. D. Prowse et al., 2009). Although adaptation through a shift from ice road usage to all season roads is possible, construction of all season roads would require climate change adaptive hydrological engineering as roadways often will need to cross waterways (Bouchard, 2020). Currently constructed all season roads are impacted due to the loss of instability through permafrost thaw (Bouchard, 2020). Significant economic impacts are also expected as “resource extraction industries” rely on winter roads which cross ice covered rivers and lakes, and infrastructure used to contain hazardous materials on industrial sites often relies on the impermeability of frozen soil (Walsh et al., 2005).

2.5. Gaps in Research

Although climate change has provided an interest in Arctic hydrological processes, ongoing work in this field continues to be limited by available data for all fields of study. Hydrology is not a standalone field of science, but frequently provides input and boundary conditions to further studies of marine and terrestrial environments. Modelled data often is the only serially and spatially continuous option for further studies. Large scale modelling of the pan-Arctic particularly, and across the entire domain has not been done often. Particularly studies have been concentrated at river outlets, and assessments of model performance across the domain has not been done. In order to provide innovative and relevant information for further studies, modelled data must be spatially complete and provide increasing complexity of model outputs by not just focusing hydrological studies on streamflow but also temperature outputs.

There are few studies which incorporate multiple secondary hydrological inputs although they are related and together can inform further study of ecological, biological and community impacts. As understanding within the scientific community of climate change evolves and the urgency of adaptive planning increases, the incorporation of the newest available climate data becomes more important. Although the more commonly represented in literature single model applications with intensive efforts on model calibration aid in regional studies, using flexible modelling frameworks which can efficiently incorporate large data sets and model into the far future are important in providing updated information for adaptive strategy planning.

Communities are increasingly concerned by changes they are experiencing in regard to permafrost thaw and decreases in ice thickness, however comprehensive data are unavailable, most notably for river ice thickness studies. The production of large-scale modelled information of these changes for permafrost and ice thickness, environmental markers impacting community function, fills a large gap in scientific knowledge available for remote communities.

3. Methodology

3.1. Observed Data

Due to the spatial scale of the modelling efforts, significant care was given to finding observed data to ground truth model outputs. As previously mentioned, observed data are sparce in the arctic and so model outputs are compared to observed data occurs at certain locations in the model domain which represent “data dense” areas. Comparison between observed and modeled variables occurs across various regions, this split up is necessary to ensure that the data used were consistent across measurement techniques and were taken across a reasonably similar time period. In addition to observed data, a general comparison was done to other modelled data products. These data are spatially continuous and provides an opportunity for more direct comparison and adds additional quality checks to the observed data used to assess the AHYPEv4 model performance. The following sections describe the observed and modelled data sources in detail used to assess model performance in calculating water temperature, river ice thickness, soil temperature and soil moisture.

3.1.1. Observed Water Data

Observed water data are split up into two stream characteristics, first water temperature and secondly river ice thickness. These were explored separately, and data was obtained from different sources. Firstly, stream water temperature data was obtained from Water Survey of Canada (WSC) at a daily resolution for the entire historical study period as spot measurements extracted from the Environment and Climate Change Canada Historical Hydrometric Data web site (Canada, n.d.), and from the US Fish and Wildlife Service (US FWS) which had data available at an hourly resolution for 2004 to 2017 (United States

Fish Wildlife and Service, 2017). We can expect water temperature measurements to have an accuracy of +/- 0.2°C to 0.5°C depending on the instrumentation used (Wilde, 2006).

As can be seen in Figure 4, WSC spot measurements are available across Canada including extremely high latitude (far North) and remote locations. The data record length is impacted by station access, with longer data records being available in lower latitudes where stations are closer to population centers. There is also a high concentration of longer records in the west, notably in the Rockies and along the Mackenzie River. The longest record from a single WSC gauge covers almost 21 years (gauge number 10BE009 “Teeter Creek near the mouth”). The US FWS measurements are continuous with records ranging from 1 to 7 years. The spatial coverage is not as spread out as the WSC data, with small clusters of observation locations in 6 different areas in southern and central Alaska. The stations are located inland are within the Yukon River basin mainly occurring in the upstream portion of the basin.

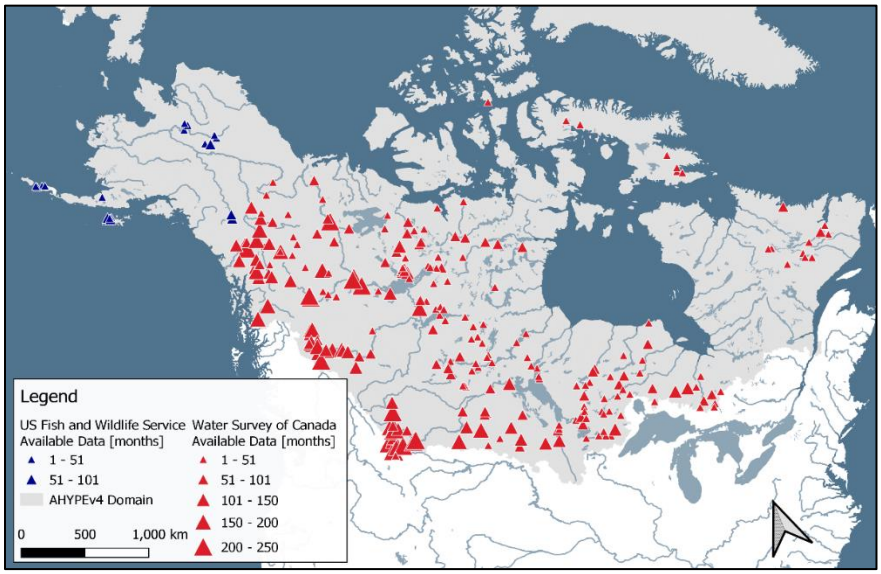

Figure 4 Spatial availability of stream temperature measurements at stations across Canada (WSC) and Alaska (US FWS).

Data are available across the historical period until 2017. As can be seen in Figure 5 most data from WSC are available from 1996 to 2012. As these are spot measurements you can see the cyclical annual variation in data availability. Many locations likely became inaccessible for water temperature measurements due to ice cover. US FWS data are available starting in 2004, and as it is continuous it does not have the same cyclical properties as the WSC data. There is a significant increase in data availability starting in 2015, and most data are available in the two-year period starting in mid-2015 and ending mid-2017.

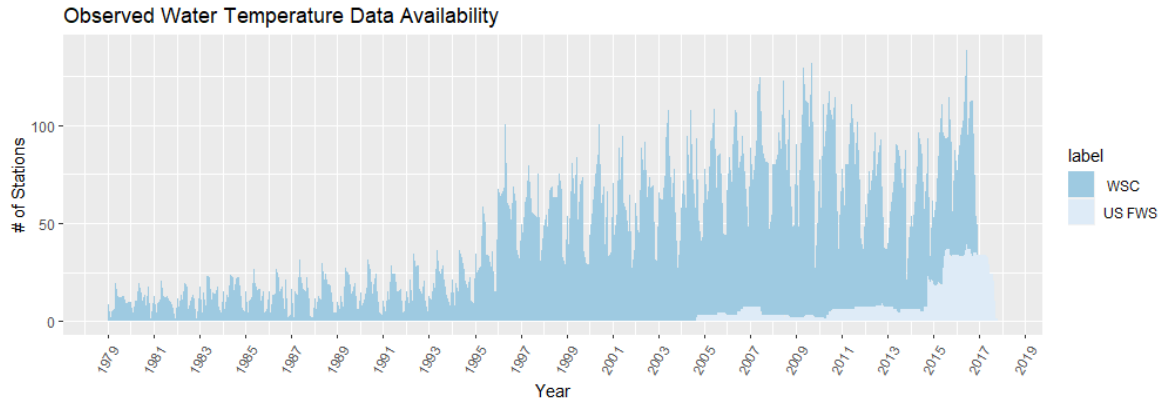

Figure 5 Temporal availability for stream temperature measurements across the comparison period, on a daily scale.

There is a total of 355 stations, as some stations are in very close proximity, they only cover 279 AHYPE subbasins which although finely discretized in some cases contain multiple measurement stations. How these cases are handled in comparison is explained in detail in section 4.1 *Model Performance - Water Temperature and River Ice* which covers the model performance over the historical period.

Table 1 Summary of stream temperature data stations, their temporal extent, and coverage of AHYPE subbasins.

Source	Station Count	Subbasin Count	Temporal Extent
WSC	296	259	1979-01 to 2016-12
US FWS	59	20	2004-08 to 2017-10

River ice thickness data were firstly obtained from the Canadian River Ice Database (CRID) , of which version 3 is currently available with the most recent data available up until 2016 (De Rham et al., 2020). Secondly additional data were obtained from the National Snow and Ice Data Center (NSIDC) which provides significant spatial coverage of Northern Russia as can be seen in Figure 6 (Vuglinsky, 2000a). The CRID dataset provides a single river ice thickness measurement per hydrological year, which can be treated as a maximum river ice thickness for that ice on season as measurements were intentionally taken just prior to ice melt (De Rham et al., 2020). Russian observations are “semi-continuous” with multiple measurements taken per month. Figure 6 shows the spatial distribution of stations, as well as record lengths. The Russian observations have a record of at least 9 years with the longest being 16 years long. CRID data covers major rivers across Canada, with long data records spanning up to 37 years available mostly in Western Canada.

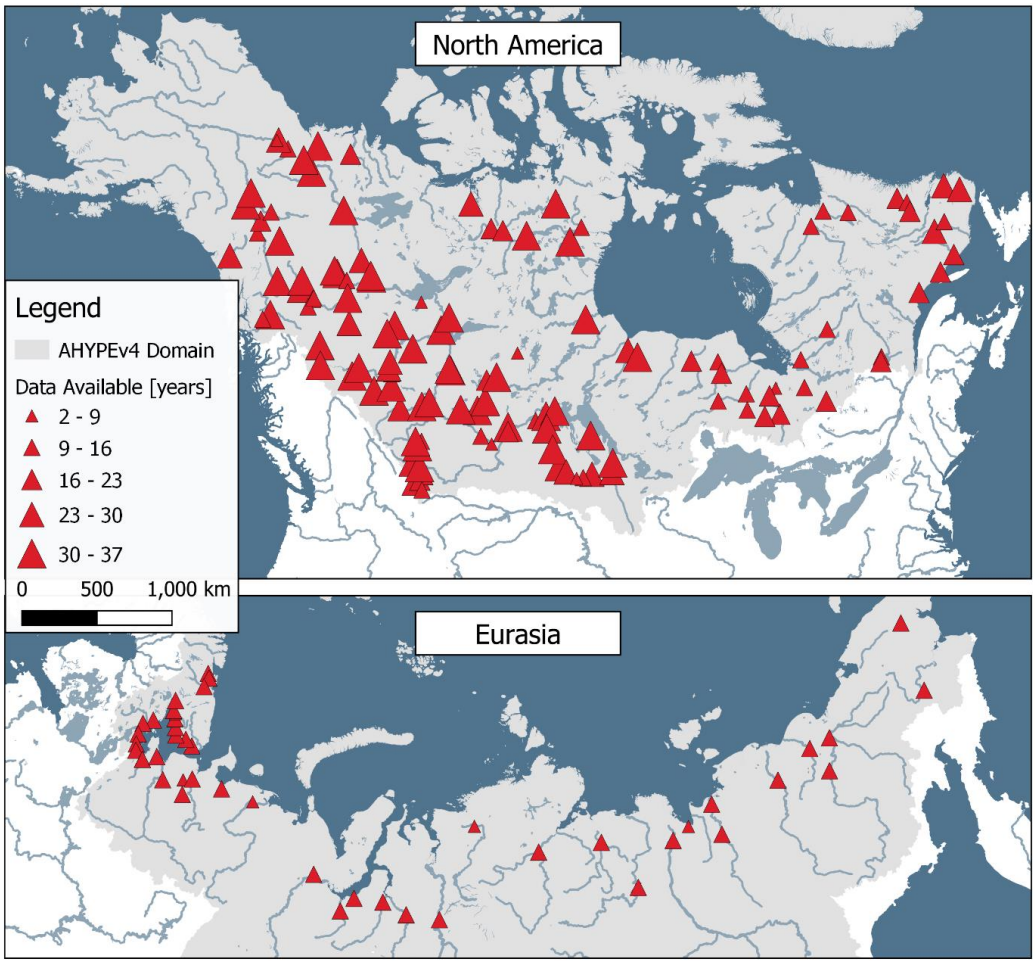

Figure 6 Spatial Availability of river ice thickness measurements at stations across Canada (CRID) and Russia (NSIDC).

CRID data are available for most of the historical period until 2015. As is shown in Figure 7 most observations are in the first seven years, with a steady decline in observations until 2000 from which point on data are available at around 75 stations. NSIDC observations are available only at the beginning of the historical period, with the most stations reporting observations until 1986. Availability of observations is reported on an annual basis, showing only if measurements occurred in that Water Year and therefore do not show the annual cycling which we can expect occur due to ice on and off seasons.

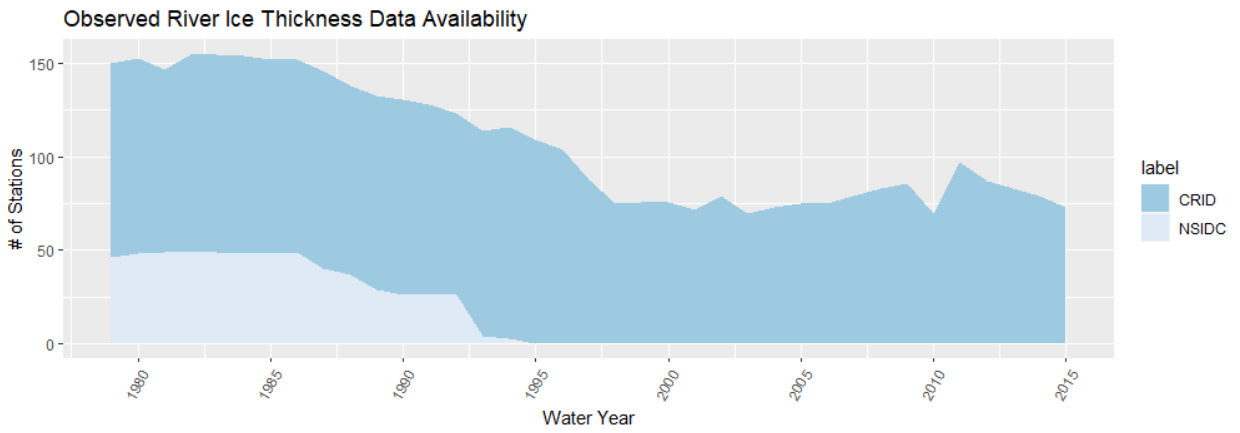

Figure 7 Annual temporal availability for river ice thickness measurements across the comparison period.

Unlike other observed data, the stationing of the CRID data at 107 stations within our historical period equates to covering 107 AHYPE v4 subbasins. The NSIDC data almost has the same property, however the dense stationing in western Russia causes only 46 subbasins to be covered by 50 stations as is summarized in Table 2. Both data sources cover the start of the historical period, with the CRID dataset extending 10 years beyond the Russian data.

Table 2 Summary of river ice thickness data stations, their temporal extent, and coverage of HYPE subbasins.

Source	Station Count	Subbasin Count	Temporal Extent
CRID	107	107	1979 – 2015
NSIDC	50	46	1979 – 1994

3.1.2. Observed Soil Data

Observed soil temperature and soil moisture data was obtained through the international soil moisture network (ISMN). It includes a collection of data from various observational networks, including the Bonanza Creek Long Term Ecological Research Network (BNZ-LTER)(Chapin et al., 2022), the Soil Climate Analysis Network (SCAN), Snow Telemetry (SNOTEL) Network, and the U.S. Climate Reference Network (USCRN). Stations were chosen with data available at 0.2m and 1.0m depth to be comparable with the soil layer

set up in the AHYPEv4 model which is described in Section 3.2.2. Stations were required to have continuous data records for this comparison and stations with only spot measurements were avoided. The data sources chosen had continuous data available at hourly intervals over various time periods. Any data that was flagged was removed to reduce errors. Flagged data includes measurements which were outside of the reasonable measurement range or considered questionable for another reason by the data provider or observations of soil moisture during which the soil would be frozen as this impacts the sensors/measurement method. Data outside of the reasonable measurement range was defined by ISMN as >60 °C and <60°C for soil temperature and for soil moisture this is defined as <0 m^3/m^3 or > 0.6 m^3/m^3. Additionally, the data was reviewed manually and values which were inconsistent or showed significant jumps outside of a reasonable range were removed manually even if they were not flagged.

Figure 8 shows the spatial distribution of the soil observation data stations. The area of focus for this comparison is Alaska, with stations varying in proximity to rivers and covering a generous area, due to the difficulty in retrieving soil moisture data. Model performance was assessed in detail over a smaller domain in order to allow for a direct comparison to observed data rather than a reanalysis product which may introduce its own modelling biases and spatial smoothing of observation data. Additionally, initial plans were to gather observed data to aid in the calibration of soil modelling, which is why data that was temporally continuous over similar periods, and utilized consistent measurement practices was selected. As can be seen, most frequently stations will have both soil temperature (ST) and soil moisture (SM) data available at depth of 0.2 m. There are only

three stations which have only soil moisture observations, this is likely due to the soil temperature data having to be removed due to quality flags.

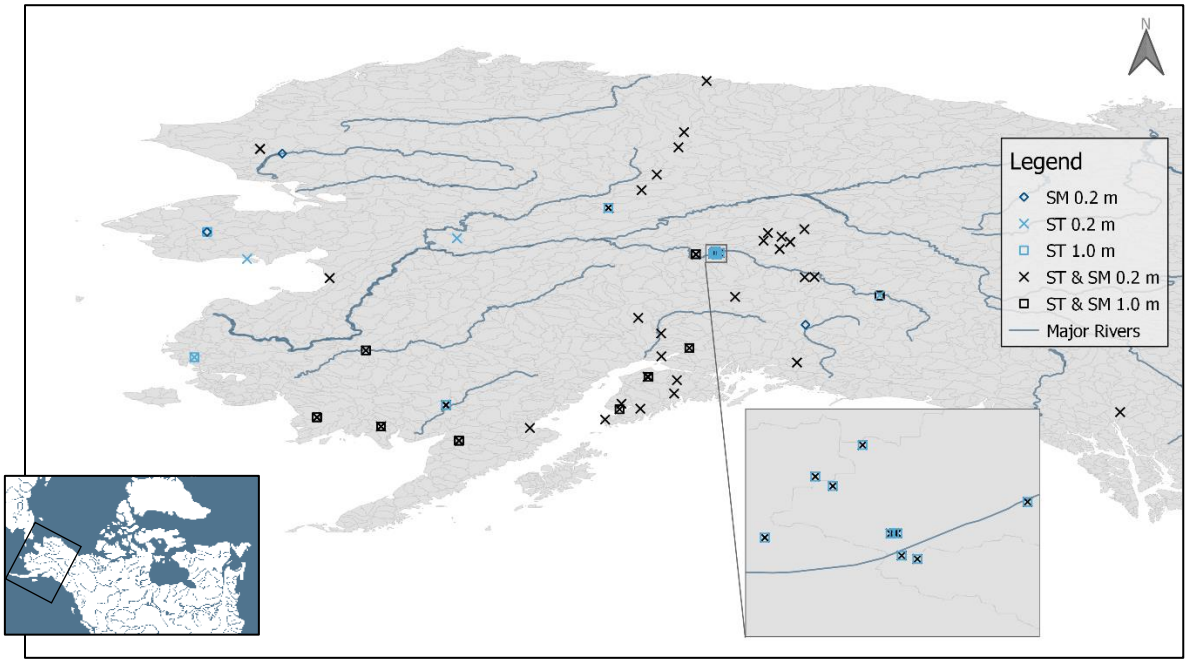

Figure 8 Spatial Availability of soil data with observations at 1.0 m and 0.2 m depths for soil moisture (SM) and soil temperature (ST).

Figure 9 shows the majority of data are available from 2006 to 2017 on a daily scale. Additionally, there is significantly less data available at the 1.0m depth. This is due to the initial data search being done for depths of 0.2 and 0.5 meters to fit a different soil calculation configuration in AHYPE. This new soil layer configuration was not used in this application of AHYPE due to the large study domain which proved itself too large for the addition of more complex soil layers. Fortunately, observed data at a depth of 1.0 meters was included in the original data download even though the station choice was not made specifically for this depth. Soil Moisture data clearly shows seasonal cycling, with most stations not reporting data in the winter months when the ground is at temperatures where soil moisture sensors are not reliable or operational. Additionally, we see that there is less seasonal cycling for soil moisture observations at 1.0 m depths, and data are mostly

available towards the end of the historical period with the most stations reporting observations from 2012 to 2017.

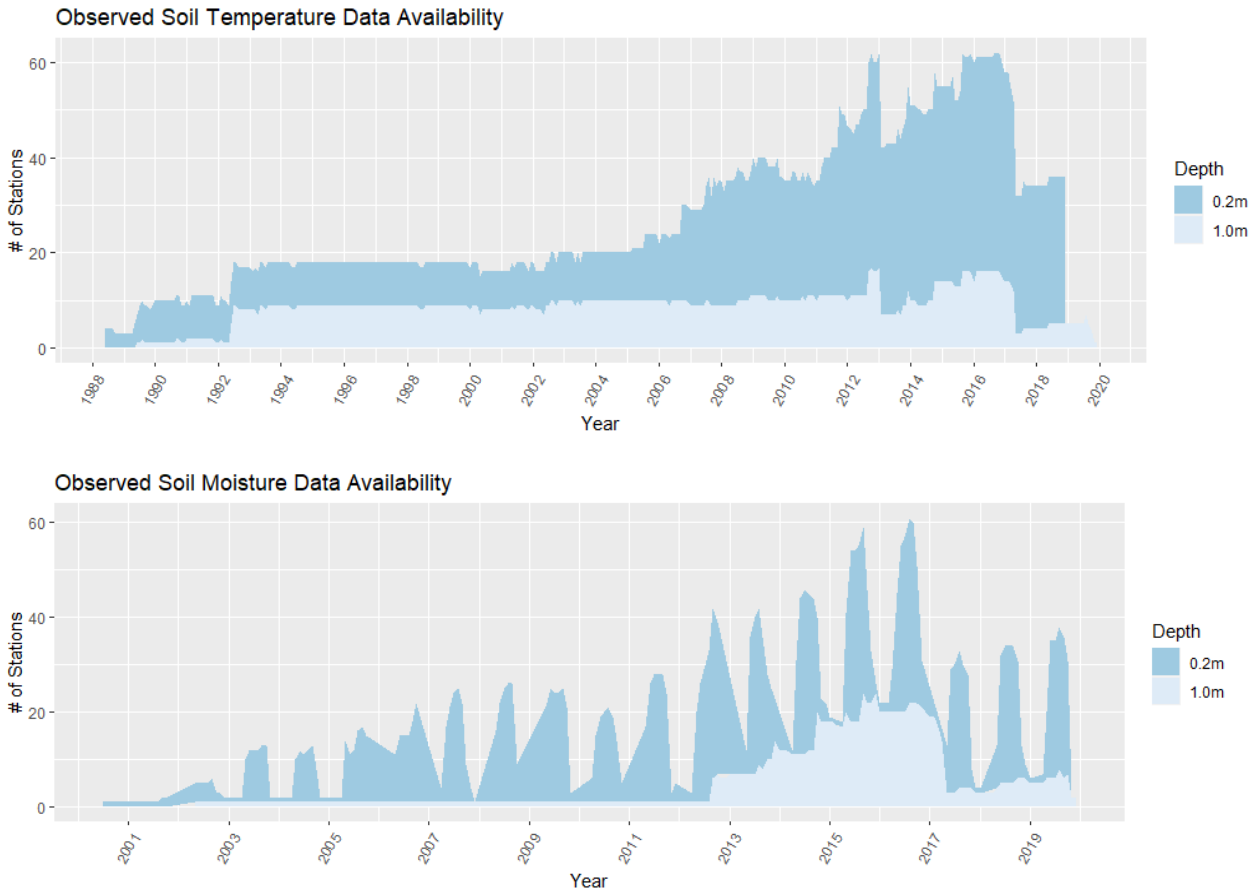

Figure 9 Temporal data availability over the comparison period on a daily scale, note the difference in time scale between the different data types.

Table 3 below summarizes the station information for both soil data variables. In addition to the station count it is important to note that similarly to water temperature observations there may be multiple stations within a single model subbasin. Therefore, less subbasins are covered than there are stations available.

Table 3 Summary of soil temperature and moisture data stations, their temporal extent, and coverage of AHYPE subbasins.

Variable	Depth [m]	Station Count	Subbasin Count	Temporal Extent
ST	1.0	32	15	1989-06 to 2019-12
ST	0.2	66	41	1988-06 to 2019-12
SM	1.0	13	9	2004-08 to 2019-12
SM	0.2	64	40	2002-09 to 2019-10

3.1.3. Modeled Water Data

Modeled data are used as supplementary data due to its spatial and temporal continuity. A recent water temperature modeling effort produced a new 1-D dynamic energy routing model (DynWat). It is a high-resolution physically based water temperature model, producing water temperature available at a 10-km spatial resolution from 1960-2014 (Wanders et al., 2019). The model solves for the transport of water and energy and is an adaptation of Beek et al. (2012) and therefore includes processes from that model as well as additional processes. For example, some of the processes included in the DynWat model are lateral energy transport, ice formation, ice breakup, and thermal mixing in large bodies. Model performance was assessed with correlation (R), the root mean square error (RMSE) and bias.

3.1.4. Modeled Soil Data

Modeled data are used to supplement the sparsely available soil moisture data for the assessment of HYPE model's skill in calculating this variable. In-situ measurements of soil moisture were only available for a small spatial area, and so the Global Land Evaporation Amsterdam Model (GLEAM) data are used to assess performance across the entirety of the domain. It should be understood that this comparison is not between modeled outputs and measurements but instead between two model outputs and

therefore is not a way to ground truth the model but can give insight into how the HYPE model compares to other modeling efforts.

GLEAM produces modeled soil moisture data for the surface and root zone (Martens et al., 2017; Miralles et al., 2011). It covers a lengthy time period from 1980 to 2020 as one of its intended applications is to investigate the impacts of climate change on terrestrial hydrology, similarly to this thesis. All GLEAM outputs are available for download at different time scales (daily, monthly, or annually) across a 0.25° global grid. The modelling effort is forced through various sets of satellite observations and where needed utilizes reanalysis data to fill in data gaps in order to produce its multi-decadal record. GLEAM was validated over the 2011-2015 period by comparing model results to in-situ measurements. Metrics used to assess GLEAM model performance were the unbiased root mean square difference (uRMSD) and correlation (R).

3.2. HYPE Model

HYPE is a semi-distributed hydrological model created by the Swedish Meteorological and Hydrological Institute (SMHI). It has the benefit of global application, customizability, with limited input requirements. These qualities have made the HYPE model an ideal candidate for compatibility with ocean modelling, having been used to create freshwater ocean inputs for long term studies of ocean circulation, and climate change studies, having been applied in particular to studying the Hudson Bay (A. Bajracharya et al., 2020) (Stadnyk et al., 2020). Both applications resonate with the goals of this study, with the creation of freshwater outputs being a secondary outcome of this study. The following sections will provide an overview of how HYPE computes the main model outputs that will be examined in this study, which include water temperature, lake and river ice

thickness, soil temperature and soil moisture. Special care is taken to explain some of the considerations that HYPE makes during computation as well as some of the required simplifications necessary to make large scale hydrologic modelling feasible.

3.2.1. Modelling Water Temperature, Lake and River Ice Thickness

The following processes are described on the HYPE wiki detailing tracer methods (SMHI, 2023b). Water Temperature can be modeled several different ways within the AHYPE model. The method used for this study which is described in this section is modelling water temperature as a tracer. With this method water temperature follows the path of water within the AHYPE model and is calculated in degrees Celsius. This tracer is labeled as “T2” within HYPE and is computed at different stages within the hydrological simulation. The three stages at which temperature output are available (HYPE variable name in brackets) are: the outflow from the outlake (ccT2), the soil water(csT2), and local runoff from soil water(coT2). This study utilizes the outflow from the outlake (ccT2) water temperature, which is also the outflow at the subbasin scale, in order to correspond to previous studies that have looked at outflow and water temperature simultaneously.

The tracer routine considers different sources of heat originating from precipitation, point sources, soil temperature and runoff. Precipitation on land is equal to the air temperature and is limited to temperatures >0°C. Precipitation on rivers and lakes is dependent on the model components and is determined using a weighted average of snowfall on open water, snowfall on frozen water, or rain within the subbasin. It is possible to control the initial state of water temperature for some water bodies such as soil water, river and lake sources. Point sources may have constant temperatures specified within the model

forcing files and can be added to rivers and lakes; aquifer temperatures can also be set. Snow and glacier melt is assumed to have a temperature of 0°C.

Temperature is calculated differently for rivers and lakes, with the method dependent on water depth. River water is determined using the temperatures of the inflow(s). When included in HYPE, river temperature can be affected by irrigation withdrawals, abstractions, point sources, constructed wetlands, or water from aquifers. Lake water is simulated via a thermocline, with the lake water divided into an upper and lower layer provided the lake is deep enough relative to its area to support a thermocline. Shallow lakes with a calculated thermocline depth (calculated from the lake area) deeper than the actual lake depth are treated as a single water layer (Hanna, 1990). Precipitation events on open water influence the water temperature. If the precipitation type is rain, then the rain is considered to have the same temperature as the air. If the precipitation is in the form of snow, the model simulates a heat exchange, considering the heat required to melt snowfall on lakes and rivers without an ice cover. When an ice cover is present, snow is assumed to be the same temperature as the upper layer of water for lakes or average temperature for rivers so as not to affect the current temperature state. A single precipitation event can takes all these different possible scenarios as a weighted average for a water body to calculate how its temperature is influenced by for example a mixed rain and snow event, or when partial ice cover is present. As a simplification for this model, evaporation does not impact the temperature of rivers, lakes, or floodplains.

Ice growth is calculated using an adaptation of a simple thermodynamics model as described by Leppäranta (M. Lepparanta, 1983; Matti Lepparanta, 1993), which is driven by air temperature and precipitation. Lake and river ice is represented using a floating

snow-covered ice sheet, which distributes ice into at least three distinct layers: snow, snow ice and black ice. A fourth layer of slush ice is introduced if the snow layer becomes submerged. As a simplification, the ice mass balance does not interact with the mass balance of lakes and river water, an assumption that is considered reasonable for rivers and lakes that do not freeze to the bottom due to their size. This means that ice processes do not affect the water balance by removing water to form the ice cover or adding water when the ice cover thaws. The only interaction between ice processes and water processes is through the influence of ice and snow melt on water temperature and ice cover which hinders evaporative processes. Lake and river water temperature considers the melt water input from ice to have a temperature of 0°C. Ice cover prevents evaporation from occurring in the model. It is considered to have an insulating effect on water bodies, cutting off surface heat exchanges with the atmosphere.

Ice growth initialization is determined by the thermodynamics of the water surface heat balance. Shallow lakes and rivers use mean water temperatures for the freezing temperature threshold and deep lakes use the temperature of an upper layer. When the heat balance indicates the water temperature falls below the freezing point, ice growth is initialized and calculated for a fraction of the water surface required to maintain the water temperature at the freezing point within the heat balance. Ice cover continues gradually until the surface of the lake is fully ice covered following this process.

The two ice layers, black ice and middle layer of snow ice grow through different processes. The bottom ice layer, black ice, is modeled through a modified Stefan's equation (M. Lepparanta, 1983). The growth equation is only applied if no slush ice layer is present (submerged snow ice); slush ice needs to be frozen first, along with an air

temperature below the freezing temperature. Within rivers, the rate of ice growth is limited by the heat flow from water which depends on the calculated water velocity. Heat from black ice growth is released upward to the atmosphere through the overlaying ice and snow layers. Heat transfer is driven by the temperature gradient between the underlaying (assumed freezing) water temperature and overlying air temperature, dependent on a heat exchange coefficient set for the air. No heat is transferred into river or lake water from ice growth. The median layer of snow ice growth comes from the freezing of the slush layer. This process is considered to release less heat than black ice growth, and the resulting heat is conducted to surface air through the snow layer only.

Snow and ice melt are modeled with a simple temperature index model, which is triggered when air temperature is > 0°C. Melt occurs from the top layer (snow) down to the black ice layer. The snow layer is completely melted before any ice melt is calculated. Internal radiation is also considered when calculating the rate of ice melt. The model considers that the final ice break up is considered to have occurred when the ice thickness is zero or the porosity is below a threshold that may differ between lakes and rivers.

3.2.2. Modelling Soil Temperature and Soil Moisture

The following section is an overview of how HYPE simulates soil temperature and moisture; a detailed description of these processes can be found on the HYPE wiki maintained by SMHI (SMHI, 2023a). The HYPE model simulates three soil layers and allows for the definition of different soil properties for each layer.

Soil temperature is based on three temperature sources including the soils history, the calculated temperature of the soil at a deep depth, below the defined soil layers, this has a constant assumed weight for influence on the above soil layers, and the air temperature

which varies in weight depending on snow cover. The model used for soil temperature calculation is based on Lindström et al. (2002). Soil temperature from the previous time step is dependent on the soil depth as well as the land use. Once soil temperatures drop below zero, part of the soil water will freeze as a function of the soil temperature in each soil layer, limiting water movement through the soil and evaporation.

Soil moisture is dependent on the soils ability to retain water. When only a single value is set for the parameters determining the soils water retention capabilities for all soil layers, the retention capability is distributed evenly depending on the soil layer thickness. However, retention capability can also be calculated for each layer individually if parameters differ among layers. The fraction of water for a soil layer is calculated from soil temperature, water in that soil layer, the porosity of the soil and other soil type parameters. HYPE assumes that the upper soil layer can hold more water than its pore volume however standing water is not treated separately. The soil frost depth is calculated if soil temperature drops below zero and is dependent on water content and other soil parameters. The soils liquid fraction is calculated based on soil temperature (with all soil water as liquid when the soil temperature is >0°C) and is distributed equally in all portions of the soil water within that layer. The model also accounts for the expansion of frozen water in the soil pores by decreasing the volume available within that layer for liquid water.

3.3. AHYPE Performance (1979-2019)

Since one of the novelties of this study is the application of a new iteration of the HYPE model, specifically AHYPE version 4, it is important to report model performance. The model was not calibrated specifically for the model outputs being assessed within this study, and therefore it can be assumed that model performance would likely be improved

through a model calibration unique to each state variable analyzed. Due to the scale of the model, data management to retrieve, prepare and post-process observations is not insignificant, and is further complicated by varying spatial resolution, time gaps, and quality issues. The computational requirements of calibration itself made a re-calibration of the model (let alone multiple calibrations for different state variables) out of scope, however data availability for calibration of all state variables was the biggest limiting factor, making calibration beyond the scope of this project. Instead, the focus is on how the model performs in its current state and each parameter comparison (modeled AHYPE to observed) concludes with remarks on the limitations of available observed data and qualitative guidance on how the model outputs are interpreted as a part of this study. Another consideration that should be made when interpreting model performance results is that observed data are available for individual stations or point measurements. But model output is either on a subbasin average scale, or for the subbasin outlet which may be at a slightly different location. Therefore, we would not expect a perfect match even if the model performed perfectly.

Hydrological model performance is assessed over the historical time period (1979 – 2019) by comparing model output to available, representative observed data sets described in Section 3.1. The AHYPEv4 model was run over the historical time period, with a spin up period of ten years using HydroGFDv3 forcing data to initialize hydrological storages prior to commencing the historical period simulation. HydroGFDv3 data are intended to be used in large (global or continental) scale hydrological simulation; and have commonly been used with HYPE, particularly for applications in the northern hemisphere. They are based on ERA data, making them consistent with most commonly applied ocean model

forcing data as well. The historical period is a product of the e5 (ERA5) reanalysis model corrected with gpcch (GPCCv8) and cru (CRUts4.03) data sets, and has a comparable performance to similar available data sets (Berg et al., 2021).

Observed data were available for each model output on various spatial and temporal scales. Comparison was done on a monthly time step where observed data at a monthly temporal scale was available to accommodate the complexity of the model, the large domain of analysis, and to specifically focus on climatology rather than event-based analysis. The model is not expected to capture the day-to-day variability accurately, but its performance is more accurately assessed over monthly hydro climatological means. Some comparisons are done on annual or decadal time scales depending on the type of observed data available. Spatially, observed data were available on a station basis for various sizes of domains. To compare station data to model outputs on a subbasin scale pre-processing of observed data involved matching each station to the subbasin within which it is located. Then, if multiple stations are within the same subbasin, the average observed value would be used.

Evaluation metrics used are the Root Mean Squared Error (RMSE), a root mean squared normalized using the standard deviation ($NRMSE_{\sigma}$) of the observed data, and the model bias. Normalized metrics afford comparison of performance in the highly heterogenous and variable environment within the large AHYPE model domain, as site specific attributes such as latitude or river size have a significant impact on the parameters of interest. Additionally, model bias is calculated to assess if the model generally over or underestimates the output parameters of interest. Although these metrics are often used in hydrological studies to assess streamflow, this study is primarily investigating

secondary hydrologic model state variables, such as water and soil temperature, river ice thickness and soil moisture. RMSE has been used in notable large scale studies of water temperature, along with bias (Wanders et al., 2019). Studies of model performance in predicting water temperature are still relatively new in literature compared to the extensive research that has gone into how we measure and report model performance of streamflow predictions.

The RMSE is the mean of the square root of the squared difference between the simulated model output (sim) and the observed data of the same parameter (obs). Therefore, the RMSE takes on the units of the parameter compared, for example units of °C when comparing simulated water temperatures to observed water temperatures. The lower the RMSE, the closer the modeled values are to the observed values and the better the model performance.

$$RMSE = \sqrt{mean((sim - obs)^2)}$$

The NRMSE then uses the observed data set to normalize the quantified error. This was done using the standard deviation (σ). Due to being normalized, the NRMSE is unitless. When interpreting the NRMSEσ “low” values reflect better model performance, where “low” is considered to be a RMSE less than half of the standard deviation (Singh et al., 2005). Following this reasoning values ranging from 0-0.5 are considered to be a GOOD model performance, values from 0.5-1.0 to be a FAIR performance and values above 1.0 to be a POOR performance.

$$NRMSE_{\sigma} = \frac{\sqrt{mean((sim - obs)^2)}}{\sigma_{obs}}$$

Finally, the Bias is calculated by taking the average of the difference between the simulated and the observed. This will yield a number which is positive if the model generally overpredicts the parameter, or negative if it generally underpredicts the parameter. An unbiased model will have a bias close to zero. The bias takes on the units of the parameter being compared.

$$Bias = mean(sim - obs)$$

Box plots presented in the following sections were produced using the ggplot2 geom_boxplot() function. Hinges represent the 25th and 75th percentiles, and whiskers extend up to 1.5* IQR, where IQR is the distance between the 25th and 75th percentiles, beyond these outliers are shown as points. None of these parameters are altered between plots to allow for transparent interpretation of the results.

3.4. Climate Change Projections

Climate change projections used to force the future model runs use bias corrected data from the Inter-Sectoral Impact Model Intercomparison Project (ISIMIP) which utilizes CMIP6 Global Climate Models (GCMs). The forcing variables used have been bias adjusted and statistically downscaled with the ISIMIP3BASD method introduced by Lange and applied to the third phase of ISIMIP. This method first bias-adjusts climate data at the GCMs spatial resolution using an aggregated observational data set, and then downscales the GCM data to a higher resolution using a stochastic method (Lange, 2019). The observational data sets used in this method are the EartH2Observe, WFDEI, and ERA-Interim data. Gridded future projection data was remapped to AHYPE subbasins using EASYMORE, a publicly available software (Shervan & Knoben, 2019). From the available ISIMIP3 data covering a total of 10 different GCMs, a representative

set of 3 GCMs were chosen to encompass a range of temperature and precipitation changes. CanESM5 global model scenarios show higher global mean precipitation increases relative to MIROC6 model, MRI-ESM2 sits between these two models in projected global mean precipitation increases. These combined with the different temperature warming scenarios, create a representative set for most other climate models in the ISIMIP project (Lange, 2021). Table 4 summarizes the climate models and their shared socioeconomic pathways (SSPs).

Table 4 Summary of Climate Models and their shared socioeconomic pathways used to force AHYPE model in the future period (2020-2100)

Global Climate Model	ssp126	ssp585
CanESM5	✓	✓
MIROC6	✓	✓
MRI-ESM2-0		✓

Both of the SSPs are part of the “Tier 1” scenarios reported by IPCC, they cover socio-economic assumptions, levels of climate mitigation, land use and air pollution controls (Calvin et al., 2023). The two shared socioeconomic pathways represent opposing ends of future human response to climate change. SSP1-2.6 or ssp126 is the low warming scenario with a 2°C increase in global mean temperature expected by 2100, it is within the SSP1 socio-economic family which assumes a sustainable future. SSP5-8.5 or ssp585 is the very high warming scenario with a warming of more than 4°C by 2100 globally. This new method of categorizing future climate change response to projected greenhouse gas emissions has replaced the representative concentration pathways previously used by the IPCC to show future trajectories of CO_2 concentrations, ssp126 (CMIP6) corresponds to the previously used RCP 2.6 (CMIP5) and ssp585 (CMIP6) corresponds to the previously used RCP 8.5 (CMIP5) (Meinshausen et al., 2020).

3.4.1. Mean Temperature Rise

Instead of defining static 30-year time windows as future periods for analysis or moving time windows, this study utilizes mean temperature rise thresholds over the AHYPE domain. This is a method that has been introduced through global climate change studies and allows for a more consistent analysis across climate models (Calvin et al., 2023). Future analysis periods are by individual GCM simulation by the year when a threshold of mean temperature rise within the model domain is exceeded, alleviating the need to separate analyses by time periods or SSP. Mean annual temperature rise was determined for each GCM and SSP combination across the model domain using the AHYPE forcing files to define the year of exceedance first the Mann-Kendall trend is computed with a pre-whitening method, this method is described in detail in section 3.5.2. Trend is used to define warming thresholds instead of absolute difference from the baseline period to filter out the noise of (sub)annual temperature variability.

Three mean warming thresholds of 1, 2.5 and 5°C rise were selected for each model and SSP combination, meaning that each climate scenario has a different future period of analysis (summarized in Table 5) for each warming threshold. Due to the ssp126 representing a low warming scenario, the two GCM and ssp combinations with this scenario do not have a temperature rise high enough to reach the mid (2.5°C) and highest (5°C) thresholds.

Table 5 Summary of the years of mean annual temperature rise exceedance for each GCM and ssp combination. These represent the ending years of the analysis periods for each combination, with the starting year being 2020. The combinations with the low warming scenario of ssp126 do not exceed the higher thresholds of 2.5 and 5°C.

	1	2.5	5
CanESM5 ssp126	2065	-	-
CanESM5 ssp585	2027	2038	2056
MIROC6 ssp126	2076	-	-
MIROC6 ssp585	2030	2045	2070
MRI-ESM2-0 ssp585	2035	2059	2099

Figure 10 shows the pre-whitened Mann-Kendall trends for annual temperature for all GCM and ssp combinations. It clearly shows the spread in warming scenarios that are represented in this study by the future scenarios which were chosen. Trends show when each scenario crosses the temperature rise thresholds, which is how the values in Table 5 were calculated.

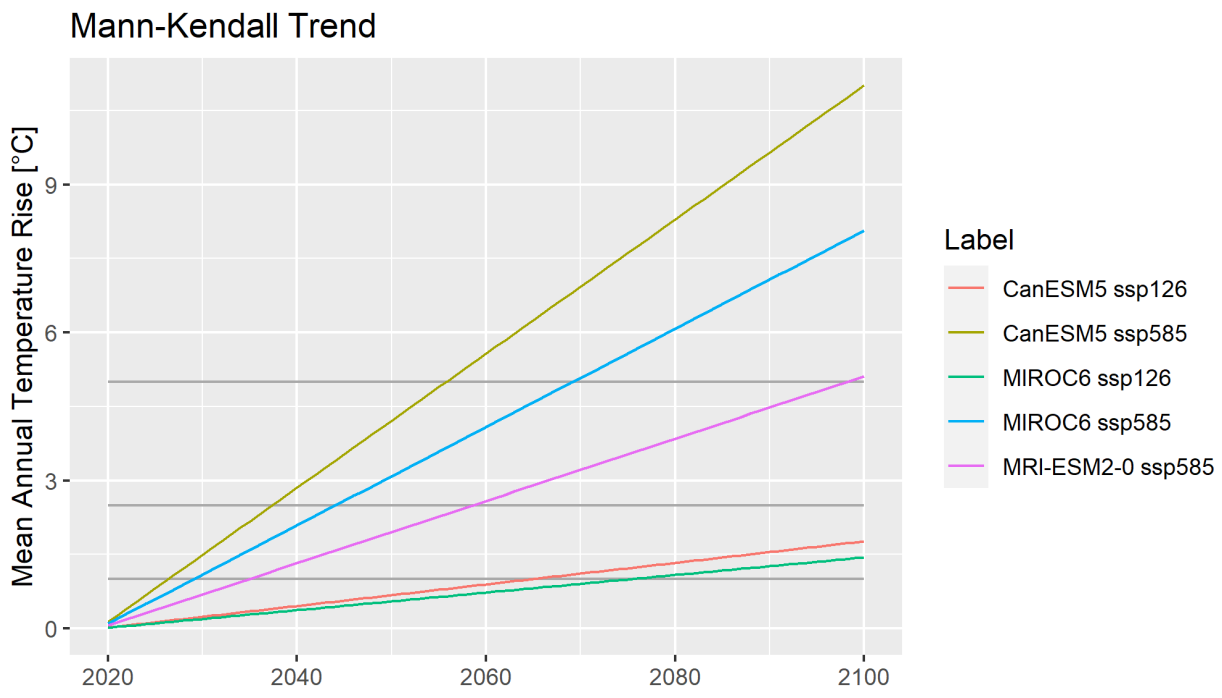

Figure 10 Mean annual temperature rise from 2020 to 2100 for each GCM and ssp combination used in this study, shown by its Mann-Kendall trend. Temperature thresholds of 1°C, 2.5°C, and 5°C are shown in the dark grey lines.

3.5. Analysis

The following section describes the methods used in the analysis of modelled results for the historical period and future period. This includes the temporal and spatial scales for which the analysis is available, since the model domain is of significant size it is beneficial to view the results from various spatial and temporal aggregations. Since the time horizon extends well into the far future, a climatological approach to data analysis is appropriate. The following sections first provide an overview of the temporal and spatial scales that are presented in the results and analysis sections of this thesis, then will describe the trend and change point tests utilized and conclude with a description of how values modeled in Greenland impact the overall AHYPE analysis results and why it is omitted from further analysis.

3.5.1. Temporal and Spatial Scales

Temporal scale can refer to the model output aggregation considered, as well as the time "window" of data included in analysis. Due to the climatological approach of this study, annual averages of model outputs are utilized, which is an appropriate aggregation when looking at long term changes. As for the time window, these vary depending on the application. Trend tests of annual averages are done for the historical period, the whole future period and future time windows determined by the mean temperature rise thresholds for each climate model. Trend tests are also applied to seasonal averages across the entire future period. Seasonal analysis is limited to water and soil temperature since those model outputs are analyzed for their average values. River ice thickness is omitted from the seasonal analysis as the maximum river ice thickness is examined and this is not applicable to seasonal changes. Change point tests are done for the future

period only, as the method used is capable of detecting a single change point and benefits from the availability of a longer time series.

The two different spatial scales of historical and future analysis are the continental scale and the watershed scale. The continental scale assesses trends and change points for aggregated results across Eurasia and North America separately, and also compares them to aggregated model outputs for the AHYPE domain as a whole (excluding Greenland as described in section 3.6). The aggregation is done by taking the average of the model output at each timestep across each domain. This large spatial scale analysis addresses objectives one and two of this thesis, by looking at the overall trends on a continental scale, and addresses objective four by examining the agreements and disagreements among the climate models. The second spatial category is the watershed scale. The method is similar as the continental scale, but model outputs are aggregated for each of the 12 largest rivers (by volume) watersheds. This finer spatial scale is not applied to all temporal scales previously described, but only to the analysis of trends and change points for the entire future period. This addresses objective three of this thesis and will provide analysis for the discussion of hot spots and pan-arctic community impact. Finer spatial discretization such as for example doing the analysis for each subbasin or every watershed contained within the AHYPE model is not done in this analysis, as we don't expect model performance to be accurate on a subbasin scale across the entire AHYPE model domain and computational demands increase exponentially with a finer spatial discretization of model results. Additionally, when considering that one of the major goals with this study is to inform arctic studies on the ocean scale, it is important to

understand what is occurring within the rivers that are considered to be the largest freshwater contributors to the Arctic Ocean and the Arctic marginal seas.

Seasonal trends were only explored for river water temperature and soil temperature, as river ice thickness analysis is focused on maximum thickness which is an annual occurrence. Due to the study being of the entire arctic domain the choice of how to determine seasons presented a unique challenge. In the Arctic domain a traditional understanding of spring, summer, fall and winter does not accurately represent seasonal shifts. Instead, the year is split into three seasons based on the hydrologic year as it is defined in Canada, beginning with October to January which should capture temperatures during the “cooling” season when many of the lower and mid latitudes experience the formation of ice. The second season has been defined as February to May to capture the warming period where ice break up occurs at many of the river ice thickness measurement stations. Observed changes and trends in these months will give insight on shifts in the timing of ice break up. The remaining months, June to September capture the ”summer” months which tend to be the wettest. These seasons have been intentionally increased to four months from the traditional three month windows to try and capture the variability in climate across the domain. Seasonal analysis was done for the continental scale only.

3.5.2. Trend Tests

The trend test utilized is a pre-whitened application of the Mann-Kendall trend test which has been utilized in other hydrological studies which Arctic application (Feng et al., 2021), and provides the slope of a trend line, along with a p-value to describe statistical significance of the trend. It is a nonparametric test, and without pre-whitening has been

shown to produce errors when dealing with time series with a positive serial correlation. Serial correlation tends to occur in annual timeseries on various scales (even the annual average scale), as oscillating patterns in values are often seen and data points are not independent. To avoid these errors, that lead to the detection of significant trends when data are not independent from one year to the next, pre-whitening is used. The pre-whitening method used in this study is the one employed by Yue (2002). This method takes the trend approximated by the Theil-Sen approach, if there is a trend (slope does not equal to zero), then the sample data are “detrended”, and a lag-1 serial correlation coefficient is calculated. This allows for the removal a lag-1 autoregressive process, after this the series is independent. Finally, this method blends the original series and residual series. This blended series still contains the true trend but has removed any influence of the autocorrelation. This application follows previous hydrological studies which use this method to detect changes within hydrological regimes and is able to detect statistically significant trends ($p < 0.05$) even though the timeseries has been “detrended” (Déry & Wood, 2005). Pre-whitening and the Mann-Kendall trend test were done in R using the modifiedmk package.

3.5.3. Change Points

The statistical test used for change point detection is the pettitt test(Pettitt, 1979). It is a nonparametric ranking test which detects a single break in a trend and will report if it is statistically significant. It does this by testing the null hypothesis that there is no change in a sequence, against the alternative that there is a change in the sequence. The pettitt test is known to be less sensitive to outliers than other tests (Verstraeten et al., 2006).

The biggest limitation is that the pettitt test only detects the first detectable change point. The pettitt test was applied to the data in R using the trend package.

3.6. Greenland

Greenland is a significant contributor of freshwater inputs into the Arctic Ocean, and it is included in the AHYPEv4 domain. However, there is low confidence that the AHYPE model can capture the complexity of Greenland's glacial hydrology. Although AHYPE incorporates glaciers into the model, it is not explicitly a glacial model which is what is required to properly model the hydrological processes. Considering this, further analysis and discussion of the AHYPEv4 domain excludes Greenland. Appendix F contains the historical trend analysis of the AHYPE domain which includes Greenland and shows that the inclusion of Greenland creates a bias in trends. Water and temperatures are modelled colder but its greatest impact is on model domain river ice thicknesses. Greenland ice thicknesses are modelled significantly thicker than anywhere else in the model domain, and for the historical and future projections ice thicknesses in Greenland have strong increasing ice thickness trends. To illustrate the impact of Greenland, the following figures are presented to show future trends in ice thickness for Greenland, the whole AHYPE domain, and finally the AHYPE domain excluding Greenland. The annual maximum ice thickness across the entire AHYPE domain shows the influence Greenland model outputs have on the overall results. When comparing trends for the AHYPE domain which include and exclude Greenland, we see that Greenland alters the directionality of the trend. Although deeper analysis would be required to determine exactly why the AHYPE model projects increases in very thick river ice over Greenland (almost ten times thicker than

averages maximum ice thickness across the entire AHYPE domain), it is likely impacted by the glacial influence.

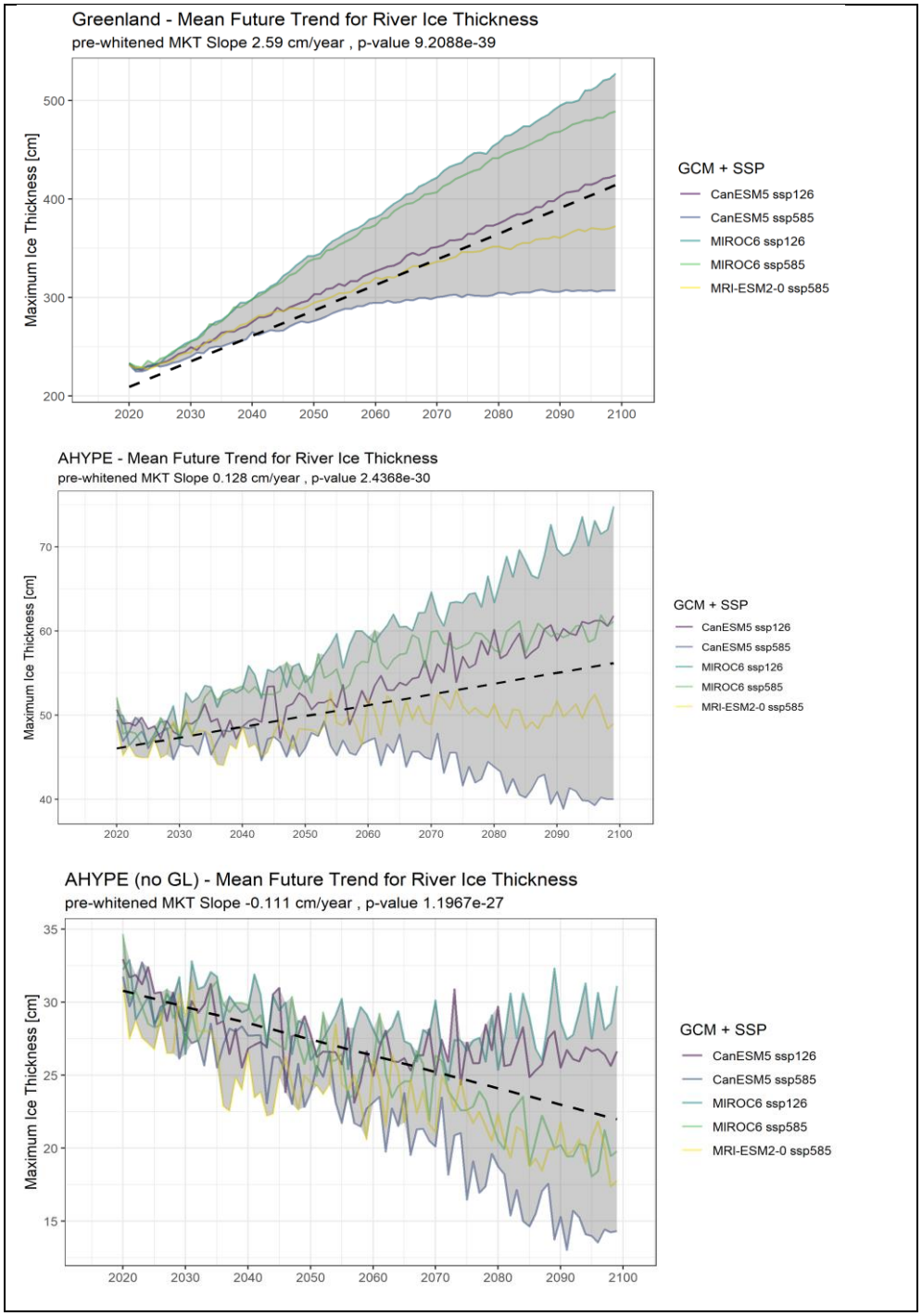

Figure 11 Illustration of the impact modelled results across Greenland have on the overall AHYPE domain. Shown through the timeseries of annual maximum ice thickness [cm] in Greenland, AHYPE, and AHYPE without Greenland domains. Individual GCM+SSP values are shown in solid colored lines, and the mean pre-whitened MKT is shown in a black dashed line.

4. Historical Period (1979-2019) Model Performance, Modelling Results and Analysis

The following historical analysis of the modeled results is presented in order to assess model performance and establish a baseline for future trend analysis. The methodology for model performance assessment is described in section 3.3. An initial review of historical trends will provide the background information to determine whether future trends significantly diverge from an observation driven model of the past. The following sections (4.3 to 4.4.3) outline the historical Mann-Kendall trends (MKT) calculated using the pre-whitening method as outlined in Section 3.5.2 over the historical period (1979-2019). Historical modeled trends are first presented for water temperature and river ice, followed by soil temperature and establish the baseline for future analysis. Each model output is reported on at a continental scale, and then for the watersheds which contain the 12 largest rivers (by volume) in the pan-Arctic. Finally, a seasonal analysis of trends is included for water and soil temperature at the continental scale. Trend analysis does not go to a finer spatial resolution than the watershed scale to reflect the results of the model performance assessment. Model performance varied across the outputs analyzed in this study; however, errors due to the difficulty of the model capturing details at the subbasin scale in some subbasins will average out when examining trends at these larger spatial scales.

4.1. Model Performance - Water Temperature and River Ice

4.1.1. Water Temperature

Water temperature measurements in Alaska (US FWS) and Canada (WSC), previously described in section 3.1.1, are compared to modeled water temperatures at subbasin outlets (CCT2) where observed data exist. Observed and modelled data may not

necessarily be compared at the exact same location since station data can reside anywhere within the subbasin, leading to possible mismatches as the subbasin size increases. We assume the observations are sufficiently representative of river water temperatures within the main river of that subbasin, on average, when comparing monthly average temperatures. No continuous observed water temperature data sets were available on the Eurasian continent, which results in this comparison being isolated to the North American continent.

Table 6 below summarizes the model evaluation of stream temperature across the North American domain. Results are reported separately by data source, rather than being aggregated since measurement techniques slightly differ between the reporting agencies. A full summary of model performance, not aggregated across all stations, but rather by subbasin is provided in Appendix B, and is also visually summarized in Figure 13.

Table 6 Summary of model performance metrics including RMSE, NRMSE and Bias based on comparison to WSC and US FWS data for monthly average water temperature.

Water Temperature Metrics Summary

	AVG		MAX		MIN	
	WSC	**US FWS**	**WSC**	**US FWS**	**WSC**	**US FWS**
RMSE [°C]	3.73	2.66	77.80	5.36	1.14	1.17
NRMSE$_\sigma$	0.74	0.74	29.58	2.88	0.15	0.22
BIAS [°C]	0.56	0.69	48.36	2.40	-6.96	-2.84

Model performance, on average, is better across all metrics for Alaska. This is likely a result of these data being comprised of continuous observations instead of the discontinuous time series with inherent seasonal variability available for Canada, and an artefact of the relatively smaller subbasins for the Alaskan domain. The maximum RMSE appears high for WSC, however the RMSE generally does not exceed 6°C with only two subbasins exceeding that value out of 259. We see that when interpreting average model

performance using the NRMSEσ, it is within the fair performance range at 0.74 for both WSC and US FWS networks. The average model bias suggests that water temperature is slightly overestimated for North America by the AHYPEv4 model (i.e., the model is warm).

The same information as in the above table is shown in the following collection of boxplots in Figure 12, which provide the added benefit of showing data spread and their outliers more clearly. For clarity, the RMSE and NRMSEσ use a log scale on the y-axis due to outliers in the WSC comparison.

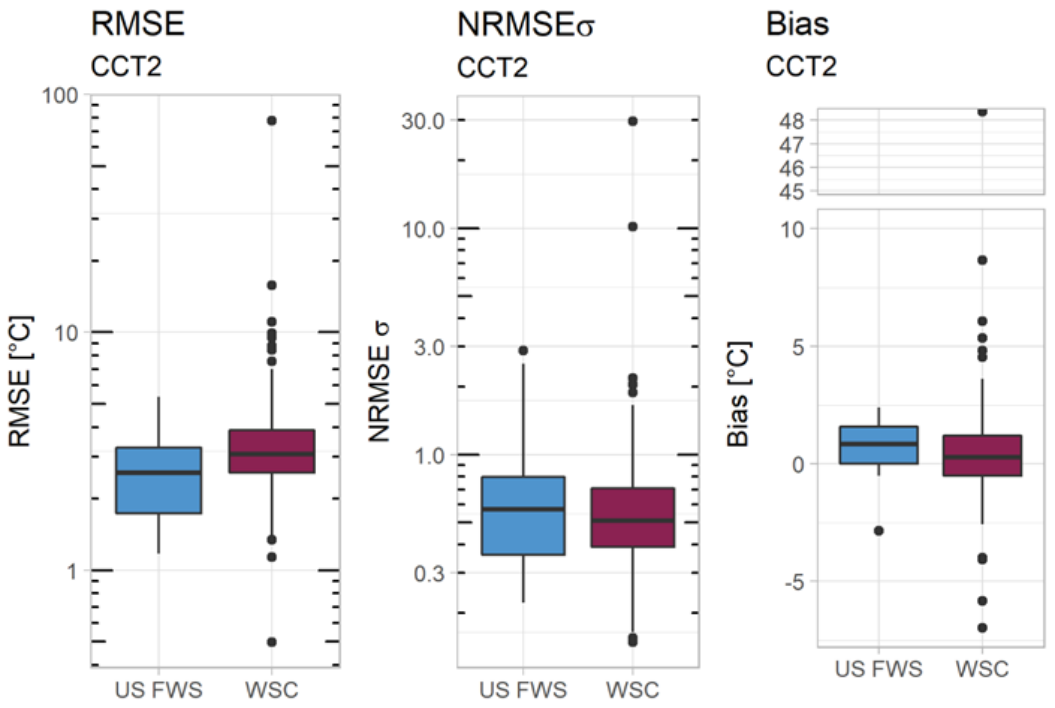

Figure 12 Boxplots summarizing model performance metrics for modelling water temperature using the tracer method. The model output "CCT2" is compared to observed water temperature by the US FWS and WSC. From left to right the metrics compared are the RMSE (log scale), NRMSE (log scale), and the bias. Outliers are shown by dots.

The metric spread is much wider for WSC observations even though the average performance is similar between the two domains, which could be due to the lack of continuous measurements in the WSC observations. The boxplots support the model

overprediction of water temperatures since the bias is generally positive, while also showing that WSC has a much more balanced spread in values. RMSE sit between one and five for most stations, and as previously mentioned the NRMSEσ can be interpreted to showing that an overall fair model performance.

Figure 13 below shows the spatial distribution of the NRMSEσ. The colour scale has been set to match the definition of good (0 to 0.5), fair (0.5 to 1) and poor (>1) performance. There appears to be spatial patterning, lending insight into regions where model processes are most accurately representing the physical processes influencing water temperature. Regions where model performance is strongest occur within the Canadian prairies and northwestern Ontario. Poor performance exists within high latitude or altitude regions, and at stations with shorter records closer to lakeshores or river outlets.

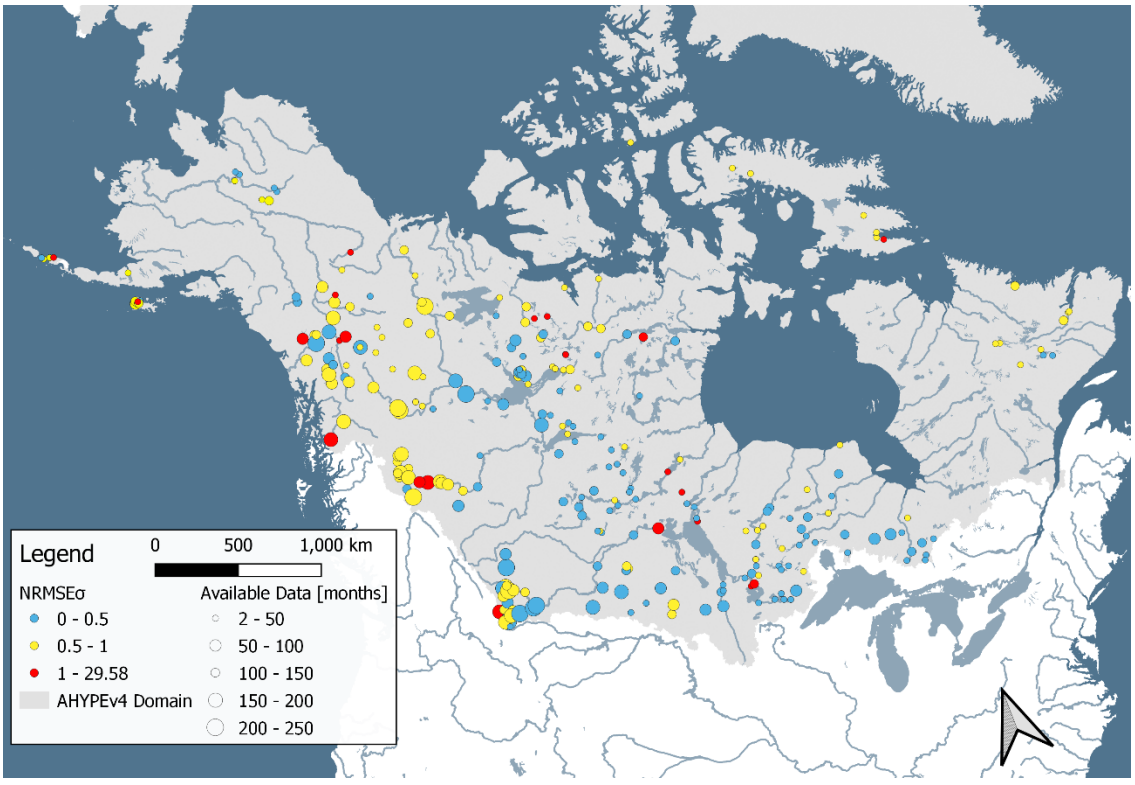

Figure 13 Model performance based on the RMSE normalized by the observed data standard deviation (NRMSE) across Canada and Alaska for the monthly average water temperature. Symbol size indicates the months of data available.

The spatial distribution of the model bias is provided in Figure 14 below, showing the overall positive bias and overestimated water temperature at stations with longer records, shown by the larger circles. Higher biases are seen in high latitude and altitude regions such as the Rocky Mountains in Western Canada, corresponding to the patterns we observe from NRMSEσ. These are at the headwaters of several watersheds and errors in temperature simulation may propagate downstream through the model. Negative biases of greater than 2 degrees are mostly at stations with short observation records which could mean that the timing of the model is affecting these scores.

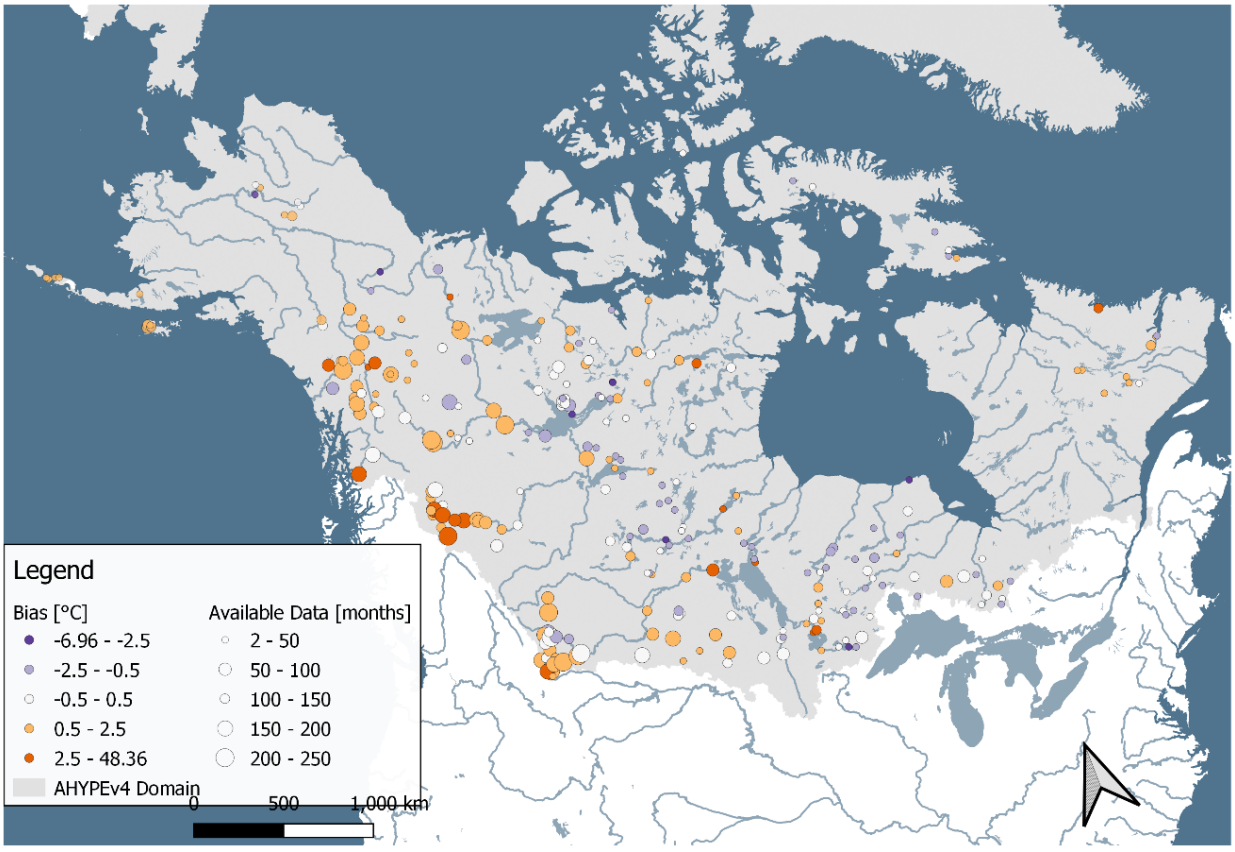

Figure 14 Spatial distribution of model performance modelling water temperature in degrees Celsius based on the bias across Canada (WSC) and Alaska (US FWS) for the monthly average water temperature. Symbol size indicates the months of data available.

Comparison to Modeled Water Temperature

As discussed in Section 3.1.3, modelled AHYPEv4 water temperature outputs are also compared to other water temperature modelling efforts. The model compared to here is the DynWat modelled global water temperature which was described previously. Since DynWat data are available for up to 2014, the comparison was split into decadal periods from 1981 to 2010 to capture as much data as possible beyond the AHYPE spin up period and the conclusion of DynWat data availability. The modelled data are provided for visual comparison on the following two pages, including the average decadal water temperature for both models, and the change in water temperature across each decade.

Figure 15 below shows the decadal average water temperature for both models. Variance in spatial discretization stands out between the two models. As well as some numerical issues with AHYPEv4 modelling, which present as average 0 degrees temperatures or blue speckling in several sections of the model domain. These are also amplified due to the spatial aggregation from a subbasin scale modelling output to gridded data for the creation of comparable plots. Aside from these, the patterning between the two models are similar with clear decreases in average temperature with increasing latitudes and altitude. Water temperature increases along major rivers, particularly visible for the Ob, Yenisei and Lena (listed from West to East) in Eurasia, which are highlighted in warmer temperatures that stand out more drastically in the AHYPEv4 modelling, likely due to increased residence time and storages of water being routed into the outlet rivers.

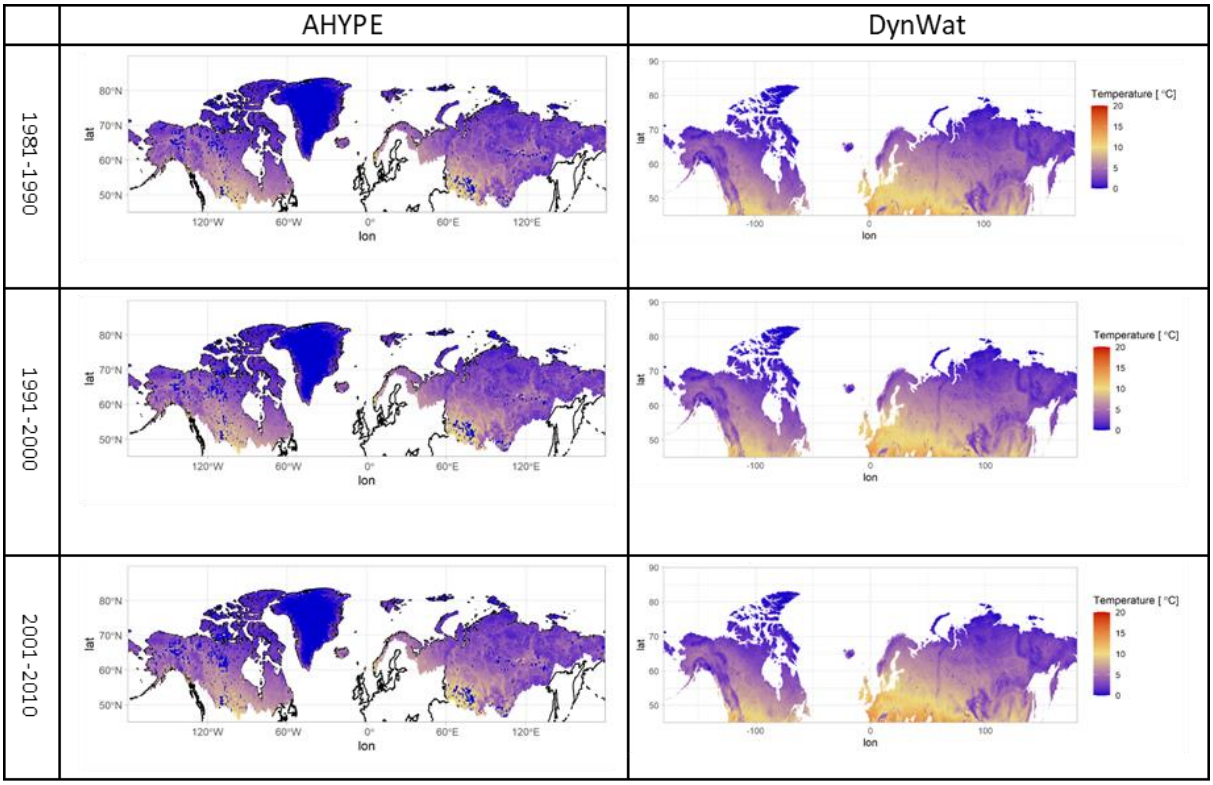

Figure 15 Comparison of decadal average water temperature modelled by AHYPE and DynWat.

Figure 16 below, summarizes the change in annual temperature from the start to the end of each decade, 1981 to 1990, 1991 to 2000, and finally 2001 to 2010. These are the decades covered by both the historical AHYPEv4 model run and the DynWat model. When reviewing the visual comparison, it is evident that the overall patterns in change in water temperature are the same. Interesting is the shift from clear warming across central Eurasia from 1981-1990, and the shift towards cooling in the later portion of the period (2001-2010). Numerical issues for AHYPE modelled water temperatures are still seen scattered through northern and central Canada, as well as the southwestern corner of Eurasia where scatters (shown in white) of decadal changes which fall far outside of the legend range are omitted from the plot. This could be due to numerical instabilities in lower flow subbasins.

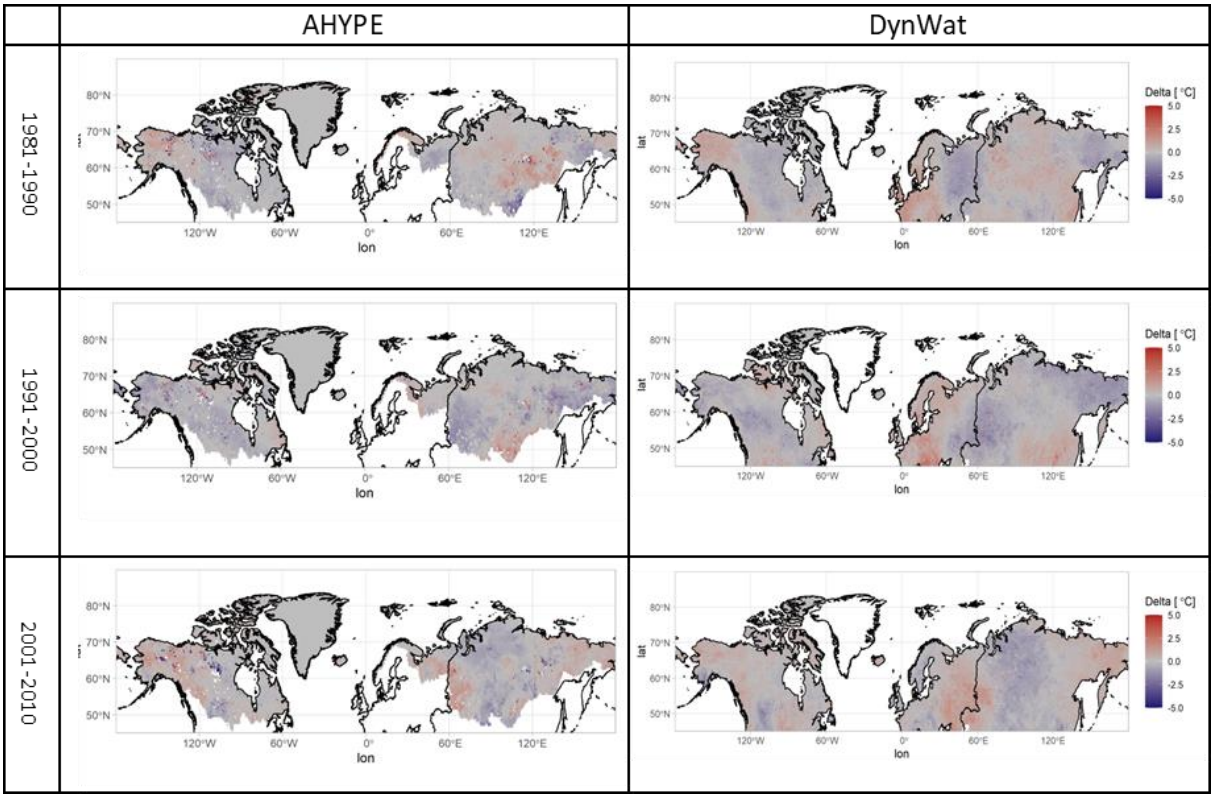

Figure 16 Comparison of decadal change in average annual water temperature modelled by AHYPE and DynWat.

As a result of the above comparisons, AHYPEv4 is found to show reasonable skill in predicting water temperature, on average. When interpreting water temperatures modelled by AHYPE, the positive bias of the modelled values should be considered. It is not guaranteed that this bias is carried forward into a study of future periods where the model encounters conditions that were not included in the historical period (i.e., increased rate of warming), since we know that future temperatures are projected to significantly increase depending on the climate scenario. Since this study focuses on understanding future trends and changes in water temperature and not their absolute value, the AHYPE model shows that it can be appropriately used for this application with the current model process for water temperature.

4.1.2. Ice Thickness

Similar to water temperature, ice thickness outputs are compared against two separate data sets; one that covers Canadian stations (CRID), and one that covers Russian stations (NSIDC) (described in detail in Section 3.1.1). Ice thickness is compared using the maximum modelled value to the maximum observed value. This is due to the ice thicknesses monitoring practices: measurements of ice thickness are usually taken for the average ice thickness across a river cross section near ice break up, which is when ice thickness is at its maximum. This is the practice for the CRID data set, whereas NSIDC is comprised of several measurements, and it is not known if observations are taken just prior to ice break up. In order to properly assess the model's skill in matching observed ice thicknesses, we compare the observations to maximum modelled values.

There are limitations to the comparison of a modelled subbasin average river ice thickness, and measurements physically taken at station locations. Not only is it not expected of the model to capture exact observed river ice thickness when it should be producing a subbasin average, it is also important to consider the errors which are embedded within the observed data set. Historical river ice thickness measurements are not necessarily taken with rigorous attention to quality. The NSIDC data set notes that many observations are taken "visually" with no specifics into the techniques used or where within the river cross-sections measurements were taken (Vuglinsky, 2000b). Human errors when compiling observed data from various sources can also be a factor and are noted as potential errors within the CRID dataset but are also applicable to the NSIDC data. Additionally, noted for the CRID data set is that measurements are not necessarily taken at consistent locations as safety is a major concern when taking field

measurements, and most measurements are taken near bridge sites where bridge hydraulics impact the formation of ice which may produce a thicker ice thickness than other portions of the same river not influenced by bridge pier hydraulics (De Rham et al., 2020). For these reasons, model performance in this comparison should be done by considering errors in both the modeled and observed data, which is increasingly important when not just comparing averages but maximum modelled thicknesses to a ice thickness measurements which are reported to likely be the maximum.

Model performance is summarized in Table 7 below, followed by boxplots and the spatial distribution of the NRMSEσ and Bias. Results are reported separately by data source, rather than being aggregated since measurement techniques slightly differ between the reporting agencies. A full summary of model performance not aggregated across all stations, but rather on a subbasin scale is provided in Appendix B and visually summarized in Figure 20 and Figure 21.

Table 7 Summary of model performance metrics including RMSE, NRMSE, and Bias based on comparison to CRID (Canada) and NSIDC (Russia) data for maximum annual river ice thickness.

River Ice Thickness Metrics Summary

	AVG		MAX		MIN	
	CRID	NSIDC	CRID	NSIDC	CRID	NSIDC
RMSE [m]	0.45	0.48	1.60	2.74	0.04	0.18
$NRMSE_{\sigma}$ [m/m]	2.99	10	9.45	182	0.55	1.12
BIAS [m]	-0.40	-0.38	0.06	0.47	-1.57	-1.38

As shown in the summary table, the average root mean square error is around 0.45 meters for CRID and similarly at 0.48 meters for the NSIDC data. Using the same categorization of performance based on the NRMSEσ that 0-0.5 is good, 0.5-1 is fair and >1 is poor, the best model performance, or minimum value, can be interpreted as fair with

a NRMSEσ of 0.55 m/m. However even the best performing stations in the comparison of modelled to NSIDC observations, the NRMSEσ remains poor with values at or exceeding 1.12. Bias is similar between the two domains, the average bias for both is close to -0.4 meters.

The same information as in Table 7 is shown in the following collection of boxplots in Figure 17. These provide the added benefit of showing data spread and their outliers more clearly. For clarity, the NRMSEσ boxplot in the center uses a log scale on the y-axis due to outliers in the NSIDC.

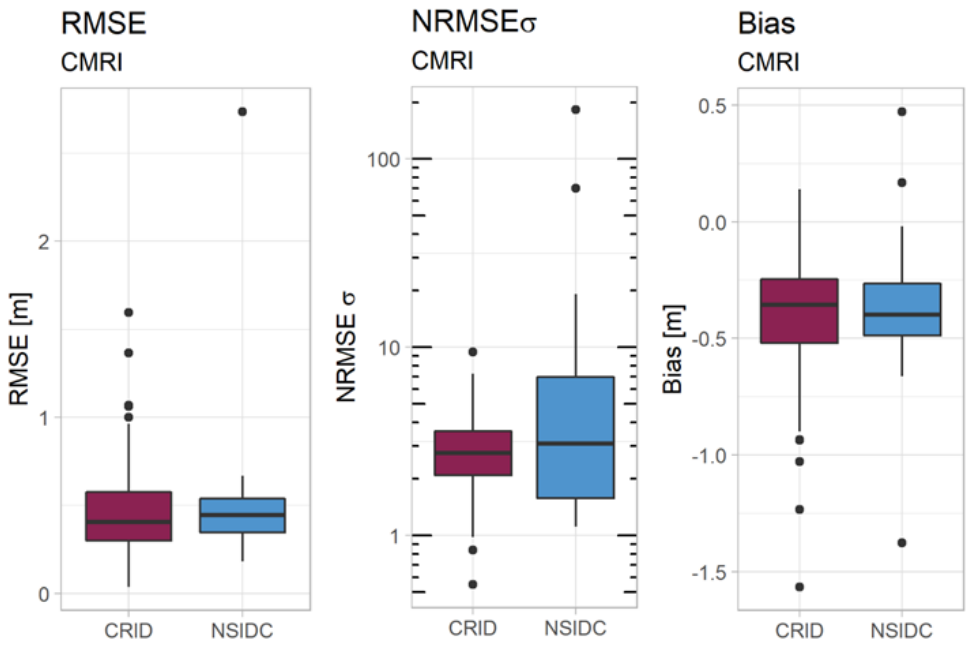

Figure 17 Boxplots summarizing model performance metrics for modelling maximum river ice thickness. The model output "CMRI" is compared to observed river ice thickness in Canada (CRID) and Russia (NSIDC). From left to right the metrics compared are the RMSE, NRMSE (log scale), and the bias. Outliers are shown by dots.

When reviewing the spread of metrics, the NRSMEσ for NSIDC data stand out. This could be due to the inconsistencies in the measurement record, which may not reflect the maximum river ice thickness in the same way the CRID data do, and also much shorter record lengths. Therefore, standard deviation (variability) for the NSIDC is also

significantly higher. As mentioned previously, RMSE is similar for both comparison domains with the average sitting just below half a meter of river ice thickness.

In order to take a closer look at how modeled and observed river ice thicknesses differ between the Canadian and Russian comparisons, a closer look at the individual data points in the comparison is presented in Figure 18 and Figure 19. The scatterplot describing the relationship between AHYPE modeled and observed NSIDC data (Figure 18), shows that there are concerns with the observed data set. Observed river ice thickness does not go beyond 1.0 m, except for a singular measurement. There is also a significant number of observations at around 0.1m, which are unlikely to all be maximum river ice thickness measurements.

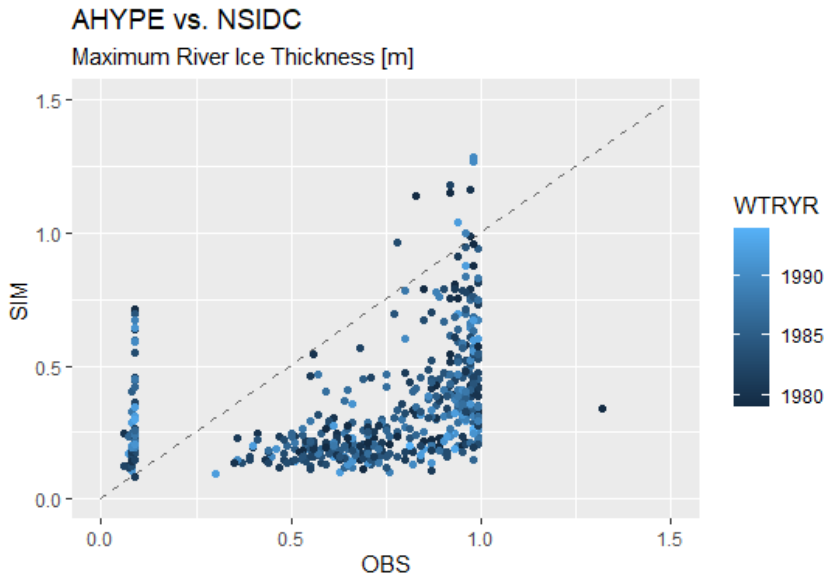

Figure 18 Observed maximum river ice thickness by water year (WTRYR) form the NSIDC data set versus AHYPE modelled maximum river ice thickness by water year.

The scatterplot describing the relationship between AHYPE modeled and observed CRID data (Figure 19) shows a more “organic” set of observations, with a concentration of observations below 1m ice thickness and various measurements that go beyond that.

AHYPE clearly performs better at matching lower river ice thicknesses. This could be impacted by the river ice thickness having been observed near bridges which produce thicker ice cover than perhaps a natural channel. It is clear that AHYPE does not model the same spread in river ice thicknesses as what is observed.

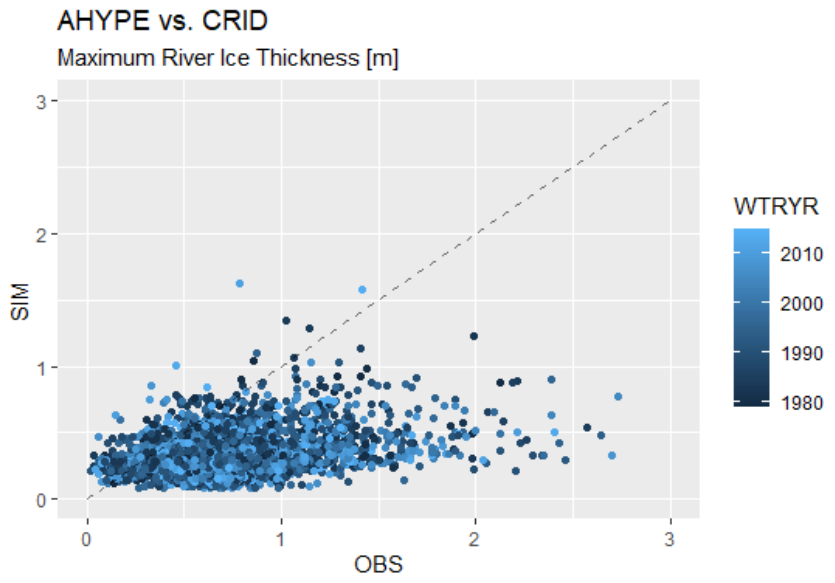

Figure 19 Observed maximum river ice thickness by water year (WTRYR) form the CRID data set versus AHYPE modelled maximum river ice thickness by water year.

Figure 20 shows the RMSE across the two domains instead of the NRMSEσ which was shown for water temperature. This is because there is low spatial variance in model performance when plotting the NRMSEσ, and the model generally performs “poorly” for river ice thickness, as by the ranges defined for the interpretation of NRMSEσ. However, model performance should not be labeled poor as there are clear issues with observed data not representing the same thing as the model. Clearly shown are the differences in record length, with observed data records being much shorter across Russia. For the RMSE performance is best for the Canadian observation stations in the eastern prairies and in the southeastern corner of the Hudson Bay. RMSE are higher at higher latitudes,

which makes sense as we know AHYPE does not model as high ice thicknesses as are recorded, and this is where at cooler climates thicker river ice is able to develop. In the Russian observations, the RMSE does not have a clear spatial pattern. But does show lower RMSE at some very high latitude locations. This does not have the same impact on the RMSE as in Canada, because the Russian observations do not go beyond 1m ice thickness depth.

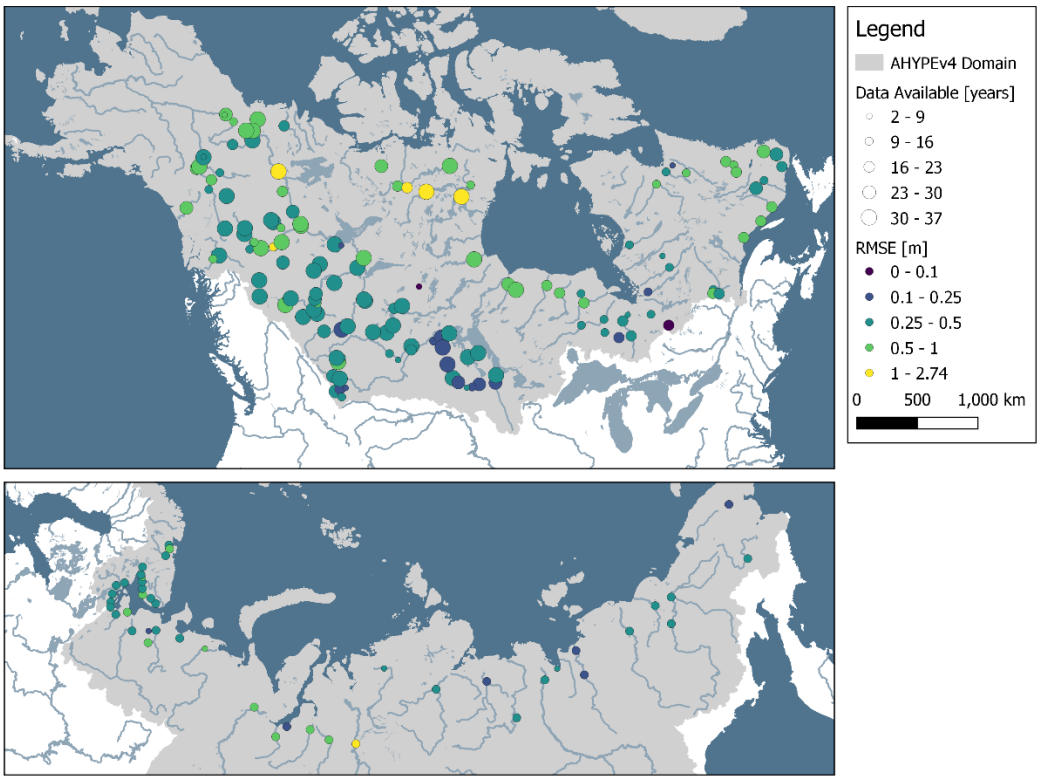

Figure 20 Model performance based on the RMSE across Canada and Russia for the maximum annual ice thickness. Symbol size indicates the months of data available.

More interesting is the spread of Bias across the various observation stations in the Canadian and Russian domains. Canadian stations mostly indicate negative bias at high latitudes, due to the thicker ice observed here which modelled thicknesses do not reach. The model generally shows greater overestimation of river ice thickness near coasts and major river outlets to the Arctic Ocean. Russian stations indicate negative bias with

particularly strong negative biases near the Kara Sea where both the Ob and the Yenisey have their outlets, some of these biases could be due to the influence of ocean water temperatures and ice aggregation in the major deltas which these outlets drain into.

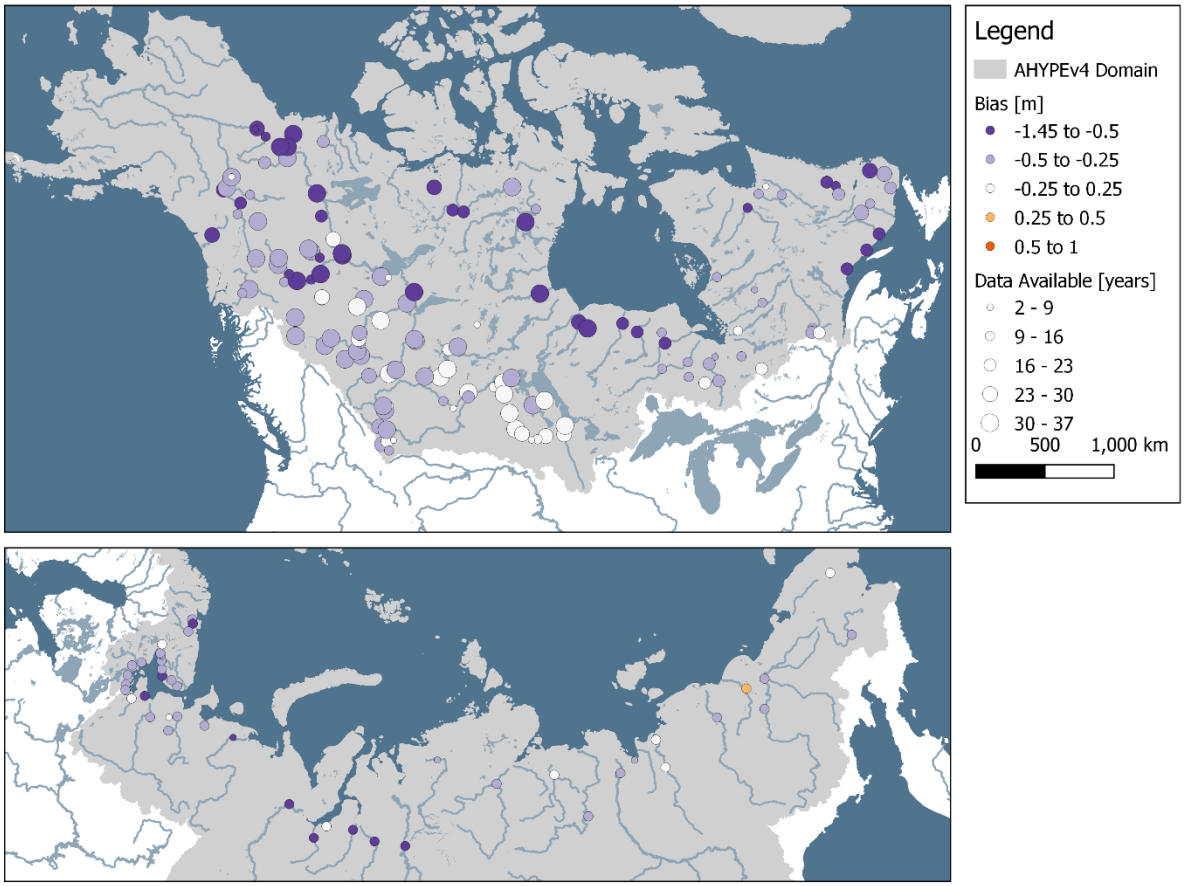

Figure 21 Model performance based on the Bias across Canada and Russia for the maximum annual ice thickness. Symbol size indicates the months of data available.

AHYPEv4 underpredicts river ice thickness when compared to point observations available. RMSE on average are at 0.5m and best performing stations show errors as small as 0.04m. Analysis of ice thickness from the model will proceed as there is also significant uncertainty in the observed data available for comparison. River ice thickness for a domain this size and at the subbasin scale is not available from one consistent hydrologic model. Analysis will focus on larger scale averages such as the continental

scale and watershed scale for large rivers, where errors average out. Additionally, the model's tendency to under-estimate river ice thickness will be considered when discussing the modelled results, particularly for future scenarios. It is likely that model performance can be significantly improved when utilizing AHYPE for smaller domain applications where models can be specifically calibrated to a particular watershed. In this application, since it is an assessment of changes in ice thickness and trends the model can still be used understanding its performance for this model output compared to observed data. It should also be remembered that observations are sparce and prone to error, and a more comprehensive assessment is necessary to understand how both model performance and observed records could be improved for ice thickness.

4.2. Model Performance - Soil Temperature and Moisture

Modelled soil temperature and soil moisture outputs are compared to observed data from the international soil moisture network described in Section 3.1.2. When finding a dataset to assess model performance care was taken to find observed data that utilized consistent measurement methods and covered a continuous time period. High quality and continuous data were only available for a small portion of the model domain, in Alaska where other studies of soil have been undertaken. Observed data at a 0.2 meter depth is compared to modeled soil moisture (SML1) and temperature (STM1) at 0.3 meters which corresponds to the bottom of the first soil layer and observed data at a 1.0 meter depth is compared to modeled soil moisture (SML2) and temperature (STM2) also at 1.0 meters, the bottom of the second soil layer. Data preparation was necessary and any flagged data in the observational data set were removed as described in Section 3.1.4. It is anticipated that observations (point, or in-situ measurements) would not be explicitly and exactly

representative of AHYPE outputs, averaged across an area or subbasin, however, the comparison at least suggests if the model is performing within an expected range of reliability. Soil moisture data contains significant gaps by nature of their collection as it is impossible to take observations once temperatures drop below 0°C and liquid water content within the soils freezes into solid water content. Additional, far more intensive methods of data collection are needed to collect information about solid water content, and that information was not publicly available across this domain.

4.2.1. Soil Temperature

Performance metrics evaluation AHYPEv4s ability to calculate soil temperature for both soil depths in the observed data set are summarized in Table 8 below.

Table 8 Summary of model performance metrics including RMSE, NRMSE, and Bias based on the comparison of average monthly soil temperature at 0.2 m depth (observed) vs. 0.3 m depth (model) and 1.0 m (observed and model).

	AVG		MAX		MIN	
	0.2 m	**1.0 m**	**0.2 m**	**1.0 m**	**0.2 m**	**1.0 m**
RMSE [°C]	4.9	4.1	12.3	8.4	1.3	1.6
NRMSE$_\sigma$	1.5	1.7	4.9	5.1	0.4	0.4
BIAS [°C]	-0.3	1.9	2.4	5.2	-5.5	0.1

The average RMSE for both models is at almost 5 degrees Celsius for a depth of 0.2 meters and just above 4 degrees for a depth of 1.0 meters. The average NRMSEσ is classified within the *poor* performance range for both soil depths, however, as can be seen from the minimum values, some stations do fall into the *good* performance category. The bias for each depth is varied, with the overall bias higher at the 1.0 meter depth than the 0.2 meter depth, and the model being more likely to underpredict soil temperature at the 0.2 meter depth. Values for the AHYPEv4 model are similar to other studies, Alizamir et al. (2021) reported RMSE of between 2.4 – 4.6°C during the testing phase of different

data based models at a 10 cm soil depth, and 1.3 – 3.8°C at a 20 cm soil depth. Bayatvarkeshi et al. (2021) reported the average RMSE for different machine learning models which ranged from 0.4 – 2.3°C.

The same information as in the table is shown in the following collection of boxplots in Figure 22. These provide clarity on the spread of the model performance and the presence of outliers.

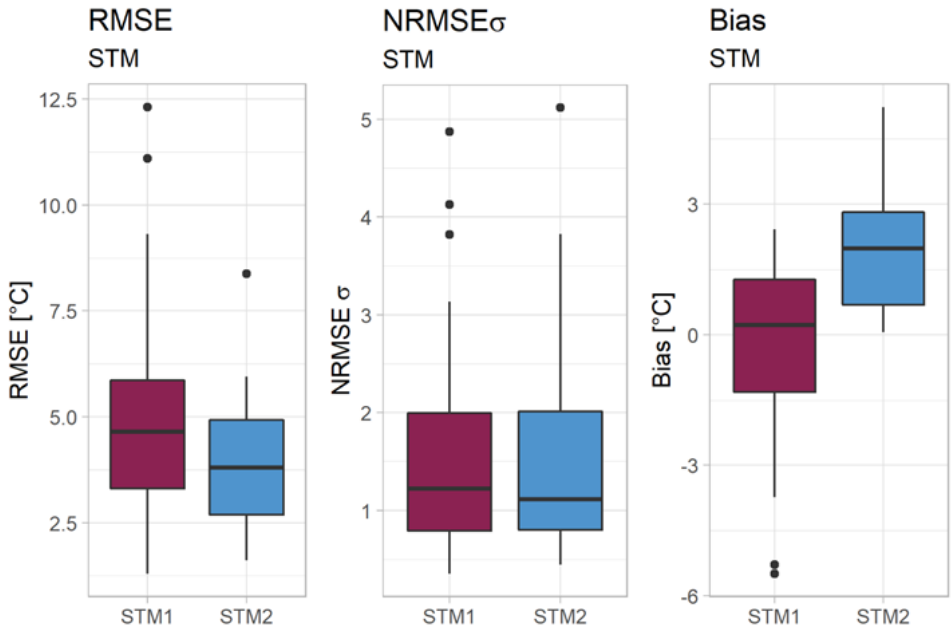

Figure 22 Boxplots summarizing model performance metrics for modelling average monthly soil temperature at depth 1 (0.2m obs vs. 0.3m mod) and at depth 2 (1.0 m). The model output STM1 and STM2 are compared to observed soil temperature. From left to right the metrics compared are the RMSE, NRMSE, and the bias. Outliers are shown by dots.

Boxplots show that although the RMSE results are slightly higher for the shallower depth, the average and spread of the NRMSEσ is very similar between both depths. Temperature deviations are slightly higher for the first depth where temperatures are more likely to vary at shallower depths since surface temperatures have a greater and more direct influence. The bias is positive at the lower depth, indicating the model is not predicting cool enough temperatures (is too warm) at the lower depths for all subbasins.

Figure 23 below shows the spatial distribution of the NRMSEσ and the Bias for each soil depth. In additional to model performance and data availability the maps also highlight the mean subbasin elevations.

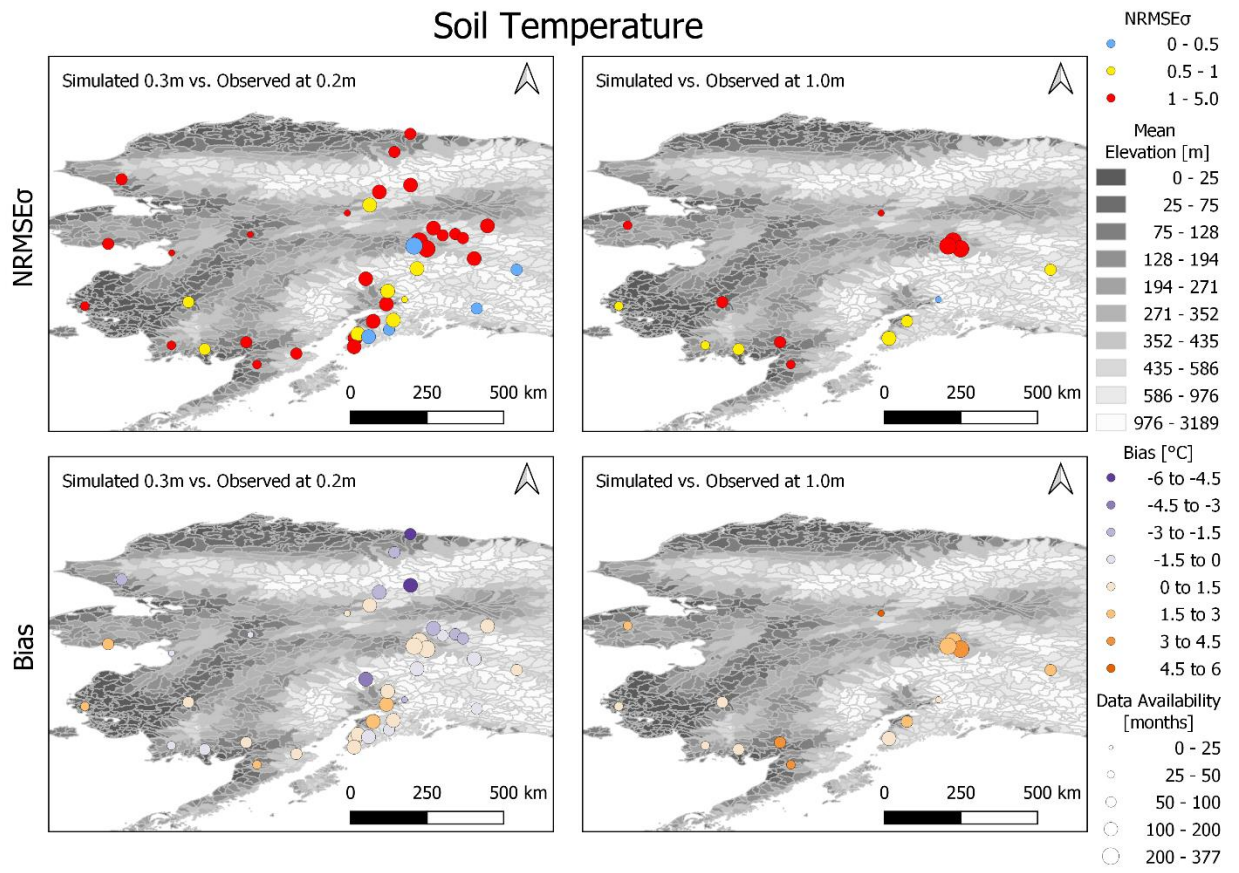

Figure 23 Model performance based on the NRMSEσ and Bias for the average monthly soil temperature at depth 1 (0.2 m observed and 0.3 m simulated) and at depth 2 (1.0 m). Symbol size indicates the months of data available. Subbasins are shaded to show mean subbasin elevation, darker shading indicates lower elevations.

Spatially performance is best in the southeastern portion of the comparison domain, this is where the majority of stations with fair or good performance are located, for both soil depths. Performance is poor at 0.2 m depth along the Alaskan coast but is fair for several stations at the lower soil depth of 1.0 m. Overall, there are positive biases at the lower soil depths. At the upper soil depths, negative biases are mostly present in central and northern Alaska. Stations at lower latitudes seem to have a smaller positive bias. There

are no obvious correlations between model performance and subbasin elevation. It is likely that the movement of water through the various soil layers is causing biases, if water is infiltrated too quickly less water will be available for heat transfer in the upper layers causing a modelling of cooler temperatures at the shallower depth as well as modelling of too warm temperatures at the lower depths. This may be due to soil parameters not being represented accurately within the model; however, soil classification data is difficult to find at this scale resolution. Model calibration for soil temperature would like improve performance at this resolution.

Although AHYPE has variable model performance when it comes to modelling soil temperature, performance is not unexpected for an uncalibrated large-scale model being compared to station-based observations across a small domain. The model was not specifically calibrated for soil state variables, or for performance in this region, nor is it entirely representative of the spatial heterogeneity in soil properties, landcover, and physiography at finer (in-situ) scales. Additionally, this comparison is of a single (or aggregated in-situ stations) to a subbasin, across which the average soil temperature is modeled for a region (92 to 3372 km^2). These spatial resolutions are quite different, and measurements of soil temperature could vary significantly within the subbasin. Additionally, calculated the average RMSE are comparable to other more detailed modelling applications of soil temperature modelling. For the purposes of model evaluation in this research, model performance is considered adequate for assessing future changes in soil temperature at the large scale (across multiple basins and aggregated regions), and because there simply are no other data or observations that can be used to inform climate resiliency and adaptation measures in Canada's North and

the across the Arctic region. In this sense, this work presents a novel application for a hydrologic model to be used to assess soil temperature alongside water temperature at the pan-Arctic scale.

4.2.2. Soil Moisture

Performance metrics evaluating AHYPE's ability to calculate soil moisture for both soil depths are summarized in Table 9 below.

Table 9 Summary of model performance metrics including RMSE, NRMSE, and Bias based on the comparison of average monthly soil moisture at 0.2 m depth (observed) vs. 0.3 m depth (model) and 1.0 m (observed and model).

	AVG		MAX		MIN	
	0.2 m	**1.0 m**	**0.2 m**	**1.0 m**	**0.2 m**	**1.0 m**
RMSE [mm/mm]	0.303	0.107	0.531	0.204	0.073	0.037
NRMSE$_\sigma$	8.0	5.0	26.7	22.1	1.7	1.3
BIAS [mm/mm]	0.295	0.050	0.530	0.191	0.022	-0.127

AHYPE's modelled soil moisture averaged across each subbasin (92 to 3372 range km^2) is a difficult comparison to observed station soil moisture. Performance is better at lower depths (1 m) across all metrics and shows lower RMSE, NRMSEσ and smaller bias. The average RMSE at the lower depth (1 m) is only 0.107 mm/mm compared to 0.303 mm/mm at the shallower depth (0.2 m), or RMSE of approximately 10% and 30% soil moisture, respectively. At shallower depths (0.2 m, the majority of subbasins have a RMSE between 0.2 to 0.3 mm/mm, and at the deeper depth (1 m) the majority are between 0.1 to 0.2 mm/mm (Figure 25). Better performance at deeper depths is encouraging, however this depth also has fewer soil moisture observations therefore it is difficult to comment on whether performance is truly better across the entire AHYPE domain. Deeper soil layers are also known to be less heterogeneous and therefore will be influenced less by variability in the soil permeability, and permafrost variability.

A collection of boxplots (Figure 24) demonstrate the variability in model error for soil moisture. These provide the added benefit of showing data spread and their outliers more clearly. Note that SML1 refers to the shallow soil depth (the comparison of observed data at a 0.2m and modeled data (SML1) at 0.3m depth), and that SML2 refers to the lower soil depth (the comparison of observed and modeled data (SML2) at 1.0m). The NRMSEσ is presented with a logarithmic scale due to the presence of outliers.

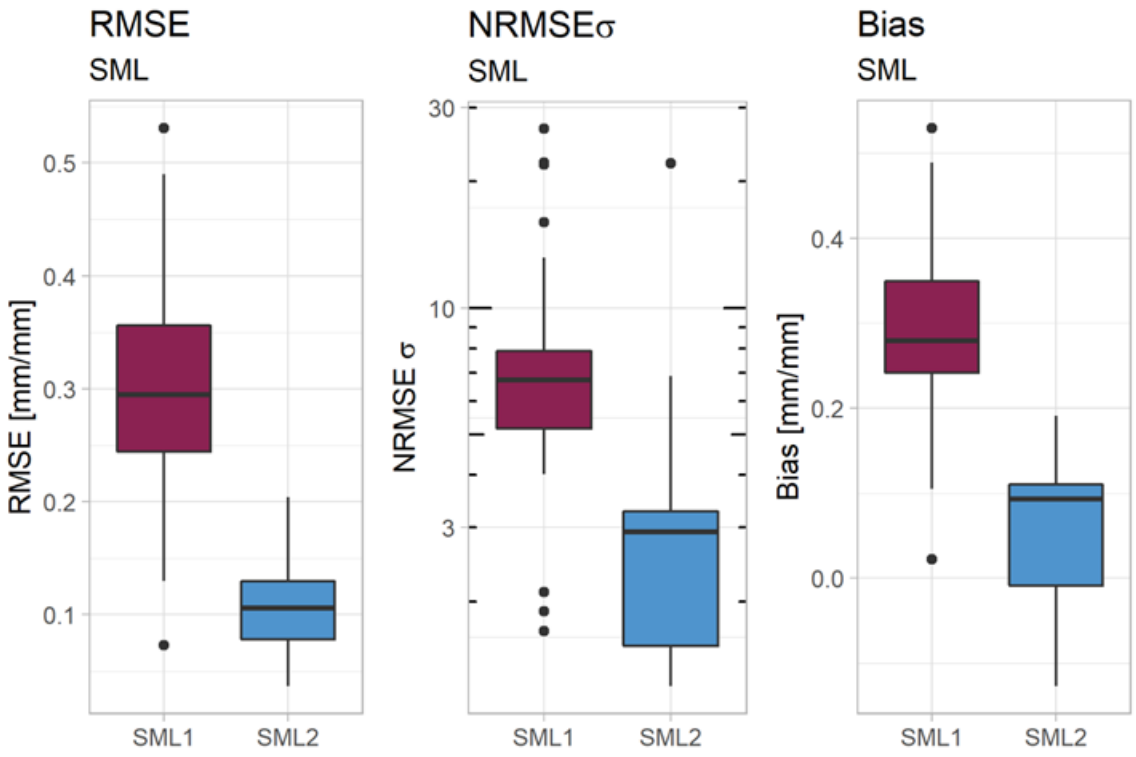

Figure 24 Boxplots summarizing model performance metrics for modelling average monthly soil moisture at depth 1/SML1(0.2m obs vs. 0.3m mod) and at depth 2/SML2 (1.0 m). The model output SML1 and SML2 are compared to observed soil moisture. From left to right the metrics compared are the RMSE, NRMSE, and the bias. Outliers are shown by dots.

Using the previous definitions for the interpretation for the NRMSEσ, where values above 1 are considered poor model performance, suggests all points of comparison have *poor* model performance. Something to be considered when interpreting the NRMSEσ particularly for soil moisture is that performance is normalized by the standard deviation

and soil moisture has little fluctuation (standard deviation) particularly in the observed soil moisture since moisture freezes as temperatures drop below zero, at which point the observations are no longer viable for comparison to the model. The observations below zero represent only liquid water content (a small fraction of soil moisture), while the model preserves the solid and liquid water mass. AHYPE at this time does not include the advanced thermodynamic equations required to numerically separate liquid from solid water content mass balance, therefore a direct comparison of liquid water contents is not possible. Due to this, the NRMSE is not used in the spatial analysis as with previous analyses, but instead it is focused on the RMSE which is easier to interpret. Finally, model Biases are generally positive, at both soil depths, indicating the model tends to be wetter than what is observed.

Below, spatial plots show the RMSE and Bias metrics for all individual subbasins included in the previously summarized metrics. As the distribution of the NRMSEσ metric does not exist outside of the “poor” range, the RMSE is shown instead to allow for a better assessment of spatial trends and model performance across the comparison domain.

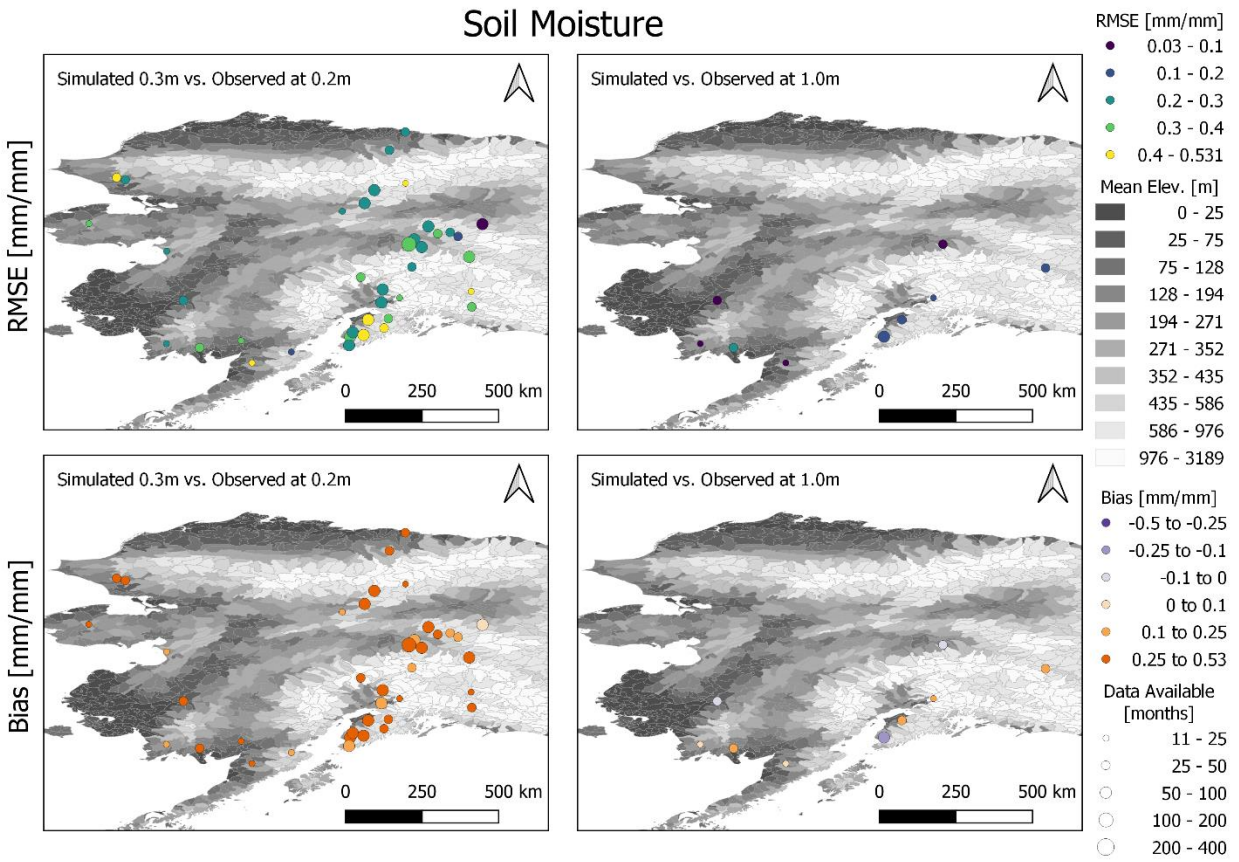

Figure 25 Model performance based on the NRMSEσ and Bias for the average monthly soil moisture at the shallow depth (0.2 m observed and 0.3 m simulated) and at the deep depth (1.0 m). Symbol size indicates the months of data available.

The spatial plots also indicate the sparcity of observations, overall, for soil moisture relative to soil temperature stations. There are no clear spatial trends among either of the metrics. Better performing subbasins those that have a lower RMSE (dark blue), are close to less well performing subbasins (yellow). The biases are all positive (orange) at the shallow depth (0.2m), and and only a few subbasins show slightly negative (light purple) biases at the deeper depth (1 m).

Comparison to Modeled Soil Moisture

AHYPE soil moisture was also compared to a global modeled soil moisture product from the GLEAM model described in Section 3.1.4. Similarly to the comparison between

modeled data for water temperature this comparison was done qualitatively (visually) to further understand AHYPE model performance relative to the best available modeled products globally products. Neither of the two modeled datasets can be considered as “truth”, but this method offers insight into the degree of trust and agreement between AHYPE and other modeled reanalyses used for the pan-Arctic region. This comparison was done on a decadal scale for both average decadal soil moisture as well as the change in soil moisture across the decade by taking the difference between the first and final year. Since GLEAM data was available for the surface and for the root zone the comparison is done first at the surface with AHYPE modeled soil moisture in the first soil layer, and then for the root zone using a the average soil moisture AHYPE models for the two upper soil layers.

The first set of maps (Figure 26) show the decadal average soil moisture from the upper AHYPE soil layer compared to the modeled GLEAM surface soil moisture, for the first decade within the comparison period. As there is little variation between decades in soil moisture modelling the complete set of maps is available in Appendix E. Comparing AHYPE modeled soil moisture to GLEAM we see differing patterns in soil moisture. AHYPE does not model areas with high soil moisture like GLEAM near the Hudson Bay and in Northern Eurasia. Additionally, AHYPE simulates lower soil moisture in central and northern Canada and there is some disagreement between the two models in the soil moisture patterns across Eurasia. We do see agreement on lower soil moisture modeled just west of the Hudson Bay in both models, and higher soil moisture tendencies agree across the prairies. This is encouraging as this area has been the focus of multiple

AHYPE studies particularly the Nelson River watershed (A. Bajracharya et al., 2020; A. R. Bajracharya et al., 2023; Stadnyk et al., 2020).

The second set of maps (Figure 27) show the same comparison; however, for the root zone soil layer which indicates similar patterns as for the soil surface layer.

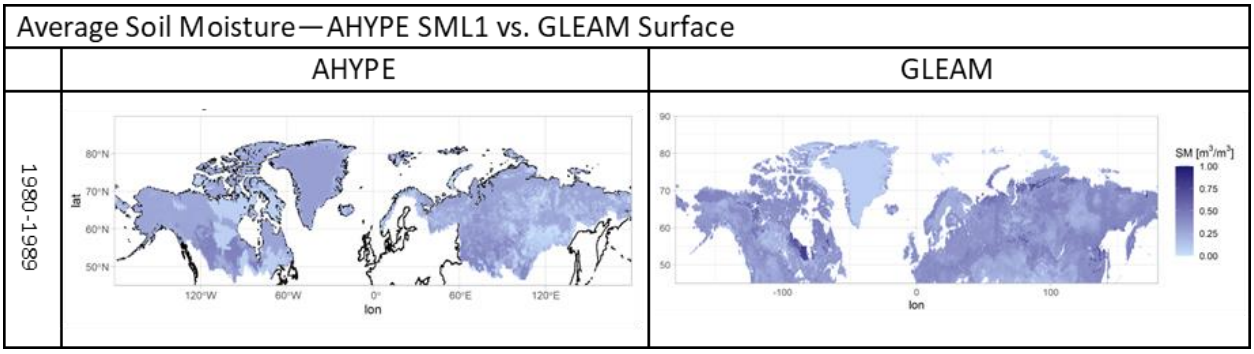

Figure 26 Visual comparison of average decadal modeled soil moisture at the soil surface between AHYPE and GLEAM. Darker blue colors indicate a higher soil moisture content for this soil layer.

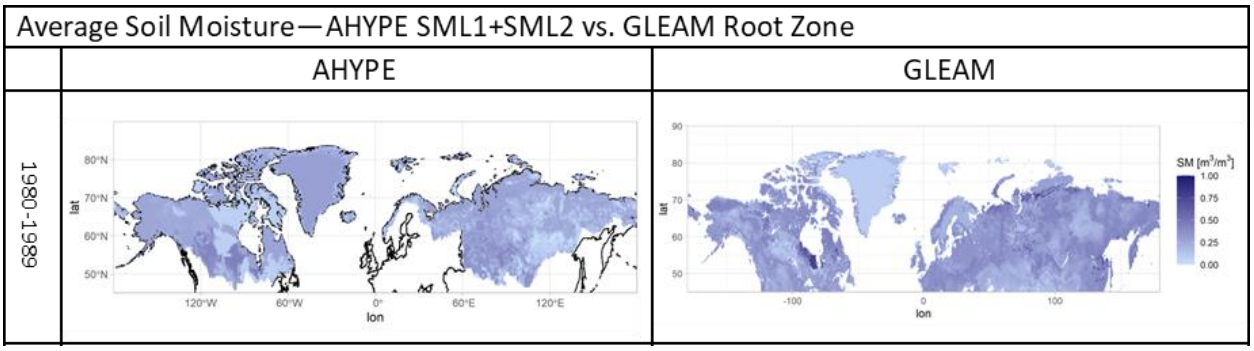

Figure 27 Visual comparison of average decadal modeled soil moisture in the root zone soil layer between AHYPE and GLEAM. Darker blue colors indicate a higher soil moisture content for this soil layer.

More insightful for this particular study is how the models compare in their ability to model soil moisture change. Figure 28 and Figure 29 on the following pages show the comparison between the two models first for the surface soil layer and then for the root zone. The AHYPE model simulated soil moisture changes across each decade are much lower compared to the GLEAM model. Across each historical decade AHYPE simulates the same spatial patterns in modeled change as the GLEAM model; however, relative

changes in soil moisture across the decade are simulated much smaller in the AHYPE model.

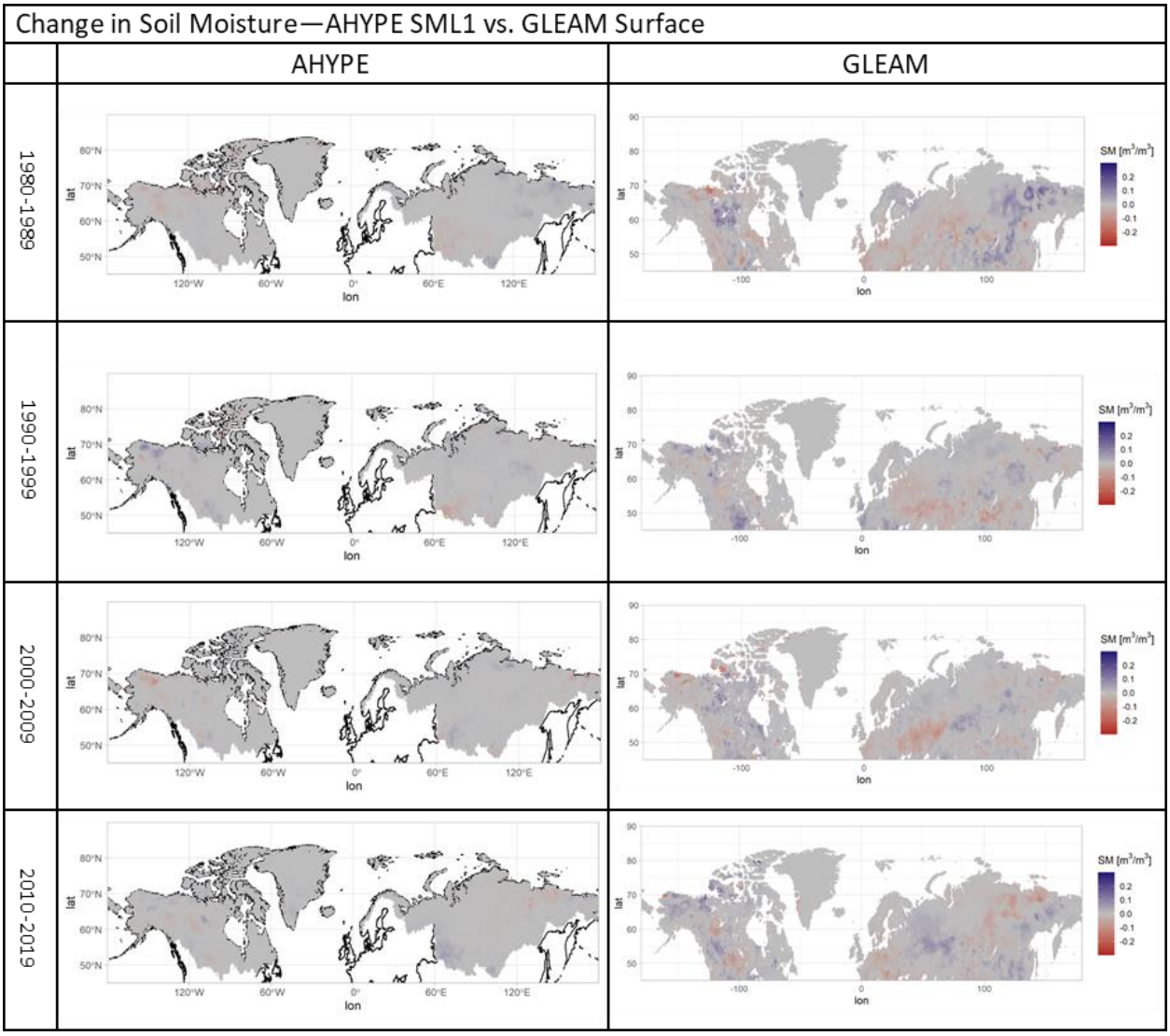

Figure 28 Visual comparison of decadal change in modeled soil moisture in the soil surface layer between AHYPE and GLEAM. Darker blue colors indicate an increase in soil moisture, red colors indicate a decrease in soil moisture and grey shows very little or no change.

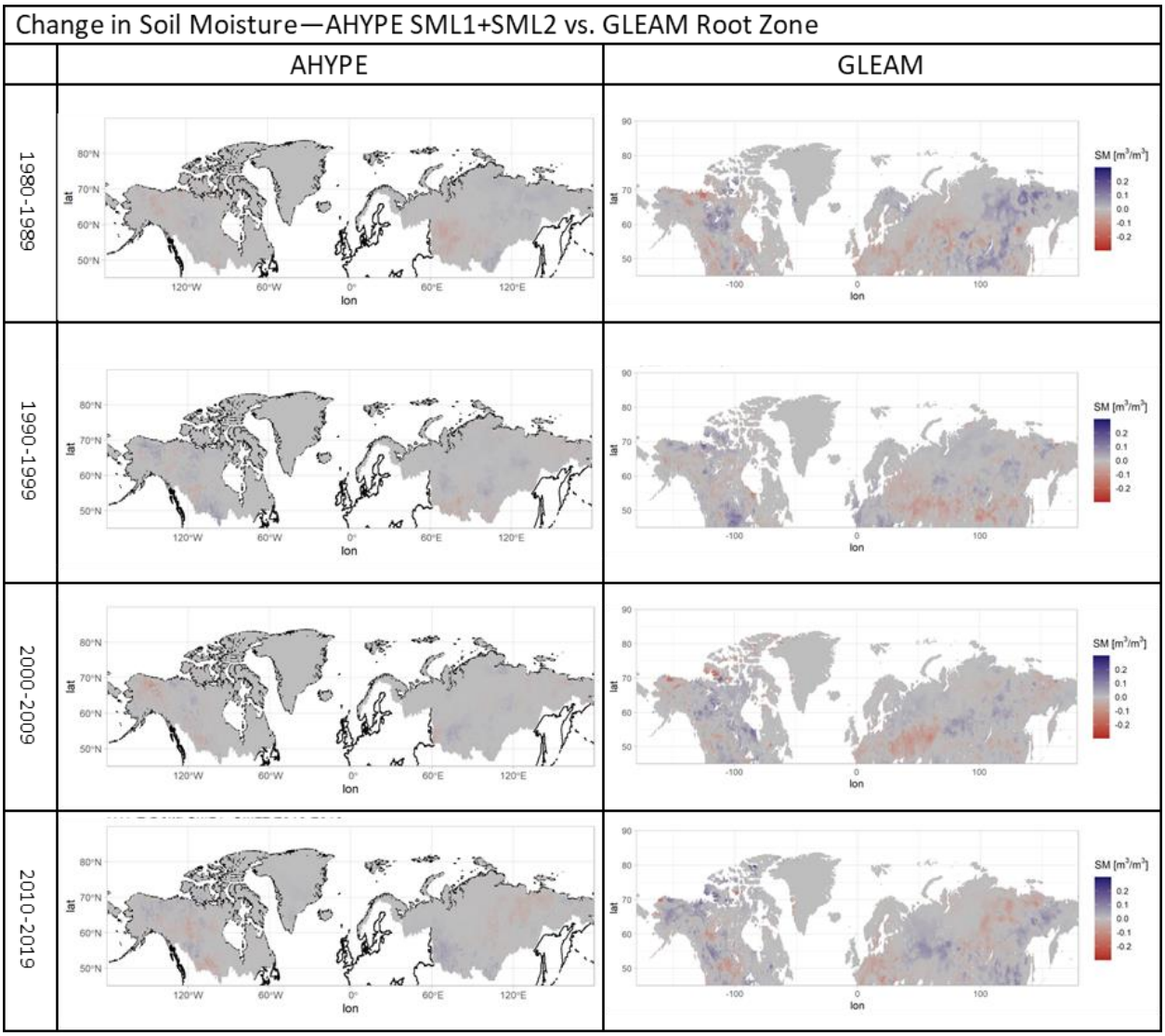

Figure 29 Visual comparison of decadal change in modeled soil moisture in the root zone soil layer between AHYPE and GLEAM. Darker blue colors indicate an increase in soil moisture, red colors indicate a decrease in soil moisture and grey shows very little or no change.

In conclusion, it is impossible to adequately and properly assess AHYPE model performance with the observational data available for the pan-Arctic basins. This is something that was anticipated when performing a pan-Arctic study, as it is a general understanding that observational data are sparse and improvements to observational network density and observational standards are necessary. However, from the data available and used, we can confidently conclude the AHYPE model appears to simulate

a wetter soil than observed. This can be at least partially attributed to the presence of permafrost/solid water content in the soils in these regions, and AHYPE's lack of physical thermodynamic components. When reviewing other modelled data available for the region, however, we see that AHYPE simulates dryer soils, on average. This is encouraging as it suggests that AHYPE may be a better choice than the currently available products for climate resiliency and adaptation information in the pan-Arctic region. Finally, the AHYPE modelling of soil moisture does not model the same intensity of historical changes as other modelling efforts.

Soil moisture is not carried forward into the analysis of modelled trends at this time, as it does not directly correlate to the research objectives. However, it is important to understand the state of modelled soil moisture within the AHYPE model as it is impactful for the understanding of modeled soil temperatures.

4.3. Water Temperature and River Ice Trends

4.3.1. Continental Scale

Water Temperature

The first type of analysis on historical trends for water temperature was done on the continental scales by averaging annual temperatures across the AHYPE domain excluding Greenland, and then the North American and Eurasian continents separately. Trends in annual average water temperature are summarized in Table 10 below. All trends are statistically significant as p-value is less than 0.05 for all spatial scales. The AHYPE domain has an increase of 0.14°C/decade in the historical period, North America has the lowest amount of warming at 0.11°C/decade and Eurasia shows the fastest warming at 0.17°C/decade.

Table 10 Summary of MKT with pre-whitening for average annual water temperature (CCT2) over the historical period, including the p-value indicating statistical significance of the trend.

Spatial Scale	Slope [°C/year]	p-value
AHYPE*	0.014	2.16×10^{-7}
North America	0.011	6.41×10^{-4}
Eurasia	0.017	5.30×10^{-8}

The same trends as above are shown in the time series plot (Figure 30) below. Average annual water temperatures are very similar between the continents and become even more similar near the end of the historical period. In the first half of the historical period the North American continent has higher annual water temperatures, and in the latter half during colder years North America has the lowest temperatures. This is because of the quicker warming trends in Eurasia which cause the Eurasian water temperatures to overtake those in North America.

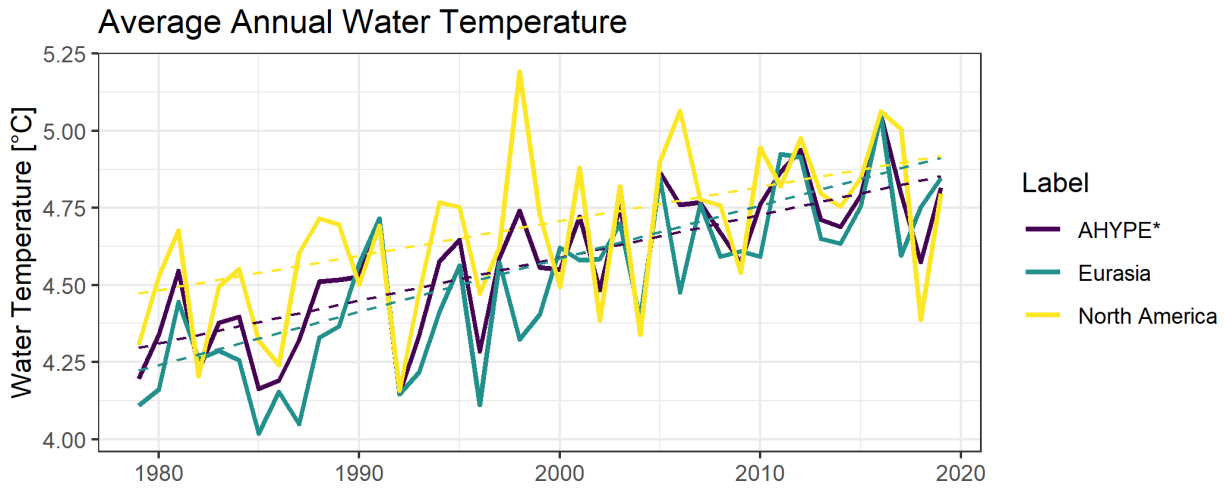

Figure 30 Time series of the average annual water temperature (CCT2) in the solid lines, including the pre-whitened MKT for each spatial domain in the dashed lines. The entire AHYPE domain has a trend of 0.0139 °C/year, Eurasia has a trend of 0.0172 °C/year, and North America has a trend of 0.0111 °C/year. All trends are statistically significant.

A recent study of historical trends in water temperatures focused on Arctic river outlets for the period of 1979-2013, but reported a similar overall trend of 0.16 °C/decade for Arctic River outlets (Park et al., 2017). This is a comparable number to the overall trends

we are seeing here. These trends establish the baseline that average annual water temperatures are warming for the AHYPE model excluding Greenland, and the North American and Eurasian continent. The Eurasian continent is warming faster than North America.

River Ice Thickness

Trends in river ice thickness are anticipated to be decreasing given increasing trends in air (water) temperature (Terry Prowse et al., 2011; Yang et al., 2002). Results of the historical trend analysis for continental river ice thickness are summarized in Table 11 below. The trends are not all significant (significance indicated in **bold**). The historical trend in North America has a p-value of above 0.05. The whole AHYPE domain, excluding Greenland, and Eurasia both have statistically significant negative trends. Maximum annual ice thickness decreases by around 1.1 cm/decade in Eurasia and 0.6 cm/decade for the AHYPE domain.

*Table 11 Summary of MKT with pre-whitening for maximum annual river ice thickness (CMRI) over the historical period, including the p-value indicating statistical significance of the trend. Significant trends indicated in **bold.***

Spatial Scale	Slope [cm/year]	p-value
AHYPE*	**-0.062**	**0.029**
North America	-0.027	0.477
Eurasia	**-0.113**	**0.006**

The same trends are shown in the timeseries plot below (Figure 31). River ice thickness shows high interannual variability. Neither of the two continents shows a consistently higher maximum river ice thickness. Insignificant trends for the North American continent correspond to a lower water temperature rise for the continent during the historical period.

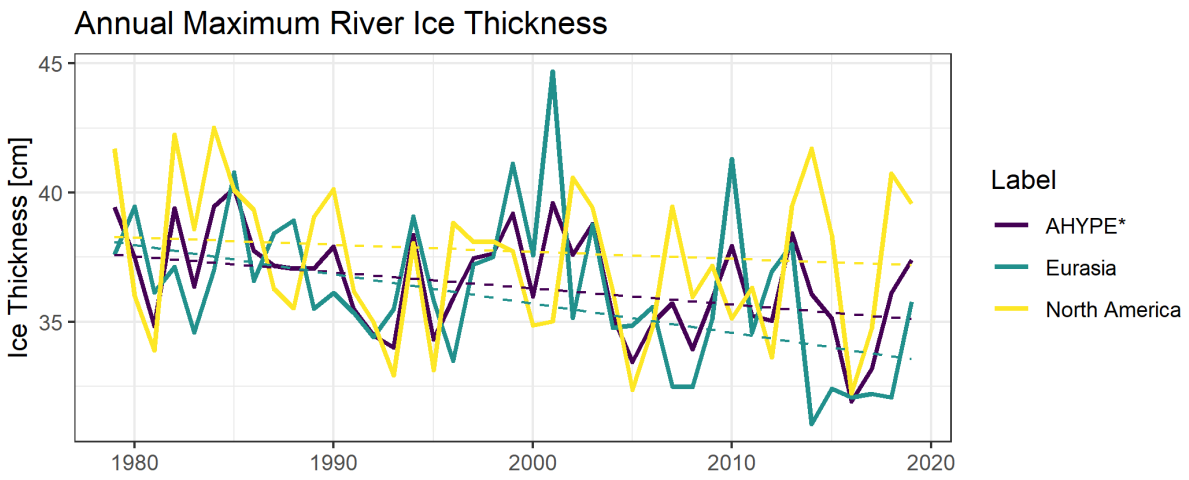

Figure 31 Time series of the maximum annual river ice thickness (CMRI) in the solid lines, including the pre-whitened MKT for each spatial domain in the dashed lines. The AHYPE domain excluding Greenland has a trend of -0.062 cm/year, Eurasia has a trend of -0.113 cm/year, and North America has a trend of -0.027 cm/year. Trends for the AHYPE domain and Eurasia are statistically significant.

Historical trends in river ice indicate decreasing river ice thickness across Eurasia and insignificant trends in North America over the historical period, as expected with the previously discussed increases in water temperature and as reported in the literature (Terry Prowse et al., 2011). Other modelling efforts by Park et al. (2016) for river ice thickness modeled decreases of 0.3cm/year from 1990-2009 for Siberian rivers, this is not directly comparable to the AHYPE Eurasian modelling of ice thickness but does indicate that the AHYPE historically modelled trends are within a reasonable range.

The baseline established from historical trends in maximum river ice thickness is that overall model trends show a clear decrease over the historical period. However, river ice thickness is only exhibiting statistically significant trends in Eurasia and trends are not detectable in North America.

4.3.2. Watershed Scale

Water Temperature

Analysis was also done at a finer spatial resolution on a watershed scale for the 12 largest rivers within the AHYPE domain. Trends are shown below (Figure 32) in both table and time series format, followed by Figure 33 which is a map of the spatial distribution of the ranked trends. The watersheds vary in their overall average temperatures, with lower temperatures in Eurasian watersheds, and the highest in North American, which are generally found in lower latitudes (e.g., Nelson-Churchill River basin). Additionally, all trends are statistically significant, except for the two largest watersheds in Canada which show statistically insignificant trends, the Nelson and Mackenzie River watersheds. In general, individual watershed trends are higher than those which were seen on the continental and model scale. This can be expected as large-scale averaging can level out warmer temperatures.

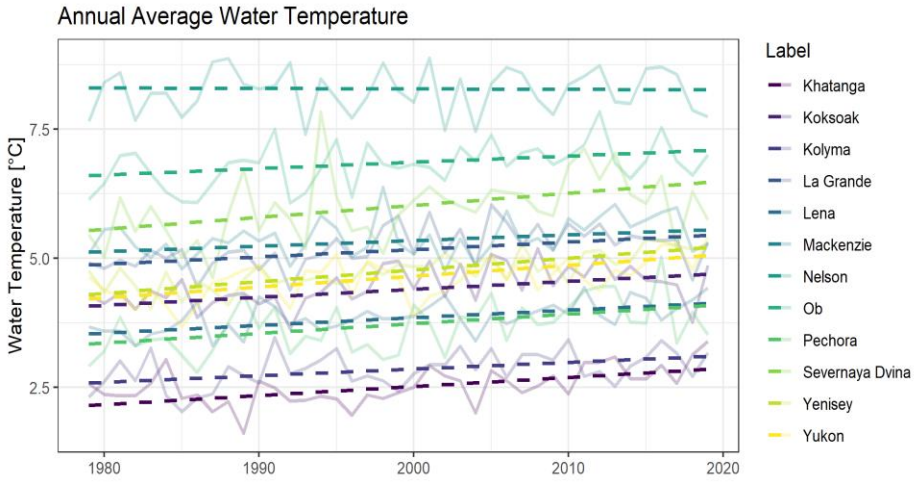

Watershed	Slope [°C/ year]
Khatanga	**0.017**
Koksoak	**0.015**
Kolyma	**0.013**
La Grande	**0.014**
Lena	**0.015**
Mackenzie	0.011
Nelson	-0.001
Ob	**0.012**
Pechora	**0.019**
S. Dvina	**0.023**
Yenisey	**0.023**
Yukon	**0.021**

Figure 32 Timeseries of annual average water temperature for each of the 12 largest watersheds in the AHYPE domain, pre-whitened MKT are denoted by dashed lines and average water temperatures are solid lines. Summarized in the table on the right are the same trends as shown in the plot, and statistically significant trends

The following map highlights that on the watershed scale the majority of the higher trends (orange) are in Eurasia and the majority of the lower trends are in North America (blue), particularly in Canada. This agrees with the continental trends previously discussed. The Ob watershed is a spatial outlier in Eurasia and has a much lower trend compared to the surrounding watersheds.

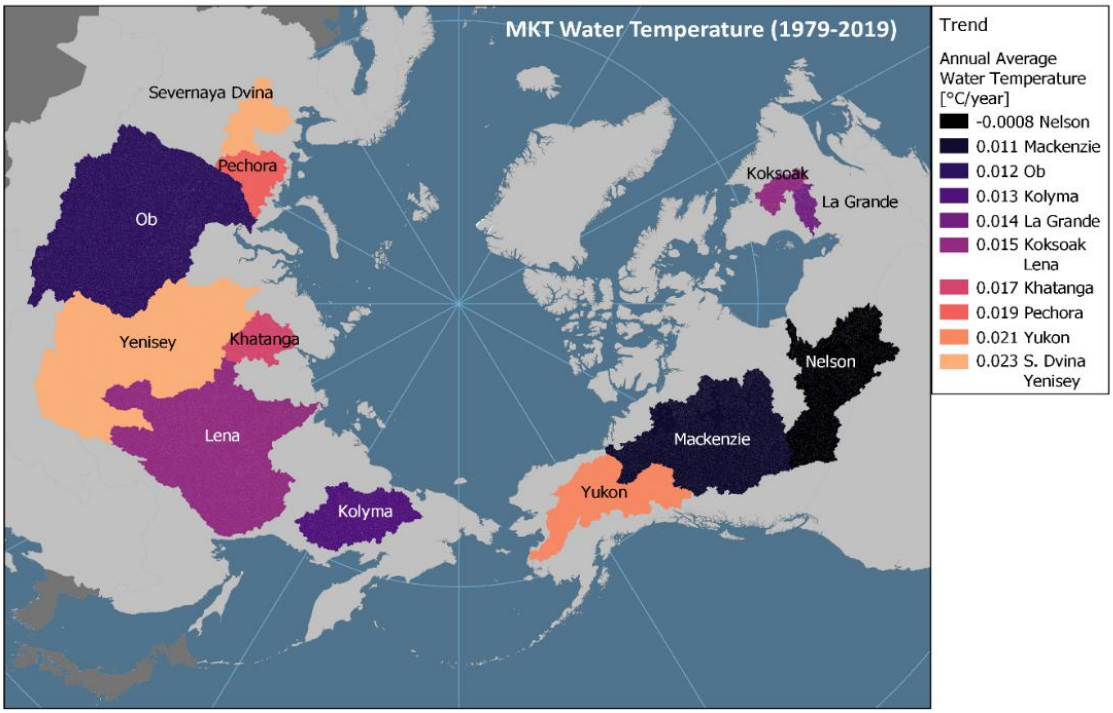

Figure 33 Map of annual water temperature trends for each of the twelve largest watersheds in the pan-Arctic. Watersheds are ranked by trend from lowest to highest. Trends for the Nelson and Mackenzie watersheds are not significant.

The baseline established for water temperature trends on a watershed scale is that most watersheds are showing statistically significant warming in the historical period. However, two large North American watersheds are not. Additionally, at the watershed scale trends are slightly higher than those calculated at the continental scale.

River Ice Thickness

Trends in river ice thickness on the watershed scale are not as clear as those for water temperature. Trends are shown as a time series plot and in table format in Figure 34

below. Unlike water temperature, most watersheds are showing little to no change across the historical period. Only two watersheds show significant trends of a decrease of 2.3 cm/decade for the Kolyma watershed and 2.4 cm/decade for the Khatanga watershed. It should be noted that these two watersheds are among the top four watersheds for the thickest modeled river ice thickness. A final observation when reviewing the timeseries is that watersheds with thicker river ice, on average, have a greater interannual variation compared to watersheds with thinner average river ice thickness.

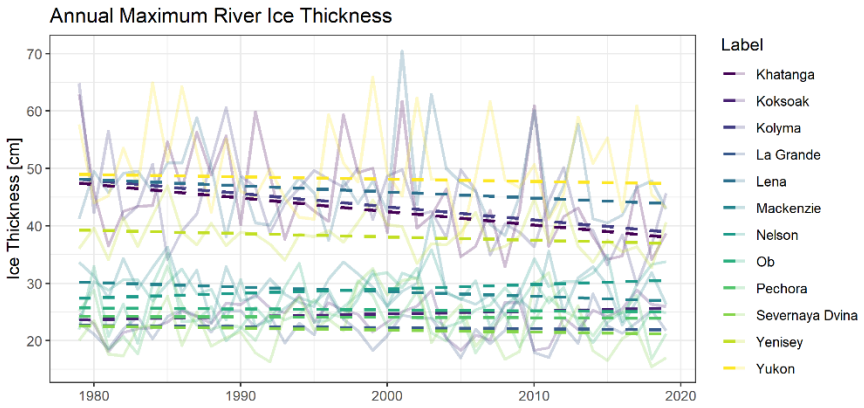

Watershed	Slope [cm/ year]
Khatanga	**-0.24**
Koksoak	0.05
Kolyma	**-0.23**
La Grande	-0.02
Lena	-0.11
Mackenzie	-0.08
Nelson	0.08
Ob	-0.019
Pechora	-0.008
S. Dvina	-0.034
Yenisey	-0.059
Yukon	-0.039

Figure 34 Timeseries of maximum annual ice thickness for each of the 12 largest watersheds in the AHYPE domain, pre-whitened MKT are denoted by dashed lines and maximum ice thickness are solid lines. Summarized in the table on the right are the same trends as shown in the plot, and statistically significant trends are shown in bold.

Many of the trends are statistically insignificant and show little to no change throughout the historical period. The most notable spatial observation shown in Figure 35 below, is that the significant trends are both in smaller Eurasian watersheds at higher latitudes and are what contributed to the statistically significant trend being calculated at the continental scale for Eurasia. Of interest is that there is no consistent correlation between water

temperature trend and river ice thickness trend. All significant trends in water temperature showed increasing temperatures, however there are few significant trends in ice thickness. This could be due to the high interannual variability that tends to be observed in ice thickness (Arp et al., 2019). Modeled maximum annual ice thickness varies up to 20 cm from one year to the next. It would also be expected that the watersheds with the highest warming trends would show decreases in river ice thickness over the same period, however, the Khatanga and the Kolyma did not have the highest trends in water temperature. Something that the two watersheds do have in common is that they are among the highest initial maximum annual ice thicknesses, and this could be interpreted as the reason why they show significant loss of river ice thickness. However, the Yukon River also has one of the highest initial thicknesses, and highest warming trends, but does not exhibit a statistically significant trend for river ice thickness.

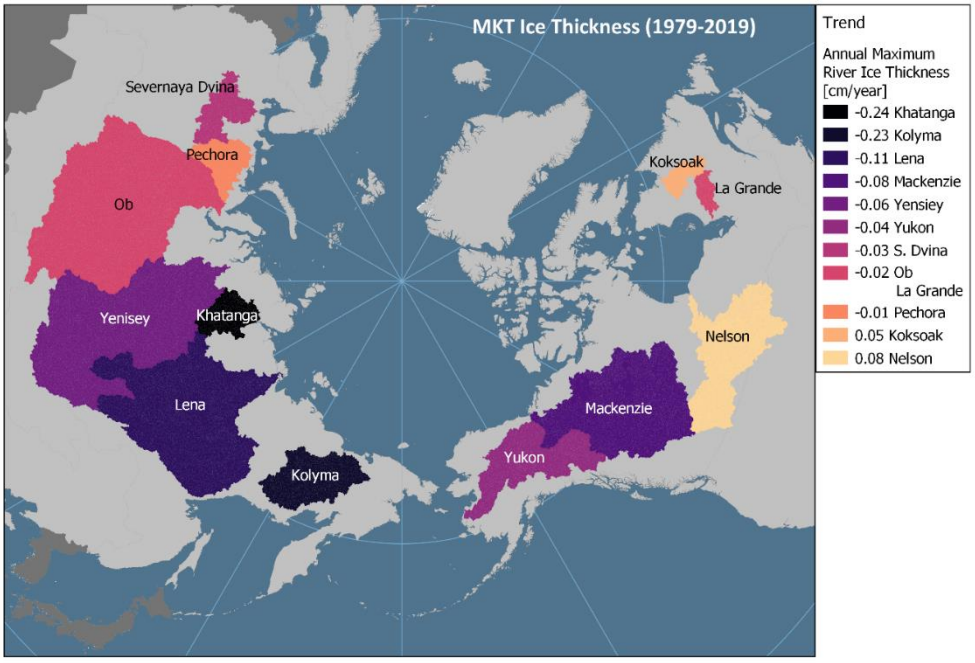

Figure 35 Map of maximum annual river ice thickness trends for each of the twelve largest watersheds in the pan-Arctic. Watersheds are ranked by trend from lowest to highest. Trends for the Nelson and Mackenzie watersheds are not significant.

The baseline established through the analysis of historical maximum annual river ice thickness trends is that there are few significant trends at the watershed scale for the historical period. Only the Khatanga and Kolyma show decreases in river ice thickness of 2.3 and 2.4 cm/decade.

4.3.3. Seasonal Trends

A seasonal analysis of historical trends was done for water temperature across three seasons which have been defined in four-month climatological chunks; October to January to compensate for longer ice-on, cold periods in the North, February to May and finally June to September. This seasonal split looks at average temperatures in each of these seasons and their change across the historical period. Seasonal trend results are shown in Table 12 below. The first season, October to January, represents the cooling period across most portions of the basin. This is when many areas rely on cooling air temperatures to initiate freezing of rivers and lake surfaces. Over the historical period, changes are gradual and consistent across all spatial scales. Showing very slight warming of approximately a fifth of a degree over the decade. February to May is when temperatures begin to increase across the pan-Arctic domain. This season has the greatest divergence in trends across the different spatial scales, as anticipated due to latitudinal gradients and differences of the basins in the pan-Arctic domain (warming is delayed at higher latitudes). Showing a similar trend to the first season for the entire AHYPE domain, but a negligible and statistically insignificant trend for the North American continent. The sign suggests temperatures are cooling for this season historically, however the trend is small and insignificant statistically, which suggests that temperatures are in fact steady. The greatest change occurs during the June to September period were

warming is up to 0.35°C/decade in Eurasia, and 0.23°C/decade for North America with the whole domain falling somewhere in between. Except for the February to May trend in North America, all trends are considered significant.

Table 12 Results of seasonal trend analysis across the large spatial domains (AHYPE, North America, and Eurasia). For each season the pre-whitened MKT is presented along with its statistical significance. P-values which show statistical significance are shown in bold.

	October to January		February to May		June to September	
Spatial Scale	**Slope [°C/year]**	**p-value**	**Slope [°C/year]**	**p-value**	**Slope [°C/year]**	**p-value**
AHYPE*	**0.006**	**3.53×10^{-5}**	**0.0052**	**0.0016**	**0.030**	**5.78×10^{-7}**
North America	**0.007**	**0.001**	-0.00013	0.95	**0.0227**	**1.39×10^{-4}**
Eurasia	**0.006**	**0.003**	**0.01**	**7.82×10^{-5}**	**0.035**	**2.78×10^{-7}**

To supplement the table, trends and timeseries of seasonal average temperature are shown in Figure 36 below. October to January clearly shows the similarity in trends and temperatures across all spatial domains. Although trends are clearly visible at this resolution, it should be noted that major labels on the y-axis are in increments of 0.2 °C, and therefore over the entire period, the greatest change <0.25°C (North America). The February to May seasonal temperatures indicate the variation in trends but similarities for average temperature across all domains. The June to September seasonal temperatures indicate a much greater variance in temperatures, although similar trends. Eurasia shows the greatest amount of warming with temperatures increasing up to North American levels near the end of the historical period.

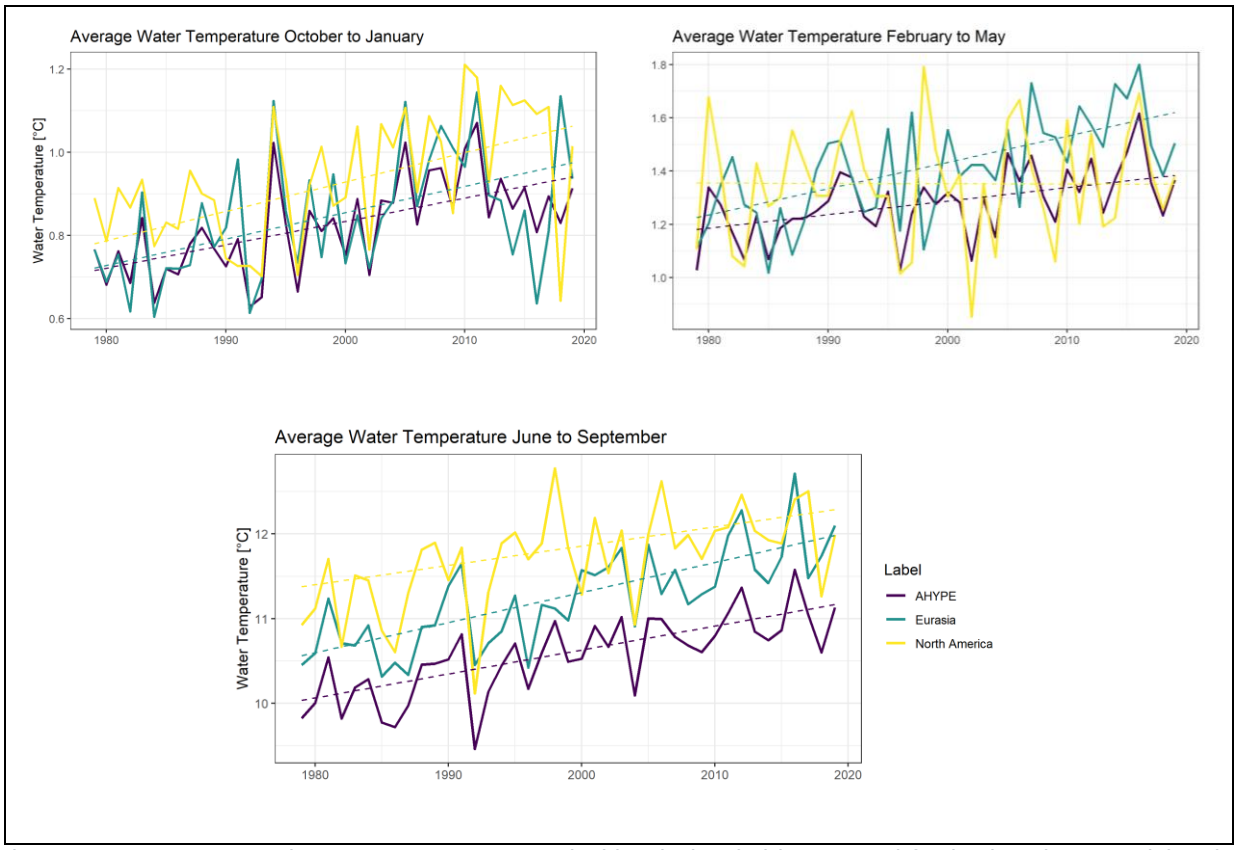

Figure 36 Average seasonal water temperatures over the historical period (1979-2019) for the three large spatial scales (AHYPE, North America and Eurasia). Pre-whitened MKT are shown in dashed lines while seasonal temperatures are shown by solid lines.

Seasonal analysis of water temperature in the historical period tells a story of differing trend patterns for each season. The greatest changes have occurred during the “summer” season from June to September which should have a relatively lower impact on the formation of river ice. The slight increases in water temperature for the cooling season suggest that ice-on conditions could be pushed further into the winter season. Ice break-up occurs in the February to May season and shows differing trends for the three different spatial scales but show a relatively stable baseline for this season across the historical period suggesting that future changes in this season will greatly impact current conditions.

4.4. Soil Temperature Trends

4.4.1. Continental Scale

Historical trends in soil temperature are important for establishing a baseline for future trend analysis. Trends in soil temperature for the large spatial domains are summarized in Table 13 below. All trends are shown to be statistically significant as shown by the p-value being less than 0.05 for all spatial scales. All three spatial scales have positive trends which show a historical increase in soil temperature as is expected(Oelke & Zhang, 2004). Eurasian soil temperature is increasing at almost twice the rate compared to North America. Trends range from 0.24 °C/decade in North America which has the slowest soil temperature increase to 0.41 °C/decade in Eurasia which is has the fastest change in soil temperature over the historical period.

*Table 13 Summary of MKT with pre-whitening for average annual soil temperature (STMP) over the historical period, including p-value indicating statistical significance of the trend. Significant trends are highlighted by **bold** text.*

Spatial Scale	Slope [°C/year]	p-value
AHYPE*	**0.0320**	**2.09×10^{-11}**
North America	**0.0239**	**4.538×10^{-7}**
Eurasia	**0.0410**	**8.605×10^{-11}**

Trends are also shown in the timeseries plot below (Figure 37). Eurasia, which as mentioned has the fastest soil temperature trend, has a higher soil temperature to begin with. Following the trend slope for Eurasia, it is an increase of almost a 1 degree Celsius every 25 years, whereas the other two domains are closer to taking 40 years for an increase in one degree. This is not what is expected from soil temperature warming, as some literature suggests cooler temperatures should show faster warming trends (Royer et al., 2021). However, we assume some model bias is occurring in the actual soil

temperatures modelled, as was presented in section 4.2. Even though the temperature values may be unexpected in relation to the trends, general trends do agree with other soil temperature studies.

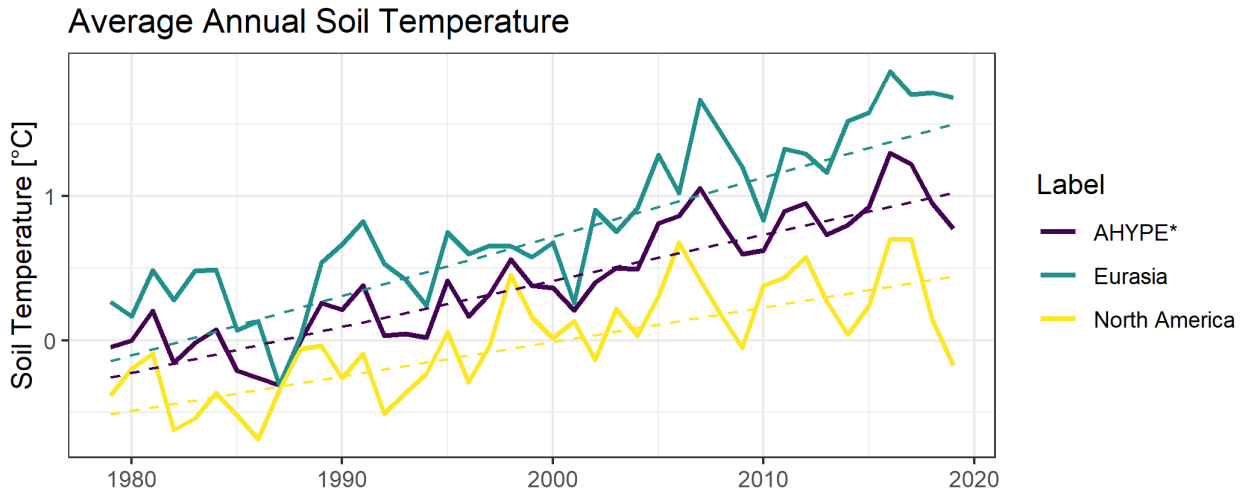

Figure 37 Time series of the average annual soil temperature (STMP) in the solid lines, including the pre-whitened MKT for each spatial domain in the dashed lines. The AHYPE domain excluding Greenland has a trend of 0.0320 °C/year, Eurasia has a trend of 0.0410 °C /year, and North America has a trend of 0.0239 °C /year. All trends are statistically significant.

The baseline established for the overall AHYPE model historical trends in average annual soil temperature are significant warming of around 0.3°C/decade. This agrees with the study done by Smith et al. (2022) for the period of 1980-2020, which reported the same warming trend (0.3°C/decade) for warmer permafrost soils, assuming that overall modeled averages across the pan-arctic are representative of the warmer permafrost soils. Additionally, we establish that over the historical period Eurasian pan-Arctic soil temperatures were warming more rapidly than North American pan-Arctic soil temperatures.

4.4.2. Watershed Scale

Soil temperature trends at a watershed spatial scale for the 12 largest rivers in the pan-Arctic domain are summarized in Figure 38 below. All trends are statistically significant,

except the trend in the Nelson River watershed which has one of the highest average soil temperatures but does not show a significant change in modeled soil temperature over the historical period. The highest trends occur in watersheds with the lowest average soil temperatures such as the Khatanga, and Kolyma which have warming trends of over 0.5°C/decade. They also have average temperatures below the zero-degree threshold throughout the historical time frame. Trends in watersheds with average temperatures above zero appear to have similar and slower warming trends for soil temperature, usually between 0.2-0.4°C/decade. This observation, that trends for warmer watersheds are lower lines up with our understanding of warming feedback cycles in the arctic (Royer et al., 2021).

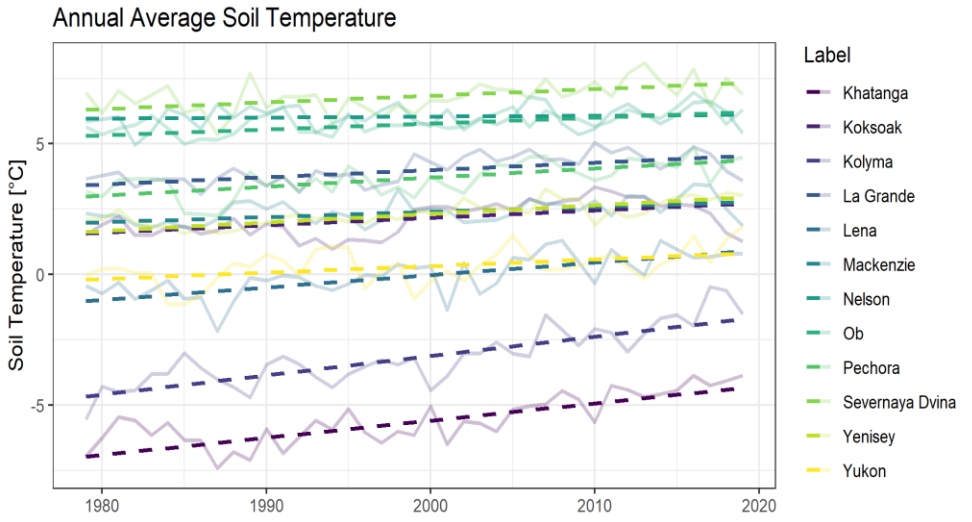

Watershed	Slope [°C /year]
Khatanga	**0.066**
Koksoak	**0.028**
Kolyma	**0.074**
La Grande	**0.028**
Lena	**0.047**
Mackenzie	**0.019**
Nelson	0.004
Ob	**0.023**
Pechora	**0.035**
S. Dvina	**0.026**
Yenisey	**0.033**
Yukon	**0.025**

Figure 38 Timeseries of average annual soil temperature for each of the 12 largest watersheds in the AHYPE domain, pre-whitened MKT are denoted by dashed lines and average soil temperatures are solid lines. Summarized in the table on the right are the same trends as shown in the plot, and statistically significant trends are shown in bold.

The spatial distribution of these trends is shown in Figure 39 below. Visible is the split between higher (orange) and lower (blue) trends between the two continents. Once again, the Ob is a spatial outlier compared to the surrounding watersheds and reports one of the lowest warming trends in soil temperature. This is likely due to its high overall average

soil temperature. The two highest trending watersheds are also at the highest latitude which coincides with the coolest overall soil temperatures and is expected as stronger positive feedbacks cause more pronounced warming at higher latitudes (Royer et al., 2021).

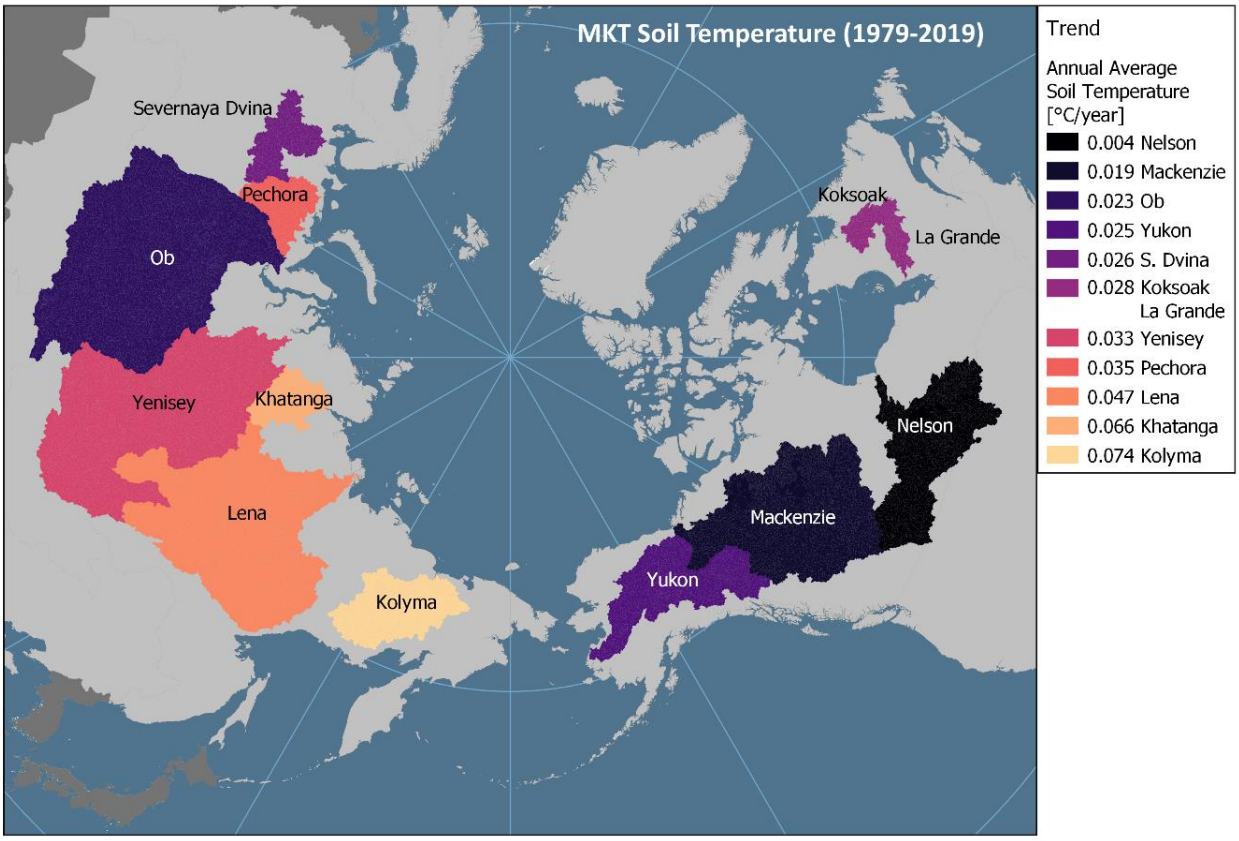

Figure 39 Map of average annual soil temperature trends for each of the twelve largest watersheds in the pan-Arctic. Watersheds are ranked by trend from lowest to highest. Trend for the Nelson watershed is not significant.

The baseline established for annual soil temperature trends at the watershed scale is that watersheds with higher soil temperatures have slower warming trends and those with cooler average soil temperatures are warming faster. Most watersheds which are "warmer" (>0°C) have trends around 0.3°C/decade, and the "colder" (<0°C) watersheds have trends up to 0.74°C/decade. This is similar to trends calculated by Smith et al. (2022)

who reported warming of 0.3°C/decade in warmer permafrost and warming closer to 1°C for those with colder permafrost since the 1980s.

4.4.3. Seasonal Trends

Finally, the same seasonal trend analysis that was done for water temperature was also done for soil temperature at the continental spatial scale and are summarized in Table 14 below. All seasonal trends are significant for soil temperature and show little seasonal variation which is very different from water temperature. The fastest warming occurs in Eurasia for all seasons. Warming trends range from 0.02 to 0.045°C /year.

Table 14 Results of seasonal trend analysis of soil temperature across the large spatial domains (AHYPE, North America, and Eurasia). For each season the pre-whitened MKT is presented along with its statistical significance. P-values which show statistical significance are shown in **bold.***

	October to January		February to May		June to September	
Spatial Scale	**Slope [°C/year]**	**p-value**	**Slope [°C/year]**	**p-value**	**Slope [°C/year]**	**p-value**
AHYPE*	**0.030**	**$2.1x10^{-11}$**	**0.030**	**$1.22x10^{-8}$**	**0.035**	**$8.25x10^{-10}$**
North America	**0.026**	**$6.1x10^{-9}$**	**0.023**	**$5.84x10^{-6}$**	**0.022**	**$2.11x10^{-5}$**
Eurasia	**0.038**	**$6.3x10^{-11}$**	**0.040**	**$2.45x10^{-7}$**	**0.045**	**$2.45x10^{-11}$**

The same information as in the table above is shown in Figure 40 below. Temperatures are very similar for the coldest season (February to May) for all three spatial domains. is the largest variance in soil temperatures is in the summer months where Eurasia clearly has higher soil temperatures than North America. This divide was evident in trend analysis for the average annual soil temperature, and we now see that this divide is not present across all seasons. Temperatures are nearly indistinguishable for the October to January cooling period and begin to diverge for the February to May warming period. This could points to cooler temperatures being similar (those <0°C), but warmer temperatures in the Oct to Jan season, and summer months differing across the two continents.

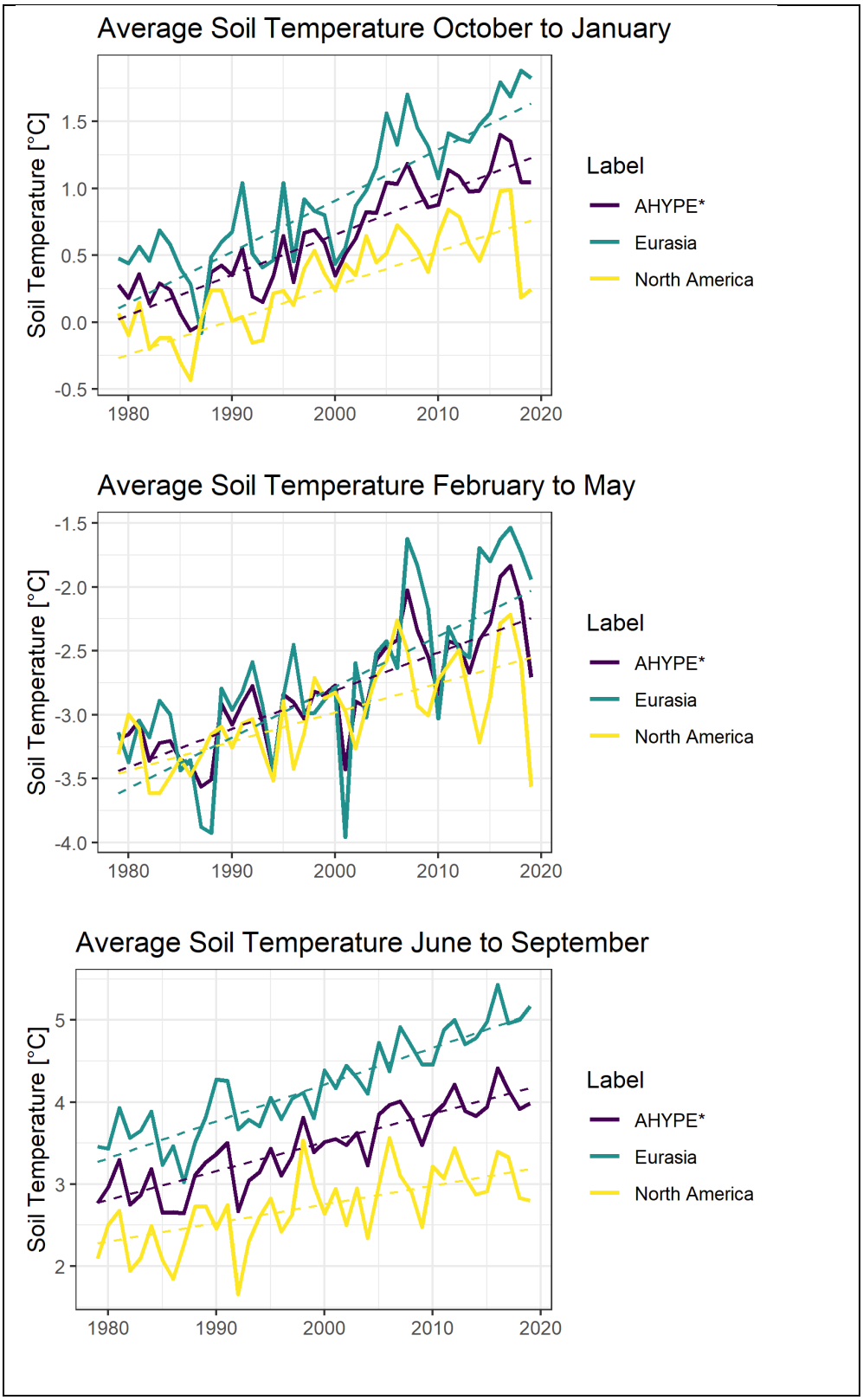

Figure 40 Average seasonal water temperatures over the historical period (1979-2019) for the three large spatial scales (AHYPE without Greenland, North America and Eurasia). Pre-whitened MKT are shown in dashed lines while seasonal temperatures are shown by solid lines.

5. Results and Analysis of Future Projections

Pre-whitened Mann-Kendall Trends will be discussed first at the continental scale and at the watershed scale for the entire future period. Analysis is first done for annual average, or in the case of river ice thickness maximum, values. At the continental scale, analysis is also done for seasonal values for water temperature and soil temperature only. Analysis will also be done for the time periods defined for each GCM and ssp combination by the mean temperature rise discussed in section 3.4.1 at the continental scale. Change point analyses are completed for the continental and 12 largest river basins for the entire future period.

5.1. Trend Analysis at the Continental Scale

Water Temperature

Future trends in water temperature at the continental scale are summarized in Table 15 below. Trends indicate accelerated water temperature warming relative to that from the modeled historical period. Trends approximately double from the historical to the mean trend for the whole AHYPE domain in the future period (excluding Greenland). The North American trends nearly triple, as they had historically shown the slowest rate of rise but accelerate rapidly in future periods. All water temperature warming trends are statistically significant and vary only slightly between the domains. Trends range from less than 0.01 °C/yr for the model runs, which were forced with GCM and ssp combinations under low warming scenarios, to almost 0.07°C/yr for the highest warming scenario combined with the CanESM5, which has the most significant change in temperature and precipitation for the future period as described in section 3.4.

*Table 15 Summary of Water Temperature pre-whitened Mann-Kendall trends (°C /year) for the whole future period. Statistically significant trends are shown in bold. Colour shows trend ranking and darker shades of red show larger positive trends. The historical trend is also included in the summary. *Note that AHYPE does not include Greenland.*

2020-2100		Domain		
		AHYPE*	North America	Eurasia
	Historical (1989-2019)	**0.014**	**0.011**	**0.017**
	Future Mean	**0.031**	**0.032**	**0.031**
GCM + SSP	CanESM5 ssp126	**0.0093**	**0.0086**	**0.0078**
	CanESM5 ssp585	**0.0687**	**0.0692**	**0.0677**
	MIROC6 ssp126	**0.0080**	**0.0082**	**0.0070**
	MIROC6 ssp585	**0.0458**	**0.0457**	**0.0458**
	MRI-ESM2-0 ssp585	**0.0250**	**0.0259**	**0.0244**

The time series of the future modeled annual average water temperature and the mean pre-whitened MKT for each domain is shown below. There is very little difference across the domain for the future period. Noticeable is the divergence among the GCM+SSP combinations: the modeled range in water temperature increases from around 1°C to 2°C over only 30 years, suggesting notable uncertainty in the rate of warming across the Arctic domain in future periods. The CanESM5 model combined with higher warming shows the largest divergence from the other models and provides the upper boundary for future modeled results.

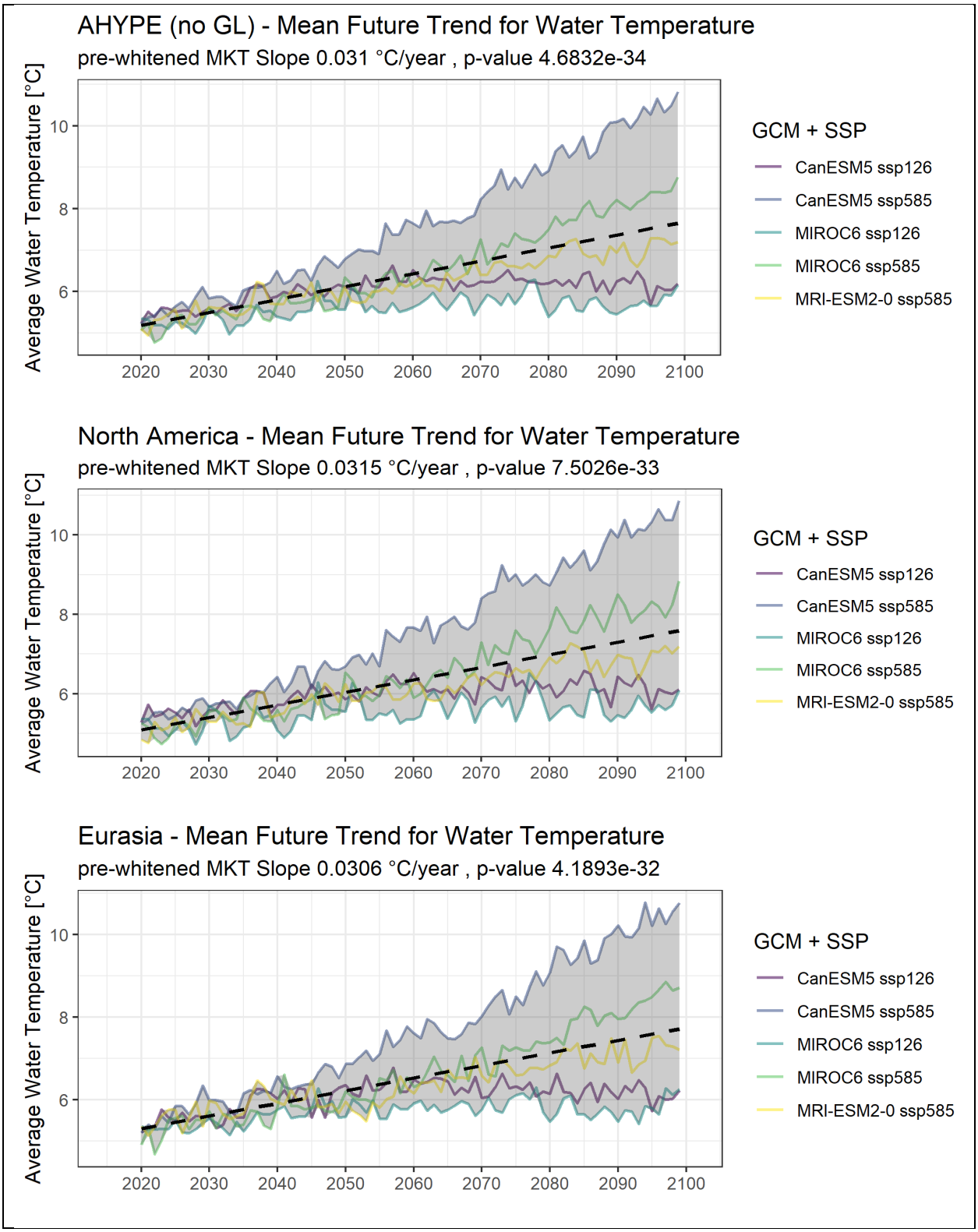

Figure 41 Time series plots for AHYPE without Greenland, North America, and Eurasia showing the time series of modeled annual average water temperature into the future for each GCM+SSP combination. The mean pre-whitened MKT is shown as the black dashed line. The range in modeled water temperatures is shaded in grey.

Trends in water temperature rise for each mean temperature rise (MTR) period are summarized in the following tables. Not all models show statistically significant trends at the 1 degree warming level. GCM+SSP combinations which reach 1°C warming are less likely to have significant trends. The lower warming GCM+SSP combinations show significant trends for all domains. The least number of significant trends are for the North American domain. Although counter intuitive in light of the overall future period analysis, this occurs because the MTR periods were calculated using the overall warming trend. For North America, and the other spatial domains as well, the quicker warming trends for the ssp585 scenarios produced very short MTR periods for 1°C warming. This means trends are calculated over short near future time periods, during which warming is slower than the overall trends, but also statistically significant trends are not produced as interannual variability lowers trend significance signals over short periods.

The subsequent warming levels of 2.5 and 5°C only include the higher warming scenarios, and all trends are significant. Significant trends range from 0.013-0.063°C/year for the 1°C MTR, 0.014-0.043°C/year for 2.5°C MTR, and finally 0.024-0.049°C/year for 5°C.

Table 16 Summary of the pre-whitened MKT (°C/yr) for each domain, GCM+SSP combination for the mean temperature rise of 1°C, 2.5°C and 5°C. The length of each warming period is also summarized in the years column. Each column shows the sorting of trends with shading in red, darker red shows a faster warming trend. Statistical significance is shown in bold.

GCM + SSP	MTR 1°C	Domain			
		AHYPE	*North America*	*Eurasia*	*years*
	CanESM5 ssp126	**0.021**	**0.018**	**0.025**	45
	CanESM5 ssp585	**0.059**	0.028	0.092	7
	MIROC6 ssp126	**0.013**	**0.013**	**0.013**	56
	MIROC6 ssp585	**0.063**	0.059	**0.061**	10
	MRI-ESM2-0 ssp585	0.013	0.024	0.026	15

GCM + SSP	MTR 2.5°C	Domain			
		AHYPE	*North America*	*Eurasia*	*years*
	CanESM5 ssp585	**0.041**	**0.038**	**0.043**	18
	MIROC6 ssp585	**0.030**	**0.032**	**0.020**	25
	MRI-ESM2-0 ssp585	**0.021**	**0.027**	**0.014**	39

GCM + SSP	MTR 5°C	Domain			
		AHYPE	*North America*	*Eurasia*	*years*
	CanESM5 ssp585	**0.0491**	**0.049**	**0.049**	36
	MIROC6 ssp585	**0.035**	**0.035**	**0.034**	50
	MRI-ESM2-0 ssp585	**0.025**	**0.026**	**0.024**	79

River Ice Thickness

River ice thickness trends are anticipated to continue to be negative into the future (decreasing ice thickness), as warmer temperatures will decrease ice seasonality, causing thinner maximum ice thicknesses each season. The trends discussed in this section, as a reminder, are those for the average maximum ice thickness across the spatial domain. Table 17 below summarizes the pre-whitened Mann-Kendall trends (cm/year) for the 2020-2100 period. Compared to the historical trends, the mean future trends model significantly quicker loss in annual maximum ice thickness across the AHYPE domain, not including Greenland. North America which shows no statistically

significant trend in the historical, has a significant trend for future periods. For Eurasia there is little change between the historic and future periods. Mean trends are similar, with each around -0.1 cm/year, or a loss of 1 cm per decade. Future trends are higher for the North American domain, which is the reverse of what was observed in the historical modeled predictions.

Table 17 Summary of River Ice thickness pre-whitened Mann-Kendall trends (cm/year) for the whole future period. Statistically significant trends are shown in bold. Colour shows trend ranking, positive trends are red and negative are blue. The historical trend is also included in the summary.

2020-2100		Domain		
		*AHYPE**	*North America*	*Eurasia*
	Historical (1989-2019)	**-0.062**	-0.027	**-0.113**
	Future Mean	**-0.111**	**-0.118**	**-0.103**
GCM + SSP	*CanESM5 ssp126*	**-0.051**	**-0.069**	**-0.019**
	CanESM5 ssp585	**-0.222**	**-0.238**	**-0.109**
	MIROC6 ssp126	**-0.032**	-0.022	**-0.016**
	MIROC6 ssp585	**-0.148**	**-0.157**	**-0.080**
	MRI-ESM2-0 ssp585	**-0.113**	**-0.114**	**-0.051**

The timeseries of annual maximum ice thickness for each domain follows in Figure 42. Inter-annual variation in ice thickness is much higher (as expected) than for the temperature model outputs. Examining the time series progressions, lower warming scenarios (scenarios with greater ice thicknesses) decrease faster up until around 2070 after which they appear to level off near the end of the period. This is most noticeable in the AHYPE and North American domain. GCM+SSP combinations with higher warming (lower ice thicknesses) decrease noticeably in ice thickness throughout the whole future period. Eurasia shows the least change in ice thickness and the most agreement between the scenarios.

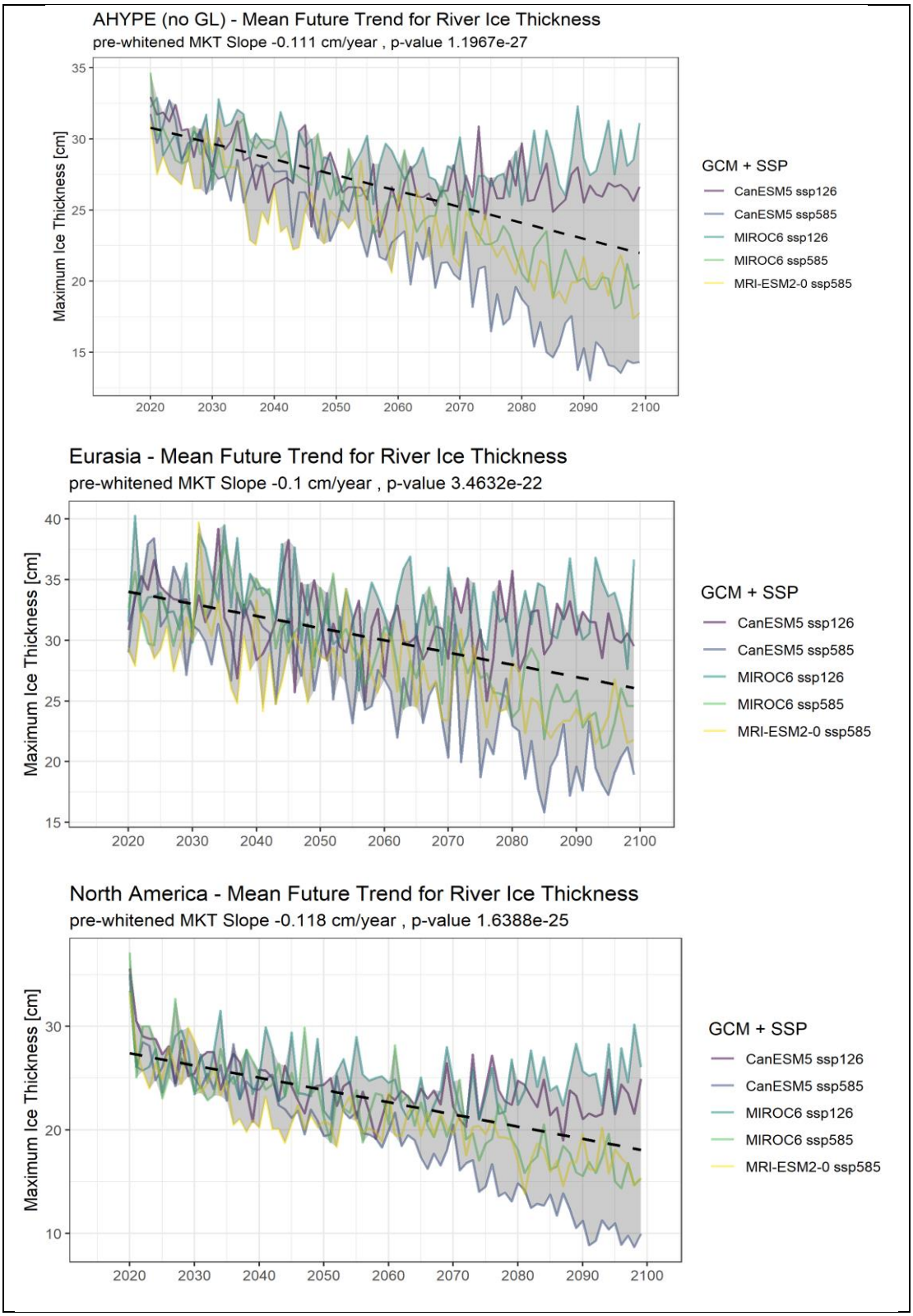

Figure 42 Time series plots for AHYPE without Greenland, North America, and Eurasia showing the time series of modeled annual maximum ice thickness into the future for each GCM+SSP combination. The mean pre-whitened MKT is shown as the black dashed line. The range in modeled water temperatures is shaded in grey.

Trends in maximum river ice thickness for each mean temperature rise period are summarized in the following tables. Higher warming scenarios have no statistically significant trend for the 1°C temperature rise period. The two low warming scenarios have significant trends for all domains and range from -0.068cm/yr to -0.142cm/yr. The 2.5°C temperature rise period indicates statistically significant trends for only two of the three GCM+SSP combinations, and Eurasia only has a significant trend for the CanESM5 ssp585 scenario, which is the most extreme for warming and precipitation changes. Trends range from -0.142 to -0.4 cm/yr for this warming period. Finally, all trends are significant for the 5°C temperature rise and range from 0.106 to 0.212 °C. It is interesting that for river ice thickness, the most significant trend is in the 2.5°C rise.

Table 18 Summary of the pre-whitened MKT (cm/yr) for each domain, GCM+SSP combination for the mean temperature rise of 1°C, 2.5°C and 5°C. The length of each warming period is also summarized in the years column. Each column shows the sorting of trends with shading in red, darker red shows a faster warming trend. Statistical significance is shown in bold.

	MTR 1°C	Domain			
		*AHYPE**	*North America*	*Eurasia*	*years*
GCM + SSP	CanESM5 ssp126	**-0.127**	**-0.142**	**-0.099**	45
	CanESM5 ssp585	-0.2177	-0.416	-0.296	7
	MIROC6 ssp126	**-0.074**	**-0.070**	**-0.068**	56
	MIROC6 ssp585	-0.231	-0.295	-0.143	10
	MRI-ESM2-0 ssp585	0.047	-0.129	0.173	15

	MTR 2.5°C	Domain			
		*AHYPE**	*North America*	*Eurasia*	*years*
GCM + SSP	CanESM5 ssp585	**-0.2463**	**-0.189**	**-0.400**	18
	MIROC6 ssp585	-0.057	-0.119	0.050	25
	MRI-ESM2-0 ssp585	**-0.142**	**-0.188**	-0.067	39

	MTR 5°C	Domain			
		*AHYPE**	*North America*	*Eurasia*	*years*
GCM + SSP	CanESM5 ssp585	**-0.2015**	**-0.201**	**-0.212**	36
	MIROC6 ssp585	**-0.121**	**-0.139**	**-0.109**	50
	MRI-ESM2-0 ssp585	**-0.113**	**-0.114**	**-0.106**	79

Soil Temperature

Annual soil temperatures for the large domains are summarized in Table 19 below, including modeled historical trends as the baseline and the projected future mean trends. Trends follow a similar pattern for all domains and are ranked by the intensity of their projected rate of warming. The most rapid warming is modelled in GCM+SSP combinations which represent the greater warming scenarios in the future period, and slower warming rates are modeled under lower warming scenarios. Future mean trends are higher than those which were modeled historically. Noticeable is a shift from the Eurasian continent having the quickest warming under the historical period to North America in the future period. This is true for all future scenarios; mean trends range from 0.52°C/year to 0.0.57°C/year and scenario trends range from 0.16 °C/year up to 1 °C/year.

Table 19 Summary of River Ice thickness pre-whitened Mann-Kendall trends (cm/year) for the whole future period. Statistically significant trends are shown in bold. Colour shows trend ranking, larger positive trends are a darker red. The historical trend is also included in the summary.

2020-2100		Domain		
		*AHYPE**	*North America*	*Eurasia*
	Historical (1989-2019)	**0.032**	**0.024**	**0.041**
	Future Mean	**0.054**	**0.057**	**0.052**
GCM + SSP	*CanESM5 ssp126*	**0.0195**	**0.0214**	**0.0168**
	CanESM5 ssp585	**0.1056**	**0.1088**	**0.1023**
	MIROC6 ssp126	**0.0164**	**0.0161**	**0.0156**
	MIROC6 ssp585	**0.0788**	**0.0828**	**0.0771**
	MRI-ESM2-0 ssp585	**0.0530**	**0.0558**	**0.0499**

Time series of annual soil temperatures for each domain are shown in Figure 43. Trends and temperatures are similar across all domains. CanESM5+ssp126, MIROC+ssp585 and MRI-ESM2-0+ssp585 scenarios all show similar warming until around 2060 when modeled average soil temperatures diverge more clearly. All high warming scenarios

increase continually throughout the future period, but those with lower warming level off around 2050.

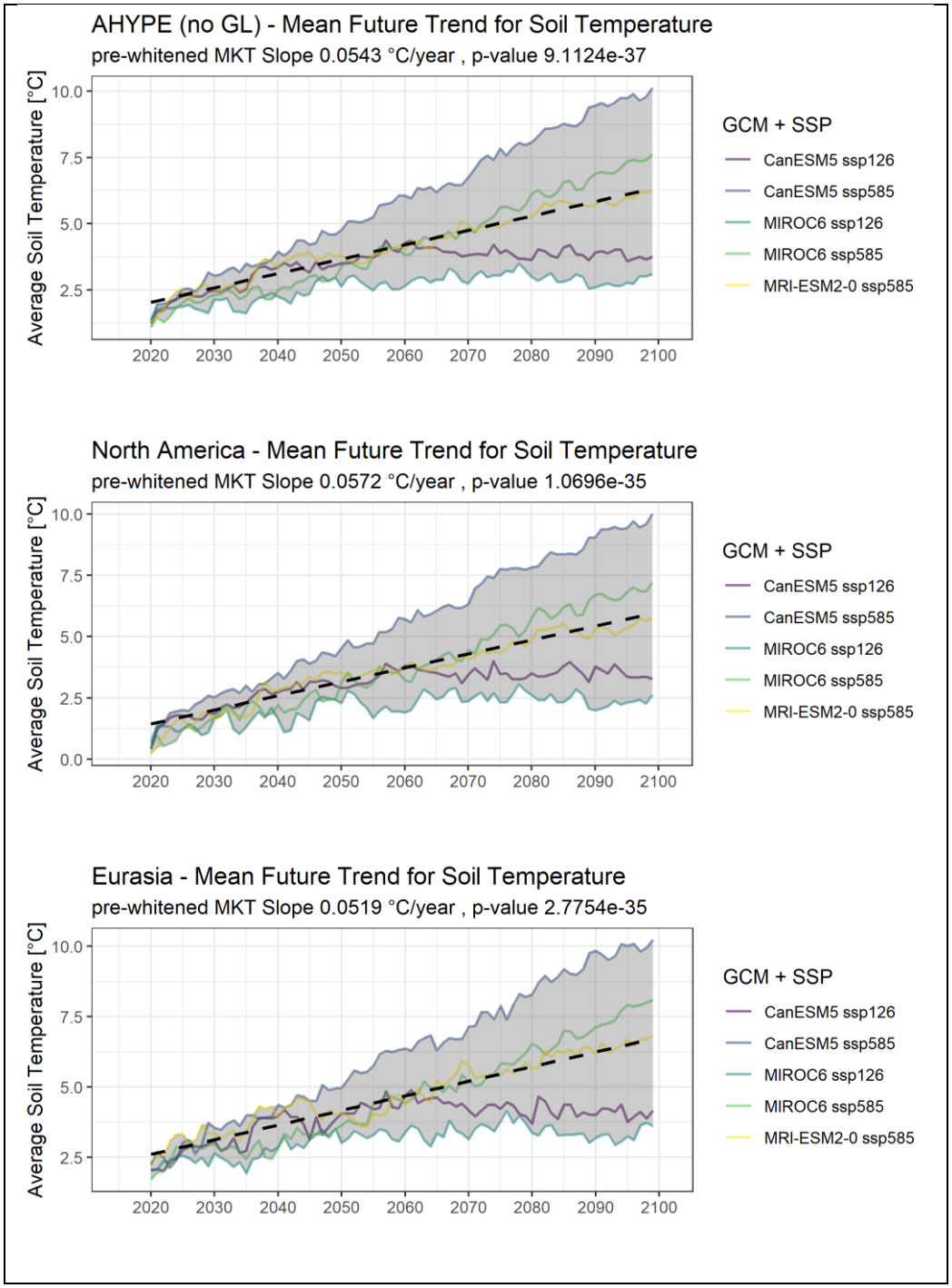

Figure 43 Time series plots for AHYPE without Greenland, North America, and Eurasia showing the time series of modeled annual average soil temperature into the future for each GCM+SSP combination. The mean pre-whitened MKT is shown as the black dashed line. The range in modeled water temperatures is shaded in grey.

Trends in average annual soil temperature rise for each mean temperature rise period are summarized in Table 20. Unlike water temperature and river ice thickness, most trends indicate statistical significance, even those at lower MTR periods over shorter time periods. The largest trends are observed for the 1°C mean temperature rise and for high warming scenarios with short rapid warming periods, meaning the largest changes occur within the near future (10 years) for high warming scenarios. Warming trends are the highest in North America. Trends range from 0.026-0.153°C/yr in the 1°C temperature rise period, from 0.034-0.0998°C/yr in the 2.5°C period, and from 0.05-0.099°C/yr in the 5°C period.

Table 20 Summary of the pre-whitened MKT (°C/yr) for each domain, GCM+SSP combination for the mean temperature rise of 1°C, 2.5°C and 5°C. The length of each warming period is also summarized in the years column. Each column shows the sorting of trends with shading in red, darker red shows a faster warming trend. Statistical significance is shown in bold.

GCM + SSP	MTR 1°C	Domain			
		AHYPE	*North America*	*Eurasia*	*years*
	CanESM5 ssp126	**0.051**	**0.052**	**0.052**	45
	CanESM5 ssp585	**0.1075**	**0.153**	0.080	7
	MIROC6 ssp126	**0.026**	**0.027**	**0.027**	56
	MIROC6 ssp585	**0.117**	**0.129**	**0.103**	10
	MRI-ESM2-0 ssp585	**0.049**	**0.056**	**0.043**	15

GCM + SSP	MTR 2.5°C	Domain			
		AHYPE	*North America*	*Eurasia*	*years*
	CanESM5 ssp585	**0.0998**	**0.093**	**0.094**	18
	MIROC6 ssp585	**0.051**	**0.069**	**0.034**	25
	MRI-ESM2-0 ssp585	**0.054**	**0.073**	**0.037**	39

GCM + SSP	MTR 5°C	Domain			
		AHYPE	*North America*	*Eurasia*	*years*
	CanESM5 ssp585	**0.0983**	**0.099**	**0.094**	36
	MIROC6 ssp585	**0.065**	**0.071**	**0.060**	50
	MRI-ESM2-0 ssp585	**0.053**	**0.056**	**0.050**	79

5.1.1. Continental Seasonal Trends

Seasonal trends were only calculated for water and soil temperature since river ice thickness analysis is focused on the maximum annual ice thickness. Seasonal analysis provides an important insight into changes anticipated for the pan-Arctic domain. We understand that changes in temperature are not occurring equally throughout the year, and so by dividing the year into seasons, this provides insight into when changes are occurring most pronounced and rapidly, and how (if) that will impact freeze/thaw cycles for the ground and water.

Water Temperature

Seasonal pre-whitened Mann Kendall trends (°C/year) are summarized in the following Table 21, including the historical model trends which are the baseline for comparison. Warming is similar across all three domains. February to May shows similar future trends for all three domains of around 0.02°C/year. June to September projects a rate of warming of 0.053°C/year, and finally October to January ranges from 0.018-0.02°C/year warming and is the only season showing slight variations among the domains. Eurasia is warming slightly slower than North America in this season. Comparing across the seasons, the most rapid rate of warming occurs in summer from June to September. Similar trends are projected for the break-up and thaw season from February to May, and the ice-on season from October to January. This is similar to the historical period for the AHYPE domain, but the North American continent had no significant warming during Feb-May compared to Oct-Jan, and Eurasia had much higher warming during Feb-May than what was modelled for Oct-Jan historically. Trends significantly increase from the historical period to the future period across all seasons, and all future trends show statistical significance

which is notable for North America during the Feb-May season which previously showed no detectable trend.

Table 21 Summary of the pre-whitened MKT (°C/yr) for each domain, GCM+SSP combination for each season. Each section shows the sorting of trends with shading in red, darker red shows a faster warming trend. Statistical significance is shown in bold.

	Feb - May	Domain		
		AHYPE*	N. America	Eurasia
GCM + SSP	Historical (1989-2019)	**0.005**	-0.0001	**0.010**
	Future Mean	**0.020**	**0.020**	**0.020**
	CanESM5 ssp126	**0.005**	**0.003**	**0.006**
	CanESM5 ssp585	**0.046**	**0.045**	**0.046**
	MIROC6 ssp126	**0.005**	**0.004**	**0.004**
	MIROC6 ssp585	**0.030**	**0.033**	**0.028**
	MRI-ESM2-0 ssp585	**0.013**	**0.014**	**0.011**
	June - Sep	**Domain**		
		AHYPE*	N. America	Eurasia
GCM + SSP	Historical (1989-2019)	**0.030**	**0.023**	**0.035**
	Future Mean	**0.053**	**0.053**	**0.053**
	CanESM5 ssp126	**0.017**	**0.018**	**0.013**
	CanESM5 ssp585	**0.109**	**0.108**	**0.110**
	MIROC6 ssp126	**0.016**	**0.016**	**0.015**
	MIROC6 ssp585	**0.080**	**0.080**	**0.082**
	MRI-ESM2-0 ssp585	**0.046**	**0.047**	**0.045**
	Oct - Jan	**Domain**		
		AHYPE*	N. America	Eurasia
GCM + SSP	Historical (1989-2019)	**0.006**	**0.007**	**0.006**
	Future Mean	**0.019**	**0.020**	**0.018**
	CanESM5 ssp126	**0.006**	**0.006**	**0.005**
	CanESM5 ssp585	**0.050**	**0.055**	**0.045**
	MIROC6 ssp126	**0.003**	**0.004**	**0.001**
	MIROC6 ssp585	**0.024**	**0.023**	**0.024**
	MRI-ESM2-0 ssp585	**0.015**	**0.015**	**0.015**

Timeseries of seasonal average water temperature are shown on Figure 44. As expected from the previous table, trends for each domain are quite similar. Into the future the modelled upper bound increases most significantly for all seasons, however, lower bounds for the GCM+SSP scenarios show very little change for the Feb-May and Oct-

Jan season and increases for the Jun-Sep season. This contributes to the overall higher trends in the June-Sep season.

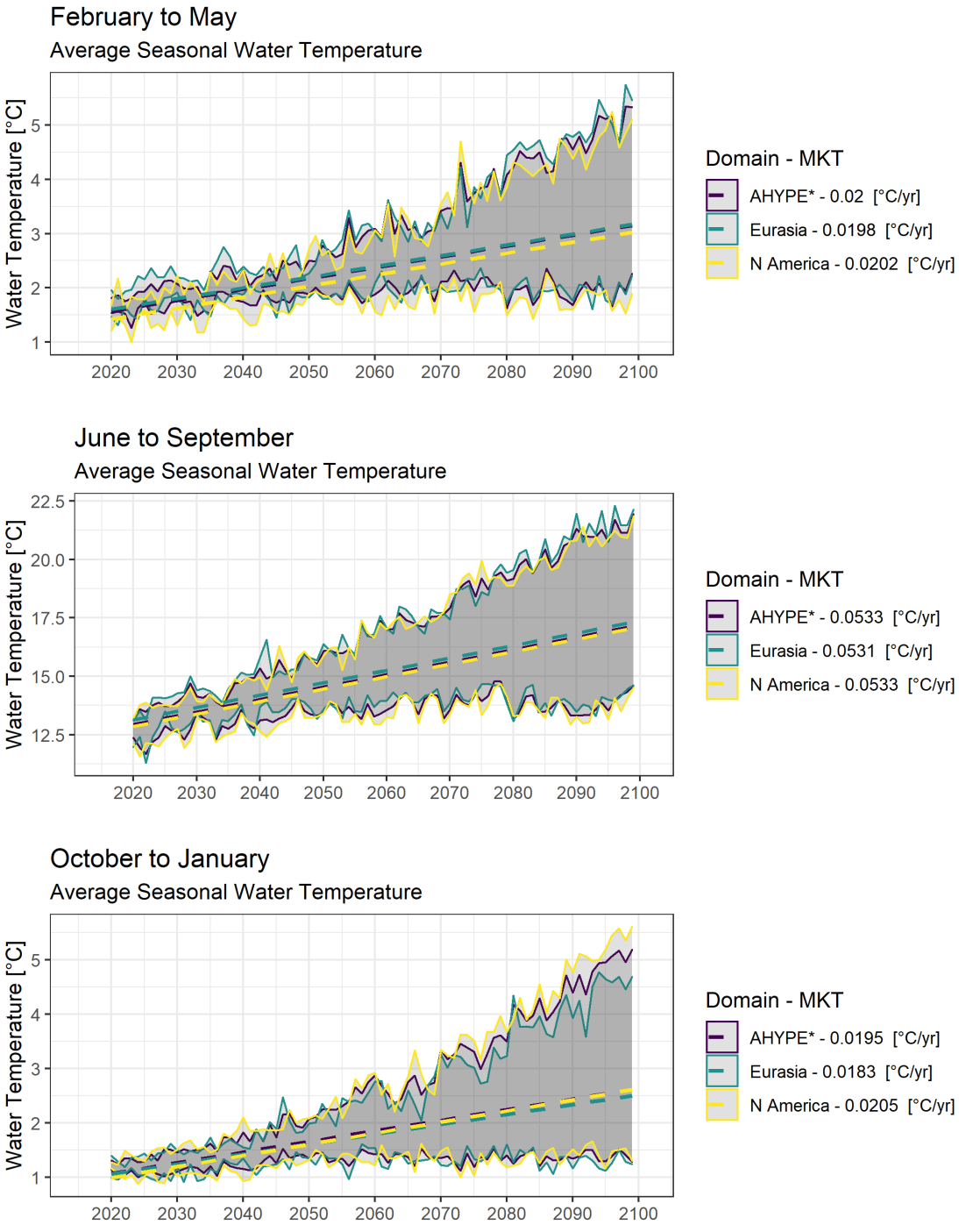

Figure 44 Time series plots for AHYPE without Greenland, North America, and Eurasia showing the time series of modeled seasonal average water temperature into the future. GCM+SSP combinations upper and lower bounds are shown by the ribbon. The mean pre-whitened MKT for each domain is shown as a dashed line.

Soil Temperature

All soil temperature pre-whitened Mann-Kendall trends are summarized in Table 22 by domain and season. Soil temperature shows a slight variation in seasonality among the spatial domains. North America has slightly higher trends than Eurasia and the AHYPE (pan-Arctic) domain trends land in between. February to May trends range from 0.052 to 0.055°C/year, June to September season from 0.057 to 0.065°C/year which is the largest difference among the domains, and the October to January season ranges from 0.046-0.051°C/year rise in soil temperature, all seasonal trends are statistically significant for all seasons and future scenarios. Comparing between the various seasons the summer season has the fastest warming trends and also the widest spread between domains. Soil temperature shows a more significant difference between the Feb and May thaw season and Oct to Jan frozen season. Trends in the thaw season (Feb-May) are slightly higher than those in the ice-on season (Oct-Jan).

Table 22 Summary of the pre-whitened MKT (°C/yr) for each domain, GCM+SSP combination for each season. Each section shows the sorting of trends with shading in red, darker red shows a faster warming trend. Statistical significance is shown in bold.

	Feb - May	Domain		
		AHYPE*	N. America	Eurasia
GCM + SSP	Historical (1989-2019)	**0.030**	**0.023**	**0.040**
	Future Mean	**0.054**	**0.055**	**0.052**
	CanESM5 ssp126	**0.022**	**0.024**	**0.020**
	CanESM5 ssp585	**0.102**	**0.102**	**0.101**
	MIROC6 ssp126	**0.016**	**0.015**	**0.015**
	MIROC6 ssp585	**0.077**	**0.081**	**0.076**
	MRI-ESM2-0 ssp585	**0.054**	**0.056**	**0.051**

	June - Sep	Domain		
		AHYPE*	N. America	Eurasia
GCM + SSP	Historical (1989-2019)	**0.035**	**0.022**	**0.045**
	Future Mean	**0.061**	**0.065**	**0.057**
	CanESM5 ssp126	**0.021**	**0.023**	**0.018**
	CanESM5 ssp585	**0.118**	**0.124**	**0.113**
	MIROC6 ssp126	**0.019**	**0.019**	**0.018**
	MIROC6 ssp585	**0.089**	**0.095**	**0.086**
	MRI-ESM2-0 ssp585	**0.057**	**0.062**	**0.053**

	Oct - Jan	Domain		
		AHYPE*	N. America	Eurasia
GCM + SSP	Historical (1989-2019)	**0.030**	**0.026**	**0.038**
	Future Mean	**0.049**	**0.051**	**0.046**
	CanESM5 ssp126	**0.017**	**0.020**	**0.015**
	CanESM5 ssp585	**0.097**	**0.101**	**0.093**
	MIROC6 ssp126	**0.014**	**0.014**	**0.012**
	MIROC6 ssp585	**0.070**	**0.073**	**0.068**
	MRI-ESM2-0 ssp585	**0.048**	**0.050**	**0.046**

Timeseries of seasonal average soil temperatures are shown in Figure 45 on the following page. An intercomparison of the spatial domains and their timeseries provide an insight into why North America shows slightly higher trends than the other domains. And it is likely due to the overall lower soil temperatures in North America for all seasons. Additionally, we see the similarity in trends and lower and upper bounds during the Feb-

May season for all three domains and a significant difference between them in the Jun-Sep season. The Oct-Jan season has a greater difference in trends among the three domains than the Feb-May season, similar upper simulation bounds for all three domains and greater variability in the lower bounds or low warming scenarios. The variability throughout the seasons (shown in the spread among the future projections for each domain) aligns with our expectations of future climate change in the Arctic and the modeled trends. Summer (Jun-Sep) with its warmer temperatures shows the most significant warming and also the greatest variability among the domains; this carries over into the following ice-freeze-up season which is impacted by a lengthening of the summer season in portions of the domains.

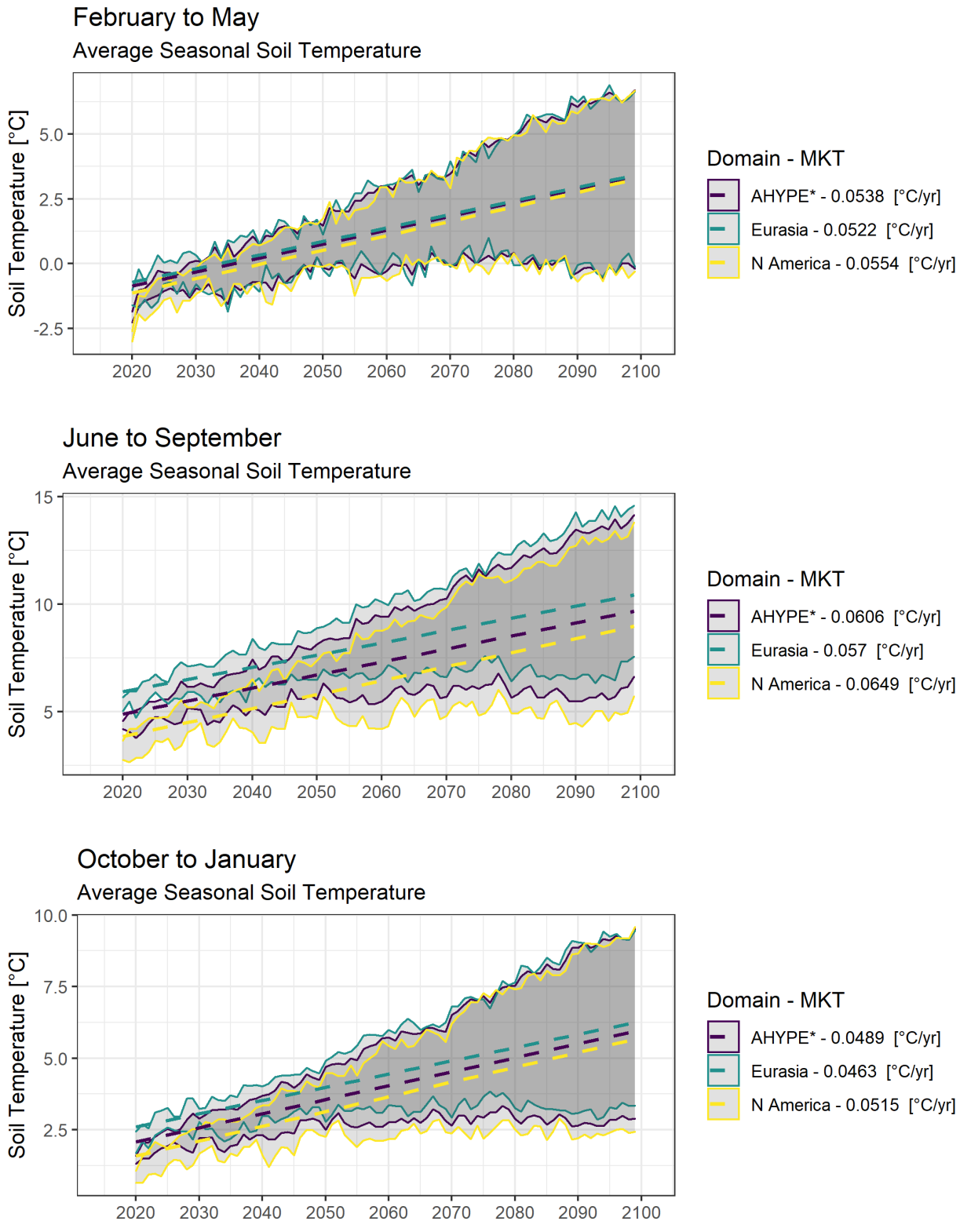

Figure 45 Time series plots for AHYPE without Greenland, North America, and Eurasia showing the time series of modeled seasonal average soil temperature into the future. GCM+SSP combinations upper and lower bounds are shown by the ribbon. The mean pre-whitened MKT for each domain is shown as a dashed line.

5.2. Continental Change Points

The following sections summarize the change point analysis (by year), which were computed using the Pettitt test (Pettitt, 1979). Included in the various GCM +SSP combinations is the future modeled ensemble mean.

Water Temperature

Change points for water temperature range from 2045 to 2067. Earlier change points occur in the lower warming GCM+SSP scenario combinations. In general, change points occur earlier for the Eurasian domain. Change points detected in the ensemble mean are detected in 2057 for Eurasia, and 2062 for AHYPE and North America. There is an agreement in the change point analysis among the differing spatial domains that lower warming scenarios have earlier change points, and those with higher warming have later change points. Four out of five scenarios suggest that Eurasia has earlier change points than North America, although most are within one or two years of each other. The largest continental difference in change points is for the CanESM5 ssp126 scenario which shows a seven-year difference in change points between the two continents.

When examining the time series (Figure 41) and calculating trends before and after the change point (Appendix C) we see a pattern in how trends change before and after the change point. Increases in trends after the change point are indicated in the table by “(+)” and decreases by “(-)”. It is evident that higher warming scenarios have increases in trends after their change point, and slower warming scenarios show a decrease in trends. MRI-ESM2-0 ssp585 is the only high warming scenario which has a decrease in trend after the changepoint, but only for North America. It is a very small decrease, around 5%. The observation of how the trends change corresponds to the socio-economic responses

of these scenarios, as the lower warming is supposed to see a mitigation in response to climate change, which should cause decreases in trends in the future.

Table 23 Summary of calculated change points (by year) for average annual water temperature (CCT2) using the single change point pettitt test for each domain, GCM+SSP combination, and ensemble mean over the entire future period. Lighter shading shows later change points and darker shading shows change points which occur earlier in the future period. GCM+SSP combinations have been ranked to by change point timing. Changes in trends after the change point are shown in parentheses.

Change Points - CCT2			
Model	AHYPE*	N. America	Eurasia
MIROC6 ssp126	2046 (-)	2046 (-)	2045 (-)
CanESM5 ssp126	2053 (-)	2056 (-)	2049 (-)
CanESM5 ssp585	2059 (+)	2059 (+)	2059 (+)
MIROC6 ssp585	2062 (+)	2063 (+)	2062 (+)
MRI-ESM2-0 ssp585	2065 (+)	2067 (-)	2065 (+)
Mean	2062	2062	2057

River Ice Thickness

Change points for river ice thickness range from 2043 to 2072. Earlier change points tend to occur in the lower warming GCM+SSP scenario combinations. Change points detected in the ensemble mean are in 2055 for Eurasia and 2056 for AHYPE and North America. Eurasia and the AHYPE domain have identically identified changepoints. There is agreement among the spatial domains that low warming scenarios (ssp126) have earlier change points and higher warming scenarios (ssp585) produce later change points. For water temperature, there was agreement among the future scenarios that Eurasia had consistently earlier change points than North America. For river ice thickness however, North America has earlier change points for low warming scenarios, and later change points than Eurasia for higher warming scenarios. The changes in trends (Appendix G) from before to after the change point shows that trends are becoming more positive, “(+)” means less ice thickness loss per year after the change point, for lower warming

scenarios. And trends that are becoming more negative, "(-)" means an increase in ice thickness losses per year or a more rapid trend after the change point, for higher warming scenarios. This is in agreement with water temperature trends before and after the change point as well. For river ice thickness the exception is the CanESM5 ssp585 scenario for Eurasia, which also shows a more positive trend after the change point, or a slower loss of river ice thickness after the changepoint. The combination of North America having earlier change points for low warming scenarios where annual ice thickness losses decrease after the change point, and having later change points for high warming scenarios where annual ice thickness losses increase after the change point, leads to North America experiencing more rapid ice thickness losses for a shorter time span in the future period compared to Eurasia, regardless of the future scenario. This does not necessarily mean that Eurasia is experiencing greater ice thickness losses overall, as section 5.1 showed Eurasia having overall slower annual ice thickness loss trends. However, we do know that Eurasia is experiencing its more rapid losses for longer than North America.

Table 24 Summary of calculated change points (by year) for modelled maximum annual river ice thickness (CMRI) using the single change point pettitt test for each domain, GCM+SSP combination, and ensemble mean over the entire future period. Lighter shading shows later change points and darker shading shows change points which occur earlier in the future period. GCM+SSP combinations have been ranked to by change point timing. Changes in trends after the change point are shown in parentheses (note that trends in CMRI are generally negative).

Change Points - CMRI			
Model	AHYPE*	N. America	Eurasia
MIROC6 ssp126	2047 (+)	2043 (+)	2047 (+)
CanESM5 ssp126	2051 (+)	2046 (+)	2051 (+)
CanESM5 ssp585	2055 (-)	2062 (-)	2055 (+)
MIROC6 ssp585	2056 (-)	2064 (-)	2056 (-)
MRI-ESM2-0 ssp585	2065 (-)	2072 (-)	2065 (-)
Mean	2056	2056	2055

Soil Temperature

Change points for soil temperatures range from 2046 to 2062. The change point for the ensemble mean future projection of annual soil temperature is 2061 for all domains. There is agreement in domains in change points, and there is very little variability between domains. The largest difference is between North America and Eurasia for the CanESM5 ssp126 future projection where the change points are six years apart, but all other projections either completely agree or show a difference of one year between the two continents. There is an agreement among the three domains that, just like with water temperature and river ice thickness, earlier change points occur in the lower warming scenario GCM+SSP combinations. There is a general agreement among future scenarios and domains that trends after the change points (found in Appendix G) are lower for low warming scenarios (ssp126), and higher for higher warming scenarios (ssp585). One ensemble member, the MRI-ESM2-0 ssp585 scenario, is in disagreement with this and shows lower trends after the change point for the AHYPE domain and Eurasia.

Notable is that for one of the low warming future scenarios (CanESM5 ssp126) trends change from warming to cooling at the change point for all three domains. However, these low warming scenarios are becoming increasingly unrealistic in their modeled socio-economic response, as current climate warming is exceeding expectations. The central result of this analysis is that mid-century, trends warming in soil temperature are expected to either become less severe or become cooling trends under a low warming scenario with significant socio-economic response or are expected to become more severe under higher warming with fairly high agreement between the different future scenarios.

Table 25 Summary of calculated change points (by year) for modelled annual average soil temperature (STMP) using the single change point pettitt test for each domain, GCM+SSP combination, and ensemble mean over the entire future period. Lighter shading shows later change points and darker shading shows change points which occur earlier in the future period. GCM+SSP combinations have been ranked to by change point timing. Changes in trends after the change point are shown in parentheses.

Change Points - STMP			
Model	AHYPE*	N. America	Eurasia
MIROC6 ssp126	2046 (-)	2046 (-)	2046 (-)
CanESM5 ssp126	2053 (-)	2056 (-)	2050 (-)
CanESM5 ssp585	2059 (+)	2059 (+)	2059 (+)
MRI-ESM2-0 ssp585	2059 (-)	2060 (+)	2061 (-)
MIROC6 ssp585	2062 (+)	2062 (+)	2062 (+)
Mean	2061	2061	2061

5.3. Trend Analysis at the Watershed Scale

All trend results for the future period will be presented in the following section, but further discussed in their relevance to thesis objective three in the discussion section 6.2 which covers potential “hotspots” and how those are related to pan-arctic communities and ice roads.

Water Temperature

Pre-whitened Mann-Kendall trends in water temperature over the future period are summarized in the following table. Comparing future mean trends to the historical modeled trends we see all future trends are statistically significant, and higher than those which were modeled for the historical period. Statistically significant historical trends range from 0.012-0.023°C/year and future mean trends range from 0.018-0.043°C/year. When comparing the watersheds to each other by their ranks in trends, some watersheds remained in their relative trend standing. For example, the Severnaya Dvina watershed is amongst the highest trends in both the historical and future period and the Kolyma watershed among the lowest trends. Notable differences between the historical and future

trends are the Mackenzie and Nelson which go from statistically insignificant trends to trends in the middle (Mackenzie) and upper (Nelson) end of the future mean trend range. This means there is a significant influence of future climate warming on water temperatures in the Nelson River watershed which is not present in the historical.

Table 26 Summary of pre-whitened Mann-Kendall trends for average annual water temperature in each of the 12 largest river watersheds. Historical trends are provided for comparison, and trends are ranked by colour. Darker reds show faster warming trends. Statistical significance is shown in bold text.

	Watershed											
	Khat.	*Kok.*	*Kol.*	*LaGr.*	*Lena*	*Mack.*	*Nel.*	*Ob*	*Pech.*	*S.Dvi.*	*Yen.*	*Yuk.*
Hist.	**0.017**	**0.015**	**0.013**	**0.014**	**0.015**	0.011	-0.001	**0.012**	**0.019**	**0.023**	**0.023**	**0.021**
Future Mean	**0.023**	**0.031**	**0.018**	**0.032**	**0.030**	**0.030**	**0.041**	**0.035**	**0.039**	**0.043**	**0.033**	**0.027**
CanESM5 ssp126	**0.005**	**0.007**	0.003	**0.008**	**0.008**	**0.009**	**0.012**	**0.009**	**0.010**	**0.011**	**0.009**	**0.010**
CanESM5 ssp585	**0.051**	**0.075**	**0.046**	**0.073**	**0.068**	**0.066**	**0.087**	**0.081**	**0.086**	**0.095**	**0.071**	**0.064**
MIROC6 ssp126	**0.006**	**0.005**	**0.007**	**0.009**	**0.004**	**0.008**	**0.011**	**0.007**	**0.009**	**0.009**	**0.006**	0.003
MIROC6 ssp585	**0.033**	**0.046**	**0.021**	**0.045**	**0.041**	**0.046**	**0.056**	**0.056**	**0.067**	**0.071**	**0.049**	**0.041**
MRI-ESM2-0 ssp585	**0.019**	**0.024**	**0.015**	**0.025**	**0.029**	**0.022**	**0.038**	**0.026**	**0.024**	**0.029**	**0.029**	**0.017**

Spatially, the two watersheds at the highest latitude (Khatanga and Kolyma) have the slowest warming trends. The Nelson now stands out in North America with a much higher warming trend than other watersheds on that continent. Finally, in Eurasia the higher trends are concentrated in the western portion of the continent, and lower trends are concentrated in the east.

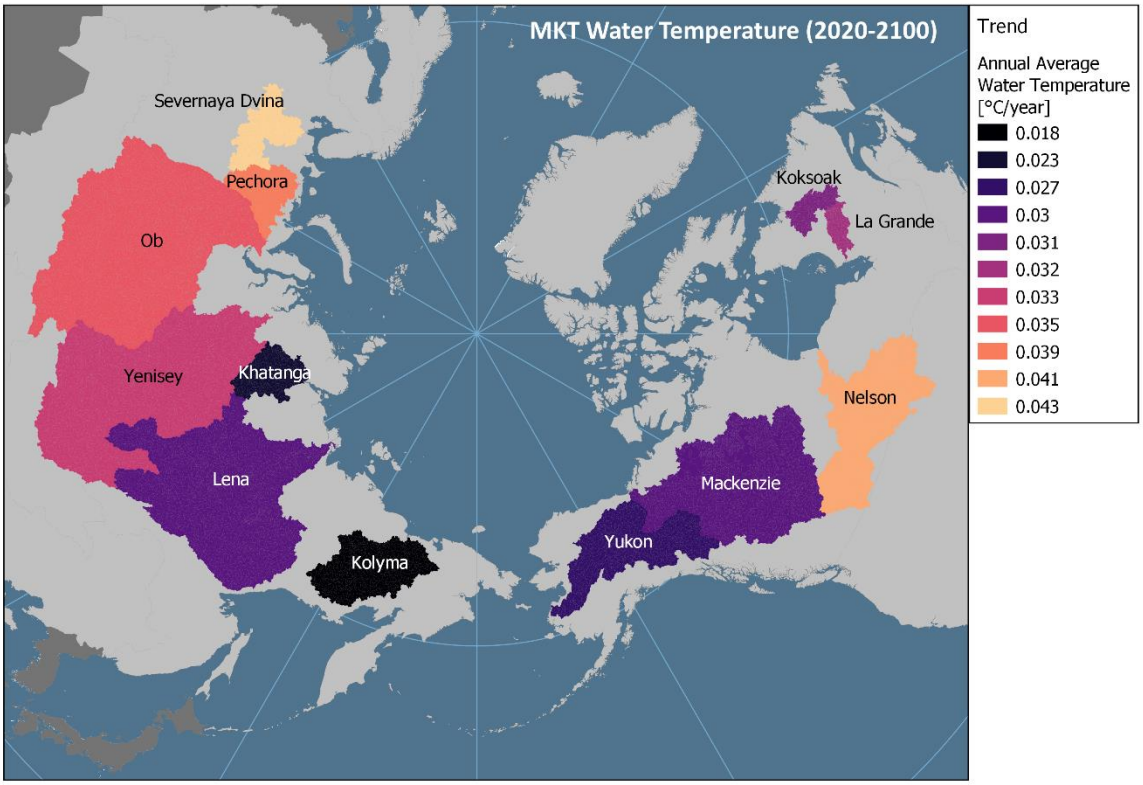

Figure 46 Map of future annual water temperature trends for each of the twelve largest watersheds in the pan-Arctic. Watersheds are ranked by trend from lowest to highest.

River Ice Thickness

Pre-whitened Mann-Kendall trends in maximum annual river ice thickness for each watershed are summarized in the following table. All future mean trends are considered statistically significant, but among the ensembles lower warming scenarios only one watershed has a statistically significant trend. Even some higher warming GCM+ssp combinations are statistically insignificant in some watersheds, only the most extreme change scenario (for temperature and precipitation), CanESM5 ssp585, has significant trends for all watersheds. Comparing future mean trends to historical and statistically significant trends there is a decrease in future trends in the Khatanga and Kolyma watershed which have historical trends ranging from -0.23 to -0.24cm/year and future

mean trends ranging from -0.09 to -0.11cm/year for those two watersheds. All other watersheds changed from statistically insignificant trends in the historical period to significant trends in the future. Overall, future mean trends range from -0.03 to -0.11cm/year. It is interesting that although the Khatanga and Kolyma did not have very high water temperature increase trends in the future, they are still among the highest trends in future river ice thickness losses. At the watershed scale there is a higher uncertainty of the impacts of climate warming among the future ensemble, as changes in both temperature and precipitation impact ice growth differently. But there is a greater agreement among the various watersheds as the trends have less variability for the future period.

Table 27 Summary of pre-whitened Mann-Kendall trends for annual maximum river ice thickness in each of the 12 largest river watersheds. Historical trends are provided for comparison, and trends are ranked by colour. Darker reds show faster warming trends. Statistical significance is shown in bold text.

	Watershed											
	Khat	*Kok.*	*Kol.*	*LaGr.*	*Lena*	*Mack.*	*Nel.*	*Ob*	*Pech.*	*S.Dvi.*	*Yen.*	*Yuk.*
Historical (1989-2019)	**-0.24**	-0.05	**-0.23**	-0.02	-0.11	-0.08	0.08	-0.02	-0.01	-0.03	-0.06	-0.04
Future Mean	**-0.09**	**-0.03**	**-0.11**	**-0.06**	**-0.09**	**-0.09**	**-0.11**	**-0.07**	**-0.05**	**-0.09**	**-0.10**	**-0.10**
CanESM5 ssp126	-0.03	-0.02	-0.02	-0.02	-0.04	**-0.05**	-0.04	-0.01	-0.02	-0.03	-0.02	-0.02
CanESM5 ssp585	**-0.13**	**-0.12**	**-0.20**	**-0.13**	**-0.17**	**-0.19**	**-0.27**	**-0.21**	**-0.14**	**-0.28**	**-0.22**	**-0.23**
MIROC6 ssp126	-0.02	-0.01	-0.04	**-0.04**	0.00	-0.01	-0.02	0.00	-0.01	-0.02	0.00	0.01
MIROC6 ssp585	**-0.17**	0.00	**-0.16**	-0.03	**-0.17**	**-0.12**	**-0.12**	**-0.05**	-0.05	**-0.13**	**-0.10**	**-0.13**
MRI-ESM2-0 ssp585	**-0.06**	**-0.04**	**-0.13**	**-0.06**	**-0.12**	**-0.09**	**-0.07**	**-0.08**	-0.04	-0.03	**-0.16**	**-0.12**

The trends spatial distributions are shown in Figure 47, slower warming trends (orange) are mainly in smaller watersheds in eastern Canada (Koksoak and the La Grande) and

western Eurasia (Pechora). Most watersheds have mean future trends around -0.10 cm/year or a loss of 1 cm/decade in maximum annual river ice thickness. The Nelson River watershed which had one of the highest water temperature trends also has one of the fastest trends for river ice thickness losses. This could indicate that water temperature is a significant influence on how river ice thickness is determined for this watershed.

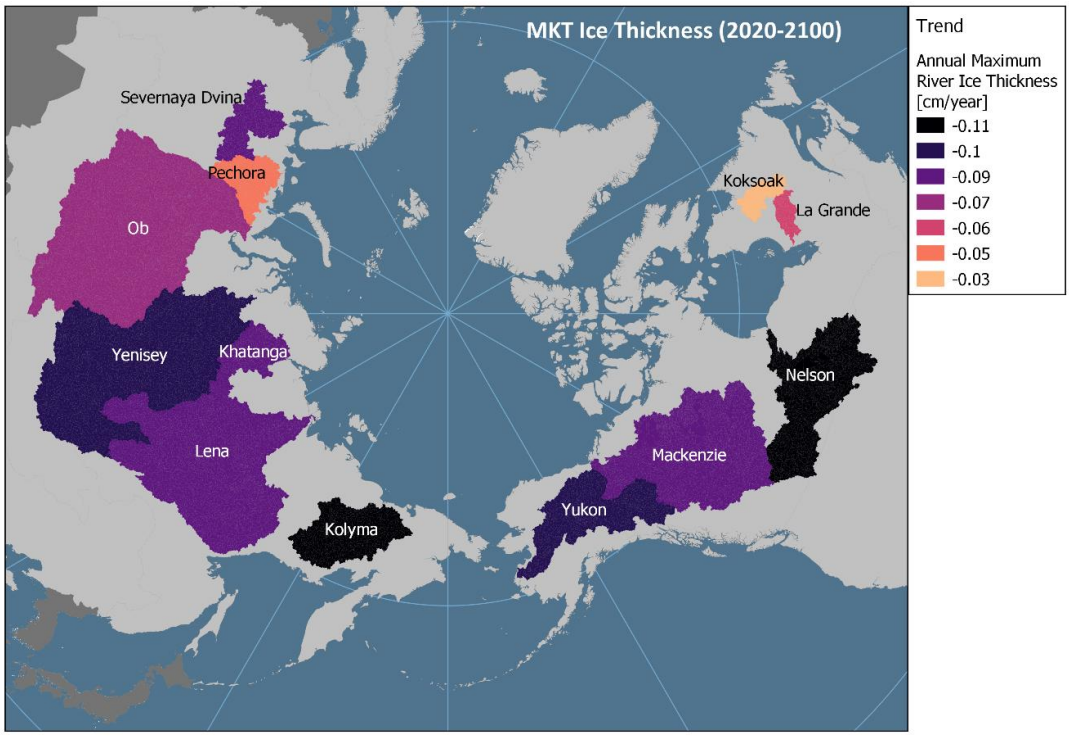

Figure 47 Map of future annual maximum river ice thickness for each of the twelve largest watersheds in the pan-Arctic. Watersheds are ranked by trend from lowest to highest.

Soil Temperature

Pre-whitened Mann-Kendall trends for the annual average soil temperature in each watershed are summarized in the following table. Unlike water temperature and river ice thickness all future trends in soil temperature are statistically significant for all future warming scenarios. Historical warming trends have a range of 0.019-0.074°C/year and future trends have a similar range of 0.032-0.07°C/year. The upper limit of soil warming

trends did not increase in the future period, but the lower limit did. This means that even the slowest warming watersheds for soil temperature have modeled warming that is more rapid in the future period, pointing to more intense thawing of permafrost soils in the future. Most watersheds show an increase in trend into the future, except for the Kolyma watershed which loses its rank as having the fastest soil temperature increase over the historical period, and moves into second place to the Khatanga watershed, another high latitude watershed. Higher warming trends in high latitude watersheds suggest that colder soils with more permafrost will be warming the quickest. This could be due to a combination of increased air temperatures, and precipitation which both insulates the soils as snow and increases percolation into the soils introducing additional heat. The Nelson watershed also shows a significant change between the historical and future period where it had an insignificant trend, and in the future period is in the middle of the trend range.

Table 28 Summary of pre-whitened Mann-Kendall trends for average annual soil temperature in each of the 12 largest river watersheds. Historical trends are provided for comparison, and trends are ranked by colour. Darker reds show faster warming trends. Statistical significance is shown in bold text.

2020-2100		Watershed											
		Khat	*Kok.*	*Kol.*	*LaGr*	*Lena*	*Mac.*	*Nel.*	*Ob*	*Pech*	*S.Dvi*	*Yen.*	*Yuk.*
	Historical (1989-2019)	**0.066**	**0.028**	**0.074**	**0.028**	**0.047**	**0.019**	0.004	**0.023**	**0.035**	**0.026**	**0.033**	**0.025**
	Future Mean	**0.070**	**0.052**	**0.059**	**0.049**	**0.051**	**0.051**	**0.048**	**0.041**	**0.041**	**0.032**	**0.049**	**0.052**
GCM + SSP	*CanESM5 ssp126*	**0.024**	**0.021**	**0.017**	**0.019**	**0.016**	**0.019**	**0.016**	**0.017**	**0.016**	**0.012**	**0.016**	**0.020**
	CanESM5 ssp585	**0.126**	**0.099**	**0.126**	**0.093**	**0.110**	**0.099**	**0.094**	**0.083**	**0.078**	**0.065**	**0.103**	**0.108**
	MIROC6 ssp126	**0.024**	**0.012**	**0.017**	**0.014**	**0.018**	**0.012**	**0.014**	**0.007**	**0.010**	**0.006**	**0.007**	**0.013**
	MIROC6 ssp585	**0.106**	**0.078**	**0.077**	**0.073**	**0.081**	**0.076**	**0.067**	**0.064**	**0.065**	**0.047**	**0.069**	**0.074**
	MRI-ESM2-0 ssp585	**0.064**	**0.055**	**0.063**	**0.052**	**0.060**	**0.046**	**0.047**	**0.040**	**0.034**	**0.026**	**0.051**	**0.044**

Spatially, faster soil temperature increases are modeled in eastern portion of Eurasia and western North America. The Khatanga and Kolyma, the watersheds with the highest latitudes have the fastest mean warming trends. The watersheds with lower latitudes, which generally have a higher average soil temperature, such as the Ob, Yenisey and Nelson either have lower mean warming trends or are in the middle of the trend range.

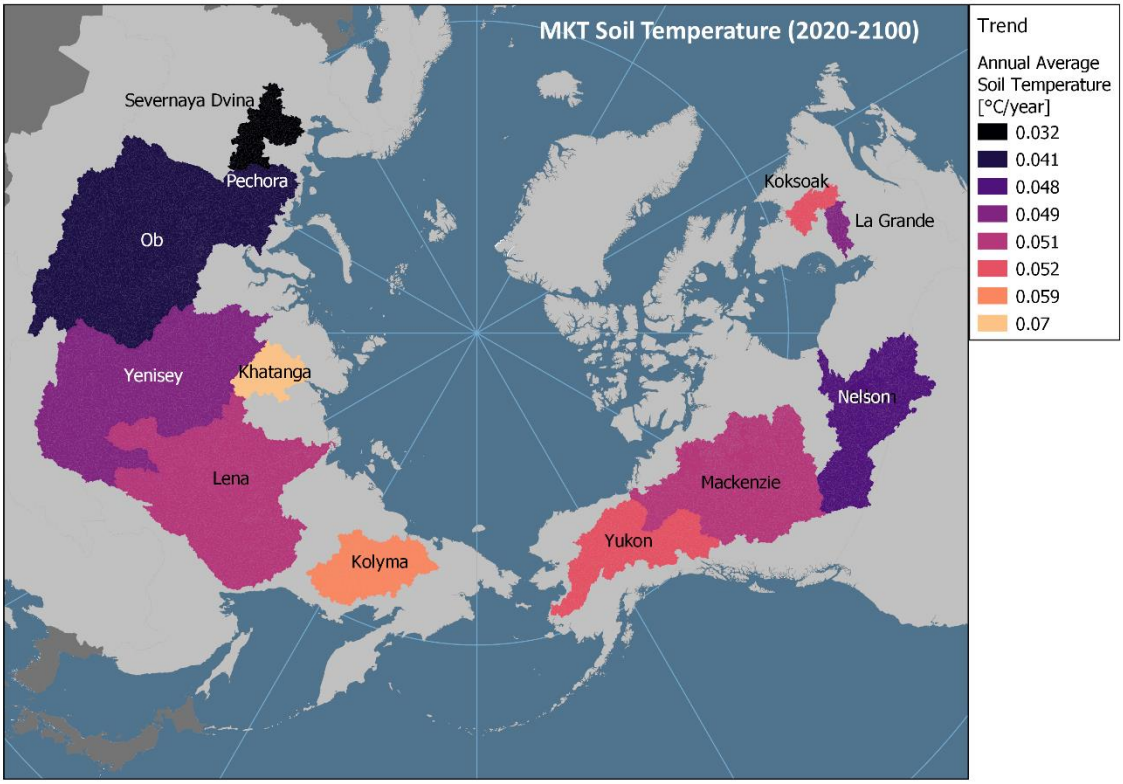

Figure 48 Map of future annual soil temperature trends for each of the twelve largest watersheds in the pan-Arctic. Watersheds are ranked by trend from lowest to highest.

6. Discussion

6.1. Continental Trends

Water Temperature

The analysis is conclusive that modeled trends at the pan-arctic and continental scale show accelerated future warming of freshwater temperature. Trends for North America, and Eurasia show warming of 0.3°C/decade when assessing the mean modeled annual water temperatures for the entire future period. An acceleration in warming is not surprising but confirms the urgency for adaptation. Historical increases in water temperature have already led to changes in arctic fish species biodiversity, as warming temperatures expand habitats for fish species which thrive in warmer temperatures and increase competition among species for limited resources (Pörtner et al., 2019). Accelerated warming does not necessarily lead to an expansion of habitat but limits migration and increase competition, and species that are sensitive to high temperatures are at further risk (Campana et al., 2020; Kangur et al., 2016). Sensitivity to high temperatures is of prominent concern because from the seasonal analysis it was established that summer freshwater temperatures are warming at the highest rate. Seasonally, summer warming (June-Sep) is calculated to be closer to 0.5°C/decade, over twice as high as warming in the shoulder seasons (Oct-Jan and Feb-May) which have warming around 0.2°C/decade. Increased warmer freshwater inflows to the Arctic Ocean can impact its ability to operate as a carbon sink, along with impacting marine coastal ecosystems (Meredith et al., 2019). Increased future trends in freshwater warming predispose the Arctic to a decreased ability to regulate global temperatures effectively.

Highly important is not just an understanding of future trends, but what impacts current climate warming mitigation practices may have on the trends. Encouragingly, lower

warming scenarios, those which are meant to represent a socio-economic response to lower emissions do show that warming trends could decrease around the mid-century. Higher warming scenarios however, those which we are trending towards currently, do warn us that inaction could lead to a further acceleration in warming in the latter half of the century.

Ice Thickness

Future modeled ice thickness trends, project losses of around 1 cm/decade of annual maximum ice thickness at the continental scale. Ice thickness is of great concern to many communities, and those which rely on it for travel have already noticed changes in ice and have been hindered by shorter ice-on seasons and increased safety concerns surrounding the travel of ice. This is even more concerning when considering that historical continental scale trends for maximum river ice thickness were much lower, and statistically insignificant, in North America. However, changes in ice thickness were still noticeable by community groups (Tam et al., 2013). Future projections show much clearer trends, for both North America and Eurasia which have similar future projections.

Since maximum river ice thickness was the point of analysis, we can expect that average ice thicknesses, which would be lower, are experiencing changes. As often discussed in literature, ice on and ice thaw timing is of high importance and seeing significantly increasing trends in the maximum ice thickness alone signals that other ice factors are also projected to have accelerated change.

Similarly to water temperature trends, in light of the socio-economic response to climate warming, lower warming scenarios with a significant response to lower emissions do show a change in river ice thickness trends prior to the middle of the century in North

America. There is more disagreement among climate models and continents for river ice thickness as its relationship to air temperature and precipitation is much more complicated than water and soil temperatures. In some low warming scenarios, trends are not significant before or after detected change points. Due to the model and continental disagreements it is difficult to determine the exact impact mitigation has on future trends. It is clear that in North America, under a higher warming scenario, modeled trends show increased losses in maximum river ice thickness in the latter half of the century.

Soil Temperature

Throughout the analysis soil temperature has shown clear warming signals with agreement between all climate models and warming scenarios. Just as with water temperature, future modeled trends project more rapid warming in the future, with the ensemble average at around 0.5°C/decade for all continents. Future modeled trends increase for all continents, but North American warming trends double from the historical to the future.

The concern with projected soil temperature increase is its impact on permafrost. And increases in warming solidify the loss of permafrost cover at all permafrost densities. Permafrost thaw decreases the structural strength of soil which communities rely on when constructing infrastructure, changes hydrologic conductivity, and further releases stored carbon (Mohammadi & Hayley, 2023; Walvoord & Kurylyk, 2016). Increased modeled trends in future warming ring the warning bell that already observed permafrost thaw are expected to continue, at increasing speeds.

Seasonally, summer temperatures in soil show the highest increases in soil temperature. This is likely due to the lack of insulating effects that snow has in the winter months, which protect soil from warmer air temperatures. Additionally, we know that future warming produces increased precipitation and with that, increased snow cover may mitigate some warming during snow cover months. However, once permafrost melt occurs and water moves more freely throughout the soil warming becomes more rapid as liquid water moves heat through the soil. And increases in summer precipitation likely also contribute to this increased warming.

When reviewing the possible impact of socio-economic response to climate warming on soil temperature trends there is some disagreement among the climate models in the higher warming scenarios. For low warming scenarios, an accelerated response to mitigate the rate of global temperature rise could produce lower warming trends by the mid-century. However, even then warming is expected to continue. And it is difficult to know if it would be possible to reduce warming enough to slow down the feedback effects which are not all represented in this modelling exercise (ie. changes in landscape due to permafrost thaw). For high warming scenarios, most models show increases in trends for the latter half of the century, but one model shows a slight decrease in trends.

6.2. “Hot Spots”

This section discusses the results in the context of whether there are any “hotspots” in the 12 largest river basins in the pan-Arctic domain for the three model outputs. Hotspots are areas which are changing more rapidly than others. These will be discussed also in context of where communities are likely to be impacted by these changes, and where we know Canadian ice roads are present, as this data was readily available. Communities

are often located near rivers, and therefore are relevant to the discussion of trends in all three model outputs whether they are water or soil related.

According to Ramage et al. (2021) there are 1162 settlements in the Arctic Circumpolar Permafrost Region, which is contained in the AHYPE domain. These are home to approximately five million people. 638 of these defined settlements are within the 12 largest rivers watersheds and are home to just over three million people. The following map shows the permafrost settlements and their population size. The majority of large settlements are in the Ob and Lena watersheds. In general, more settlements are in Eurasia, in North America settlements are concentrated in Alaska in the Yukon watershed but generally have lower populations. Some watersheds such as the Severnaya Dvina and Nelson watershed show no permafrost settlements; however, that does not mean there are no settlements in these areas that are not impacted by the changes discussed in the following sections. It should be noted that for the Nelson watershed there are communities which rely on the construction of winter roads and can therefore be significantly impacted.

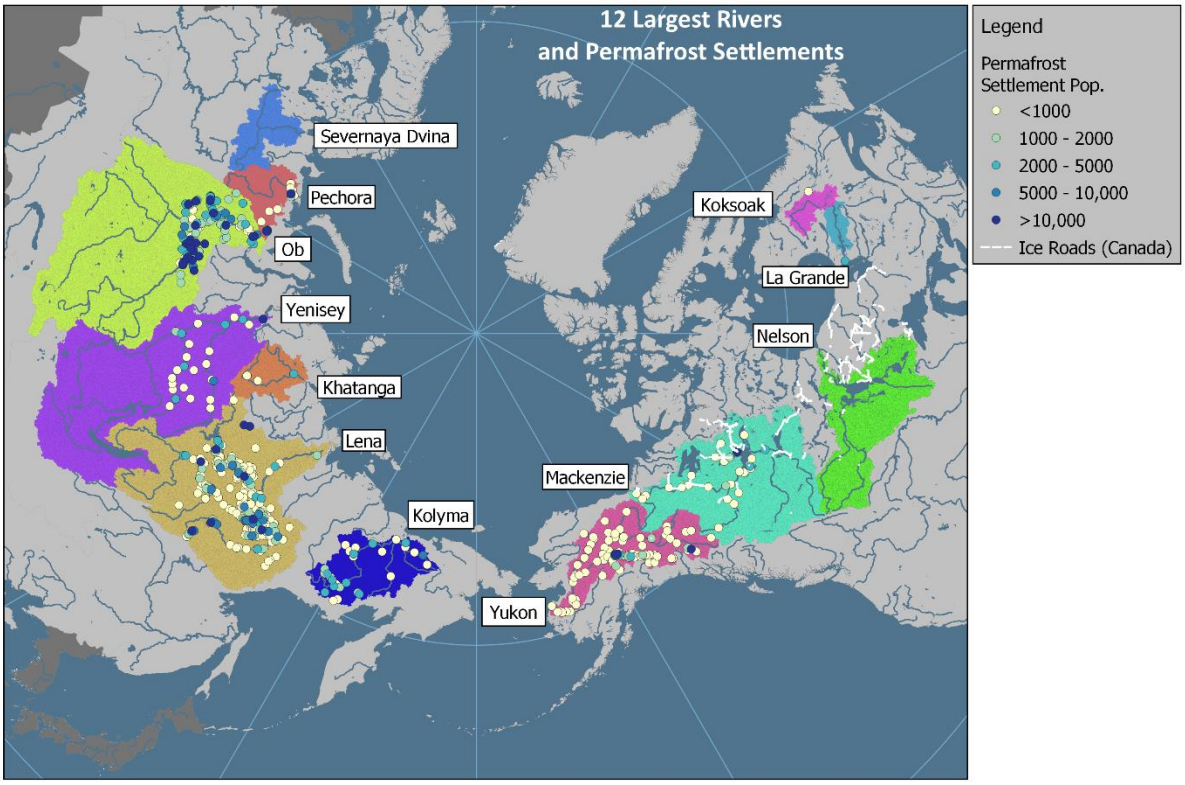

Figure 49 Map of the 12 Largest River Watersheds and the permafrost settlements contained within them. Additionally, Canadian ice roads are shown in white.

Water Temperature

Trends in water temperature were previously presented in detail in Section 5.3, and all future mean trends are statistically significant for the future period. Future trends range from around 0.2-0.4°C/decade which does not provide a significant range in water temperatures that a single watershed could be considered an outlier or significant hot spot from the others. However, the Ob watershed contains a significant amount of permafrost settlements concentrated around rivers and also has the fourth fastest warming trend at 0.35°C/decade. The Lena and Yukon watershed which also have a significant number of permafrost settlements have lower trends of around 0.3°C/decade, but as noted this is not a huge difference to the Ob due to the small range in trends. Finally, the Nelson watershed has one of the fastest warming trends of around

0.4°C/decade, and although it does not contain permafrost settlements there are known settlements which rely on ice roads which would be significantly affected by the warming of freshwater in local rivers.

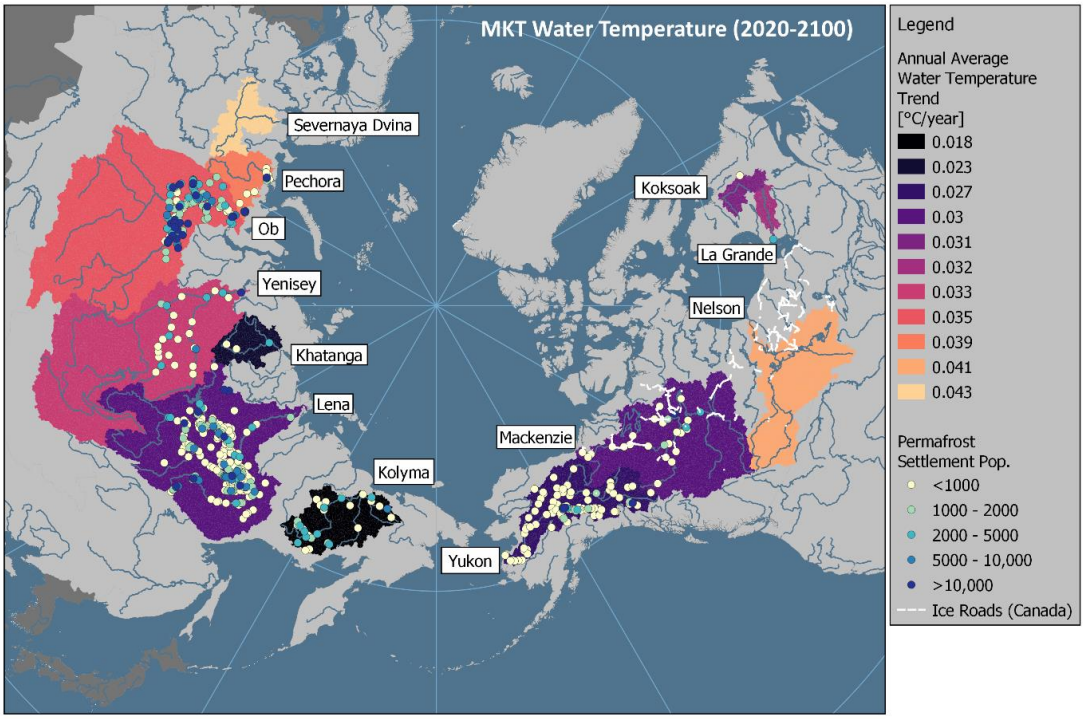

Figure 50 Future trends (slope of the pre-whitened MKT) for annual water temperatures in the 12 Largest River Watersheds. Permafrost settlements within the 12 largest rivers and Canadian ice roads are also shown.

Ice Thickness

Mean future trends in river ice thickness were also all statistically significant, and there is a larger spread to them than for water temperature. For river ice thickness hot spots are in darker colors and include the Nelson, Kolyma, Mackenzie, Yenisey, Lena and Khatanga which all have mean trends of a loss of 1 cm/decade in maximum annual river ice thickness. When considering the highest warming future scenario, they can have almost twice that at around 2 cm/decade of maximum river ice thickness being lost.

For the Nelson, Yukon, and Mackenzie which we know contain ice roads this is particularly important, knowing that they are experiencing some of the highest ice

thickness loss rates. Additionally, the Lena, Yenisey and Kolyma all have large numbers of communities around their major rivers which means they likely also utilize ice roads, although no official spatial information is available on them.

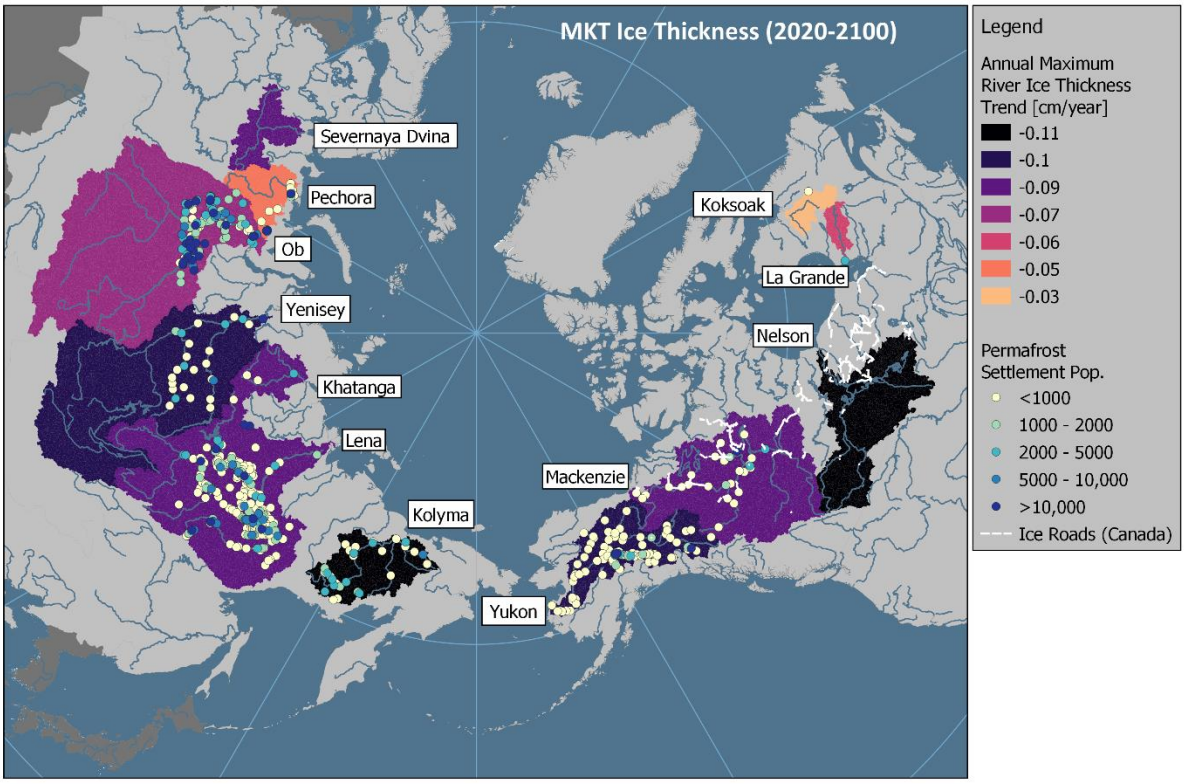

Figure 51 Future trends (slope of the pre-whitened MKT) for annual maximum ice thickness in the 12 Largest River Watersheds. Permafrost settlements within the 12 largest rivers and Canadian ice roads are also shown.

Soil Temperature

Future modeled mean trends in soil temperature for the 12 largest river watersheds are all statistically significant. The trends have a range from 0.3-0.7°C/decade in soil temperature, and the hotspot for soil temperature warming should be easily spotted in Figure 52 below which shows the pre-whitened Mann-Kendall trends ranked by their intensity. The Khatanga watershed, at a high latitude is clearly a hotspot for soil temperature warming. Its warming trend sits at 0.7°C/decade, around 0.1°C faster per

decade than the next watershed which is the Kolyma watershed. Both of these would be amongst those with significant continuous permafrost cover, and warming may trigger feedback cycles and could have significant impacts on infrastructure where we know warming can occur more rapidly.

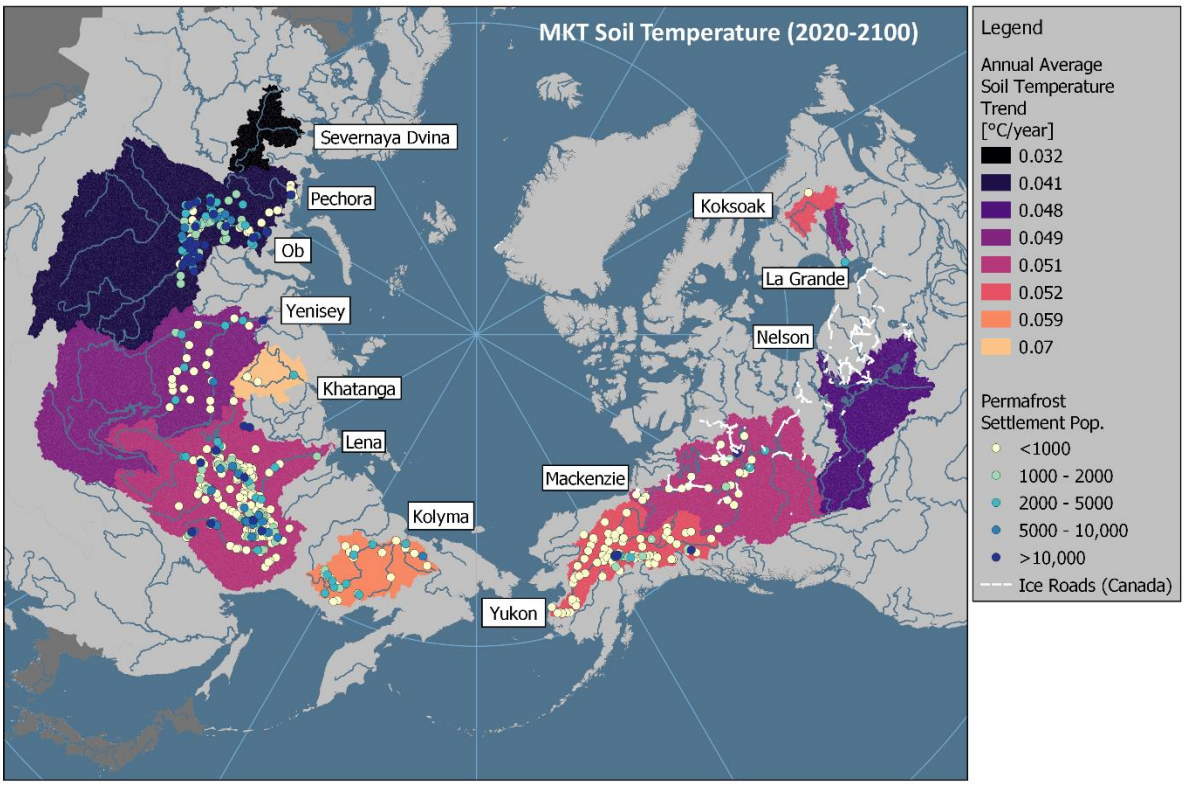

Figure 52 Future trends (slope of the pre-whitened MKT) for annual soil temperatures in the 12 Largest River Watersheds. Permafrost settlements within the 12 largest rivers and Canadian ice roads are also shown.

6.3. Model Uncertainty

There are several uncertainties in this model application, including uncertainties introduced by forcing data sets and model capability. Data uncertainly stems from the two forcing data sets, one for the historical period and the second for future projections. These data have different methods of bias correction and underlying global climate weather data. HydroGFDv3 was the data utilized for the historical period, which is a product of the

ERA5 reanalysis model, and is corrected with GPCCv8 and CRUts4.03 (Berg et al., 2021). Modelling over the future projections is done with CMIP6 data from ISIMIP. The underlying global data products are the EartH2Observe, WFDEI, and ERA-Interim data used for bias adjustments (Lange, 2019). Therefore, there is some discontinuity between the values modeled from the historical to future period. To adjust for this, trends were compared from the historical to future period, and not absolute modeled values of temperature or ice thickness.

Another limitation is the ability to assess model performance due to observed data available. Although this has been previously discussed, observational data in the Arctic does not have a broad coverage of the domain and is also done on a station basis for the model outputs analyzed here. Therefore, although we can determine how the model performs at these station locations, it is difficult to draw conclusions for the entire model domain and all possible hydrological landscapes this model covers. Due to this, model results are treated with caution and assessed on larger scales rather than trusting in model output at a subbasin scale analysis is limited to the watershed scale.

In regard to calculations of permafrost and soil temperature, the active layer thickness was not discussed or computed as a part of this thesis. There is little trust in the ability of AHYPE to calculate active layer thickness reliably, and therefore this was left out of the model output analysis and discussion. Also, permafrost cover was not explicitly calculated due to the overall positive bias in soil temperature calculations by AHYPE. Due to this, many subbasins were modeled too warm which are in the warmer permafrost area (close to 0°C) and therefore permafrost classification for the 12 largest watersheds was inaccurate as they contain a significant portion of subbasins in the warmer permafrost

range. Instead, the decision was made to discuss permafrost from the lens of soil temperature trends in warming and those results applied to how this may impact current permafrost areas.

7. Summary and Conclusion

The pan-Arctic domain experiences air temperature warming at a rate approximately 2.4 times faster than the global average. Polar amplification and climate feedback cycles, such as the release of carbon stored in permafrost thaw, ensure that any change to the terrestrial environment perpetuates further changes in climate. These impact the hydrologic cycle, ecology, and pan-Arctic communities. Studies of the pan-Arctic pose a significant challenge when solely based on observational data. Available observational records are limited due to the high cost and difficulty maintaining continuous observation stations within Arctic environments. Data-driven methods are continually improving and have rapidly evolved throughout recent decades. It remains, however, difficult for studies to gather enough reliable, temporally complete, and consistently archived data to make observations about pan-Arctic climate beyond the local scale. This is why studies of physically modeled data are required to analyze changes in the pan-Arctic environment. The pan-Arctic is very large, covering around 26 million km^2, and includes a network of diverse rivers and environments which eventually contribute their freshwater flows to the Arctic Ocean. This is how terrestrial changes in the pan-Arctic, at the global scale, impact overall global ocean circulation, and climate regulation as well. The pan-Arctic is also home to diverse habitat, and resilient communities which reside on permafrost, and rely on a frozen environment. Communities and policy makers are concerned about the risks

that permafrost thaw, increased water temperatures and losses in river ice impose on the predictability of the environment that they rely on.

This study analyzes the trends of modeled soil temperature, water temperature, and river ice thickness for the historical period (1979-2019) and future projections (2020-2100). Hydrologic modelling using the AHYPEv4 model is performed, which produces model outputs at a subbasin scale. Model performance shows that AHYPEv4 can be applied to perform large basin trend assessment for this study, but limited observational data lowers the conclusiveness of model performance at the individual subbasin scale. Analysis therefore proceeded at the continental and watershed scale, where errors tend to average out by model output aggregation.

Trends assessed in this study directly impact pan-Arctic ecology, and communities through permafrost thaw, increased water temperature and a decrease in maximum river ice thickness. Providing a new data set of modeled hydrological parameters which can be applied to further study of the pan-Arctic terrestrial and marine environment. The study introduced further novel results by utilizing the newest future climate projection data sets available. Future climate forcing data for air temperature and precipitation from various models submitted to the sixth phase of the Coupled Model Intercomparison Project, CMIP6, allow for updated future projections. To capture uncertainty of future climate projections and socioeconomic response, this study analyzes an ensemble of climate models (CanESM5, MIROC6, and MRI-ESM2-0) and future warming scenarios (ssp1-2.6 and ssp5-8.5) which capture the extreme ends of likely future changes. The study analyzes trends on various spatial scales. Firstly, for the entire pan-Arctic domain,

continental scale comparing North America and Eurasia, and at the watershed scale for the 12 largest rivers (by historical volumes).

Trends were calculated using the Mann-Kendall trend test with pre-whitening applied to annual time series. The results of the analysis showed that modeled trends of aggregated results for the entire pan-Arctic increase in the future period. Soil temperature trends increase from 0.032°C/year to 0.054°C/year, water temperature trends increase from 0.014°C/year to 0.031°C/year, and maximum ice thickness trends change from -0.062 cm/year to -0.111 cm/year. The study was also able to accomplish its objective of providing future trends at the continental scale in freshwater temperature, maximum river ice thickness, and soil temperature, a discussion of hotspots in the pan-Arctic domain by reviewing trends at the watershed scale, and a look at how future projections agree or disagree on future trends.

Future Continental Trends in Freshwater Temperature

Water temperature trends are in agreement among the continents in the future period. Future mean trends of 0.32°C/decade in North America and 0.31°C/decade are expected into the future, nearly tripling for North America which had a mean trend of 0.11°C/decade in the historical period and nearly doubling for Eurasia which had a mean trend of 0.017°C/decade. Uncertainty in future projected temperatures increases as it progresses into the future. Seasonal trends show higher warming during the months of June to September, where seasonal trends increase up to 0.53°C/decade for both continents, and the colder seasons have lower warming of around 0.2°C/decade. This poses serious concerns for the ecological impacts of water temperature changes and fish species sensitive to high temperatures will feel the most immediate effects of climate warming.

Inaction to mitigate climate warming, which is modeled by the higher warming scenarios, suggests that warming is expected to further increase around 2060. The climate model ensemble from this study is in general agreement on this. If a lower warming scenario is attained warming trends are projected to slow just before 2050 but are not expected to reverse. Inaction to mitigate climate warming is not an option if the extreme loss of Arctic ecosystems sensitive to high temperatures is to be avoided.

Future Continental Trends in River Ice Thickness

Model results for trends in maximum annual river ice thickness not surprisingly (given its complexity and variability) show the most disagreement among the climate models and continents. Losses of ice thickness and length of ice cover have already been noticed at the community scale in North America. This is concerning because projected future trends show increases in ice thickness compared to the historical period for North America. The historical period showed no statistically significant average trend, but in the future maximum ice thickness losses of -1.2 cm/decade can be expected. Eurasia shows a slight slowing in ice thickness loss from the historical to future period, with a historical trend of -1.1 cm/decade and a future trend of -1.0 cm/decade. As with water temperature, inaction to climate mitigation is expected to lead to increased losses of ice thickness after around 2055. Further impacts to communities into the future should be expected, and alternative strategies put in place where ice roads are heavily relied on for travel and the transportation of supplies.

Future Continental Trends in Soil Temperature

Soil temperature was discussed in this study in relation to permafrost thaw. Permafrost underlays a significant portion of the pan-Arctic and as such increases in soil temperature will contribute to permafrost thaw where temperature changes are great enough. Although

model performance does not provide confidence to make conclusions about the modelled temperatures, the resulting trends in temperature change are in alignment with other soil temperature studies. This study found that modeled soil temperatures below zero (those presented as permafrost in the model) are warming much faster than those above zero. As the model has an overall warm bias, soil temperatures could actually be increasing at much faster rates than what is predicted in these model results.

A strong warming signal for soil temperature increases throughout this study is detected, and soil temperature consistently provides the highest portion of significant trends among the various temporal analyses. For the entire future period, modeled soil temperature warming trends more than double for North America. Historical mean trends sit at 0.24°C/decade, and future mean trends are up to 0.57°C/decade. In Eurasia, increases into the future are not as high as it had much higher historical trends than North America. Eurasia's historical trend of 0.41°C/decade increased up to 0.52°C/decade into the future period.

Seasonal warming is modeled to be much higher in the summer months (June to September) for soil temperature. And summer average soil temperature warming trends are up 0.65°C/decade in North America and 0.57°C/decade in Eurasia. This could be due to snow cover providing an insulating effect during the other seasons and helping lower the effects of air temperature increases. There are disagreements about the effects of climate warming mitigation between the climate models. The majority of models show an increase in warming trends around 2060 with the higher warming scenarios, however, MRI-ESM2-0 projects a decrease in the trend for Eurasia and also the overall pan-Arctic.

Soil temperature warming is expected to continue to increase into the future. This poses significant risks for communities and their infrastructure as soil warming produces further permafrost thaw. This model does not include the effects of environmental changes from permafrost thaw which alter the hydrologic properties of the subbasins by increasing connectivity, erosion, and shrubification through increased temperature rises. Overall, we can conclude that actual soil temperature rise may likely be even higher than what was presented in this study because of these simplifications and due to the model's warm bias.

Hot Spots for Change

Trends at the watershed scale were presented for the identification of "hot spots" or watersheds which show more significant trends than others within the pan-Arctic. This informs future studies of which watersheds are of greatest importance when applying climate studies at the regional scale. Watersheds such as the Ob, Lena, Yukon, and Mackenzie are among the largest and contain some of the highest permafrost settlement concentrations. These watersheds are already at the top of the list for further study as mitigation and adaptation is necessary here to preserve communities and economic activity.

Future trends in water temperature did not show a particular "hot spot" since trends were reasonably consistent ranging from 0.2°C/decade to 0.4°C/decade. However, compared to historical trends, the Nelson River Watershed could be considered a hot spot for change as it had no statistically significant change in water temperature for the historical period, and the second highest trend in the future period. This could have significant impacts on communities and ice roads in this watershed. There are no permafrost

settlements reported in the Nelson watershed, however, communities still rely on water for transport and changes make the environment unpredictable.

Trends in river ice thickness show hot spots of change as large watersheds such as the Nelson, Mackenzie, Yenisey and Lena, but also the Khatanga and Kolyma which are smaller high latitude watersheds in Eurasia. These all have modeled trends in mean annual maximum river ice thickness of -0.9 to -1.1 cm/decade. The Mackenzie and Nelson watersheds contain networks of known river ice roads, and high trends in ice thicknesses losses there could significantly impact community travel and access to supply shipments. Although little information is available on Eurasian ice roads, the watersheds impacted in Eurasia likely also face the same consequences to ice thickness losses.

Trends in soil temperature show significant hot spots of warming in the two small high latitude watersheds in Eurasia, the Kolyma and Khatanga. These are the coldest in average soil temperatures and are showing the highest increases in soil temperature at 0.6°C/decade to 0.7 °C/decade. There are more permafrost settlements in the Kolyma which show a need for future study of impacts in this higher latitude watersheds. Losses of continuous permafrost cover found in these watersheds are expected to trigger significant feedback cycles, create losses in soil stability and strength, and change hydrologic conductivity.

7.1. Recommendations for Future Work

This study provides a comprehensive large scale hydrologic data set for further study of the pan-Arctic. Modelling of the marine environment, ocean circulation, and sea ice studies all benefit from improved boundary conditions which modeled freshwater flows provide. More complex marine modelling is also possible through the modelled water

temperatures which go beyond the basic contribution of freshwater volumes. Further regional studies of identified hot spots would benefit a more detailed community focused analysis to inform specific adaptation practices. In North America studies in the Mackenzie and Nelson watersheds are beneficial, as these often show significant changes in trends between the historical and future period. They also contain ice road infrastructure which remote communities heavily rely on.

Model performance would be improved through regional applications and model calibration to regional conditions as new datasets – observed and remotely sensed - emerge. Global streamflow monitoring initiatives from the remote sensing community, such as the surface water ocean topography mapping mission (SWOT), provide a significant opportunity here (Biancamaria et al., 2016).

References

Alizamir, M., Kim, S., Zounemat-Kermani, M., Heddam, S., Shahrabadi, A. H., & Gharabaghi, B. (2021). Modelling daily soil temperature by hydro-meteorological data at different depths using a novel data-intelligence model: deep echo state network model. *Artificial Intelligence Review*, *54*(4), 2863–2890. https://doi.org/10.1007/s10462-020-09915-5

Arp, C. D., Whitman, M. S., Jones, B. M., Nigro, D. A., Alexeev, V. A., Gädeke, A., Fritz, S., Daanen, R., Liljedahl, A. K., Adams, F. J., Gaglioti, B. V., Grosse, G., Heim, K. C., Beaver, J. R., Cai, L., Engram, M., & Uher-Koch, H. R. (2019). Ice roads through lake-rich Arctic watersheds: Integrating climate uncertainty and freshwater habitat responses into adaptive management. *Arctic, Antarctic, and Alpine Research*, *51*(1), 9–23. https://doi.org/10.1080/15230430.2018.1560839

Bajracharya, A., Awoye, H., Stadnyk, T., & Asadzadeh, M. (2020). Time variant sensitivity analysis of hydrological model parameters in a cold region using flow signatures. *Water (Switzerland)*, *12*(4). https://doi.org/10.3390/W12040961

Bajracharya, A. R., Ahmed, M. I., Stadnyk, T., & Asadzadeh, M. (2023). Process based calibration of a continental-scale hydrological model using soil moisture and streamflow data. *Journal of Hydrology: Regional Studies*, *47*(August 2022), 101391. https://doi.org/10.1016/j.ejrh.2023.101391

Bayatvarkeshi, M., Bhagat, S. K., Mohammadi, K., Kisi, O., Farahani, M., Hasani, A., Deo, R., & Yaseen, Z. M. (2021). Modeling soil temperature using air temperature features in diverse climatic conditions with complementary machine learning models. *Computers and Electronics in Agriculture*, *185*(April), 106158. https://doi.org/10.1016/j.compag.2021.106158

Beltaos, S., & Bonsal, B. (2021). Climate change impacts on Peace River ice thickness and implications to ice-jam flooding of Peace-Athabasca Delta, Canada. *Cold Regions Science and Technology*, *186*(December 2020), 103279. https://doi.org/10.1016/j.coldregions.2021.103279

Berg, P., Almén, F., & Bozhinova, D. (2021). HydroGFD3.0 (Hydrological Global Forcing Data): A 25 km global precipitation and temperature data set updated in near-real time. *Earth System Science Data*, *13*(4), 1531–1545. https://doi.org/10.5194/essd-13-1531-2021

Biancamaria, S., Lettenmaier, D. P., & Pavelsky, T. M. (2016). The SWOT Mission and Its Capabilities for Land Hydrology. *Surveys in Geophysics*, *37*(2), 307–337. https://doi.org/10.1007/s10712-015-9346-y

Bishop, K., & L, M. O. (2002). *Soil frost and runoff at Svartberget , northern Sweden — measurements and model analysis*. *3392*(January 2001), 3379–3392. https://doi.org/10.1002/hyp.1106

Bolduc, C., & Lamoureux, S. F. (2018). Multiyear variations in High Arctic river temperatures in response to climate variability. *Arctic Science*, *4*(4), 605–623. https://doi.org/10.1139/as-2017-0053

Bouchard, C. (2020). *Arctic Highways as Critical Infrastructure*. https://www.naadsn.ca/wp-content/uploads/2020/08/20-Aug_Bouchard_Policy-Primer-1.pdf

Box, J. E., Colgan, W. T., Christensen, T. R., Schmidt, N. M., Lund, M., Parmentier, F. J. W., Brown, R., Bhatt, U. S., Euskirchen, E. S., Romanovsky, V. E., Walsh, J. E., Overland, J. E., Wang, M., Corell, R. W., Meier, W. N., Wouters, B., Mernild, S., Mård, J., Pawlak, J., & Olsen, M. S. (2019). Key indicators of Arctic climate change: 1971-2017. *Environmental Research Letters*, *14*(4), 45010. https://doi.org/10.1088/1748-9326/aafc1b

Braun, M., Thiombiano, A. N., Vieira, M. J. F., & Stadnyk, T. A. (2021). Representing climate evolution in ensembles of GCM simulations for the Hudson Bay System. *Elementa: Science of the Anthropocene*, *9*(1), 1–19. https://doi.org/10.1525/elementa.2021.00011

Bring, A., Fedorova, I., Dibike, Y., Hinzman, L., Mård, J., Mernild, S. H., Prowse, T., Semenova, O., Stuefer, S. L., & Woo, M. K. (2016). Arctic terrestrial hydrology: A synthesis of processes, regional effects, and research challenges. *Journal of Geophysical Research G: Biogeosciences*, *121*(3), 621–649. https://doi.org/10.1002/2015JG003131

Bring, Arvid, & Destouni, G. (2011). Relevance of hydro-climatic change projection and monitoring for assessment of water cycle changes in the arctic. *Ambio*, *40*(4), 361–369. https://doi.org/10.1007/s13280-010-0109-1

Brown, K. A., Holding, J. M., & Carmack, E. C. (2020). Understanding Regional and Seasonal Variability Is Key to Gaining a Pan-Arctic Perspective on Arctic Ocean Freshening. *Frontiers in Marine Science*, *7*(August), 1–25. https://doi.org/10.3389/fmars.2020.00606

Brown, N. (2022). tsp ("Teaspoon"): A library for ground temperature data. *Journal of Open Source Software*, *7*(77), 4704. https://doi.org/10.21105/joss.04704

Calvin, K., Dasgupta, D., Krinner, G., Mukherji, A., Thorne, P. W., Trisos, C., Romero, J., Aldunce, P., Barrett, K., Blanco, G., Cheung, W. W. L., Connors, S., Denton, F., Diongue-Niang, A., Dodman, D., Garschagen, M., Geden, O., Hayward, B., Jones, C., … Ha, M. (2023). IPCC, 2023: Climate Change 2023: Synthesis Report. Contribution of Working Groups I, II and III to the Sixth Assessment Report of the Intergovernmental Panel on Climate Change [Core Writing Team, H. Lee and J. Romero (eds.)]. IPCC, Geneva, Switzerland. *European University Institute*, *2*, 2–5. https://eur-lex.europa.eu/legal-content/PT/TXT/PDF/?uri=CELEX:32016R0679&from=PT%0Ahttp://eur-lex.europa.eu/LexUriServ/LexUriServ.do?uri=CELEX:52012PC0011:pt:NOT%0Ahttps://www.ipcc.ch/report/ar6/syr/

Campana, S. E., Stefánsdóttir, R. B., Jakobsdóttir, K., & Sólmundsson, J. (2020). Shifting fish distributions in warming sub-Arctic oceans. *Scientific Reports*, *10*(1), 1–14. https://doi.org/10.1038/s41598-020-73444-y

Canada, W. S. of. (n.d.). *Historical Hydrometric Data*. https://wateroffice.ec.gc.ca/mainmenu/historical_data_index_e.html

Casagrande, F., Neto, F. A. B., de Souza, R. B., & Nobre, P. (2021). Polar amplification and ice free conditions under 1.5, 2 and 3◦c of global warming as simulated by cmip5 and cmip6 models. *Atmosphere*, *12*(11). https://doi.org/10.3390/atmos12111494

Chadburn, S. E., Burke, E. J., Cox, P. M., Friedlingstein, P., Hugelius, G., & Westermann, S. (2017). An observation-based constraint on permafrost loss as a function of global warming. *Nature Climate Change*, *7*(5), 340–344. https://doi.org/10.1038/nclimate3262

Chapin, F. S., Ruess, R., Mack, M. C., & LTER, B. C. (2022). *Bonanza Creek LTER: Hourly Soil Moisture (VWC) at Various Depths from 2002 to Present in the Bonanza Creek Experimental Forest near Fairbanks, Alaska*. Environmental Data Initiative. https://doi.org/https://doi.org/10.6073/pasta/d5b1b4d9f137271de7a9893393c8b7c8

Cold, H. S., Brinkman, T. J., Brown, C. L., Hollingsworth, T. N., Brown, D. R. N., & Heeringa, K. M. (2020). Assessing vulnerability of subsistence travel to effects of environmental change in interior Alaska. *Ecology and Society*, *25*(1). https://doi.org/10.5751/ES-11426-250120

De Rham, L., Dibike, Y., Beltaos, S., Peters, D., Bonsal, B., & Prowse, T. (2020). A Canadian River Ice Database from the National Hydrometric Program Archives. *Earth System Science Data*, *12*(3), 1835–1860. https://doi.org/10.5194/essd-12-1835-2020

Déry, S. J., & Wood, E. F. (2005). Decreasing river discharge in northern Canada. *Geophysical Research Letters*, *32*(10), 1–4. https://doi.org/10.1029/2005GL022845

Dobinski, W. (2011). Permafrost. *Earth-Science Reviews*, *108*(3–4), 158–169. https://doi.org/10.1016/j.earscirev.2011.06.007

Feng, D., Gleason, C. J., Lin, P., Yang, X., Pan, M., & Ishitsuka, Y. (2021). Recent changes to Arctic river discharge. *Nature Communications*, *12*(1), 1–9. https://doi.org/10.1038/s41467-021-27228-1

Ford, J. D., & Pearce, T. (2010). What we know, do not know, and need to know about climate change vulnerability in the western Canadian Arctic: A systematic literature review. *Environmental Research Letters*, *5*(1). https://doi.org/10.1088/1748-9326/5/1/014008

Greenan, B. J. W., James, T. S., Loder, J. W., Pepin, P., Azetsu-Scott, K., Hamme, R. C., Gilbert, D., Tremblay, J.-E., Wang, X. L., & Perrie, W. (2019). Changes in Oceans Surrounding Canada. In *Canada's Changing Climate Report: Vol. Chapter 7*.

Hanna. (1990). Evaluation of models predicting mixing depth. *Canadian Journal of Fisheries and Aquatic Sciences*, *47*, 940–947.

Henry, H. A. L. (2008). Climate change and soil freezing dynamics: Historical trends and projected changes. *Climatic Change*, *87*(3–4), 421–434. https://doi.org/10.1007/s10584-007-9322-8

Hirota, T., Pomeroy, J. W., Granger, R. J., & Maule, C. P. (2002). An extension of the force-restore method to estimating soil temperature at depth and evaluation for frozen soils under snow. *Journal of Geophysical Research Atmospheres*, *107*(24), ACL 11-1-ACL 11-10. https://doi.org/10.1029/2001JD001280

Hu, X. M., Ma, J. R., Ying, J., Cai, M., & Kong, Y. Q. (2021). Inferring future warming in the Arctic from the observed global warming trend and CMIP6 simulations. *Advances in Climate Change Research*, *12*(4), 499–507. https://doi.org/10.1016/j.accre.2021.04.002

Jiang, D., Xu, Y., Lu, Y., Gao, J., & Wang, K. (2022). Forecasting Water Temperature in Cascade Reservoir Operation-Influenced River with Machine Learning Models. *Water (Switzerland)*, *14*(14), 1–22. https://doi.org/10.3390/w14142146

Kangur, K., Ginter, K., Kangur, P., Kangur, A., Nõges, P., & Laas, A. (2016). Changes in water temperature and chemistry preceding a massive kill of bottom-dwelling fish: an analysis of high-frequency buoy data of shallow Lake Võrtsjärv (Estonia). *Inland Waters*, *6*(4), 535–542. https://doi.org/10.1080/IW-6.4.869

Kotowych, N., Smalås, A., Amundsen, P. A., & Primicerio, R. (2023). Climate warming accelerates somatic growth of an Arctic fish species in high-latitude lakes. *Scientific Reports*, *13*(1), 1–11. https://doi.org/10.1038/s41598-023-43654-1

Lammers, R. B., Pundsack, J. W., & Shiklomanov, A. I. (2007). Variability in river temperature, discharge, and energy flux from the Russian pan-Arctic landmass. *Journal of Geophysical Research: Biogeosciences*, *112*(4), 1–15. https://doi.org/10.1029/2006JG000370

Lange, S. (2019). Trend-preserving bias adjustment and statistical downscaling with ISIMIP3BASD (v1.0). *Geoscientific Model Development*, *12*(7), 3055–3070. https://doi.org/10.5194/gmd-12-3055-2019

Lange, S. (2021). *ISIMIP3b bias adjustment fact sheet*. 39. https://www.isimip.org/documents/413/ISIMIP3b_bias_adjustment_fact_sheet_Gnsz7CO.pdf

Leach, J. A., & Moore, R. D. (2019). Empirical Stream Thermal Sensitivities May Underestimate Stream Temperature Response to Climate Warming. *Water Resources Research*, *55*(7), 5453–5467. https://doi.org/10.1029/2018WR024236

LeBlanc, R. T., Brown, R. D., & FitzGibbon, J. E. (1997). Modeling the effects of land use change on the water temperature in unregulated urban streams. *Journal of Environmental Management*, *49*(4), 445–469. https://doi.org/10.1006/jema.1996.0106

Lembrechts, J. J., van den Hoogen, J., Aalto, J., Ashcroft, M. B., De Frenne, P., Kemppinen, J., Kopecký, M., Luoto, M., Maclean, I. M. D., Crowther, T. W., Bailey, J. J., Haesen, S., Klinges, D. H., Niittynen, P., Scheffers, B. R., Van Meerbeek, K., Aartsma, P., Abdalaze, O., Abedi, M., … Lenoir, J. (2022). Global maps of soil temperature. *Global Change Biology*, *28*(9), 3110–3144. https://doi.org/10.1111/gcb.16060

Lepparanta, M. (1983). A growth model for black ice, snow ice and snow thickness in subarctic basins. *Nordic Hydrology*, *14*(2), 59–70. https://doi.org/10.2166/nh.1983.0006

Lepparanta, Matti. (1993). A review of analytical models of sea-ice growth. *Atmosphere - Ocean*, *31*(1), 123–138. https://doi.org/10.1080/07055900.1993.9649465

Martens, B., Miralles, D. G., Lievens, H., Van Der Schalie, R., De Jeu, R. A. M., Fernández-Prieto, D., Beck, H. E., Dorigo, W. A., & Verhoest, N. E. C. (2017). GLEAM v3: Satellite-based land evaporation and root-zone soil moisture. *Geoscientific Model Development*, *10*(5), 1903–1925. https://doi.org/10.5194/gmd-10-1903-2017

McClelland, J. W., Holmes, R. M., Peterson, B. J., & Stieglitz, M. (2004). Increasing river discharge in the Eurasian Arctic: Consideration of dams, permafrost thaw, and fires as potential agents of change. *Journal of Geophysical Research Atmospheres*, *109*(18), 1–12. https://doi.org/10.1029/2004JD004583

Mehdizadeh, S., Ahmadi, F., & Kozekalani Sales, A. (2020). Modelling daily soil temperature at different depths via the classical and hybrid models. *Meteorological Applications*, *27*(4), 1–15. https://doi.org/10.1002/met.1941

Meinshausen, M., Nicholls, Z. R. J., Lewis, J., Gidden, M. J., Vogel, E., Freund, M., Beyerle, U., Gessner, C., Nauels, A., Bauer, N., Canadell, J. G., Daniel, J. S., John, A., Krummel, P. B., Luderer, G., & Meinshausen, N. (2020). *The shared socio-economic pathway (SSP) greenhouse gas concentrations and their extensions to 2500*. 3571–3605.

Meredith, M., Sommerkorn, M., Cassotta, S., Derksen, C., Ekaykin, A., Hollowed, A., Kofinas, G., Mackintosh, A., Melbourne-Thomas, J., Muelbert, M. M. C., Ottersen, G., Pritchard, H., & Schuur, E. A. G. (2019). Polar regions. In *IPCC Special Report on the Ocean and Cryosphere in a Changing Climate*. https://doi.org/10.1016/S1366-7017(01)00066-6

Miralles, D. G., Holmes, T. R. H., De Jeu, R. A. M., Gash, J. H., Meesters, A. G. C. A., & Dolman, A. J. (2011). Global land-surface evaporation estimated from satellite-based observations. *Hydrology and Earth System Sciences*, *15*(2), 453–469. https://doi.org/10.5194/hess-15-453-2011

Mohammadi, Z., & Hayley, J. L. (2023). Qualitative evaluation of thaw settlement potential in permafrost regions of Canada. *Cold Regions Science and Technology*, *216*(August), 104005. https://doi.org/10.1016/j.coldregions.2023.104005

Muñoz-Carpena, R., Carmona-Cabrero, A., Yu, Z., Fox, G., & Batelaan, O. (2023). Convergence of mechanistic modeling and artificial intelligence in hydrologic science and engineering. *PLOS Water*, *2*(8), e0000059. https://doi.org/10.1371/journal.pwat.0000059

Null, S. E., Viers, J. H., Deas, M. L., Tanaka, S. K., & Mount, J. F. (2013). Stream temperature sensitivity to climate warming in California's Sierra Nevada: Impacts to coldwater habitat. *Climatic Change*, *116*(1), 149–170. https://doi.org/10.1007/s10584-012-0459-8

Oelke, C., & Zhang, T. (2004). A model study of circum-arctic soil temperatures. *Permafrost and Periglacial Processes*, *15*(2), 103–121. https://doi.org/10.1002/ppp.485

Park, H., Yoshikawa, Y., Oshima, K., Kim, Y., Ngo-Duc, T., Kimball, J. S., & Yang, D. (2016). Quantification of warming climate-induced changes in terrestrial Arctic river ice thickness and phenology. *Journal of Climate*, *29*(5), 1733–1754. https://doi.org/10.1175/JCLI-D-15-0569.1

Park, H., Yoshikawa, Y., Yang, D., & Oshima, K. (2017). Warming water in arctic terrestrial rivers under climate change. *Journal of Hydrometeorology*, *18*(7), 1983–1995. https://doi.org/10.1175/JHM-D-16-0260.1

Pettitt, A. N. (1979). A Non-Parametric Approach to the Change-Point Problem Published by : Wiley for the Royal Statistical Society A Non-parametric Approach to the Change-point Problem. *Journal of the Royal Statistical Society. Series C (Applied Statistics)*, *28*(2), 126–135.

Podkowa, A., Kugler, Z., Nghiem, S. V., & Brakenridge, G. R. (2023). Ice Freeze-Up and Break-Up in Arctic Rivers Observed With Satellite L-Band Passive Microwave Data From 2010 to 2020. *Water Resources Research*, *59*(6). https://doi.org/10.1029/2022wr031939

Pörtner, H.-O., Roberts, D. C., Masson-Delmotte, V., Zhai, P., Poloczanska, E., Mintenbeck, K., Tignor, M., Alegría, A., Nicolai, M., Okem, A., Petzold, J., Rama, B., Weyer, N. M., & (eds.). (2019). IPCC, 2019: Technical Summary. In *IPCC Special Report on the Ocean and Cryosphere in a Changing Climate*. Cambridge University Press. https://doi.org/10.1017/9781009157964.002

Prowse, T., Bring, A., Mård, J., & Carmack, E. (2015). Arctic freshwater synthesis: Introduction. *Journal of Geophysical Research: Biogeosciences*, *120*(11), 2121–2131. https://doi.org/10.1002/2015JG003127

Prowse, T. D., Furgal, C., Chouinard, R., Melling, H., Milburn, D., & Smith, S. L. (2009). Implications of climate change for economic development in Northern Canada: Energy, resource, and transportation sectors. *Ambio*, *38*(5), 272–281. https://doi.org/10.1579/0044-7447-38.5.272

Prowse, Terry, Alfredsen, K., Beltaos, S., Bonsal, B., Duguay, C., Korhola, A., McNamara, J., Pienitz, R., Vincent, W. F., Vuglinsky, V., & Weyhenmeyer, G. A. (2011). Past and future changes in arctic lake and river ice. *Ambio*, *40*(SUPPL. 1), 53–62. https://doi.org/10.1007/s13280-011-0216-7

Ramage, J., Jungsberg, L., Wang, S., Westermann, S., Lantuit, H., & Heleniak, T. (2021). Population living on permafrost in the Arctic. *Population and Environment*, *43*(1), 22–38. https://doi.org/10.1007/s11111-020-00370-6

Razavi, S., Tolson, B. A., & Burn, D. H. (2012). Review of surrogate modeling in water resources. *Water Resources Research*, *48*(7). https://doi.org/10.1029/2011WR011527

Rosenzweig, C., Arnell, N. W., Ebi, K. L., Lotze-Campen, H., Raes, F., Rapley, C., Smith, M. S., Cramer, W., Frieler, K., Reyer, C. P. O., Schewe, J., Van Vuuren, D., & Warszawski, L. (2017). Assessing inter-sectoral climate change risks: The role of ISIMIP. *Environmental Research Letters*, *12*(1). https://doi.org/10.1088/1748-9326/12/1/010301

Royer, A., Picard, G., Vargel, C., Langlois, A., Gouttevin, I., & Dumont, M. (2021). Improved Simulation of Arctic Circumpolar Land Area Snow Properties and Soil Temperatures. *Frontiers in Earth Science*, *9*(June), 1–19. https://doi.org/10.3389/feart.2021.685140

Sadler, J. M., Appling, A. P., Read, J. S., Oliver, S. K., Jia, X., Zwart, J. A., & Kumar, V. (2022). Multi-Task Deep Learning of Daily Streamflow and Water Temperature. *Water Resources Research*, *58*(4), 1–18. https://doi.org/10.1029/2021WR030138

Sahoo, G. B., Schladow, S. G., & Reuter, J. E. (2009). Forecasting stream water temperature using regression analysis, artificial neural network, and chaotic non-linear dynamic models. *Journal of Hydrology*, *378*(3–4), 325–342. https://doi.org/10.1016/j.jhydrol.2009.09.037

Sándor, R., & Fodor, N. (2012). Simulation of soil temperature dynamics with models using different concepts. *The Scientific World Journal*, *2012*. https://doi.org/10.1100/2012/590287

Schneider Von Deimling, T., Lee, H., Ingeman-Nielsen, T., Westermann, S., Romanovsky, V., Lamoureux, S., Walker, D. A., Chadburn, S., Trochim, E., Cai, L., Nitzbon, J., Jacobi, S., & Langer, M. (2021). Consequences of permafrost degradation for Arctic infrastructure - Bridging the model gap between regional and engineering scales. *Cryosphere*, *15*(5), 2451–2471. https://doi.org/10.5194/tc-15-2451-2021

Shervan, G., & Knoben, W. J. M. (2019). *easymore* (0.0.0). https://doi.org/10.5281/zenodo.2628350

Singh, J., Knapp, H. V., Arnold, J. G., & Demissie, M. (2005). Hydrological modeling of the Iroquois River watershed using HSPF and SWAT. *Journal of the American Water Resources Association*, *41*(2), 343–360. https://doi.org/10.1111/j.1752-1688.2005.tb03740.x

SMHI. (2023a). *Land routines [HYPE Model Documentation]*. http://www.smhi.net/hype/wiki/doku.php?id=start:hype_model_description:hype_land

SMHI. (2023b). *Tracers [HYPE Model Documentation]*. http://www.smhi.net/hype/wiki/doku.php?id=start:hype_model_description:hype_tracer

Smith, D. M., Screen, J. A., Deser, C., Cohen, J., Fyfe, J. C., García-Serrano, J., Jung, T., Kattsov, V., Matei, D., Msadek, R., Peings, Y., Sigmond, M., Ukita, J., & Zhang, X. (2019). The Polar Amplification Model Intercomparison Project (PAMIP) contribution to CMIP6: Investigating the causes and consequences of polar amplification. *Geoscientific Model Development*, *12*(3), 1139–1164. https://doi.org/10.5194/gmd-12-1139-2019

Smith, S. L., Romanovsky, V. E., Lewkowicz, A. G., Burn, C. R., Allard, M., Clow, G. D., Yoshikawa, K., & Throop, J. (2010). Thermal state of permafrost in North America: A contribution to the international polar year. *Permafrost and Periglacial Processes*, *21*(2), 117–135. https://doi.org/10.1002/ppp.690

Smith, Sharon L., O'Neill, H. B., Isaksen, K., Noetzli, J., & Romanovsky, V. E. (2022). The changing thermal state of permafrost. *Nature Reviews Earth and Environment*, *3*(1), 10–23. https://doi.org/10.1038/s43017-021-00240-1

Souaissi, Z., Ouarda, T. B. M. J., & St-Hilaire, A. (2023). Non-parametric, semi-parametric, and machine learning models for river temperature frequency analysis at ungauged basins. *Ecological Informatics*, *75*(April). https://doi.org/10.1016/j.ecoinf.2023.102107

Stadnyk, T. A., & Déry, S. J. (2021). Canadian continental-scale hydrology under a changing climate: A review. *Water (Switzerland)*, *13*(7), 1–14. https://doi.org/10.3390/w13070906

Stadnyk, T. A., MacDonald, M. K., Tefs, A., Déry, S. J., Koenig, K., Gustafsson, D., Isberg, K., & Arheimer, B. (2020). Hydrological modeling of freshwater discharge into Hudson Bay using HYPE. *Elementa: Science of the Anthropocene*, *8*. https://doi.org/10.1525/elementa.439

Stadnyk, T. A., Tefs, A. A. G., Broesky, M., Dery, S. J., Myers, P. G., Ridenour, N. A., Vonderbank, L., & Gustafsson, D. (2021). Changing freshwater contributions to the Arctic: a 90-year trend analysis (1981-2070). *Elementa: Science of the Anthropocene*, 1–26.

Tam, B. Y., Gough, W. A., Edwards, V., & Tsuji, L. J. S. (2013). The impact of climate change on the well-being and lifestyle of a First Nation community in the western James Bay region. *Canadian Geographer*, *57*(4), 441–456. https://doi.org/10.1111/j.1541-0064.2013.12033.x

Thellman, A., Jankowski, K. J., Hayden, B., Yang, X., Dolan, W., Smits, A. P., & O'Sullivan, A. M. (2021). The Ecology of River Ice. *Journal of Geophysical Research: Biogeosciences*, *126*(9), 1–28. https://doi.org/10.1029/2021JG006275

United States Fish Wildlife and Service. (2017). *In-situ stream temperature monitoring, Alaska*. Knowledge Network for Biocomplexity. https://doi.org/doi:10.5063/F19W0CRM

Václavík, T., Lautenbach, S., Kuemmerle, T., & Seppelt, R. (2013). Mapping global land system archetypes. *Global Environmental Change*, *23*(6), 1637–1647. https://doi.org/10.1016/j.gloenvcha.2013.09.004

Van Vliet, M. T.H., Ludwig, F., Zwolsman, J. J. G., Weedon, G. P., & Kabat, P. (2011). Global river temperatures and sensitivity to atmospheric warming and changes in river flow. *Water Resources Research*, *47*(2). https://doi.org/10.1029/2010WR009198

Van Vliet, Michelle T.H., Franssen, W. H. P., Yearsley, J. R., Ludwig, F., Haddeland, I., Lettenmaier, D. P., & Kabat, P. (2013). Global river discharge and water temperature under climate change. *Global Environmental Change*, *23*(2), 450–464. https://doi.org/10.1016/j.gloenvcha.2012.11.002

Verstraeten, G., Poesen, J., Demarée, G., & Salles, C. (2006). Long-term (105 years) variability in rain erosivity as derived from 10-min rainfall depth data for Ukkel (Brussels, Belgium): Implications for assessing soil erosion rates. *Journal of Geophysical Research Atmospheres*, *111*(22), 1–11. https://doi.org/10.1029/2006JD007169

Vincent, L. A., Zhang, X., Brown, R. D., Feng, Y., Mekis, E., Milewska, E. J., Wan, H., & Wang, X. L. (2015). Observed trends in Canada's climate and influence of low-frequency variability modes. *Journal of Climate*, *28*(11), 4545–4560. https://doi.org/10.1175/JCLI-D-14-00697.1

Vuglinsky, V. (2000a). *Russian River Ice Thickness and Duration, 1917 - 1992*. National Snow and Ice Data Center. https://doi.org/https://doi.org/10.7265/N5J10129

Vuglinsky, V. (2000b). *Russian River Ice Thickness and Duration, 1917 - 1992*. https://doi.org/10.7265/N5K10129

Walsh, J. E., Anisimov, O., Hagen, J. O. M., Jakobsson, T., Oerlemans, J., Prowse, T. D., Romanovsky, V., Savelieva, N., Serreze, M., Shiklomanov, A. I., Shiklomanov, I. A., & Solomon, S. (2005). Cryosphere and Hydrology. In *Arctic Climate Impact Assessment*.

Walvoord, M. A., & Kurylyk, B. L. (2016). Hydrologic Impacts of Thawing Permafrost-A Review. *Vadose Zone Journal*, *15*(6), vzj2016.01.0010. https://doi.org/10.2136/vzj2016.01.0010

Walvoord, M. A., & Striegl, R. G. (2007). Increased groundwater to stream discharge from permafrost thawing in the Yukon River basin: Potential impacts on lateral export of carbon and nitrogen. *Geophysical Research Letters*, *34*(12). https://doi.org/10.1029/2007GL030216

Wanders, N., van Vliet, M. T. H., Wada, Y., Bierkens, M. F. P., & van Beek, L. P. H. (Rens. (2019). High-Resolution Global Water Temperature Modeling. *Water Resources Research*, *55*(4), 2760–2778. https://doi.org/10.1029/2018WR023250

Weierbach, H., Lima, A. R., Willard, J. D., Hendrix, V. C., Christianson, D. S., Lubich, M., & Varadharajan, C. (2022). Stream Temperature Predictions for River Basin Management in the Pacific Northwest and Mid-Atlantic Regions Using Machine Learning. *Water (Switzerland)*, *14*(7), 1–21. https://doi.org/10.3390/w14071032

Westerveld, L., Kurvits, T., Schoolmeester, T., Mulelid, O. B., Eckhoff, T. S., P., O. P., Fritz, M., Lantuit, H., Alfthan, B., Sinisalo, A., Miesner, F., Viitanen, L.-K., & NUNATARYUK consortium. (2023). *Arctic Permafrost Atlas*. GRID-Arendal.

Wilde, F. D. (2006). Temperature. In *U.S. Geological Survey Techniques of Water-Resources Investigations* (book 9, pp. 3–15). USGS. https://doi.org/https://doi.org/10.3133/twri09A6.1

Yang, D., Kane, D. L., Hinzman, L. D., Zhang, X., Zhang, T., & Ye, H. (2002). Siberian Lena River hydrologic regime and recent change. *Journal of Geophysical Research Atmospheres*, *107*(23), ACL 14-1-ACL 14-10. https://doi.org/10.1029/2002JD002542

Yang, D., & Peterson, A. (2017). River water temperature in relation to local air temperature in the Mackenzie and Yukon basins. *Arctic*, *70*(1), 47–58. https://doi.org/10.14430/arctic4627

Yang, D., Shrestha, R. R., Lung, J. L. Y., Tank, S., & Park, H. (2021). Heat flux, water temperature and discharge from 15 northern Canadian rivers draining to Arctic Ocean and Hudson Bay. *Global and Planetary Change*, *204*, 103577. https://doi.org/10.1016/j.gloplacha.2021.103577

Yearsley, J. (2012). A grid-based approach for simulating stream temperature. *Water Resources Research*, *48*(3), 1–15. https://doi.org/10.1029/2011WR011515

Yue, S., Pilon, P., Phinney, B., & Cavadias, G. (2002). The influence of autocorrelation on the ability to detect trend in hydrological series. *Hydrological Processes*, *16*(9), 1807–1829. https://doi.org/10.1002/hyp.1095

Zheng, D., Hunt, E. R., & Running, S. W. (1993). A daily soil temperature model based on air temperature and precipitation for continental applications. *Climate Research*, *2*(3), 183–191. https://doi.org/10.3354/cr002183

Zhu, S., Nyarko, E. K., & Hadzima-Nyarko, M. (2018). Modelling daily water temperature from air temperature for the Missouri River. *PeerJ*, *2018*(6), 1–19. https://doi.org/10.7717/peerj.4894

Zhu, S., & Piotrowski, A. P. (2020). River/stream water temperature forecasting using artificial intelligence models: a systematic review. *Acta Geophysica*, *68*(5), 1433–1442. https://doi.org/10.1007/s11600-020-00480-7

Zimov, S. A., Schuur, E. A. G., & Stuart Chapin, F. (2006). Permafrost and the global carbon budget. *Science*, *312*(5780), 1612–1613. https://doi.org/10.1126/science.1128908

Appendix A – Observation Metadata

Table A- 1 Soil temperature observation stations metadata, including the SUBID within each station is contained.

AGENCY	*STATION*	*LAT*	*LON*	*ELEV*	*DEPTH [m]*	*SUBID*
BNZ-LTER	FP1A	64.6986	-148.26	184.42	1	116437
BNZ-LTER	FP2A	64.6988	-148.25	184.42	1	116437
BNZ-LTER	FP3A	64.7232	-148.15	129.9	1	116437
BNZ-LTER	FP4A	64.6788	-148.24	443.49	1	116915
BNZ-LTER	FP5A	64.6815	-148.25	443.49	1	116915
BNZ-LTER	LTER1	64.743	-148.32	443.49	1	125248
BNZ-LTER	LTER2	64.6989	-148.25	184.42	1	116437
BNZ-LTER	UP1A	64.7355	-148.3	443.49	1	116437
BNZ-LTER	UP2A	64.6955	-148.36	443.49	1	125248
BNZ-LTER	UP3A	64.7674	-148.28	423.54	1	116437
SCAN	Aniak	61.58	-159.58	17.36	1.02	127997
SCAN	Canyon_Lake	59.4243	-161.16	167.64	1.02	122480
SCAN	Canyon_Lake	59.4243	-161.16	167.64	1.02	122480
SCAN	Checkers_Creek	65.403	-164.71	99.36	1.02	127020
SCAN	Checkers_Creek	65.403	-164.71	99.36	1.02	127020
SCAN	Kanaryagak_Camp	61.36	-165.12	8.03	1.02	128245
SCAN	Kanuti_Lake	66.177	-151.74	159.72	1.02	125983
SCAN	Kanuti_Lake	66.177	-151.74	159.72	1.02	125983
SCAN	Lower_Mulchatna	59.82	-156.99	96.67	1.02	126955
SCAN	Lower_Mulchatna	59.82	-156.99	96.67	1.02	126955
SCAN	Naknek_River	58.67	-156.57	24.41	1.02	120731
SCAN	Naknek_River	58.67	-156.57	24.41	1.02	120731
SCAN	Nenana	64.683	-148.92	126.49	1.02	125248
SCAN	Schor_Garden	59.683	-151.38	119.79	1.09	103838
SCAN	Spring_Creek	61.6572	-149.13	176.78	1.02	126925
SCAN	Tok	63.35	-142.98	494	1.02	126987
SCAN	Tok	63.35	-142.98	494	1.02	126987
SCAN	Tok	63.35	-142.98	494	1.02	126987
SCAN	Weary_Lake	59.13	-159.09	9.79	1.02	115402
SCAN	Weary_Lake	59.13	-159.09	9.79	1.02	115402
SCAN	Weary_Lake	59.13	-159.09	9.79	1.02	115402
USCRN	Kenai_29_ENE	60.7257	-150.45	282	1	121089
BNZ-LTER	FP1A	64.6986	-148.26	184.42	0.2	116437
BNZ-LTER	FP2A	64.6988	-148.25	184.42	0.2	116437
BNZ-LTER	FP3A	64.7232	-148.15	129.9	0.2	116437

BNZ-LTER	FP4A	64.6788	-148.24	443.49	0.2	116915
BNZ-LTER	FP5A	64.6815	-148.25	443.49	0.2	116915
BNZ-LTER	LTER1	64.743	-148.32	443.49	0.2	125248
BNZ-LTER	LTER2	64.6989	-148.25	184.42	0.2	116437
BNZ-LTER	UP1A	64.7355	-148.3	443.49	0.2	116437
BNZ-LTER	UP2A	64.6955	-148.36	443.49	0.2	125248
BNZ-LTER	UP3A	64.7674	-148.28	423.54	0.2	116437
SCAN	Aniak	61.58	-159.58	17.36	0.2	127997
SCAN	Canyon_Lake	59.4243	-161.16	167.64	0.2	122480
SCAN	Canyon_Lake	59.4243	-161.16	167.64	0.2	122480
SCAN	Hozatka_Lake	65.198	-156.64	62.79	0.2	128008
SCAN	Hozatka_Lake	65.198	-156.64	62.79	0.2	128008
SCAN	Ikalukrok_Creek	68.08	-163	266.13	0.2	127027
SCAN	Kanaryagak_Camp	61.36	-165.12	8.03	0.2	128245
SCAN	Kanaryagak_Camp	61.36	-165.12	8.03	0.2	128245
SCAN	Kanuti_Lake	66.177	-151.74	159.72	0.2	125983
SCAN	Kanuti_Lake	66.177	-151.74	159.72	0.2	125983
SCAN	Lower_Mulchatna	59.82	-156.99	96.67	0.2	126955
SCAN	Lower_Mulchatna	59.82	-156.99	96.67	0.2	126955
SCAN	Lower_Mulchatna	59.82	-156.99	96.67	0.2	126955
SCAN	Naknek_River	58.67	-156.57	24.41	0.2	120731
SCAN	Naknek_River	58.67	-156.57	24.41	0.2	120731
SCAN	Nenana	64.683	-148.92	126.49	0.2	125248
SCAN	Nenana	64.683	-148.92	126.49	0.2	125248
SCAN	Nenana	64.683	-148.92	126.49	0.2	125248
SCAN	Schor_Garden	59.683	-151.38	119.79	0.25	103838
SCAN	Spring_Creek	61.6572	-149.13	176.78	0.2	126925
SCAN	Tok	63.35	-142.98	494	0.2	126987
SCAN	Unalakleet	63.9133	-160.75	88.39	0.2	127538
SCAN	Unalakleet	63.9133	-160.75	88.39	0.2	127538
SCAN	Ward_Farm	63.95	-145.08	384.05	0.2	117603
SCAN	Weary_Lake	59.13	-159.09	9.79	0.2	115402
SCAN	Weary_Lake	59.13	-159.09	9.79	0.2	115402
SCAN	Weary_Lake	59.13	-159.09	9.79	0.2	115402
SNOTEL	ANCHOR_RIVER_DIVIDE	59.86	-151.32	503.83	0.2	127381
SNOTEL	ATIGUN_PASS	68.13	-149.48	1463.04	0.2	126508
SNOTEL	COLDFOOT	67.25	-150.18	316.99	0.2	127006
SNOTEL	EAGLE_SUMMIT	65.49	-145.41	1112.52	0.2	126742
SNOTEL	EXIT_GLACIER	60.19	-149.62	121.92	0.2	106153
SNOTEL	GOBBLERS_KNOB	66.75	-150.67	618.74	0.2	126826

SNOTEL	GRANITE_CRK	63.94	-145.4	377.95	0.2	117603
SNOTEL	IKALUKROK_CREEK	68.08	-163	198.12	0.2	127027
SNOTEL	IMNAVIAT_CREEK	68.62	-149.3	929.64	0.2	127211
SNOTEL	KENAI_MOOSE_PENS	60.73	-150.48	91.44	0.2	121089
SNOTEL	LITTLE_CHENA_RIDGE	65.12	-146.73	609.6	0.2	115571
SNOTEL	McNeil_River_SGS	59.08	-154.28	448.65	0.2	106691
SNOTEL	MONAHAN_FLAT	63.31	-147.65	826.01	0.2	126998
SNOTEL	MONUMENT_CREEK	65.08	-145.87	563.88	0.2	123042
SNOTEL	MONUMENT_CREEK	65.08	-145.87	563.88	0.2	123042
SNOTEL	MOORE_CREEK_BRIDGE	59.59	-135.21	685.8	0.2	127396
SNOTEL	MT._RYAN	65.25	-146.15	853.44	0.2	123042
SNOTEL	MUNSON_RIDGE	64.85	-146.21	944.88	0.2	126990
SNOTEL	NUKA_GLACIER	59.7	-150.71	381	0.2	107385
SNOTEL	POINT_MACKENZIE	61.39	-150.03	76.2	0.2	107910
SNOTEL	PORT_GRAHAM	59.35	-151.85	91.44	0.2	127736
SNOTEL	PRUDHOE_BAY	70.27	-148.57	9.14	0.2	129583
SNOTEL	ROCKY_POINT	64.53	-163.42	76.2	0.2	128738
SNOTEL	SUMMIT_CREEK	60.62	-149.53	426.72	0.2	126916
SNOTEL	SUSITNA_VALLEY_HIGH	62.13	-150.04	114.3	0.2	100710
SNOTEL	TOKOSITNA_VALLEY	62.63	-150.78	259.08	0.2	117424
SNOTEL	UPPER_NOME_CREEK	65.37	-146.59	768.1	0.2	126165
SNOTEL	UPPER_TSAINA_RIVER	61.19	-145.65	533.4	0.2	121454
USCRN	Kenai_29_ENE	60.7257	-150.45	282	0.2	121089

Table A- 2 Soil moisture observation stations metadata, including the SUBID within each station is contained.

AGENCY	*STATION*	*LON*	*LAT*	*ELEV*	*DEPTH [m]*	*SUBID*
SCAN	Aniak	61.6	-159.6	17.36	1.02	127997
SCAN	Canyon_Lake	59.4	-161.2	167.64	1.02	122480
SCAN	Canyon_Lake	59.4	-161.2	167.64	1.02	122480
SCAN	Naknek_River	58.7	-156.6	24.41	1.02	120731
SCAN	Naknek_River	58.7	-156.6	24.41	1.02	120731
SCAN	Nenana	64.7	-148.9	126.49	1.02	125248
SCAN	Schor_Garden	59.7	-151.4	119.79	1.09	103838
SCAN	Spring_Creek	61.7	-149.1	176.78	1.02	126925
SCAN	Tok	63.4	-143.0	494	1.02	126987
SCAN	Weary_Lake	59.1	-159.1	9.79	1.02	115402
SCAN	Weary_Lake	59.1	-159.1	9.79	1.02	115402
SCAN	Weary_Lake	59.1	-159.1	9.79	1.02	115402
USCRN	Kenai_29_ENE	60.7	-150.5	282	1	121089
BNZ-LTER	FP1A	64.7	-148.3	184.42	0.2	116437
BNZ-LTER	FP2A	64.7	-148.3	184.42	0.2	116437
BNZ-LTER	FP3A	64.7	-148.2	129.9	0.2	116437
BNZ-LTER	FP4A	64.7	-148.2	443.49	0.2	116915
BNZ-LTER	FP5A	64.7	-148.2	443.49	0.2	116915
BNZ-LTER	LTER1	64.7	-148.3	443.49	0.2	125248
BNZ-LTER	LTER2	64.7	-148.3	184.42	0.2	116437
BNZ-LTER	UP1A	64.7	-148.3	443.49	0.2	116437
BNZ-LTER	UP2A	64.7	-148.4	443.49	0.2	125248
BNZ-LTER	UP3A	64.8	-148.3	423.54	0.2	116437
SCAN	Aniak	61.6	-159.6	17.36	0.2	127997
SCAN	Canyon_Lake	59.4	-161.2	167.64	0.2	122480
SCAN	Canyon_Lake	59.4	-161.2	167.64	0.2	122480
SCAN	Checkers_Creek	65.4	-164.7	99.36	0.2	127020
SCAN	Checkers_Creek	65.4	-164.7	99.36	0.2	127020
SCAN	Gulkana_River	62.4	-145.4	557.78	0.2	104023
SCAN	Ikalukrok_Creek	68.1	-163.0	266.13	0.2	127027
SCAN	Kanuti_Lake	66.2	-151.7	159.72	0.2	125983

SCAN	Kanuti_Lake	66.2	-151.7	159.72	0.2	125983
SCAN	Lower_Mulchatna	59.8	-157.0	96.67	0.2	126955
SCAN	Lower_Mulchatna	59.8	-157.0	96.67	0.2	126955
SCAN	Naknek_River	58.7	-156.6	24.41	0.2	120731
SCAN	Naknek_River	58.7	-156.6	24.41	0.2	120731
SCAN	Naknek_River	58.7	-156.6	24.41	0.2	120731
SCAN	Naknek_River	58.7	-156.6	24.41	0.2	120731
SCAN	Nenana	64.7	-148.9	126.49	0.2	125248
SCAN	Nenana	64.7	-148.9	126.49	0.2	125248
SCAN	Nenana	64.7	-148.9	126.49	0.2	125248
SCAN	Schor_Garden	59.7	-151.4	119.79	0.25	103838
SCAN	Spring_Creek	61.7	-149.1	176.78	0.2	126925
SCAN	Unalakleet	63.9	-160.7	88.39	0.2	127538
SCAN	Ward_Farm	64.0	-145.1	384.05	0.2	117603
SCAN	Weary_Lake	59.1	-159.1	9.79	0.2	115402
SCAN	Weary_Lake	59.1	-159.1	9.79	0.2	115402
SCAN	Weary_Lake	59.1	-159.1	9.79	0.2	115402
SNOTEL	ANCHOR_RIVER_DIVIDE	59.9	-151.3	503.83	0.2	127381
SNOTEL	ATIGUN_PASS	68.1	-149.5	1463.04	0.2	126508
SNOTEL	COLDFOOT	67.3	-150.2	316.99	0.2	127006
SNOTEL	EAGLE_SUMMIT	65.5	-145.4	1112.52	0.2	126742
SNOTEL	EXIT_GLACIER	60.2	-149.6	121.92	0.2	106153
SNOTEL	GOBBLERS_KNOB	66.8	-150.7	618.74	0.2	126826
SNOTEL	GRANITE_CRK	63.9	-145.4	377.95	0.2	117603
SNOTEL	IKALUKROK_CREEK	68.1	-163.0	198.12	0.2	127027
SNOTEL	IMNAVIAT_CREEK	68.6	-149.3	929.64	0.2	127211
SNOTEL	KELLY_STATION	67.9	-162.3	94.49	0.2	127024
SNOTEL	KENAI_MOOSE_PENS	60.7	-150.5	91.44	0.2	121089
SNOTEL	LITTLE_CHENA_RIDGE	65.1	-146.7	609.6	0.2	115571
SNOTEL	McNeil_River_SGS	59.1	-154.3	448.65	0.2	106691
SNOTEL	MONAHAN_FLAT	63.3	-147.7	826.01	0.2	126998
SNOTEL	MONUMENT_CREEK	65.1	-145.9	563.88	0.2	123042
SNOTEL	MONUMENT_CREEK	65.1	-145.9	563.88	0.2	123042
SNOTEL	MOORE_CREEK_BRIDGE	59.6	-135.2	685.8	0.2	127396
SNOTEL	MT._RYAN	65.3	-146.2	853.44	0.2	123042
SNOTEL	MUNSON_RIDGE	64.9	-146.2	944.88	0.2	126990
SNOTEL	NUKA_GLACIER	59.7	-150.7	381	0.2	107385
SNOTEL	POINT_MACKENZIE	61.4	-150.0	76.2	0.2	107910
SNOTEL	PORT_GRAHAM	59.4	-151.9	91.44	0.2	127736
SNOTEL	PRUDHOE_BAY	70.3	-148.6	9.14	0.2	129583
SNOTEL	SUMMIT_CREEK	60.6	-149.5	426.72	0.2	126916
SNOTEL	SUSITNA_VALLEY_HIGH	62.1	-150.0	114.3	0.2	100710
SNOTEL	TOKOSITNA_VALLEY	62.6	-150.8	259.08	0.2	117424

SNOTEL	UPPER_NOME_CREEK	65.4	-146.6	768.1	0.2	126165
SNOTEL	UPPER_TSAINA_RIVER	61.2	-145.7	533.4	0.2	121454
USCRN	Kenai_29_ENE	60.7	-150.5	282	0.2	121089

Table A- 3 Water temperature stations (WSC) in AHYPE domain.

River	*StationID*	*Latitude*	*Longitude*	*Province*	*SUBID*
REID	03NE001	56.4	-62.2	NL	114909
"CAMP POND"	03NE002	56.3	-62.1	NL	114909
REID	03NE011	56.3	-62.1	NL	114909
"TRIBUTARY TO REID BROOK"	03NE012	56.3	-62.1	NL	114909
"WABUSH LAKE"	03OA005	53.2	-66.8	NL	114545
"WABUSH LAKE"	03OA014	53.0	-66.9	NL	114545
FLORA	03OA015	53.0	-66.8	NL	114545
JAMES	03OB004	54.8	-66.8	NL	105344
"UNNAMED TRIBUTARY"	03OB005	54.8	-66.8	NL	105344
GOODREAM	03OB006	54.9	-67.1	NL	110843
ELROSS	03OB007	54.9	-67.1	NL	110843
HOUSTON	03OB008	54.7	-66.6	NL	105344
ATIKONAK	03OC003	53.0	-64.7	NL	111357
KEPIMITS	03OC004	52.7	-64.8	NL	117696
ATIKONAK	03OC005	52.3	-64.3	NL	103851
"ATIKONAK LAKE"	03OC007	52.7	-64.7	NL	103851
"EAST METCHIN"	03OD007	53.4	-63.2	NL	101401
CHURCHILL	03OD009	53.2	-63.3	NL	112181
CHURCHILL	03OE001	53.2	-60.8	NL	117704
MINIPI	03OE003	52.6	-61.2	NL	117705
PINUS	03OE011	53.1	-61.6	NL	105887
CHURCHILL	03OE012	53.0	-61.4	NL	105887
CHURCHILL	03OE014	53.2	-60.7	NL	117699
CHURCHILL	03PC001	53.3	-60.2	NL	101963
"LAKE MELVILLE"	03PD001	53.6	-59.5	NL	115851
SEVERN	04CA002	53.5	-91.5	ON	102967
ROSEBERRY	04CA003	52.7	-92.5	ON	106837
SEVERN	04CA004	52.7	-94.0	ON	103200
FLANAGAN	04CA005	52.5	-93.1	ON	103100
WINDIGO	04CB001	53.4	-91.8	ON	129480
PIPESTONE	04DA001	52.6	-90.2	ON	117730
ASHEWEIG	04DB001	53.7	-88.0	ON	102626
EKWAN	04EA001	53.8	-84.9	ON	117743
SUTTON	04ED001	55.2	-83.7	ON	112289
OTOSKWIN	04FA001	51.8	-89.6	ON	117747
PINEIMUTA	04FA003	52.3	-88.8	ON	129475
ATTAWAPISKAT	04FB001	52.1	-87.1	ON	117750
MUKETEI	04FC003	52.9	-86.2	ON	115579
CAT	04GA002	51.2	-91.6	ON	117756
PASHKOKOGAN	04GA003	51.0	-90.2	ON	100300

OGOKI	04GB004	50.9	-88.9	ON	117757
BRIGHTSAND	04GB005	49.6	-90.6	ON	117758
ALBANY	04GC002	51.4	-89.4	ON	120344
NAGAGAMI	04JC002	49.8	-84.5	ON	117772
"KENOGAMISIS LAKE"	04JD006	49.7	-86.9	ON	107495
"LITTLE CURRENT"	04JF001	50.7	-86.5	ON	111828
MATTAGAMI	04LA002	48.4	-81.4	ON	117783
MINISINAKWA	04LA005	47.7	-81.6	ON	103970
MOLLIE	04LA006	47.5	-81.8	ON	107213
MATTAGAMI	04LAX02	48.4	-81.4	ON	117782
"IVANHOE LAKE"	04LC002	48.2	-82.5	ON	101311
IVANHOE	04LC003	48.3	-82.4	ON	117787
NEMEGOSENDA	04LE002	47.9	-83.1	ON	105015
KAPUSKASING	04LF001	49.4	-82.4	ON	117790
MISSINAIBI	04LJ001	49.6	-83.3	ON	116833
"WATABEAG LAKE"	04MB005	48.3	-80.5	ON	102892
NEWPOST	04ME005	50.0	-81.5	ON	117836
PINCHER	05AA004	49.5	-113.9	AB	102604
CROWSNEST	05AA008	49.6	-114.4	AB	115592
OLDMAN	05AA035	49.7	-114.1	AB	117853
WILLOW	05AB041	50.1	-113.8	AB	100072
"PINE COULEE DIVERSION CANAL BELOW HEAD GATES"	05AB042	50.1	-113.8	AB	100072
"PINE COULEE RESERVOIR"	05AB044	50.1	-113.7	AB	100072
"PINE COULEE OUTFLOW BELOW RESERVOIR"	05AB045	50.1	-113.8	AB	100072
WILLOW	05AB046	49.8	-113.4	AB	100081
BELLY	05AD005	49.1	-113.7	AB	100137
"WATERTON LAKE"	05AD025	49.1	-113.9	AB	111238
WATERTON	05AD028	49.4	-113.5	AB	100172
BELLY	05AD041	49.4	-113.5	AB	100137
ST-MARY	05AE006	49.6	-112.8	AB	101167
"LAKE SHERBURNE"	05AE036	48.8	-113.5	MT	117877
OLDMAN	05AG006	49.9	-111.8	AB	100238
ELBOW	05BJ001	51.0	-114.1	AB	117919
FISH	05BK001	50.9	-114.3	AB	129429
THREEPOINT	05BL013	50.8	-114.3	AB	117926
PEKISKO	05BL023	50.5	-114.2	AB	117923
HIGHWOOD	05BL024	50.8	-113.8	AB	100378
BOW	05BM002	50.8	-113.4	AB	100403
"WESTERN IRRIGATION DISTRICT CANAL"	05BM015	51.0	-114.0	AB	100327

"EASTERN IRRIGATION DISTRICT MAIN BRANCH CANAL"	05BM020	50.7	-112.5	AB	100393
BOW	05BM021	50.8	-113.4	AB	100403
BOW	05BN012	50.0	-111.6	AB	100419
"LITTLE RED DEER"	05CB001	52.0	-114.1	AB	100440
BLINDMAN	05CC008	52.8	-114.3	AB	100443
"SOUTH SASKATCHEWAN"	05HG001	52.1	-106.6	SK	101053
NOTUKEU	05JB001	49.9	-107.2	SK	129459
QUAPPELLE	05JF001	50.7	-104.9	SK	129599
RIDGE	05JG013	51.0	-106.3	SK	129512
CUTARM	05JM015	50.6	-101.7	SK	129549
"TOBIN LAKE"	05KD004	53.7	-103.4	SK	115813
CARROT	05KH015	53.8	-101.4	MB	118107
SASKATCHEWAN	05KJ001	53.8	-101.2	MB	118109
"LAKE WINNIPEGOSIS"	05LD002	53.0	-101.0	MB	103244
MINK	05LJ019	51.4	-100.4	MB	100369
"LITTLE QUILL LAKE"	05MA002	51.9	-104.1	SK	101242
"BIG QUILL LAKE"	05MA010	51.8	-104.3	SK	100639
QUILL	05MA020	52.0	-104.3	SK	101243
"LARSEN RESERVOIR"	05NA006	49.5	-104.3	SK	129898
"MOOSE MOUNTAIN LAKE (RESERVOIR)"	05NC002	49.9	-103.0	SK	101941
ANTLER	05NF002	49.1	-101.0	MB	129971
GAINSBOROUGH	05NF007	49.1	-101.2	MB	129976
PIPESTONE	05NG003	49.6	-100.9	MB	130013
SNOWFLAKE	05OB016	49.0	-98.6	MB	130047
RED	05OC001	49.0	-97.2	MB	118216
RED	05OC008	49.8	-97.1	MB	118255
RED	05OC026	49.7	-97.1	MB	118255
RED	05OC029	49.8	-97.0	MB	118261
RED	05OJ005	50.1	-96.9	MB	118309
RED	05OJ015	49.9	-97.1	MB	118258
RED	05OJ023	50.0	-97.1	MB	118258
NAMAKAN	05PA006	48.4	-92.2	ON	101316
"LAC LA CROIX AT CAMPBELLS CAMP"	05PA011	48.4	-92.2	ON	101316
"NAMAKAN LAKE"	05PA013	48.5	-92.7	ON	100131
"RAINY LAKE"	05PB007	48.6	-93.3	ON	115834
TURTLE	05PB014	48.9	-92.7	ON	106295
ATIKOKAN	05PB018	48.8	-91.6	ON	113743
RAINY	05PC021	48.7	-94.6	ON	128894
"LAKE OF THE WOODS"	05PD011	49.7	-94.8	ON	109924
WINNIPEG	05PE001	49.8	-94.5	ON	100016

"LAKE OF THE WOODS EASTERN OUTLET"	05PE006	49.8	-94.5	ON	100016
"LAKE OF THE WOODS WESTERN OUTLET"	05PE011	49.8	-94.5	ON	100016
WINNIPEG	05PE012	49.8	-94.5	ON	100016
WINNIPEG	05PE028	49.8	-94.5	ON	100016
"LAKE OF THE WOODS WESTERN OUTLET"	05PE029	49.8	-94.5	ON	100016
WINNIPEG	05PF051	50.2	-95.1	ON	118275
STURGEON	05QA004	50.2	-91.5	ON	111508
"LAC SEUL AT LAC SEUL"	05QB001	50.3	-92.3	ON	118486
"LAC SEUL AT HUDSON"	05QB002	50.1	-92.2	ON	100127
"RED LAKE"	05QC005	51.0	-93.9	ON	101442
STURGEON	05QE009	50.4	-94.5	ON	115828
"SALVESEN LAKE"	05QE011	50.4	-94.5	ON	115828
LONG-LEGGED	05QE012	50.7	-94.0	ON	113365
"GRASSY NARROWS LAKE"	05QE015	50.2	-94.0	ON	110040
BERENS	05RC001	51.8	-93.5	ON	118300
"LAKE WINNIPEG"	05RF001	53.6	-97.8	MB	100029
"WUSKWATIM LAKE"	05TF006	55.5	-98.6	MB	103515
GUNISAO	05UA003	53.8	-97.8	MB	118318
NELSON	05UB001	54.0	-97.8	MB	100217
"PLAYGREEN LAKE"	05UB005	53.9	-98.0	MB	100217
"KISKITTO LAKE"	05UB013	54.3	-98.4	MB	100879
"KISKITTOGISU LAKE"	05UB017	54.4	-98.0	MB	102998
"CROSS LAKE"	05UD001	54.6	-97.8	MB	100258
"SIPIWESK LAKE"	05UD006	55.1	-97.5	MB	100319
"SIPIWESK LAKE"	05UD007	54.9	-98.4	MB	111912
DORE	06AG002	54.9	-107.7	SK	122720
DILLON	06BA002	55.7	-109.4	SK	118342
CHURCHILL	06BB003	55.9	-107.7	SK	103906
CANOE	06BB005	55.4	-108.0	SK	118346
HAULTAIN	06BD001	56.2	-106.6	SK	118348
"WASKESIU LAKE"	06CA002	54.0	-106.1	SK	101407
"CREAN LAKE"	06CA008	54.0	-106.2	SK	101908
"KINGSMERE LAKE"	06CA010	54.0	-106.4	SK	101209
"LAC LA RONGE AT LA RONGE"	06CB001	55.1	-105.3	SK	123922
RAPID	06CB002	55.4	-104.5	SK	100020
CHURCHILL	06CD002	55.6	-104.7	SK	118351
"WOLLASTON LAKE"	06DA001	58.5	-103.3	SK	100086
GEIKIE	06DA004	57.6	-104.2	SK	118355
WHEELER	06DA005	57.5	-105.0	SK	118357
WATHAMAN	06DC001	57.1	-103.7	SK	104669

REINDEER	06DD002	56.2	-103.2	SK	101567
WAPISKAU	06DD003	56.0	-103.3	SK	103330
CHURCHILL	06EA011	55.6	-102.8	SK	103472
"SOUTHERN INDIAN LAKE"	06EC006	57.3	-98.2	MB	115801
"SOUTHERN INDIAN LAKE"	06EC007	56.8	-99.5	MB	121327
THLEWIAZA	06HB002	60.8	-98.8	NU	118383
HANBURY	06JB001	63.6	-105.2	NT	118388
THELON	06JC002	64.5	-101.4	NU	102395
DUBAWNT	06KC003	64.2	-99.5	NU	100031
"ENNADAI LAKE"	06LA003	61.1	-101.0	NU	100269
KAZAN	06LC001	63.7	-95.9	NU	100266
THELON	06MA006	64.8	-97.1	NU	118398
BROWN	06OA007	65.9	-91.1	NU	129428
MARY	06SA001	71.2	-79.4	NU	101090
ROWLEY	06SB002	70.5	-77.4	NU	111079
INGENIKA	07EA004	56.7	-125.1	BC	118516
FINLAY	07EA005	57.1	-125.1	BC	128626
AKIE	07EA007	57.2	-124.9	BC	118518
OSPIKA	07EB002	56.5	-123.9	BC	118521
OMINECA	07EC002	55.9	-124.6	BC	129567
MESILINKA	07EC003	56.2	-124.6	BC	103800
OSILINKA	07EC004	56.1	-124.8	BC	118525
NATION	07ED003	55.4	-123.6	BC	118527
PARSNIP	07EE007	55.1	-122.9	BC	121360
PACK	07EE010	55.0	-123.0	BC	121360
PEACE	07EF001	56.0	-121.9	BC	118533
"WILLISTON LAKE"	07EF002	56.0	-123.7	BC	101568
CARBON	07EF004	55.9	-122.7	BC	119432
PEACE	07FA004	56.2	-120.8	BC	118537
PEACE	07FD002	56.1	-120.7	BC	118552
PEACE	07FD003	55.9	-118.6	AB	130742
PEACE	07FD010	56.1	-120.1	BC	118559
WAPITI	07GE001	55.1	-118.8	AB	130813
PEACE	07HA001	56.2	-117.3	AB	111554
BOYER	07JF005	57.9	-117.5	AB	127512
WATERFOUND	07LB002	58.4	-104.6	SK	103523
"FOND DU LAC"	07LE002	59.2	-105.5	SK	100003
DOUGLAS	07MA003	58.3	-109.8	SK	118611
MACFARLANE	07MB001	59.0	-108.2	SK	102029
"LAKE ATHABASCA"	07MC003	59.4	-108.9	SK	100019
SLAVE	07NB001	59.9	-111.6	AB	127718
"GREAT SLAVE LAKE"	07OB002	60.9	-115.7	NT	102551

"TAZIN LAKE"	07QC002	59.8	-109.4	SK	100568
ABITAU	07QC005	60.0	-108.8	SK	118651
TAZIN	07QC006	59.8	-108.3	SK	118652
TAZIN	07QC007	60.4	-110.7	NT	128155
CHARLOT	07QC008	59.6	-108.9	SK	100019
"NONACHO LAKE"	07QD002	61.7	-109.7	NT	100204
TALTSON	07QD004	61.9	-107.7	NT	118654
TALTSON	07QD007	60.5	-111.5	NT	114780
"KIRK LAKE OUTFLOW"	07RC003	63.7	-109.0	NT	104094
LOCKHART	07RD001	62.9	-108.5	NT	120355
SNARE	07SA002	64.0	-115.4	NT	118663
INDIN	07SA004	64.4	-115.0	NT	110807
SNARE	07SA008	64.2	-115.0	NT	110807
"GREAT SLAVE LAKE"	07SB001	62.4	-114.3	NT	107004
YELLOWKNIFE	07SB003	62.7	-114.3	NT	118667
CAMERON	07SB010	62.5	-113.5	NT	118671
"DUNCAN LAKE"	07SB012	62.8	-114.0	NT	103269
BAKER	07SB013	62.5	-114.4	NT	107004
"PROSPEROUS LAKE"	07SB014	62.5	-114.2	NT	118667
"BLUEFISH LAKE"	07SB015	62.7	-114.3	NT	100230
"PRELUDE LAKE"	07SB017	62.6	-114.0	NT	117861
YELLOWKNIFE	07SB019	63.6	-114.0	NT	108165
YELLOWKNIFE	07SB020	62.8	-114.3	NT	108215
BEAULIEU	07SC001	62.1	-113.2	NT	121067
WALDRON	07SC002	63.0	-110.5	NT	118674
HOARFROST	07SC004	62.9	-109.2	NT	100045
BARNSTON	07SC005	62.9	-110.2	NT	127175
"FLETCHER LAKE"	07SC006	63.7	-108.9	NT	106389
"LA MARTRE"	07TA001	63.1	-117.0	NT	118676
KAKISA	07UC001	60.9	-117.4	NT	100660
"AISHIHIK LAKE"	08AA005	61.2	-137.0	YT	127508
"SEKULMUN LAKE"	08AA007	61.5	-137.6	YT	123858
AISHIHIK	08AA010	61.2	-137.0	YT	128869
"AISHIHIK LAKE"	08AA012	61.6	-137.4	YT	119472
TATSHENSHINI	08AC002	60.1	-137.1	YT	108517
STIKINE	08CE001	57.9	-131.2	BC	118699
ISKUT	08CG001	56.7	-131.7	BC	118709
"ATLIN LAKE"	09AA001	59.6	-133.7	BC	100329
"BENNETT LAKE"	09AA004	60.2	-134.7	YT	112884
TUTSHI	09AA013	59.9	-134.3	BC	103600
"TAGISH LAKE"	09AA017	60.2	-134.4	YT	112884
MOON	09AA018	59.8	-134.7	BC	103600
YUKON	09AB001	60.7	-135.1	YT	101179

"MARSH LAKE"	09AB004	60.5	-134.4	YT	100451
"LAKE LABERGE"	09AB010	61.1	-135.2	YT	101179
SIDNEY	09AD002	60.8	-133.1	YT	103133
"TESLIN LAKE"	09AE002	60.2	-132.7	YT	100525
MORELY	09AE006	60.0	-132.1	YT	100835
"BIG SALMON"	09AG001	61.9	-134.8	YT	127499
YUKON	09AH001	62.1	-136.3	YT	103338
NORDENSKIOLD	09AH004	62.1	-136.3	YT	119114
DRURY	09AH005	62.2	-134.4	YT	120358
ROSS	09BA001	62.0	-132.4	YT	119117
PELLY	09BA002	62.0	-130.6	YT	119119
"SOUTH MACMILLAN"	09BB001	62.9	-130.5	YT	106962
PELLY	09BC001	62.8	-136.6	YT	119123
PELLY	09BC002	62.0	-132.4	YT	119125
"KLUANE LAKE"	09CA001	61.1	-138.5	YT	124073
HESS	09DA001	63.3	-131.5	YT	119138
"MAYO LAKE"	09DC005	63.8	-135.4	YT	119140
MCQUESTEN	09DD004	63.6	-137.3	YT	119152
KLONDIKE	09EA003	64.0	-139.4	YT	119156
"LITTLE SOUTH KLONDIKE"	09EA005	64.0	-137.6	YT	119158
KLONDIKE	09EA006	64.1	-139.1	YT	119156
WHITESTONE	09FA001	66.4	-138.4	YT	114966
RANCHERIA	10AA004	60.2	-129.6	YT	119184
HYLAND	10AD002	61.5	-128.2	YT	119194
BEAVER	10BD001	60.1	-124.9	YT	104334
TEETER	10BE009	59.5	-126.2	BC	119202
SMITH	10BE013	59.6	-126.5	BC	109081
PETITOT	10DA001	60.0	-123.0	BC	119223
LABICHE	10DB001	60.0	-124.1	YT	104654
"SOUTH NAHANNI"	10EB001	61.6	-125.8	NT	129479
PRAIRIE	10EC003	61.6	-124.8	NT	122441
LIARD	10ED002	61.7	-121.2	NT	119249
TROUT	10FA002	61.1	-119.8	NT	129461
JEAN-MARIE	10FB005	61.4	-121.2	NT	100023
KEELE	10HA004	64.1	-128.2	NT	120607
REDSTONE	10HB005	63.9	-125.3	NT	119258
CAMSELL	10JA002	65.6	-117.8	NT	101068
"GREAT BEAR"	10JC003	65.1	-123.6	NT	100005
"GREAT BEAR LAKE"	10JE002	66.6	-117.6	NT	109595
MACKENZIE	10KA001	65.3	-126.8	NT	119277
"JUNGLE RIDGE"	10KA006	65.1	-126.1	NT	119277
BOSWORTH	10KA007	65.3	-126.9	NT	119277

OSCAR	10KA008	65.4	-127.4	NT	121001
CANYON	10KA009	65.2	-126.5	NT	119277
TRAVAILLANT	10LB005	67.8	-131.9	NT	112423
TIEDA	10LB007	66.7	-129.3	NT	121194
OGILVIE	10MA002	65.4	-138.3	YT	119299
"BONNET PLUME"	10MB004	64.7	-133.7	YT	119308
COPPERMINE	10PA001	64.6	-112.0	NT	104070
YAMBA	10PA002	64.8	-111.7	NT	102208
COPPERMINE	10PB001	65.4	-114.0	NT	100244
"IZOK LAKE INFLOW"	10PB002	65.6	-112.9	NU	106003
"POINT LAKE"	10PB003	65.4	-114.0	NT	999000
"FAIRY LAKE"	10PC005	66.3	-114.0	NU	120459
HOOD	10QB001	67.3	-108.9	NU	100481
"CONTWOYTO LAKE"	10QC003	65.8	-111.2	NU	119535
ELLICE	10QD001	67.7	-104.1	NU	119337
BACK	10RA001	65.2	-106.1	NU	119340
BAILLIE	10RA002	65.0	-104.5	NU	119342
MCKEAND	10UG001	64.9	-68.3	NU	105273
"ARMSHOW SOUTH"	10UH005	63.5	-68.9	NU	101441
"ARMSHOW NORTH"	10UH006	63.6	-69.0	NU	101441
JAYNES	10UH010	63.2	-68.4	NU	111314
"LAKE GERALDINE"	10UH013	63.8	-68.5	NU	113169
MECHAM	10VC002	74.7	-94.8	NU	601229

Table A- 4 Water temperature observation stations (US-FWS).

AKOATS ID	SiteID	Lat	Lon	Sensor Placement	Waterbody name	Start date	End date	years	SUBID
1149	5.71E+14	57.2	-154.2	Main channel	Akalura River	2004	2007	3	102688
1150	5.71E+14	57.2	-154.1	Main channel	Dog Salmon River	2004	2007	3	100581
1151	5.71E+14	57.2	-154.4	Main channel	Ayakulik River	2005	2007	2	106022
1152	5.73E+14	57.4	-154.1	Main channel	Karluk River	2004	2007	3	117850
1153	6.24E+14	62.6	-141.0	Main channel	Scottie Creek	2006	2013	7	120460
1154	6.24E+14	62.7	-141.1	Main channel	Desper Creek	2006	2012	6	120460
1155	6.25E+14	62.9	-141.5	Main channel	Gardiner Creek	2006	2012	6	125027
1156	6.56E+14	66.0	-151.9	Main channel	Kanuti Kilolitna River	2010	2011	1	126094
1157	6.61E+14	66.2	-151.1	Main channel	Kanuti River tributary	2010	2015	5	118006
1158	6.62E+14	66.3	-151.1	Main channel	Kanuti River	2010	2014	4	118006
1159	6.65E+14	66.9	-151.1	Main channel	South Fork Koyukuk River	2011	2015	4	118387
1833	5.80E+14	58.0	-156.8	Main channel	Egegik River	2015	2016	1	114438
1834	6.60E+14	66.0	-152.1	Main channel	Holonada Creek	2010	2015	2	126094
1835	6.65E+14	66.9	-151.7	Main channel	Koyukuk River	2015	2016	1	125092
1848	5.52E+14	55.3	-162.7	Lakeshore	AWC 283-34-10430-0010	2016	2017	2	100308
1849	5.52E+14	55.3	-162.7	Main channel	AWC 283-34-10400	2016	2017	2	100308

1850	5.50E+14	55.0	-162.9	Main channel	AWC 283-12-11300-2014	2014	2017	4	102162
1851	5.50E+14	55.0	-162.9	Main channel	AWC 283-12-11290	2014	2017	4	102162
1852	5.52E+14	55.3	-162.3	Main channel	AWC 312-40-10100-2021-3003	2014	2017	4	100308
1854	5.52E+14	55.3	-162.3	Main channel	AWC 312-40-10100	2014	2017	4	100308
1855	5.46E+14	55.0	-163.1	Lakeshore	AWC 283-12-10100-0010	2014	2017	4	117248
1856	5.46E+14	55.0	-163.1	Main channel	AWC 283-12-10100	2014	2017	4	117248
1858	5.53E+14	55.5	-162.5	Main channel	Unnamed stream above Moffet Lagoon	2014	2017	4	104420
1859	5.53E+14	55.5	-162.5	Main channel	AWC 312-40-10300-2012	2014	2017	4	104420
1860	5.53E+14	55.4	-162.5	Main channel	AWC 312-40-10300-2006-3006	2014	2017	4	104420
1861	5.52E+14	55.4	-162.5	Main channel	AWC 312-40-10200	2014	2017	4	104420
1862	5.51E+14	55.2	-163.0	Main channel	AWC 312-20-10100	2014	2017	4	102162
1863	5.51E+14	55.1	-163.0	Main channel	AWC 312-20-10200	2014	2017	4	102162
1864	5.51E+14	55.1	-162.9	Main channel	AWC 312-20-10300	2014	2017	4	102162
1865	5.52E+14	55.3	-162.8	Main channel	AWC 312-20-11300	2014	2017	4	100308
1866	5.52E+14	55.3	-162.4	Main channel	AWC 312-40-10100-2006-3020	2014	2017	4	100308

1867	5.51E+14	55.2	-162.4	Main channel	Unnamed stream in Right Hand Valley	2014	2017	4	100308
1868	5.52E+14	55.3	-162.3	Main channel	AWC 312-40-10100-2006-3036	2014	2017	4	100308
1869	5.52E+14	55.3	-162.3	Main channel	AWC 312-40-10100-2006	2014	2017	4	100308
1870	5.52E+14	55.3	-162.4	Lakeshore	AWC 312-40-10100-2006-0010	2014	2017	4	100308
1871	5.52E+14	55.3	-162.5	Lakeshore	AWC 312-40-10100-2006-0010	2014	2017	4	100308
1872	6.54E+14	65.7	-156.1	Lake center	Willow Lake	2016	2017	2	111965
1873	6.54E+14	65.7	-156.1	Lake center	Willow Lake	2016	2017	2	111965
1874	6.61E+14	66.1	-156.3	Main channel	Dakli/Wheeler Creek	2016	2017	2	129660
1875	6.60E+14	66.1	-156.9	Main channel	Billy Hawk Creek (East Fork)	2016	2017	2	128773
1876	6.60E+14	66.1	-157.2	Main channel	Billy Hawk Creek (West Fork)	2016	2017	2	128773
1877	5.52E+14	55.3	-162.5	Main channel	AWC 283-34-10700 KL1	2014	2017	3	100308
1878	5.52E+14	55.3	-162.7	Side channel	AWC 283-34-10430 KL2	2016	2017	1	100308

1879	kdk_meacr01	57.3	-154.0	Main channel	Meadow Creek	2015	2016	1	104311
1880	kdk_omarv01	57.3	-154.0	Main channel	O'Malley River	2015	2017	2	104311
663	kdk_redlk01	57.3	-154.3	Lake (limnetic zone)	Red Lake	2011	2017	4	106022
664	kdk_karlk01	57.4	-154.0	Lake (limnetic zone)	Karluk Lake	2011	2017	4	104311
1617	kdk_akalk01	57.2	-154.2	Lake (limnetic zone)	Akalura Lake	2011	2017	1	102688
1618	kdk_akacr01	57.2	-154.2	Main channel	Akalura River	2015	2017	1	102688
1619	kdk_ayarv03	57.2	-154.4	Main channel	Ayakulik River	2015	2017	1	106022
1620	kdk_cancr01	57.3	-154.0	Main channel	Canyon Creek	2015	2017	1	104311
1621	kdk_concr01	57.3	-154.3	Main channel	Connecticut Creek	2015	2017	1	106022
1622	kdk_homlk01	57.1	-153.9	Lake (limnetic zone)	Horse Marine Lake	2015	2017	1	102688
1623	kdk_pincr01	57.3	-154.2	Main channel	Pinnell Creek	2015	2017	1	100582
1624	kdk_relrv01	57.3	-154.4	Main channel	Red Lake River	2015	2017	1	106022
1928	kdk_cascr01	57.3	-154.0	Main channel	Cascade Creek	2015	2017	2	104311
1929	kdk_eftrv01	57.4	-154.0	Main channel	East Fork Thumb River	2015	2017	2	104311
1930	kdk_falcr01	57.3	-154.0	Main channel	Falls Creek	2015	2017	2	104311
1932	kdk_soucr01	57.2	-154.3	Main channel	Southeast Creek	2015	2017	2	106022

Table A- 5 Ice thickness observation stations (CRID).

STATION ID	*STATION.NAME*	*LAT*	*LON*	*RIVER TYPE*	*SUBID*
02RD002	MISTASSIBI (RIVIERE)	48.90	-72.21	NAT	127095
02RF001	ASHUAPMUSHUAN (RIVIERE) <c0> LA T<ca>TE DE LA CHUTE AUX SAUMONS	48.69	-72.49	NAT	108849
02RG005	METABETCHOUANE (RIVIERE) EN AMONT DE LA CENTRALE SRPC	48.38	-71.99	NAT	117467
02UC002	MOISIE (RIVIERE) <c0> 5,1 KM EN AMONT DU PONT DU QNSLR	50.35	-66.19	NAT	108826
02VC001	ROMAINE (RIVIERE) AU PONT DE LA QIT	50.31	-63.62	NAT	109295
02WB003	NATASHQUAN (RIVIERE) <c0> 0,6 KM EN AVAL DE LA D<c9>CHARGE DU LAC ALIESTE	50.43	-61.71	NAT	117506
02XA003	LITTLE MECATINA RIVER ABOVE LAC FOURMONT	52.23	-61.32	NAT	117522
02XA004	RIVIERE JOIR NEAR PROVINCIAL BOUNDARY	52.16	-60.06	NAT	117524
02XC001	SAINT-PAUL (RIVIERE) <c0> 0,5 KM DU RUISSEAU CHANION	51.77	-57.60	NAT	117536
03BF001	PONTAX (RIVIERE) <c0> 60,4 KM DE L'EMBOUCHURE	51.53	-78.10	NAT	117585
03CB004	EASTMAIN (RIVIERE) A LA TETE DE LA GORGE PROSPER	52.17	-74.59	NAT	117591
03DD002	DE PONTOIS (RIVIERE) EN AMONT DE LA RIVIERE SAKAMI	53.17	-74.47	NAT	117608
03ED001	BALEINE (GRANDE RIVIERE DE LA) EN AMONT DE LA RIVIERE DENYS-1	55.24	-76.98	NAT	117624
03KC004	MELEZES (RIVIERE AUX) <c0> 7,6 KM EN AMONT DE LA CONFLUENCE AVEC LA KOKSOAK	57.67	-69.61	NAT	117673
03MB002	BALEINE (RIVIERE A LA) <c0> 40,2 KM DE L'EMBOUCHURE	57.88	-67.58	NAT	117686
03MD001	GEORGE (RIVIERE) <c0> LA SORTIE DU LAC DE LA HUTTE SAUVAGE	56.79	-65.76	NAT	117692
03NF001	UGJOKTOK RIVER BELOW HARP LAKE	55.23	-61.30	NAT	117694
03NG001	KANAIRIKTOK RIVER BELOW SNEGAMOOK LAKE	54.62	-60.98	NAT	116616
03PB002	NASKAUPI RIVER BELOW NASKAUPI LAKE	54.13	-61.43	NAT	112064
03QC001	EAGLE RIVER ABOVE FALLS	53.53	-57.49	NAT	103433
03QC002	ALEXIS RIVER NEAR PORT HOPE SIMPSON	52.65	-56.87	NAT	117710
04AB001	HAYES RIVER BELOW GODS RIVER	56.42	-92.81	NAT	117713
04AD002	GODS RIVER NEAR SHAMATTAWA	55.85	-92.09	NAT	127462

04CC001	SEVERN RIVER AT LIMESTONE RAPIDS	55.38	-88.33	NAT	117723
04DC001	WINISK RIVER BELOW ASHEWEIG RIVER TRIBUTARY	54.50	-87.23	NAT	117739
04EA001	EKWAN RIVER BELOW NORTH WASHAGAMI RIVER	53.81	-84.92	NAT	117743
04FC001	ATTAWAPISKAT RIVER BELOW MUKETEI RIVER	53.09	-85.07	NAT	117755
04GD001	ALBANY RIVER ABOVE NOTTIK ISLAND	51.64	-86.39	REG	117760
04HA001	ALBANY RIVER NEAR HAT ISLAND	51.33	-83.83	REG	117763
04JG001	KENOGAMI RIVER NEAR MAMMAMATTAWA	50.42	-84.38	REG	117777
04LD001	GROUNDHOG RIVER AT FAUQUIER	49.31	-82.04	REG	117788
04LG002	MOOSE RIVER AT MOOSE RIVER	50.81	-81.29	REG	125963
04LJ001	MISSINAIBI RIVER AT MATTICE	49.61	-83.27	NAT	116833
04LM001	MISSINAIBI RIVER BELOW WABOOSE RIVER	50.59	-82.09	NAT	117809
04NA001	HARRICANA (RIVIERE) 3,1 KM EN AVAL DU PONT-ROUTE 111 A AMOS	48.60	-78.11	NAT	109026
04NB001	TURGEON (RIVIERE) EN AMONT DE LA RIVIERE HARRICANA	49.99	-79.10	NAT	117844
05AA023	OLDMAN RIVER NEAR WALDRON'S CORNER	49.81	-114.18	NAT	117848
05AB021	WILLOW CREEK NEAR CLARESHOLM	50.02	-113.71	REG	100072
05AC003	LITTLE BOW RIVER AT CARMANGAY	50.13	-113.12	REG	100117
05AD028	WATERTON RIVER NEAR GLENWOOD	49.43	-113.48	REG	100172
05BJ001	ELBOW RIVER BELOW GLENMORE DAM	51.01	-114.09	REG	117919
05BJ004	ELBOW RIVER AT BRAGG CREEK	50.95	-114.57	NAT	117922
05BL024	HIGHWOOD RIVER NEAR THE MOUTH	50.78	-113.82	REG	100378
05CB001	LITTLE RED DEER RIVER NEAR THE MOUTH	52.03	-114.14	NAT	100440
05CC001	BLINDMAN RIVER NEAR BLACKFALDS	52.35	-113.79	NAT	100443
05CC007	MEDICINE RIVER NEAR ECKVILLE	52.32	-114.34	NAT	100456
05FF001	BATTLE RIVER AT BATTLEFORD	52.74	-108.34	REG	100940
05GC006	EAGLE CREEK NEAR ENVIRON	52.23	-107.38	REG	100978
05GG001	NORTH SASKATCHEWAN RIVER AT PRINCE ALBERT	53.20	-105.77	REG	101003
05HH001	SOUTH SASKATCHEWAN RIVER AT ST LOUIS	52.92	-105.81	REG	129447
05JM001	QU'APPELLE RIVER NEAR WELBY	50.49	-101.56	REG	129549
05KH007	CARROT RIVER NEAR TURNBERRY	53.61	-102.10	NAT	118099
05KJ001	SASKATCHEWAN RIVER AT THE PAS	53.84	-101.21	REG	118109
05LC001	RED DEER RIVER NEAR ERWOOD	52.86	-102.20	NAT	118121
05LH005	WATERHEN RIVER NEAR WATERHEN	51.85	-99.55	NAT	129714
05LM006	DAUPHIN RIVER NEAR DAUPHIN RIVER	52.00	-98.33	REG	129780

05MD004	ASSINIBOINE RIVER AT KAMSACK	51.56	-101.92	REG	129808
05ME006	ASSINIBOINE RIVER NEAR MINIOTA	50.11	-101.04	REG	196405
05MH005	ASSINIBOINE RIVER NEAR HOLLAND	49.70	-98.89	REG	129869
05NG001	SOURIS RIVER AT WAWANESA	49.60	-99.68	REG	130016
05NG021	SOURIS RIVER AT SOURIS	49.62	-100.25	REG	130007
05OC012	RED RIVER NEAR STE AGATHE	49.55	-97.19	REG	118225
05OJ010	RED RIVER NEAR LOCKPORT	50.11	-96.93	REG	127088
06AD001	BEAVER RIVER NEAR DORINTOSH	54.30	-108.60	NAT	130266
06AD006	BEAVER RIVER AT COLD LAKE RESERVE	54.36	-110.22	NAT	130273
06AG001	BEAVER RIVER BELOW WATERHEN RIVER	54.82	-107.81	NAT	122720
06BC001	MUDJATIK RIVER NEAR FORCIER LAKE	56.09	-107.59	NAT	118347
06BD001	HAULTAIN RIVER ABOVE NORBERT RIVER	56.25	-106.56	NAT	118348
06DA004	GEIKIE RIVER BELOW WHEELER RIVER	57.58	-104.19	NAT	118355
06GD001	SEAL RIVER BELOW GREAT ISLAND	58.89	-96.28	NAT	118381
06JC002	THELON RIVER ABOVE BEVERLY LAKE	64.53	-101.36	NAT	102395
06LC001	KAZAN RIVER ABOVE KAZAN FALLS	63.65	-95.85	NAT	100266
06MB001	QUOICH RIVER ABOVE ST CLAIR FALLS	64.31	-93.91	NAT	118402
07AE001	ATHABASCA RIVER NEAR WINDFALL	54.21	-116.06	NAT	100468
07BC002	PEMBINA RIVER AT JARVIE	54.45	-113.99	NAT	130505
07BE001	ATHABASCA RIVER AT ATHABASCA	54.72	-113.29	NAT	199950
07CD001	CLEARWATER RIVER AT DRAPER	56.69	-111.26	NAT	118479
07DA001	ATHABASCA RIVER BELOW FORT MCMURRAY	56.78	-111.40	NAT	118490
07EA005	FINLAY RIVER ABOVE AKIE RIVER	57.08	-125.15	NAT	128626
07EA005	FINLAY RIVER ABOVE AKIE RIVER	57.08	-125.15	NAT	128626
07EC002	OMINECA RIVER ABOVE OSILINKA RIVER	55.92	-124.57	NAT	129567
07FB001	PINE RIVER AT EAST PINE	55.72	-121.21	NAT	118540
07FC001	BEATTON RIVER NEAR FORT ST JOHN	56.28	-120.70	NAT	118546
07GE001	WAPITI RIVER NEAR GRANDE PRAIRIE	55.07	-118.80	NAT	130813
07GH002	LITTLE SMOKY RIVER NEAR GUY	55.46	-117.16	NAT	118581
07GJ001	SMOKY RIVER AT WATINO	55.71	-117.62	NAT	130847
07HA001	PEACE RIVER AT PEACE RIVER	56.24	-117.31	REG	111554
07HA005	WHITEMUD RIVER NEAR DIXONVILLE	56.51	-117.66	NAT	128116
07HC001	NOTIKEWIN RIVER AT MANNING	56.92	-117.62	NAT	118585
07JD002	WABASCA RIVER AT HIGHWAY NO 88	57.87	-115.39	NAT	118593
07KC001	PEACE RIVER AT PEACE POINT (ALBERTA)	59.12	-112.44	REG	130886
07NB001	SLAVE RIVER AT FITZGERALD (ALBERTA)	59.87	-111.58	REG	127718
07OB001	HAY RIVER NEAR HAY RIVER	60.74	-115.86	NAT	118631
07OB003	HAY RIVER NEAR MEANDER RIVER	59.15	-117.64	NAT	118634

07OC001	CHINCHAGA RIVER NEAR HIGH LEVEL	58.60	-118.33	NAT	118638
07PA001	BUFFALO RIVER AT HIGHWAY NO 5	60.71	-114.90	NAT	118639
08AB001	ALSEK RIVER ABOVE BATES RIVER	60.12	-137.98	NAT	118682
08CE001	STIKINE RIVER AT TELEGRAPH CREEK	57.90	-131.16	NAT	118699
08CF001	STIKINE RIVER ABOVE BUTTERFLY CREEK	57.49	-131.75	NAT	118707
09AE003	SWIFT RIVER NEAR SWIFT RIVER	59.93	-131.77	NAT	119106
09AH001	YUKON RIVER AT CARMACKS	62.09	-136.27	NAT	103338
09BC001	PELLY RIVER AT PELLY CROSSING	62.83	-136.58	NAT	119123
09BC004	PELLY RIVER BELOW VANGORDA CREEK	62.22	-133.38	NAT	129374
09CD001	YUKON RIVER ABOVE WHITE RIVER	63.08	-139.50	NAT	119134
09DC002	STEWART RIVER AT MAYO	63.59	-135.90	NAT	119147
09DD003	STEWART RIVER AT THE MOUTH	63.28	-139.25	NAT	119149
09EA003	KLONDIKE RIVER ABOVE BONANZA CREEK	64.04	-139.41	NAT	119156
09FB001	PORCUPINE RIVER BELOW BELL RIVER	67.44	-137.78	NAT	119173
09FC001	OLD CROW RIVER NEAR THE MOUTH	67.63	-139.70	NAT	119179
09FD001	PORCUPINE RIVER AT OLD CROW	67.56	-139.88	NAT	119181
10AA001	LIARD RIVER AT UPPER CROSSING	60.05	-128.91	NAT	119183
10AB001	FRANCES RIVER NEAR WATSON LAKE	60.47	-129.12	NAT	119188
10BB001	KECHIKA RIVER AT THE MOUTH	59.62	-127.31	NAT	104053
10BE001	LIARD RIVER AT LOWER CROSSING	59.41	-126.10	NAT	119202
10BE005	LIARD RIVER ABOVE BEAVER RIVER	59.74	-124.48	NAT	119207
10BE006	LIARD RIVER ABOVE KECHIKA RIVER	59.70	-127.23	NAT	119208
10CC002	FORT NELSON RIVER ABOVE MUSKWA RIVER	58.67	-122.64	NAT	119218
10CD001	MUSKWA RIVER NEAR FORT NELSON	58.79	-122.66	NAT	119221
10EA003	FLAT RIVER NEAR THE MOUTH	61.53	-125.41	NAT	119225
10EB001	SOUTH NAHANNI RIVER ABOVE VIRGINIA FALLS	61.64	-125.80	NAT	129479
10EC001	SOUTH NAHANNI RIVER ABOVE CLAUSEN CREEK	61.26	-124.07	NAT	100135
10ED001	LIARD RIVER AT FORT LIARD	60.24	-123.48	NAT	119228
10ED002	LIARD RIVER NEAR THE MOUTH	61.74	-121.23	NAT	119249
10GB006	WILLOWLAKE RIVER ABOVE METAHDALI CREEK	62.65	-122.90	NAT	119244
10GC001	MACKENZIE RIVER AT FORT SIMPSON	61.87	-121.36	REG	119247
10HB005	REDSTONE RIVER 63 KM ABOVE THE MOUTH	63.92	-125.30	NAT	119258
10KA001	MACKENZIE RIVER AT NORMAN WELLS	65.27	-126.85	REG	119277
10LA002	ARCTIC RED RIVER NEAR THE MOUTH	66.79	-133.09	NAT	129000
10LC002	MACKENZIE RIVER (EAST CHANNEL) AT INUVIK	68.37	-133.76	REG	102628

10LC014	MACKENZIE RIVER AT ARCTIC RED RIVER	67.46	-133.75	REG	129588
10MA001	PEEL RIVER ABOVE CANYON CREEK	65.89	-136.04	NAT	119296
10MC002	PEEL RIVER ABOVE FORT MCPHERSON	67.26	-134.89	NAT	119310
10NC001	ANDERSON RIVER BELOW CARNWATH RIVER	68.63	-128.42	NAT	119322
10QC001	BURNSIDE RIVER NEAR THE MOUTH	66.73	-108.81	NAT	104418
10RA001	BACK RIVER BELOW BEECHY LAKE	65.19	-106.09	NAT	119340
10RA002	BAILLIE RIVER NEAR THE MOUTH	65.01	-104.49	NAT	119342
10RC001	BACK RIVER ABOVE HERMANN RIVER	66.09	-96.51	NAT	119343

Table A- 6 Ice thickness observation stations (NSIDC).

Number River - Station Name Identifier	*Latitude (deg min)*	*Longitude (deg min)*	*Ice Thickness Start Year*	*Ice Thickness End Year*	*SUBID*
01 PECHENGA - PECHENGA	69 32 N	31 10 E	1963	1992	309257
02 NAMA-JOKI - LUOSTARI	69 35 N	31 42 E	1980	1992	312561
03 TITOVKA - 15.5 KM	69 33 N	31 39 E	1953	1992	312561
05 KOLA - 1429 KM	68 50 N	33 05 E	1977	1992	312713
07 SOSNOVKA - SOSNOVKA	66 29 N	40 33 E	1952	1992	312268
08 CHAPOMA - CHAPOMA	66 05 N	38 50 E	1977	1992	306887
09 CHAVANGA - CHAVANGA	66 07 N	37 47 E	1978	1992	301703
10 VARZUGA - VARZUGA	66 24 N	36 38 E	1952	1992	301701
11 OLENITSA - OLENITSA	66 29 N	35 22 E	1977	1992	306729
12 KUZREKA - KUZREKA	66 37 N	34 48 E	1977	1992	312314
13 UMBA - PAIALKA	66 43 N	34 20 E	1977	1992	313658
14 KOLVIZA - KOLVIZA	67 05 N	33 04 E	1977	1992	303988
15 PONGOMA - PONGOMA	65 20 N	34 23 E	1960	1988	313983
18 SHUYA - SHUERETSKOJE	64 45 N	34 42 E	1960	1988	304617
19 SUMA - SUMSKY POSAD	64 15 N	35 26 E	1960	1988	312743
20 NIUKHCHA - NIUKHCHA	63 55 N	36 13 E	1961	1988	302280
21 MALOSHUIKA - MALOSHUIKA	63 45 N	37 24 E	1960	1988	304926
22 ONEGA - POROG	63 49 N	38 28 E	1953	1988	310195
24 VONGUDA - VONGUDA	63 48 N	38 30 E	1981	1988	310195
27 NENOKSA - NENOKSA	64 36 N	39 10 E	1978	1988	302858
29 SEV.DVINA - UST PINEGA	64 08 N	41 55 E	1977	1988	301290
36 KULOY - KULOY	64 58 N	43 31 E	1977	1987	301472
39 MEZEN - MALONISOGORSKAYA	65 00 N	45 37 E	1953	1988	301455
40 PEZA - EGUMNOVO	65 49 N	45 06 E	1955	1988	313399
42 PESHA - VOLOKOVAYA	66 30 N	48 15 E	1965	1988	303600
43 PECHORA - OKSINO	67 38 N	52 11 E	1953	1988	412825
44 OB - SALEKHARD	66 38 N	66 36 E	1954	1994	444087
45 NADYM - NADYM	65 37 N	72 40 E	1954	1994	444050
46 PUR - SAMBURG	67 00 N	78 13 E	1954	1992	400561
47 TAZ - SIDOROVSK	66 36 N	82 17 E	1954	1994	400736
48 NYDA - NYDA	66 38 N	72 56 E	1977	1993	432508
55 ENISEY - IGARKA	67 26 N	86 29 E	1955	1989	404309
58 PYASINA - UST-TAREYA	73 13 N	89 43 E	1977	1987	415650
63 NAIBA - NAIBA	70 40 N	130 30 E	1979	1988	417051
64 LENA - KUSUR	70 41 N	127 24 E	1954	1992	401806
66 KHATANGA - KHATANGA	71 59 N	102 27 E	1960	1992	406725
67 ANABAR - SASKYLAKH	71 58 N	114 05 E	1954	1992	406722
68 OLENEK - SUKHANA	68 37 N	118 20 E	1951	1992	407625

69 YANA - YUBILEINAYA	70 45 N	136 05 E	1950	1992	433356
70 YNDIGIRKA - VORONTSOVO	69 34 N	147 32 E	1951	1992	444076
71 ALAZEYA - ANDRIUSHKINO	69 10 N	154 30 E	1961	1992	408724
72 OMOLOY - NAMY	69 23 N	134 37 E	1977	1992	432938
73 KOLYMA - SREDNEKOLYMSK	67 28 N	153 42 E	1934	1988	408739
74 KOLYMA - KOLYMSKOJE	68 44 N	158 43 E	1965	1988	432529
76 AMGUEMA - AMGUEMA	67 02 N	179 04 E	1977	1988	419658
77 ANADYR - MARKOVO	64 41 N	170 25 E	1977	1988	408821

Appendix B – Model Performance for Individual Subbasins

Table B- 1 Soil temperature model performance metrics for each subbasin.

SUBID	*Depth [m]*	*RMSE*	*NRMSE_SD*	*BIAS*	*# of monthly observations*	*Start Month*	*End Month*	*subbasin center lon*	*subbasin center lat*
116437	1	5.03	1.80	2.12	284	1989-06	2013-01	-148.1	64.8
116915	1	5.95	3.82	3.10	262	1989-08	2013-01	-147.7	64.4
125248	1	3.80	1.12	1.55	329	1992-06	2019-10	-148.3	64.5
127997	1	4.67	1.45	1.21	86	2012-09	2019-10	-159.9	61.6
122480	1	2.66	0.67	0.31	31	2014-10	2017-04	-160.8	59.4
127020	1	4.51	1.12	2.54	31	2014-10	2017-04	-164.8	65.6
128245	1	2.71	0.81	0.74	45	2013-08	2017-04	-165.2	61.4
125983	1	8.38	5.12	5.24	24	2015-06	2019-08	-151.8	66.2
126955	1	5.75	3.69	3.63	53	2012-09	2017-04	-157.0	59.6
120731	1	4.82	2.23	3.22	42	2013-10	2017-04	-156.4	58.4
103838	1	2.21	0.94	0.63	103	2002-05	2013-08	-151.4	59.8
126925	1	1.61	0.44	0.06	16	2018-06	2019-09	-148.8	61.8
126987	1	3.22	0.66	2.27	78	2012-09	2019-10	-143.1	63.3
115402	1	2.60	0.80	0.35	52	2012-09	2017-03	-159.1	59.2
121089	1	2.99	0.81	1.98	87	2012-10	2019-12	-150.4	60.6
116437	0.2	4.65	1.27	0.68	296	1988-06	2013-01	-148.1	64.8
116915	0.2	6.67	3.82	1.33	285	1989-05	2013-01	-147.7	64.4
125248	0.2	2.64	0.47	0.64	377	1988-06	2019-10	-148.3	64.5

127997	0.2	4.17	0.90	0.22	86	2012-09	2019-10	-159.9	61.6
122480	0.2	4.78	1.54	-1.10	31	2014-10	2017-04	-160.8	59.4
128008	0.2	5.87	1.82	-0.34	19	2014-10	2017-02	-156.7	65.1
127027	0.2	6.02	1.29	-2.03	99	2006-10	2015-05	-163.3	67.9
128245	0.2	4.29	1.36	2.15	45	2013-08	2017-04	-165.2	61.4
125983	0.2	9.32	4.87	0.33	24	2015-06	2019-08	-151.8	66.2
126955	0.2	4.64	1.17	1.31	53	2012-09	2017-04	-157.0	59.6
120731	0.2	4.83	2.04	1.91	43	2013-10	2017-04	-156.4	58.4
103838	0.2	4.65	1.68	1.48	103	2002-05	2013-08	-151.4	59.8
126925	0.2	4.21	0.69	-1.81	16	2018-06	2019-09	-148.8	61.8
126987	0.2	3.30	0.45	1.42	78	2012-09	2019-10	-143.1	63.3
127538	0.2	5.28	2.81	-1.32	21	2015-08	2017-04	-160.8	64.2
117603	0.2	4.87	1.22	-0.75	171	2005-08	2019-10	-145.3	63.9
115402	0.2	3.89	0.77	-0.94	56	2012-09	2017-08	-159.1	59.2
127381	0.2	2.51	0.64	0.26	135	2008-06	2019-10	-151.2	60.0
126508	0.2	11.11	2.00	-5.29	147	2007-08	2019-10	-148.5	67.6
127006	0.2	6.44	2.39	-2.26	177	2005-03	2019-12	-150.1	67.3
126742	0.2	5.02	1.06	0.86	146	2006-10	2019-10	-144.6	65.5
106153	0.2	1.88	0.39	0.00	97	2011-10	2019-10	-149.6	60.2
126826	0.2	4.20	0.76	0.30	157	2006-10	2019-10	-150.6	66.6
127211	0.2	4.64	1.11	-2.03	97	2011-10	2019-10	-149.4	69.3
121089	0.2	4.87	1.78	2.23	159	2006-10	2019-12	-150.4	60.6
115571	0.2	6.26	2.90	-0.22	97	2011-10	2019-10	-146.9	65.1

106691	0.2	4.24	1.35	0.82	89	2012-06	2019-10	-154.4	59.0
126998	0.2	2.69	0.82	-0.73	145	2007-10	2019-10	-148.2	63.3
123042	0.2	8.97	4.13	-2.64	97	2011-10	2019-10	-146.2	65.1
127396	0.2	2.39	0.79	1.45	97	2011-10	2019-10	-135.1	59.5
126990	0.2	7.97	3.13	-1.93	97	2011-10	2019-10	-145.8	64.9
107385	0.2	1.85	0.41	-0.91	149	2007-06	2019-10	-150.7	59.9
107910	0.2	3.95	1.10	1.52	104	2007-01	2015-08	-149.8	61.5
127736	0.2	3.17	1.05	1.14	104	2007-10	2019-10	-151.4	59.3
129583	0.2	12.32	2.01	-5.49	100	2011-07	2019-10	-148.5	70.3
128738	0.2	4.62	1.70	2.43	97	2011-10	2019-10	-164.0	64.6
126916	0.2	2.37	0.79	1.27	144	2007-11	2019-10	-149.4	60.7
100710	0.2	2.35	0.59	1.13	156	2006-10	2019-10	-149.7	62.2
117424	0.2	4.13	1.01	-3.73	146	2007-08	2019-12	-150.8	62.8
126165	0.2	7.20	2.82	-2.30	156	2006-10	2019-09	-147.4	65.4
121454	0.2	1.30	0.35	-0.19	79	2013-04	2019-10	-145.1	61.3

Table B- 2 Soil moisture model performance for each subbasin.

SUBID	*RMSE*	*NRMSE_SD*	*BIAS*	*# of monthly observations*	*Start Month*	*End Month*	*subbasin center lon*	*subbasin center lat*	*Depth [m]*
127997	0.078	1.569	-0.058	46	2012-09	2019-10	-159.9	61.6	1.0
122480	0.096	6.88	0.093	20	2014-10	2016-11	-160.8	59.4	1.0
120731	0.042	1.257	0.018	22	2014-08	2017-01	-156.4	58.4	1.0
125248	0.037	1.376	-0.009	34	2012-09	2019-09	-148.3	64.5	1.0
103838	0.13	22.079	-0.127	54	2004-08	2013-08	-151.4	59.8	1.0
126925	0.113	3.073	0.11	11	2018-06	2019-09	-148.8	61.8	1.0
126987	0.155	2.314	0.131	32	2012-09	2019-10	-143.1	63.3	1.0
115402	0.204	2.925	0.191	40	2012-09	2017-01	-159.1	59.2	1.0
121089	0.106	3.277	0.102	46	2012-10	2019-12	-150.4	60.6	1.0
116437	0.225	4.414	0.217	63	2003-05	2012-10	-148.1	64.8	0.2
116915	0.294	4.022	0.277	59	2003-05	2012-10	-147.7	64.4	0.2
125248	0.32	4.806	0.315	106	2002-09	2019-10	-148.3	64.5	0.2
127997	0.262	7.265	0.256	46	2012-09	2019-10	-159.9	61.6	0.2
122480	0.253	7.704	0.249	13	2015-06	2016-10	-160.8	59.4	0.2
127020	0.339	5.923	0.336	5	2015-08	2016-10	-164.8	65.6	0.2
104023	0.418	7.786	0.412	2	2019-05	2019-06	-145.2	62.1	0.2
127027	0.531	22.204	0.53	27	2006-10	2014-09	-163.3	67.9	0.2
125983	0.207	7.897	0.202	8	2015-06	2016-09	-151.8	66.2	0.2
126955	0.357	21.914	0.356	15	2014-05	2016-11	-157.0	59.6	0.2

120731	0.42	7.896	0.416	25	2013-10	2016-11	-156.4	58.4	0.2
103838	0.36	5.438	0.358	68	2002-05	2013-08	-151.4	59.8	0.2
126925	0.345	4.921	0.342	10	2018-06	2019-09	-148.8	61.8	0.2
127538	0.204	11.187	0.202	5	2016-06	2016-10	-160.8	64.2	0.2
117603	0.348	5.653	0.343	77	2005-08	2019-10	-145.3	63.9	0.2
115402	0.356	4.757	0.347	31	2012-09	2017-08	-159.1	59.2	0.2
127381	0.267	6.97	0.262	74	2008-06	2019-10	-151.2	60.0	0.2
126508	0.42	15.977	0.419	25	2013-06	2019-09	-148.5	67.6	0.2
127006	0.266	5.175	0.257	75	2005-05	2019-10	-150.1	67.3	0.2
126742	0.073	1.7	0.022	59	2006-10	2019-09	-144.6	65.5	0.2
106153	0.49	26.672	0.489	50	2011-10	2019-10	-149.6	60.2	0.2
126826	0.298	7.899	0.293	73	2006-10	2019-10	-150.6	66.6	0.2
127211	0.275	6.707	0.266	33	2012-06	2019-09	-149.4	69.3	0.2
127024	0.296	2.106	0.255	39	2012-08	2019-10	-162.9	67.8	0.2
121089	0.421	6.527	0.414	77	2006-10	2019-11	-150.4	60.6	0.2
115571	0.338	9.208	0.335	47	2011-10	2019-10	-146.9	65.1	0.2
106691	0.13	13.163	0.116	3	2019-08	2019-10	-154.4	59.0	0.2
126998	0.218	7.092	0.214	29	2011-06	2019-10	-148.2	63.3	0.2
123042	0.237	5.658	0.234	41	2011-10	2019-10	-146.2	65.1	0.2
127396	0.13	1.891	0.105	22	2013-07	2019-10	-135.1	59.5	0.2
126990	0.182	7.541	0.18	36	2012-07	2019-09	-145.8	64.9	0.2
107385	0.474	6.427	0.468	91	2007-06	2019-10	-150.7	59.9	0.2
107910	0.209	12.884	0.201	55	2007-05	2015-08	-149.8	61.5	0.2

127736	0.247	6.686	0.244	66	2007-10	2019-10	-151.4	59.3	0.2
129583	0.284	6.78	0.278	29	2011-07	2019-10	-148.5	70.3	0.2
126916	0.319	6.889	0.318	42	2013-06	2019-10	-149.4	60.7	0.2
100710	0.284	4.266	0.28	78	2006-10	2019-10	-149.7	62.2	0.2
117424	0.329	8.64	0.327	38	2012-08	2019-10	-150.8	62.8	0.2
126165	0.278	5.136	0.273	66	2006-10	2019-09	-147.4	65.4	0.2
121454	0.399	6.053	0.395	35	2013-06	2019-10	-145.1	61.3	0.2

Table B- 3 Water temperature model performance metrics for each subbasin.

SUBID	RMSE	NRMSE_SD	BIAS	OBS COUNT	START MONTH	END MONTH	LAT	LON
114909	4.77	0.92	2.74	71	1995-07	2016-08	56.4	-62.2
114545	3.92	0.65	1.70	50	1999-08	2016-11	53.2	-66.8
105344	3.58	0.80	2.40	19	2010-06	2015-08	54.8	-66.8
110843	2.80	0.52	0.62	15	2011-10	2016-08	54.9	-67.1
111357	3.96	0.70	1.16	47	1998-08	2015-06	53.0	-64.7
117696	3.22	0.48	0.93	10	1998-08	2001-03	52.7	-64.8
103851	1.38	0.23	0.04	10	1998-08	2001-03	52.3	-64.3
117704	3.92	0.68	1.73	46	1999-03	2014-10	53.2	-60.8
105887	3.79	0.61	0.69	59	1998-08	2016-10	53.1	-61.6
117699	4.72	0.60	-0.93	7	2009-07	2016-08	53.2	-60.7
102967	3.00	0.47	-0.71	68	1979-01	2016-10	53.5	-91.5
106837	4.26	0.62	-2.33	37	1980-05	2016-10	52.7	-92.5
103200	3.37	0.65	-1.06	14	2011-08	2016-10	52.7	-94.0
103100	3.46	0.65	-0.38	15	2011-08	2016-10	52.5	-93.1
129480	2.89	0.42	-0.99	78	1979-01	2016-10	53.4	-91.8
117730	3.42	0.45	-1.50	50	1993-01	2016-09	52.6	-90.2
102626	3.17	0.57	-0.95	44	1979-05	2016-09	53.7	-88.0
117743	2.93	0.44	-0.33	53	1980-01	2016-09	53.8	-84.9
112289	4.62	0.65	-2.56	5	2011-08	2012-09	55.2	-83.7
117747	3.20	0.44	-0.20	57	1979-01	2016-06	51.8	-89.6
129475	2.93	0.44	-1.13	51	1979-05	2016-06	52.3	-88.8
117750	5.10	0.73	1.77	16	2011-08	2016-09	52.1	-87.1
115579	2.17	0.36	-0.89	11	2013-10	2016-09	52.9	-86.2
117756	4.19	0.52	0.45	45	1989-05	2016-10	51.2	-91.6
100300	3.55	0.48	-0.74	17	2011-07	2016-06	51.0	-90.2
117757	3.05	0.47	-0.81	29	1985-05	2016-06	50.9	-88.9
117758	4.64	0.64	-0.24	45	1979-01	2016-10	49.6	-90.6
120344	1.90	0.23	0.09	45	1980-07	2016-06	51.4	-89.4
117772	3.21	0.46	0.75	137	1980-02	2016-08	49.8	-84.5
107495	2.74	0.38	-1.81	19	2006-01	2016-10	49.7	-86.9
111828	2.47	0.34	-0.22	60	1980-03	2016-09	50.7	-86.5
117783	3.48	0.48	1.29	64	1979-05	2016-10	48.4	-81.4
103970	1.86	0.21	-0.47	48	2003-01	2016-10	47.7	-81.6
107213	3.06	0.41	-1.29	44	2007-05	2016-10	47.5	-81.8
101311	1.56	0.24	0.01	39	2000-12	2016-10	48.2	-82.5
117787	2.82	0.32	0.36	63	2000-09	2016-10	48.3	-82.4
105015	2.05	0.26	0.27	38	2006-04	2016-10	47.9	-83.1
117790	3.00	0.37	-0.60	27	2007-05	2016-10	49.4	-82.4
116833	2.85	0.40	0.11	143	1980-01	2016-10	49.6	-83.3
102892	2.10	0.26	-0.60	14	2008-11	2016-10	48.3	-80.5

117836	3.66	0.51	-0.47	20	2009-08	2016-05	50.0	-81.5
102604	3.83	0.57	0.86	148	1996-02	2014-10	49.5	-113.9
115592	4.36	1.01	2.23	197	1995-12	2016-12	49.6	-114.4
117853	3.17	0.56	0.29	74	2008-10	2016-12	49.7	-114.1
100072	2.75	0.40	0.73	146	1997-07	2016-11	50.1	-113.8
100081	3.98	0.56	0.97	78	1999-06	2009-10	49.8	-113.4
100137	3.03	0.49	1.54	231	1980-02	2016-12	49.1	-113.7
111238	5.05	0.95	3.05	183	1997-01	2016-12	49.1	-113.9
100172	3.26	0.50	1.34	200	1995-06	2016-10	49.4	-113.5
101167	3.34	0.45	1.49	212	1995-06	2016-12	49.6	-112.8
117877	2.93	0.46	1.43	8	2000-11	2016-09	48.8	-113.5
100238	3.42	0.43	0.58	208	1996-01	2016-12	49.9	-111.8
117919	4.54	0.71	-2.03	200	1994-01	2016-12	51.0	-114.1
129429	3.10	0.49	1.00	163	1980-01	2016-11	50.9	-114.3
117923	4.68	0.74	-0.49	127	1997-02	2014-10	50.5	-114.2
100378	4.03	0.61	-0.46	202	1994-01	2016-11	50.8	-113.8
100403	3.83	0.66	-0.98	139	1990-05	2016-11	50.8	-113.4
100327	3.15	0.69	0.06	100	1997-05	2016-08	51.0	-114.0
100393	3.81	0.74	-0.91	80	1998-04	2016-06	50.7	-112.5
100419	3.54	0.44	0.48	208	1996-01	2016-12	50.0	-111.6
100440	3.28	0.46	0.64	204	1996-01	2016-12	52.0	-114.1
100443	3.49	0.47	0.81	148	1990-07	2016-11	52.8	-114.3
101053	2.87	0.35	0.90	60	1996-01	2014-06	52.1	-106.6
129459	2.94	0.35	0.02	152	1991-06	2016-10	49.9	-107.2
129599	2.70	0.33	0.96	186	1979-04	2016-06	50.7	-104.9
129512	2.98	0.36	0.96	124	1982-04	2016-07	51.0	-106.3
129549	3.33	0.40	0.69	139	1995-04	2016-05	50.6	-101.7
115813	2.89	0.37	0.86	55	1996-01	2011-06	53.7	-103.4
118109	77.80	10.15	48.36	113	1994-06	2011-10	53.8	-101.2
100369	2.87	0.38	-0.47	86	1989-04	2010-04	51.4	-100.4
101242	4.62	0.52	0.10	68	1996-03	2014-10	51.9	-104.1
100639	4.16	0.48	0.13	65	1996-03	2014-10	51.8	-104.3
101243	4.76	0.62	-1.00	78	1996-02	2016-11	52.0	-104.3
129898	3.10	0.36	0.79	28	2001-11	2014-10	49.5	-104.3
101941	3.67	0.45	1.61	15	2007-05	2015-02	49.9	-103.0
129976	4.22	0.51	-0.01	94	1996-02	2011-06	49.1	-101.2
130013	4.52	0.55	1.49	113	1995-04	2010-11	49.6	-100.9
130047	3.79	0.46	-0.09	112	1996-01	2016-10	49.0	-98.6
118216	2.33	0.26	0.35	148	1990-08	2010-10	49.0	-97.2
118255	2.54	0.31	0.20	70	1980-02	2010-08	49.8	-97.1
118261	1.44	0.23	-1.18	6	2009-03	2010-06	49.8	-97.0
118309	2.37	0.28	-0.19	25	2008-04	2010-11	50.1	-96.9
101316	2.68	0.37	-1.09	43	1985-07	2016-07	48.4	-92.2

100131	2.93	0.33	-2.56	11	2007-05	2016-03	48.5	-92.7
115834	1.34	0.18	-0.04	22	2005-01	2015-02	48.6	-93.3
106295	2.27	0.29	-0.07	48	1996-01	2016-07	48.9	-92.7
113743	3.09	0.37	-0.39	108	1996-01	2016-11	48.8	-91.6
128894	2.88	0.38	0.53	24	2004-01	2015-10	48.7	-94.6
109924	11.06	1.56	4.53	9	2003-11	2014-10	49.7	-94.8
100016	15.76	2.17	8.66	55	2001-06	2016-01	49.8	-94.5
118275	3.55	0.44	1.49	21	2001-04	2012-10	50.2	-95.1
111508	2.33	0.36	-0.55	45	1995-05	2016-10	50.2	-91.5
118486	2.95	0.43	-0.26	29	1996-09	2016-10	50.3	-92.3
100127	2.26	0.32	-1.11	35	2003-06	2016-10	50.1	-92.2
101442	3.49	0.56	1.29	19	2006-01	2016-05	51.0	-93.9
115828	3.20	0.45	-0.15	89	1980-05	2016-03	50.4	-94.5
113365	2.83	0.40	0.35	48	1996-01	2016-06	50.7	-94.0
110040	6.08	0.81	2.50	32	1996-05	2016-05	50.2	-94.0
118300	2.56	0.35	0.85	76	1979-10	2011-03	51.8	-93.5
103515	5.94	1.65	2.40	16	1996-01	2008-01	55.5	-98.6
118318	8.54	29.58	4.81	3	1997-02	1997-06	53.8	-97.8
100217	1.46	0.15	-0.84	3	1996-03	1997-06	54.0	-97.8
100258	2.27	0.19	-1.60	2	1997-01	1997-06	54.6	-97.8
111912	1.83	0.15	-1.30	2	1997-01	1997-06	54.9	-98.4
122720	3.20	0.43	1.28	73	1996-02	2016-09	54.9	-107.7
118342	1.71	0.23	0.49	71	1996-02	2016-09	55.7	-109.4
103906	2.74	0.42	-1.80	18	2006-10	2016-06	55.9	-107.7
118346	2.36	0.29	0.02	73	1996-02	2016-09	55.4	-108.0
118348	3.23	0.44	-0.65	60	1979-05	2016-09	56.2	-106.6
101407	2.87	0.42	0.57	33	1996-03	2015-10	54.0	-106.1
101908	5.74	0.78	-1.08	28	1996-03	2014-07	54.0	-106.2
101209	3.01	0.43	-0.23	30	1996-03	2015-10	54.0	-106.4
123922	1.87	0.27	0.09	49	1996-01	2016-06	55.1	-105.3
100020	1.14	0.15	-0.92	8	2014-04	2016-09	55.4	-104.5
118351	5.65	0.83	-4.06	34	1996-01	2016-06	55.6	-104.7
100086	3.02	0.64	-0.35	22	1996-02	2016-09	58.5	-103.3
118355	2.54	0.34	-1.39	36	1981-10	2016-06	57.6	-104.2
118357	2.48	0.36	-1.18	29	1996-01	2016-06	57.5	-105.0
104669	2.30	0.32	-1.39	36	1996-01	2016-06	57.1	-103.7
101567	2.34	0.41	0.03	34	1996-01	2016-06	56.2	-103.2
103330	3.01	0.39	-0.09	5	2015-04	2016-09	56.0	-103.3
103472	2.53	0.30	-1.33	17	2005-09	2016-06	55.6	-102.8
115801	3.33	0.90	0.86	13	1996-06	2010-01	57.3	-98.2
121327	6.39	2.05	2.82	18	1996-01	2011-10	56.8	-99.5
118388	2.78	0.43	0.85	36	1995-01	2016-07	63.6	-105.2
102395	2.32	0.41	0.65	60	1995-02	2016-09	64.5	-101.4

100031	4.67	1.02	2.62	61	1979-05	2016-09	64.2	-99.5
100269	1.39	0.20	0.02	34	1995-09	2016-09	61.1	-101.0
100266	1.54	0.32	0.31	98	1982-02	2016-09	63.7	-95.9
101090	2.99	0.78	-2.39	13	2006-08	2011-09	71.2	-79.4
111079	2.01	0.77	-0.01	12	2006-08	2011-09	70.5	-77.4
118516	2.26	0.50	0.64	100	1996-01	2016-10	56.7	-125.1
128626	4.18	0.84	2.01	114	1987-06	2016-10	57.1	-125.1
118518	3.20	0.80	-0.12	169	1981-05	2016-10	57.2	-124.9
118521	2.87	0.70	0.45	97	1996-01	2016-10	56.5	-123.9
129567	2.66	0.53	0.57	95	1996-01	2016-10	55.9	-124.6
103800	4.12	0.83	2.80	199	1979-01	2016-10	56.2	-124.6
118525	3.07	0.71	1.19	99	1996-04	2016-10	56.1	-124.8
118527	2.33	0.41	0.84	87	1996-01	2016-06	55.4	-123.6
121360	3.95	0.70	2.52	250	1979-02	2016-10	55.1	-122.9
118533	5.59	1.23	3.32	154	1979-01	2016-10	56.0	-121.9
101568	4.62	0.78	2.94	151	1979-02	2016-08	56.0	-123.7
119432	7.57	2.04	5.34	104	1998-02	2016-10	55.9	-122.7
118537	3.89	0.77	2.15	159	1979-06	2016-09	56.2	-120.8
118552	3.74	0.74	1.80	137	1979-07	2016-10	56.1	-120.7
130742	3.10	0.51	0.90	73	1995-05	2016-10	55.9	-118.6
118559	3.62	0.67	1.32	114	1981-01	2010-06	56.1	-120.1
130813	2.70	0.40	-0.09	133	1992-07	2016-08	55.1	-118.8
111554	2.48	0.35	0.37	53	1996-07	2016-09	56.2	-117.3
127512	3.30	0.47	0.44	34	2008-03	2016-10	57.9	-117.5
103523	2.04	0.33	-0.54	34	1996-02	2016-06	58.4	-104.6
100003	2.76	0.48	1.11	32	1996-02	2016-06	59.2	-105.5
118611	1.82	0.25	-0.05	72	1992-09	2016-09	58.3	-109.8
102029	1.59	0.23	-0.53	28	1996-02	2016-06	59.0	-108.2
100019	3.18	0.62	1.00	37	1995-01	2016-09	59.4	-108.9
127718	2.60	0.43	0.75	162	1979-01	2016-05	59.9	-111.6
102551	3.77	0.50	-1.29	104	1996-01	2016-08	60.9	-115.7
100568	3.11	0.65	1.32	15	1996-02	2016-04	59.8	-109.4
118651	2.81	0.42	-1.01	14	1995-01	2016-09	60.0	-108.8
118652	2.03	0.27	-0.76	9	2012-11	2016-09	59.8	-108.3
128155	3.02	0.40	-2.01	21	2007-05	2016-03	60.4	-110.7
100204	3.15	0.44	0.39	31	1996-02	2016-09	61.7	-109.7
118654	3.21	0.56	-0.10	31	1979-06	2012-08	61.9	-107.7
114780	1.67	0.23	-0.64	61	1994-06	2014-08	60.5	-111.5
104094	9.94	1.31	-6.96	8	2013-07	2015-02	63.7	-109.0
120355	2.91	0.64	1.32	65	1994-05	2016-09	62.9	-108.5
118663	1.84	0.30	-0.12	93	1984-07	2016-05	64.0	-115.4
110807	2.55	0.42	-0.09	131	1981-01	2016-04	64.4	-115.0
107004	5.53	0.87	0.00	100	1995-01	2016-09	62.4	-114.3

118667	2.65	0.36	-0.05	109	1984-07	2015-07	62.7	-114.3
118671	2.55	0.38	-0.58	109	1979-01	2016-09	62.5	-113.5
103269	3.20	0.56	-0.15	54	1995-01	2015-01	62.8	-114.0
100230	3.16	0.41	-0.27	68	1995-01	2015-01	62.7	-114.3
117861	2.68	0.43	0.17	61	1995-05	2015-07	62.6	-114.0
108165	2.16	0.33	-0.25	17	1998-06	2002-07	63.6	-114.0
108215	1.59	0.16	-0.81	6	2015-12	2016-09	62.8	-114.3
121067	5.29	0.66	-2.57	23	2010-04	2016-09	62.1	-113.2
118674	4.75	0.76	-0.91	29	2004-06	2016-09	63.0	-110.5
100045	3.45	0.56	-0.73	23	2010-04	2016-09	62.9	-109.2
127175	3.94	0.61	-0.15	22	2010-04	2016-09	62.9	-110.2
106389	8.52	1.22	-5.82	5	2013-07	2015-02	63.7	-108.9
118676	1.65	0.25	0.18	69	1993-11	2016-04	63.1	-117.0
100660	2.11	0.26	-1.01	18	2013-09	2016-08	60.9	-117.4
127508	3.02	0.56	1.60	172	1981-07	2016-10	61.2	-137.0
123858	4.17	0.77	1.45	99	1991-07	2016-09	61.5	-137.6
128869	2.59	0.48	0.68	214	1980-02	2016-10	61.2	-137.0
119472	4.69	0.78	1.43	96	1994-06	2016-09	61.6	-137.4
108517	2.13	0.54	-0.57	150	1988-10	2016-09	60.1	-137.1
118699	3.19	0.61	-0.46	170	1979-05	2016-09	57.9	-131.2
118709	4.29	1.28	3.63	192	1979-01	2016-08	56.7	-131.7
100329	3.64	0.79	2.20	136	1981-07	2016-11	59.6	-133.7
112884	3.78	0.79	1.20	133	1990-05	2016-10	60.2	-134.7
103600	3.91	0.89	1.81	176	1979-05	2016-09	59.9	-134.3
101179	2.80	0.47	1.41	109	1995-05	2016-12	60.7	-135.1
100451	2.84	0.50	0.39	100	1995-01	2016-10	60.5	-134.4
103133	2.67	0.51	0.72	5	2016-06	2016-11	60.8	-133.1
100525	2.40	0.38	0.56	86	1995-01	2016-11	60.2	-132.7
100835	2.76	0.51	0.29	118	1994-04	2016-11	60.0	-132.1
127499	8.45	1.46	6.06	10	1991-08	2016-09	61.9	-134.8
103338	1.99	0.30	0.87	8	2014-12	2016-07	62.1	-136.3
119114	2.55	0.43	1.12	190	1982-07	2016-09	62.1	-136.3
120358	5.36	1.03	3.25	102	1995-02	2016-09	62.2	-134.4
119117	2.64	0.46	0.72	177	1979-05	2016-09	62.0	-132.4
119119	2.61	0.57	1.46	19	2012-08	2016-05	62.0	-130.6
106962	3.41	0.73	1.73	18	1995-02	2016-09	62.9	-130.5
119123	4.42	0.75	2.20	178	1979-06	2016-09	62.8	-136.6
119125	2.81	0.55	1.64	22	2011-03	2016-09	62.0	-132.4
124073	6.98	1.47	3.48	118	1995-01	2016-09	61.1	-138.5
119138	2.56	0.56	1.15	19	1995-04	2016-09	63.3	-131.5
119140	3.85	0.67	1.21	90	1996-02	2016-08	63.8	-135.4
119152	4.24	0.85	1.80	137	1979-04	2010-06	63.6	-137.3
119156	4.07	0.86	0.56	122	1979-06	2010-06	64.0	-139.4

119158	5.10	1.54	1.92	9	1986-10	2016-07	64.0	-137.6
114966	8.76	1.24	-3.98	11	1996-01	2016-08	66.4	-138.4
119184	2.58	0.51	-0.32	146	1984-08	2016-08	60.2	-129.6
119194	2.56	0.57	0.37	10	2015-08	2016-11	61.5	-128.2
104334	3.54	0.59	1.76	13	2014-09	2016-09	60.1	-124.9
119202	2.81	0.76	1.32	246	1979-06	2016-10	59.5	-126.2
109081	2.76	0.50	0.94	206	1983-05	2016-10	59.6	-126.5
119223	2.37	0.31	0.44	27	1996-01	2016-09	60.0	-123.0
104654	3.59	0.55	0.21	10	2014-10	2016-09	60.0	-124.1
129479	2.45	0.51	-0.51	161	1980-05	2016-10	61.6	-125.8
122441	2.38	0.55	-0.32	19	2013-10	2016-10	61.6	-124.8
119249	3.23	0.47	0.76	184	1982-07	2016-11	61.7	-121.2
129461	2.56	0.34	0.98	204	1979-05	2016-07	61.1	-119.8
120607	2.64	0.55	-0.47	95	1993-09	2016-09	64.1	-128.2
119258	4.15	0.77	-1.08	93	1979-05	2016-09	63.9	-125.3
101068	2.63	0.38	-0.19	44	1995-01	2016-08	65.6	-117.8
100005	2.74	0.69	1.45	71	1987-07	2016-01	65.1	-123.6
109595	3.27	0.86	0.51	28	1995-05	2015-09	66.6	-117.6
119277	3.60	0.58	1.60	203	1979-05	2016-09	65.3	-126.9
121001	4.12	0.60	1.22	75	2001-09	2016-03	65.4	-127.4
112423	3.72	0.58	-0.62	63	2003-03	2016-08	67.8	-131.9
121194	4.69	0.72	2.50	33	2001-09	2016-08	66.7	-129.3
119299	4.88	0.87	-0.66	8	1996-03	2016-11	65.4	-138.3
119308	1.98	0.36	1.62	3	2016-08	2016-12	64.7	-133.7
104070	2.39	0.52	0.63	88	1994-07	2016-09	64.6	-112.0
102208	2.11	0.41	0.10	70	1999-09	2016-06	64.8	-111.7
100244	4.21	1.15	2.46	28	1995-03	2014-06	65.4	-114.0
106003	9.54	1.87	-2.30	4	1993-09	2008-08	65.6	-112.9
999000	4.11	1.00	2.34	61	1998-06	2016-08	65.4	-114.0
120459	3.81	0.92	2.26	77	1993-06	2016-08	66.3	-114.0
100481	3.32	0.66	-1.14	32	1992-06	2003-02	67.4	-108.9
119535	4.75	1.37	-0.36	33	1995-02	2011-09	65.8	-111.2
119337	3.27	0.75	0.90	40	1995-06	2016-08	67.7	-104.1
119340	3.54	0.77	1.13	72	1995-02	2016-08	65.2	-106.1
119342	2.70	0.54	0.24	69	1979-08	2016-08	65.0	-104.5
105273	1.84	0.70	-0.60	21	2007-04	2014-11	64.9	-68.3
101441	2.65	0.73	-1.36	30	2006-06	2014-11	63.5	-68.9
111314	2.88	1.28	1.18	31	2006-05	2014-11	63.2	-68.4
113169	2.89	0.75	0.31	28	2007-07	2016-07	63.8	-68.5
601229	2.15	0.70	0.25	14	2007-07	2016-09	74.7	-94.8
102688	2.69	0.55	0.79	101	2004-09	2017-09	57.2	-154.2
100581	1.17	0.25	-0.51	28	2004-08	2007-06	57.2	-154.1
106022	3.04	0.70	1.59	97	2005-07	2017-09	57.2	-154.4

117850	1.61	0.38	-0.02	35	2004-08	2007-06	57.4	-154.1
120460	1.48	0.24	0.22	93	2006-06	2017-05	62.6	-141.0
125027	2.18	0.43	1.06	68	2006-06	2012-10	62.9	-141.5
126094	3.78	0.83	2.08	30	2010-06	2015-09	66.0	-151.9
118006	3.25	0.61	1.87	55	2010-06	2015-09	66.2	-151.1
118387	2.06	0.38	0.02	45	2011-05	2015-09	66.9	-151.1
114438	2.52	0.60	0.52	24	2015-05	2017-04	58.0	-156.8
125092	1.78	0.27	-0.18	13	2015-06	2016-06	66.9	-151.7
100308	2.61	0.79	1.70	36	2014-09	2017-08	55.3	-162.7
102162	2.64	0.91	1.61	36	2014-09	2017-08	55.0	-162.9
117248	1.44	0.31	1.15	36	2014-09	2017-08	55.0	-163.1
104420	4.01	2.88	2.40	36	2014-09	2017-08	55.5	-162.5
111965	4.97	0.62	-2.84	14	2016-05	2017-08	65.7	-156.1
129660	1.93	0.39	0.98	11	2016-06	2017-06	66.1	-156.3
128773	1.24	0.22	-0.11	13	2016-06	2017-06	66.1	-156.9
104311	3.39	0.87	0.57	67	2011-09	2017-09	57.3	-154.0
100582	5.36	2.52	0.91	14	2015-06	2017-10	57.3	-154.2

Table B- 4 River ice thickness model performance metrics for each subbasin.

SUBID	RMSE	NRMSE_SD	OBS_MEAN	SIM_MEAN	%BIAS	BIAS	COUNT	LAT	LON
127095	0.38	2.93	0.54	0.18	-0.63	-0.36	10	48.9	-72.2
108849	0.51	4.74	0.65	0.16	-0.75	-0.49	23	48.7	-72.5
117467	0.27	2.93	0.47	0.23	-0.51	-0.25	23	48.4	-72.0
108826	0.74	4.20	0.88	0.16	-0.81	-0.72	23	50.4	-66.2
109295	0.58	3.30	0.70	0.16	-0.72	-0.54	22	50.3	-63.6
117506	0.54	3.76	0.71	0.19	-0.72	-0.52	23	50.4	-61.7
117522	0.34	3.83	0.56	0.23	-0.57	-0.32	25	52.2	-61.3
117524	0.36	7.22	0.59	0.25	-0.57	-0.34	16	52.2	-60.1
117536	0.49	3.04	0.71	0.25	-0.62	-0.46	22	51.8	-57.6
117585	0.14	1.92	0.37	0.24	-0.33	-0.13	15	51.5	-78.1
117591	0.48	6.11	0.62	0.15	-0.75	-0.47	10	52.2	-74.6
117624	0.35	3.92	0.53	0.19	-0.62	-0.33	13	55.2	-77.0
117673	0.59	3.44	0.82	0.27	-0.66	-0.55	14	57.7	-69.6
117686	0.30	1.67	0.51	0.25	-0.51	-0.27	12	57.9	-67.6
117692	0.52	4.21	0.79	0.31	-0.61	-0.48	14	56.8	-65.8
117694	0.63	5.92	0.89	0.27	-0.70	-0.62	21	55.2	-61.3
116616	0.65	5.56	0.89	0.25	-0.72	-0.64	16	54.6	-61.0
112064	0.52	2.96	0.71	0.22	-0.67	-0.49	19	54.1	-61.4
103433	0.64	5.76	0.83	0.20	-0.76	-0.63	26	53.5	-57.5
117710	0.48	3.59	0.73	0.26	-0.63	-0.46	24	52.6	-56.9
117713	0.69	2.95	0.96	0.32	-0.66	-0.64	29	56.4	-92.8
127462	0.57	4.67	0.85	0.30	-0.64	-0.55	34	55.9	-92.1
117723	0.75	5.72	1.02	0.28	-0.72	-0.74	17	55.4	-88.3
117739	0.63	4.20	0.88	0.27	-0.69	-0.61	22	54.5	-87.2
117743	0.40	3.53	0.65	0.27	-0.59	-0.39	13	53.8	-84.9
117755	0.62	4.67	0.82	0.21	-0.74	-0.61	17	53.1	-85.1
117760	0.46	5.81	0.64	0.19	-0.70	-0.45	13	51.6	-86.4
117763	0.48	4.40	0.70	0.24	-0.66	-0.46	15	51.3	-83.8
117777	0.35	7.19	0.58	0.24	-0.58	-0.34	15	50.4	-84.4
117788	0.31	3.27	0.55	0.27	-0.50	-0.28	17	49.3	-82.0
125963	0.45	5.86	0.65	0.21	-0.67	-0.44	3	50.8	-81.3
116833	0.23	2.65	0.43	0.22	-0.47	-0.21	23	49.6	-83.3
117809	0.41	3.77	0.62	0.22	-0.63	-0.39	21	50.6	-82.1
109026	0.10	2.09	0.22	0.25	0.16	0.02	19	48.6	-78.1
117844	0.33	2.73	0.56	0.24	-0.58	-0.33	10	50.0	-79.1
117848	0.31	2.38	0.48	0.20	-0.55	-0.28	28	49.8	-114.2
100072	0.19	1.08	0.29	0.20	-0.05	-0.09	17	50.0	-113.7
100117	0.15	1.18	0.31	0.24	0.35	-0.07	6	50.1	-113.1
100172	0.31	2.18	0.44	0.18	-0.55	-0.26	13	49.4	-113.5
117919	0.17	1.34	0.26	0.15	-0.24	-0.11	9	51.0	-114.1
117922	0.41	1.76	0.52	0.18	-0.55	-0.34	25	50.9	-114.6

100378	0.46	2.38	0.60	0.21	-0.52	-0.39	34	50.8	-113.8
100440	0.52	2.53	0.65	0.17	-0.70	-0.48	34	52.0	-114.1
100443	0.26	1.12	0.34	0.22	0.03	-0.12	15	52.4	-113.8
100456	0.40	2.10	0.56	0.20	-0.58	-0.36	32	52.3	-114.3
100940	0.35	1.57	0.64	0.39	-0.32	-0.25	15	52.7	-108.3
100978	0.29	1.06	0.35	0.38	0.99	0.03	3	52.2	-107.4
101003	0.27	2.63	0.58	0.36	-0.37	-0.22	37	53.2	-105.8
129447	0.32	3.33	0.68	0.40	-0.41	-0.28	19	52.9	-105.8
129549	0.27	1.46	0.59	0.43	-0.15	-0.17	33	50.5	-101.6
118078	0.15	0.83	0.26	0.28	0.84	0.02	16	53.4	-103.1
118099	0.23	2.26	0.52	0.34	-0.32	-0.18	35	53.6	-102.1
118109	0.36	3.02	0.72	0.39	-0.46	-0.34	34	53.8	-101.2
118121	0.18	1.12	0.37	0.34	0.06	-0.03	37	52.9	-102.2
129714	0.38	2.13	0.65	0.33	-0.44	-0.32	33	51.8	-99.5
129780	0.31	1.92	0.52	0.35	-0.24	-0.18	31	52.0	-98.3
129808	0.19	1.13	0.36	0.32	0.19	-0.04	32	51.6	-101.9
196405	0.23	2.07	0.56	0.41	-0.26	-0.16	29	50.1	-101.0
129869	0.18	2.06	0.54	0.44	-0.19	-0.10	29	49.7	-98.9
130016	0.22	1.44	0.33	0.39	0.58	0.06	14	49.6	-99.7
130007	0.25	1.02	0.33	0.32	0.79	-0.01	5	49.6	-100.2
118225	0.17	1.60	0.50	0.44	-0.08	-0.06	30	49.6	-97.2
127088	0.26	1.85	0.63	0.42	-0.30	-0.21	32	50.1	-96.9
130266	0.26	2.19	0.54	0.32	-0.37	-0.21	37	54.3	-108.6
130273	0.36	2.45	0.60	0.30	-0.48	-0.30	36	54.4	-110.2
122720	0.27	2.69	0.54	0.32	-0.39	-0.22	34	54.8	-107.8
118347	0.27	2.68	0.56	0.33	-0.41	-0.23	17	56.1	-107.6
118348	0.32	2.83	0.57	0.28	-0.51	-0.29	33	56.2	-106.6
118355	0.04	0.55	0.27	0.28	0.06	0.01	2	57.6	-104.2
118381	0.64	2.71	0.98	0.45	-0.51	-0.52	36	58.9	-96.3
102395	1.60	4.82	2.02	0.46	-0.77	-1.57	36	64.5	-101.4
100266	1.00	3.31	1.47	0.53	-0.62	-0.93	35	63.7	-95.9
118402	0.55	1.48	0.96	0.61	-0.24	-0.34	11	64.3	-93.9
100468	0.42	3.41	0.66	0.27	-0.58	-0.39	29	54.2	-116.1
130505	0.17	1.50	0.47	0.37	-0.18	-0.10	36	54.5	-114.0
199950	0.29	2.77	0.58	0.32	-0.44	-0.26	37	54.7	-113.3
118479	0.33	2.92	0.68	0.39	-0.42	-0.29	37	56.7	-111.3
118490	0.37	3.58	0.72	0.38	-0.47	-0.34	33	56.8	-111.4
128626	0.37	2.36	0.54	0.23	-0.54	-0.32	35	57.1	-125.1
129567	0.33	2.46	0.52	0.23	-0.52	-0.29	34	55.9	-124.6
118540	0.54	2.18	0.75	0.27	-0.61	-0.48	32	55.7	-121.2
118546	0.36	1.67	0.64	0.38	-0.32	-0.27	32	56.3	-120.7
130813	0.46	2.17	0.68	0.28	-0.57	-0.40	34	55.1	-118.8
118581	0.29	2.55	0.56	0.29	-0.46	-0.27	34	55.5	-117.2

130847	0.42	2.55	0.70	0.33	-0.49	-0.37	36	55.7	-117.6
111554	0.53	2.54	0.89	0.41	-0.53	-0.49	16	56.2	-117.3
128116	0.30	0.98	0.35	0.28	1.45	-0.06	24	56.5	-117.7
118585	0.39	1.31	0.52	0.25	-0.11	-0.27	28	56.9	-117.6
118593	0.27	2.00	0.64	0.43	-0.32	-0.21	34	57.9	-115.4
130886	0.47	3.39	0.84	0.40	-0.53	-0.45	35	59.1	-112.4
127718	0.56	3.21	0.90	0.39	-0.57	-0.52	34	59.9	-111.6
118631	0.45	2.22	0.72	0.33	-0.52	-0.39	36	60.7	-115.9
118634	0.30	3.39	0.63	0.36	-0.43	-0.27	32	59.1	-117.6
118638	0.31	2.16	0.57	0.33	-0.35	-0.24	34	58.6	-118.3
118639	0.22	1.18	0.44	0.30	-0.18	-0.14	7	60.7	-114.9
118682	0.69	2.42	0.84	0.27	-0.61	-0.57	27	60.1	-138.0
118699	0.46	2.14	0.69	0.28	-0.57	-0.41	32	57.9	-131.2
118707	0.52	1.93	0.66	0.25	-0.55	-0.42	15	57.5	-131.8
119106	0.47	4.82	0.66	0.21	-0.68	-0.45	32	59.9	-131.8
103338	0.37	2.28	0.82	0.50	-0.37	-0.32	15	62.1	-136.3
119123	0.58	4.31	0.86	0.31	-0.64	-0.56	21	62.8	-136.6
129374	0.31	2.82	0.59	0.31	-0.45	-0.27	32	62.2	-133.4
119134	0.65	3.47	0.99	0.37	-0.61	-0.61	30	63.1	-139.5
119147	0.36	3.64	0.74	0.41	-0.43	-0.33	11	63.6	-135.9
119149	0.51	3.68	0.80	0.31	-0.60	-0.48	32	63.3	-139.3
119156	0.36	2.06	0.85	0.53	-0.38	-0.32	32	64.0	-139.4
119159	0.34	1.48	0.95	0.78	-0.14	-0.18	2	64.1	-139.4
119173	0.68	4.61	1.12	0.48	-0.58	-0.65	13	67.4	-137.8
119179	0.65	2.39	0.98	0.38	-0.59	-0.60	26	67.6	-139.7
119181	0.79	9.45	1.33	0.57	-0.58	-0.76	9	67.6	-139.9
119183	0.49	5.26	0.73	0.25	-0.66	-0.48	34	60.1	-128.9
119188	0.44	3.19	0.67	0.25	-0.61	-0.42	35	60.5	-129.1
104053	0.36	3.83	0.62	0.28	-0.55	-0.34	12	59.6	-127.3
103582	0.37	2.16	0.57	0.25	-0.53	-0.32	16	59.1	-127.5
119202	0.84	3.02	1.08	0.28	-0.72	-0.80	34	59.4	-126.1
119207	1.07	2.01	1.23	0.29	-0.73	-0.94	16	59.7	-124.5
119208	0.74	3.00	0.97	0.27	-0.70	-0.70	13	59.7	-127.2
119218	0.25	1.74	0.52	0.36	-0.29	-0.17	18	58.7	-122.6
119221	0.28	2.40	0.60	0.37	-0.36	-0.23	29	58.8	-122.7
119225	0.47	2.38	0.70	0.27	-0.58	-0.42	37	61.5	-125.4
129479	0.42	3.36	0.68	0.28	-0.58	-0.40	37	61.6	-125.8
100135	0.59	2.91	0.88	0.34	-0.59	-0.54	15	61.3	-124.1
119228	0.71	5.46	1.07	0.38	-0.64	-0.69	33	60.2	-123.5
119249	0.76	3.20	1.13	0.44	-0.59	-0.70	37	61.7	-121.2
119244	0.28	2.37	0.54	0.30	-0.38	-0.24	28	62.7	-122.9
119247	0.76	3.92	1.14	0.42	-0.62	-0.72	35	61.9	-121.4
119258	0.61	3.25	0.89	0.32	-0.63	-0.57	18	63.9	-125.3

119277	1.06	4.36	1.48	0.45	-0.69	-1.03	33	65.3	-126.9
129000	0.40	4.20	0.72	0.35	-0.49	-0.36	35	66.8	-133.1
102628	0.74	3.13	1.06	0.36	-0.65	-0.70	37	68.4	-133.8
129588	0.72	3.15	1.15	0.47	-0.58	-0.68	36	67.5	-133.8
119296	0.45	2.95	0.81	0.39	-0.52	-0.42	22	65.9	-136.0
119310	0.75	3.87	1.01	0.29	-0.70	-0.72	36	67.3	-134.9
119322	0.50	3.29	0.95	0.51	-0.46	-0.44	17	68.6	-128.4
104418	0.96	2.74	1.45	0.55	-0.60	-0.90	27	66.7	-108.8
119340	0.95	3.14	1.37	0.48	-0.63	-0.89	23	65.2	-106.1
119342	1.37	2.44	1.70	0.47	-0.58	-1.23	17	65.0	-104.5
119343	0.59	1.71	1.18	0.73	-0.31	-0.45	36	66.1	-96.5
309257	0.47	4.09	0.67	0.21	-0.68	-0.46	11	69.5	31.1
312561	0.58	4.83	0.75	0.19	-0.74	-0.56	11	69.4	31.9
312561	0.58	4.83	0.75	0.19	-0.74	-0.56	11	69.4	31.9
312713	0.48	2.52	0.61	0.21	-0.35	-0.40	13	68.9	32.8
312268	0.46	1.49	0.52	0.16	-0.31	-0.36	11	66.7	40.2
306887	0.43	1.72	0.55	0.19	-0.32	-0.35	11	66.6	39.0
301703	0.57	2.47	0.70	0.17	-0.64	-0.53	11	66.2	37.7
301701	0.41	1.94	0.55	0.19	-0.44	-0.36	14	66.3	36.7
306729	0.34	1.60	0.46	0.18	-0.42	-0.28	11	66.6	35.5
312314	0.56	1.66	0.64	0.17	-0.41	-0.47	9	66.7	34.9
313658	0.47	3.33	0.65	0.20	-0.69	-0.45	14	66.7	34.3
303988	0.35	1.15	0.42	0.20	0.11	-0.22	11	67.0	33.1
313983	0.36	1.21	0.48	0.21	-0.01	-0.26	10	65.3	34.4
304617	0.34	1.57	0.49	0.21	-0.26	-0.28	10	64.7	34.2
312743	0.49	4.41	0.71	0.23	-0.68	-0.48	10	64.2	35.3
302280	0.33	2.84	0.52	0.20	-0.63	-0.33	10	63.8	36.3
304926	0.31	1.54	0.45	0.19	-0.43	-0.26	10	63.6	37.0
310195	0.30	1.26	0.43	0.21	-0.14	-0.22	10	63.7	38.5
310195	0.30	1.26	0.43	0.21	-0.14	-0.22	10	63.7	38.5
302858	0.55	5.87	0.69	0.14	-0.79	-0.55	10	64.5	39.1
301290	0.35	1.93	0.56	0.24	-0.46	-0.32	10	64.1	42.2
301472	0.24	1.31	0.39	0.22	-0.08	-0.17	9	65.2	43.7
301455	0.55	2.30	0.73	0.23	-0.46	-0.50	10	64.6	45.3
313399	0.42	1.50	0.56	0.25	0.01	-0.31	10	65.6	44.3
303600	0.41	1.31	0.52	0.23	0.07	-0.29	10	66.7	48.0
412825	0.65	7.94	0.89	0.25	-0.73	-0.64	9	67.6	52.5
444087	0.67	18.28	0.95	0.28	-0.70	-0.66	16	66.7	66.6
444050	0.61	2.69	0.85	0.28	-0.47	-0.57	15	65.6	72.6
400561	0.64	4.56	0.96	0.33	-0.65	-0.63	14	67.2	77.7
400736	0.61	8.61	0.88	0.28	-0.68	-0.60	15	66.9	81.7
432508	0.18	70.11	0.09	0.26	1.88	0.17	15	66.7	73.6
404309	2.74	1.12	1.71	0.33	-0.68	-1.38	11	67.2	86.7

415650	0.49	9.67	0.92	0.44	-0.53	-0.49	9	73.1	89.2
417051	0.44	3.34	0.88	0.47	-0.46	-0.41	9	70.8	130.4
401806	0.47	14.52	0.94	0.48	-0.49	-0.46	14	70.5	126.8
406725	0.46	12.61	0.96	0.52	-0.45	-0.44	13	71.9	102.2
406722	0.20	1.48	0.76	0.65	-0.15	-0.11	10	71.9	114.3
407625	0.44	4.97	0.90	0.48	-0.47	-0.43	13	68.7	118.3
433356	0.23	7.05	0.96	0.81	-0.16	-0.15	14	71.1	136.1
444076	0.43	12.50	0.94	0.54	-0.43	-0.40	14	69.6	147.6
408724	0.49	182.27	0.09	0.56	5.28	0.47	14	69.2	155.0
432938	0.21	7.72	0.96	0.94	-0.02	-0.02	13	69.3	134.5
408739	0.41	6.59	0.93	0.53	-0.43	-0.39	10	67.5	154.0
432529	0.50	19.15	0.97	0.48	-0.51	-0.49	10	68.6	158.2
419658	0.23	3.40	0.92	0.77	-0.15	-0.15	10	67.1	179.0
408821	0.45	1.68	0.85	0.48	-0.23	-0.37	10	64.7	170.6

Appendix C – Time Series

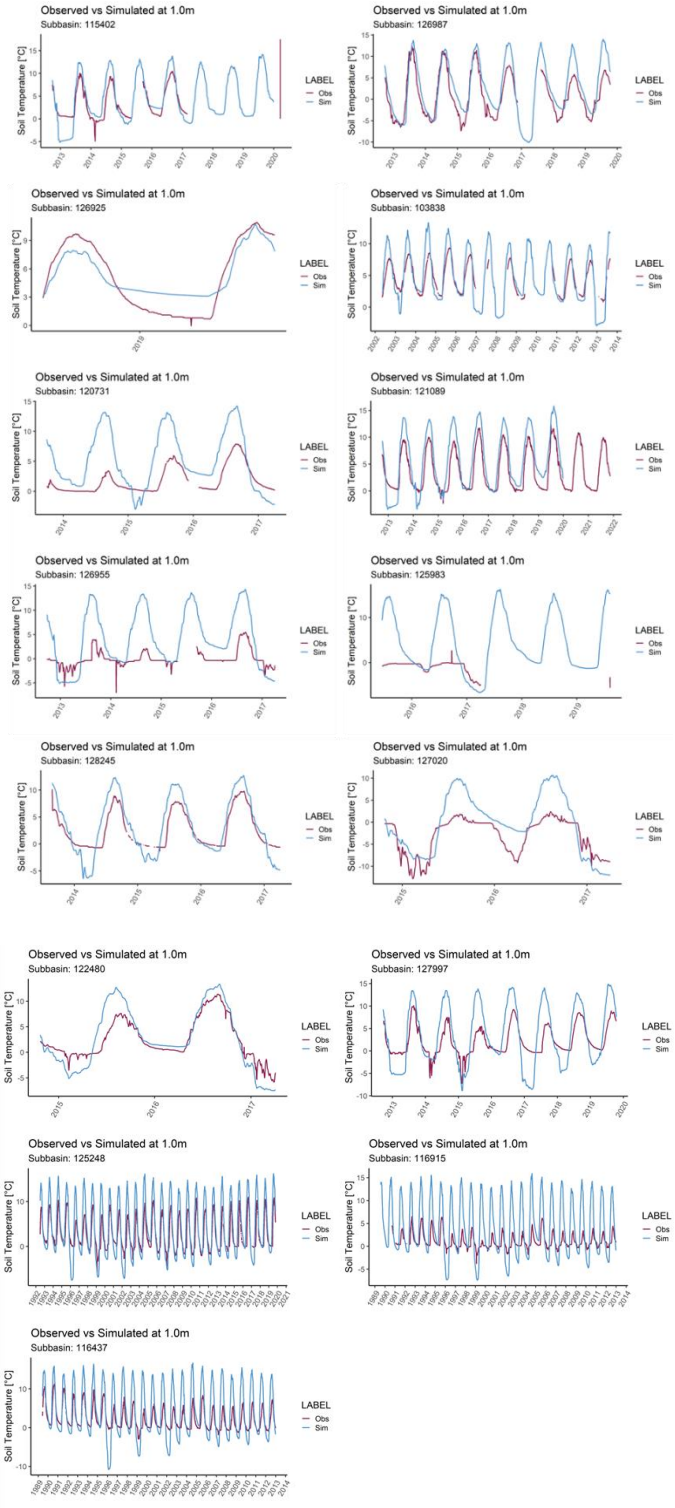

Figure C- 1 Timeseries of observed and modeled (sim) soil temperature at 1.0 m soil depth by subbasin.

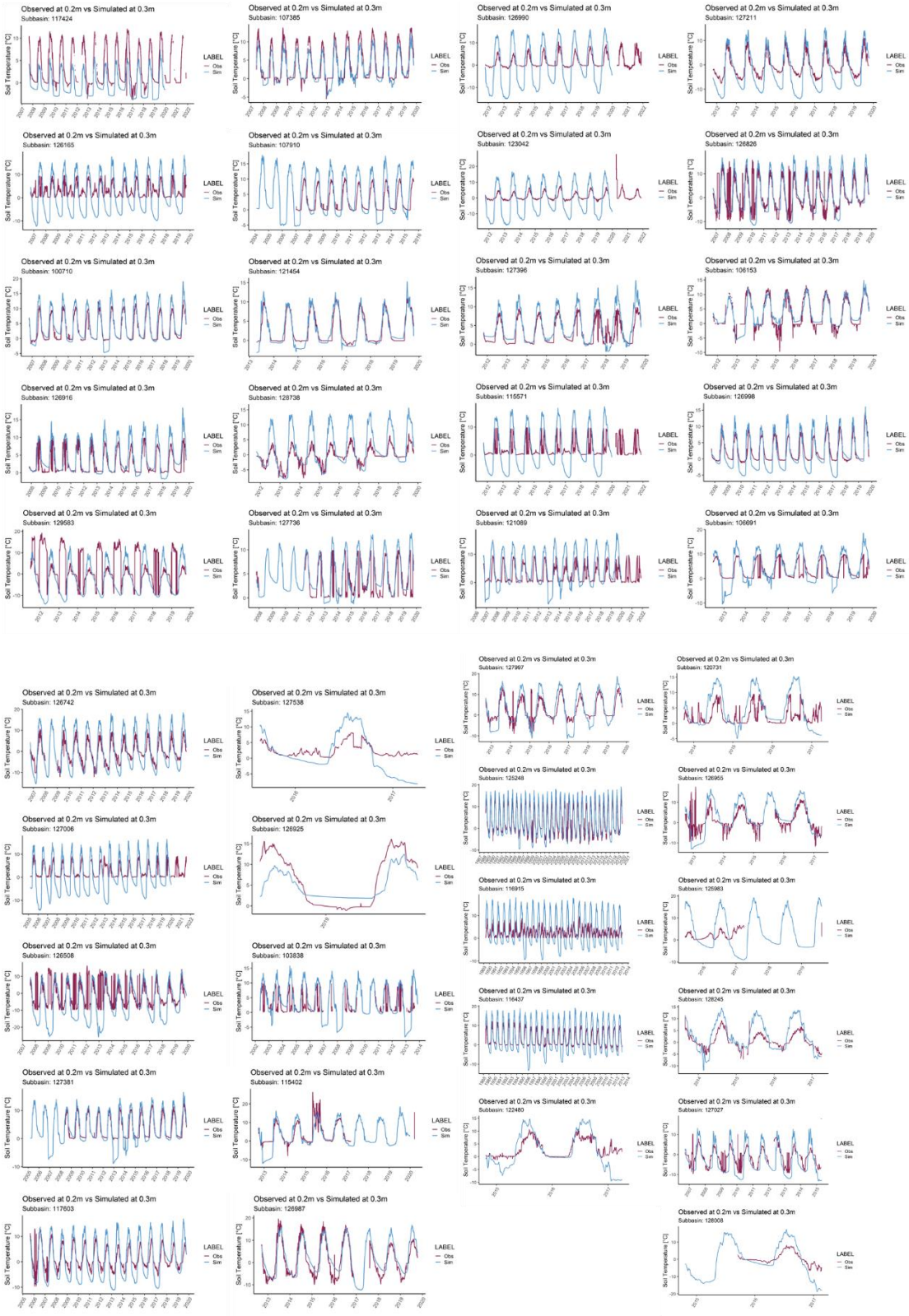

Figure C- 2 Timeseries of observed (0.2 m) and modeled (0.3 m) soil temperature for each subbasin. Observed data for some subbasins is the average of all available data stations within that subbasin.

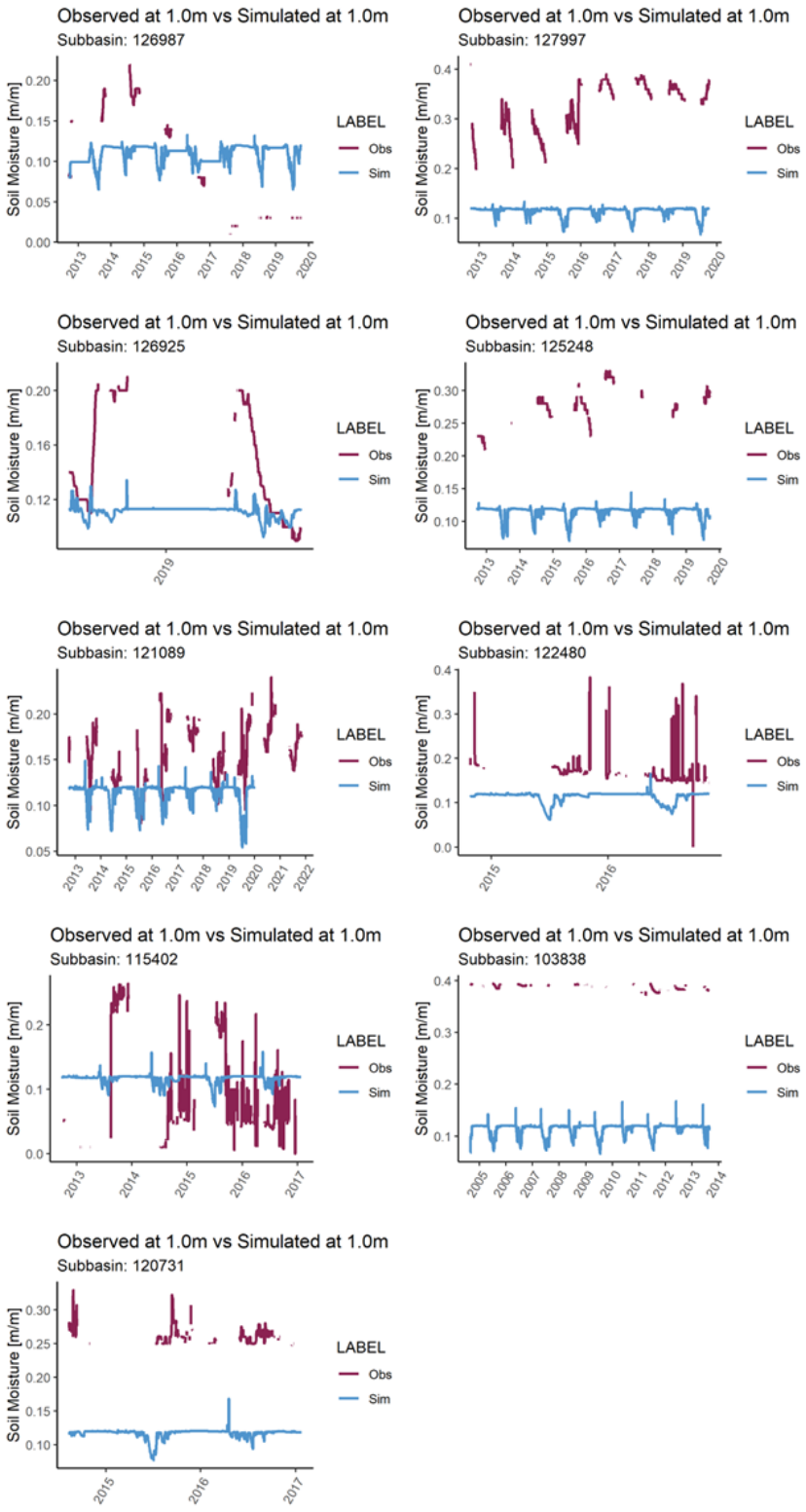

Figure C- 3 Timeseries of observed and simulated soil moisture at 1.0 m depth.

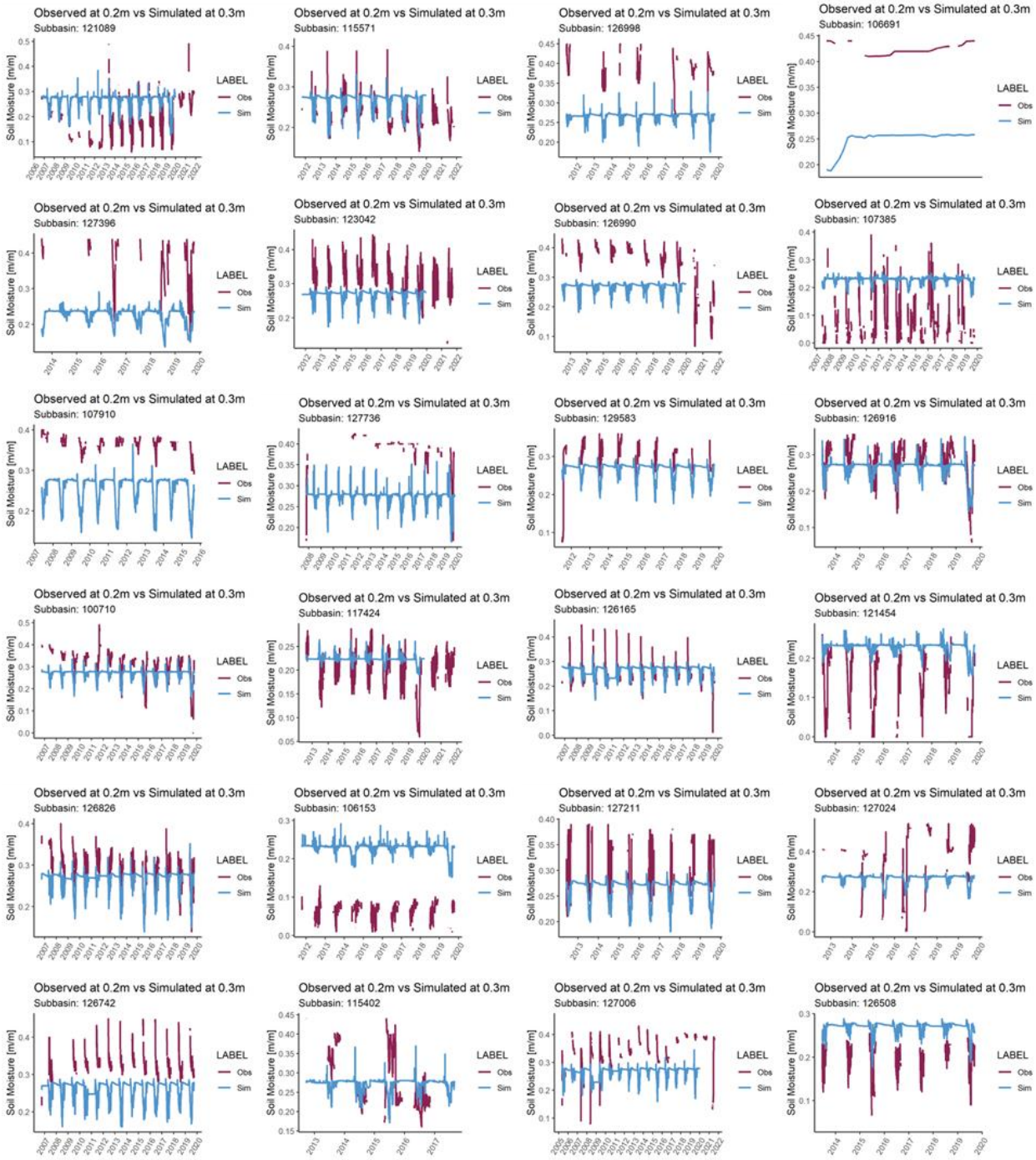

Figure C- 4 Timeseries of observed (0.2 m) and simulated (0.3 m) soil moisture. (1 – 24)

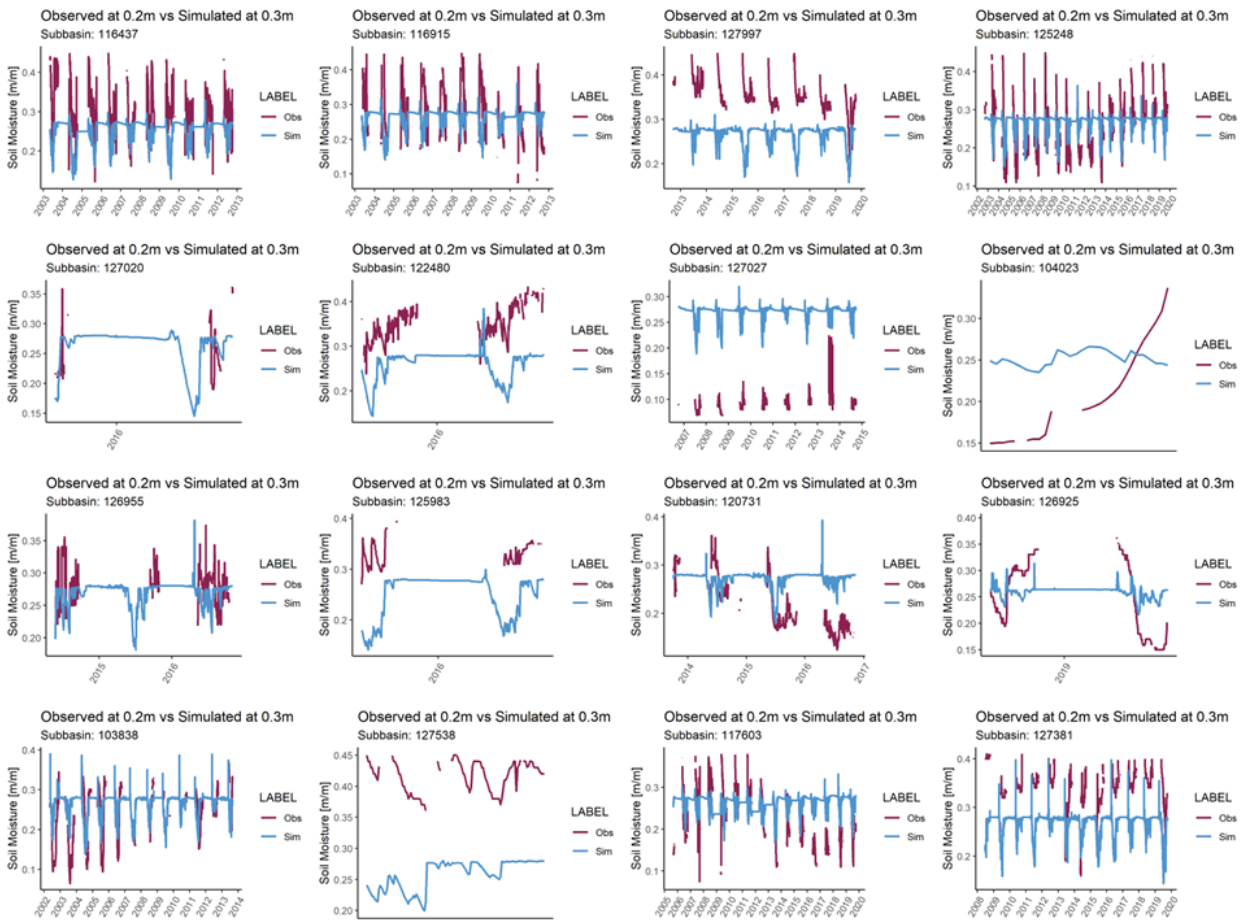

Figure C- 5 Timeseries of observed (0.2 m) and simulated (0.3 m) soil moisture. (25 – 40)

Appendix D – River Ice Thickness Plots

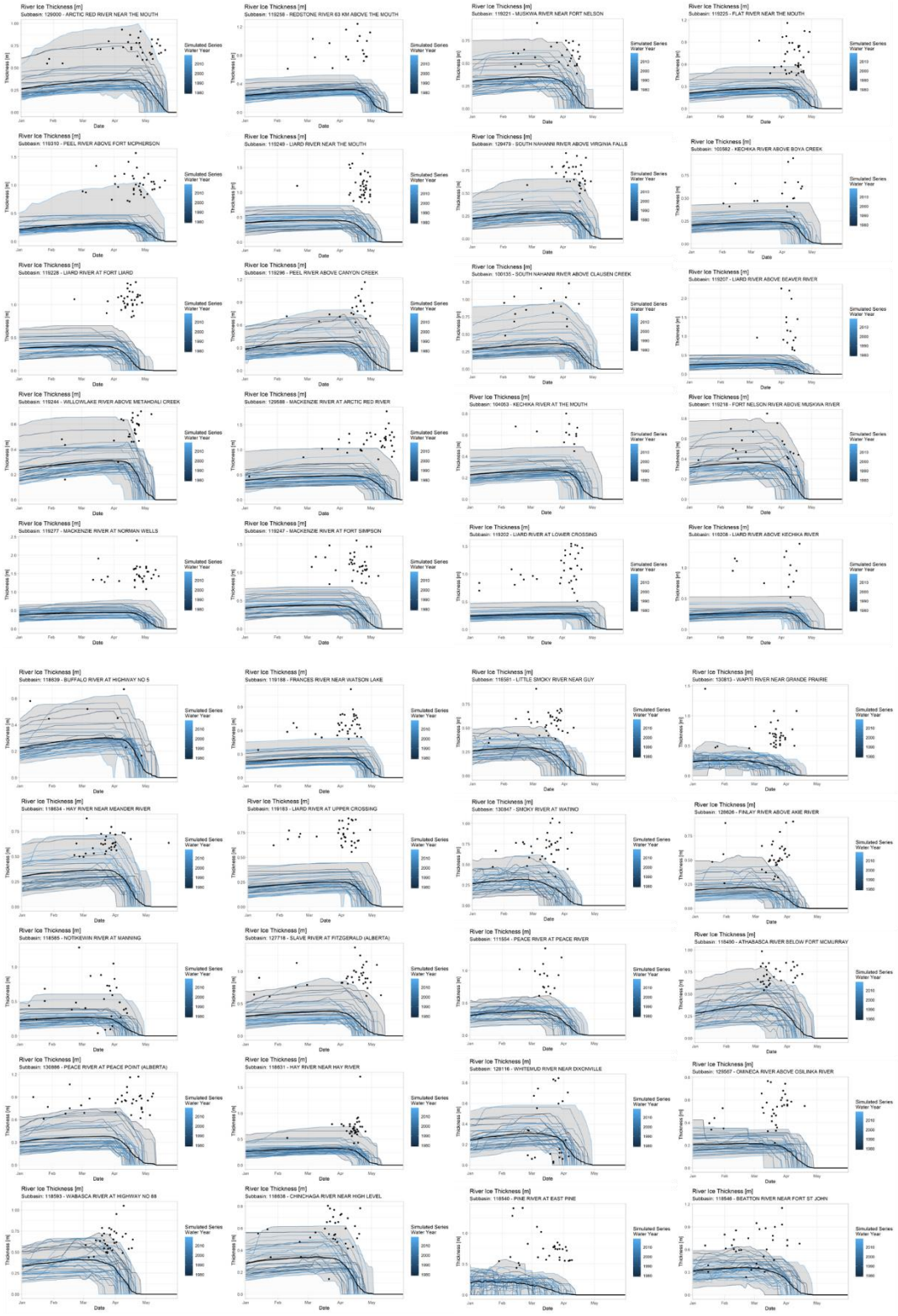

Figure D- 1 River ice thickness measurements and simulations for the ice break up season. [1-40]

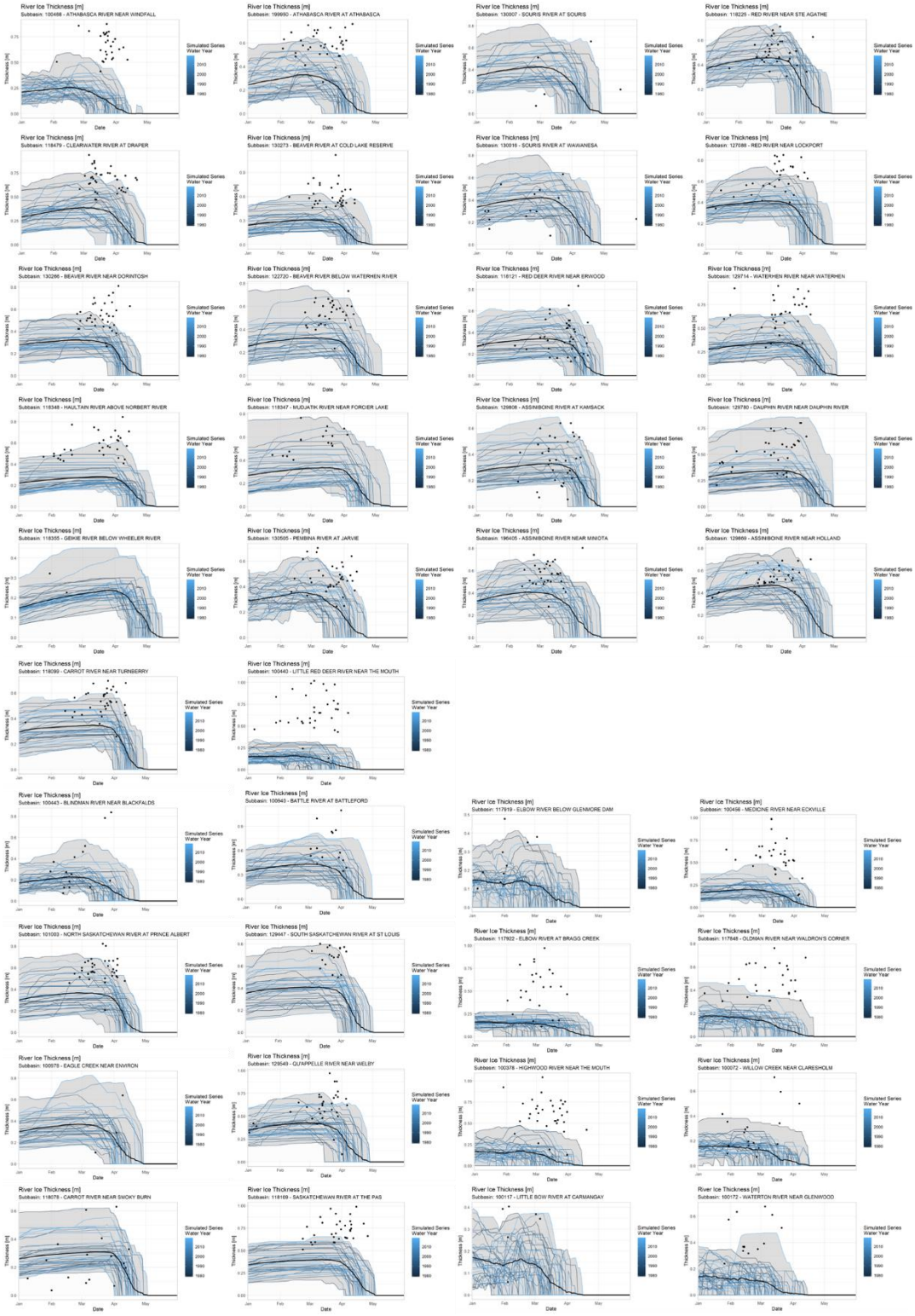

Figure D- 2 River ice thickness measurements and simulations for the ice break up season. [41-78]

Figure D- 3 Obs vs. Sim annual maximum river ice thickness, colour coded by month of observation [1-24].

Figure D- 4 Obs vs. Sim annual maximum river ice thickness, colour coded by month of observation [25-48].

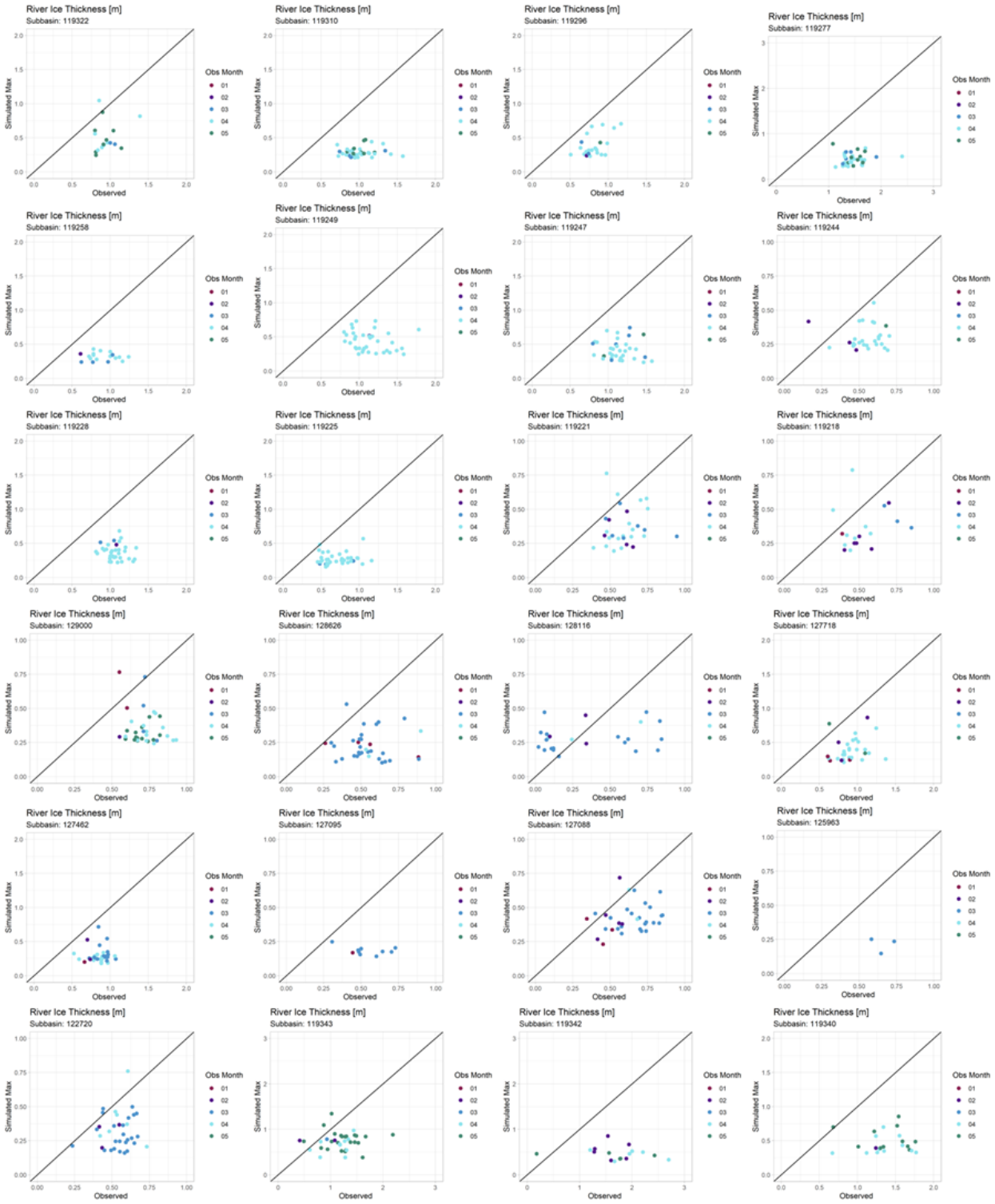

Figure D- 5Obs vs. Sim annual maximum river ice thickness, colour coded by month of observation [49-72].

Figure D- 6Obs vs. Sim annual maximum river ice thickness, colour coded by month of observation [73-96].

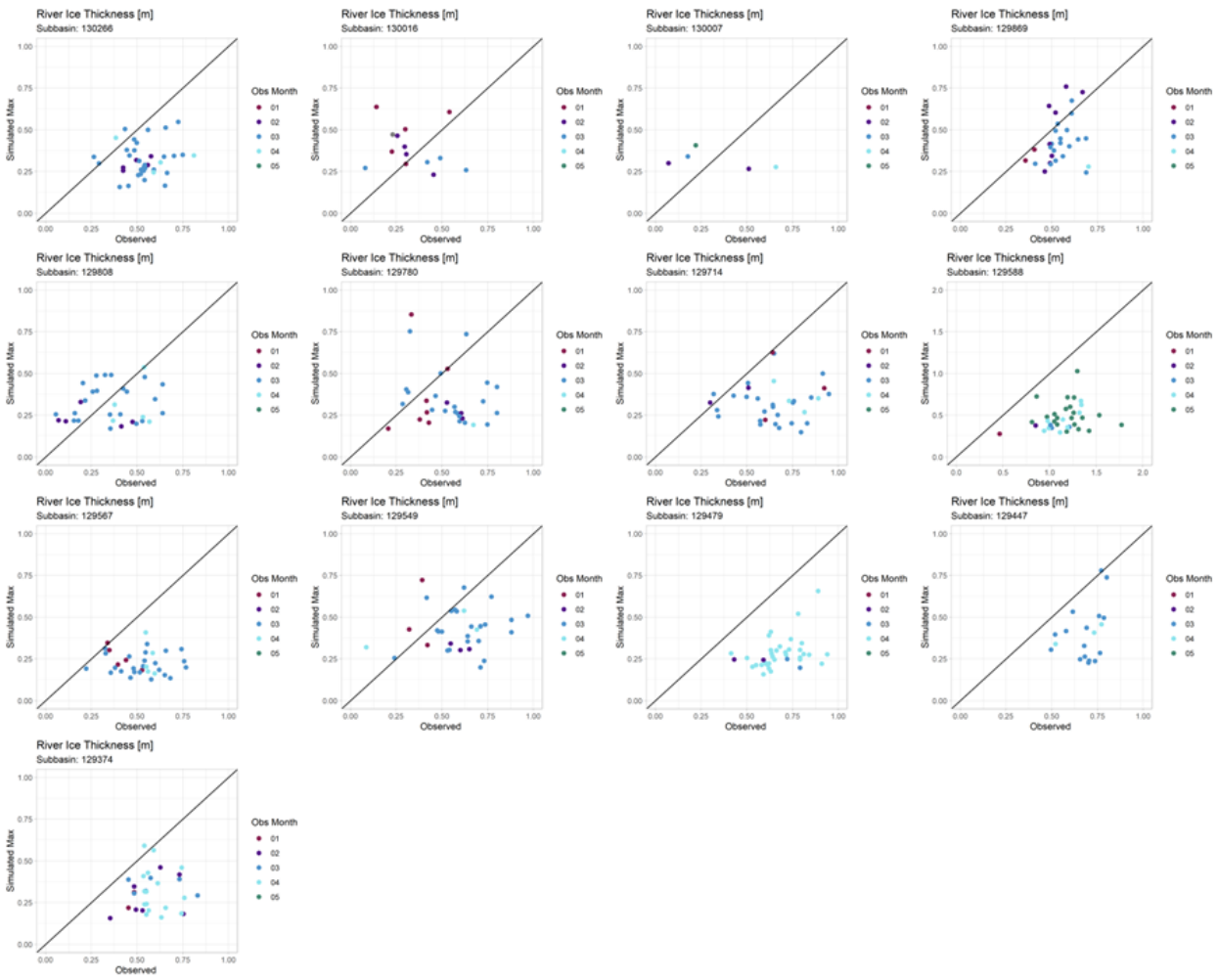

Figure D- 7Obs vs. Sim annual maximum river ice thickness, colour coded by month of observation [97-109].

Appendix E – AHYPE vs GLEAM

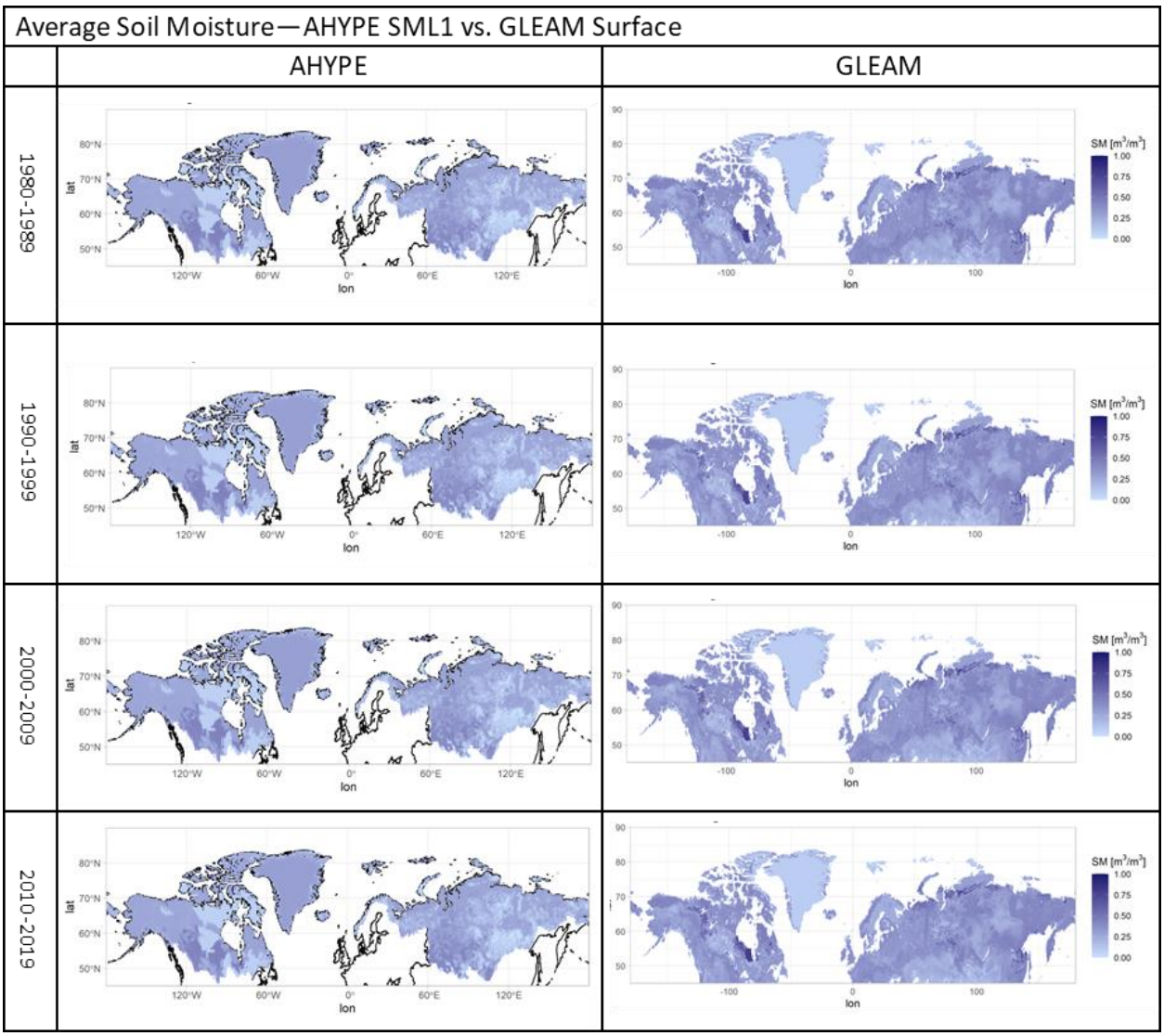

Figure E- 1 AHYPE vs. GLEAM comparison for each decade in the comparison period at the upper soil layer from AHYPE and the surface soil moisture from GLEAM.

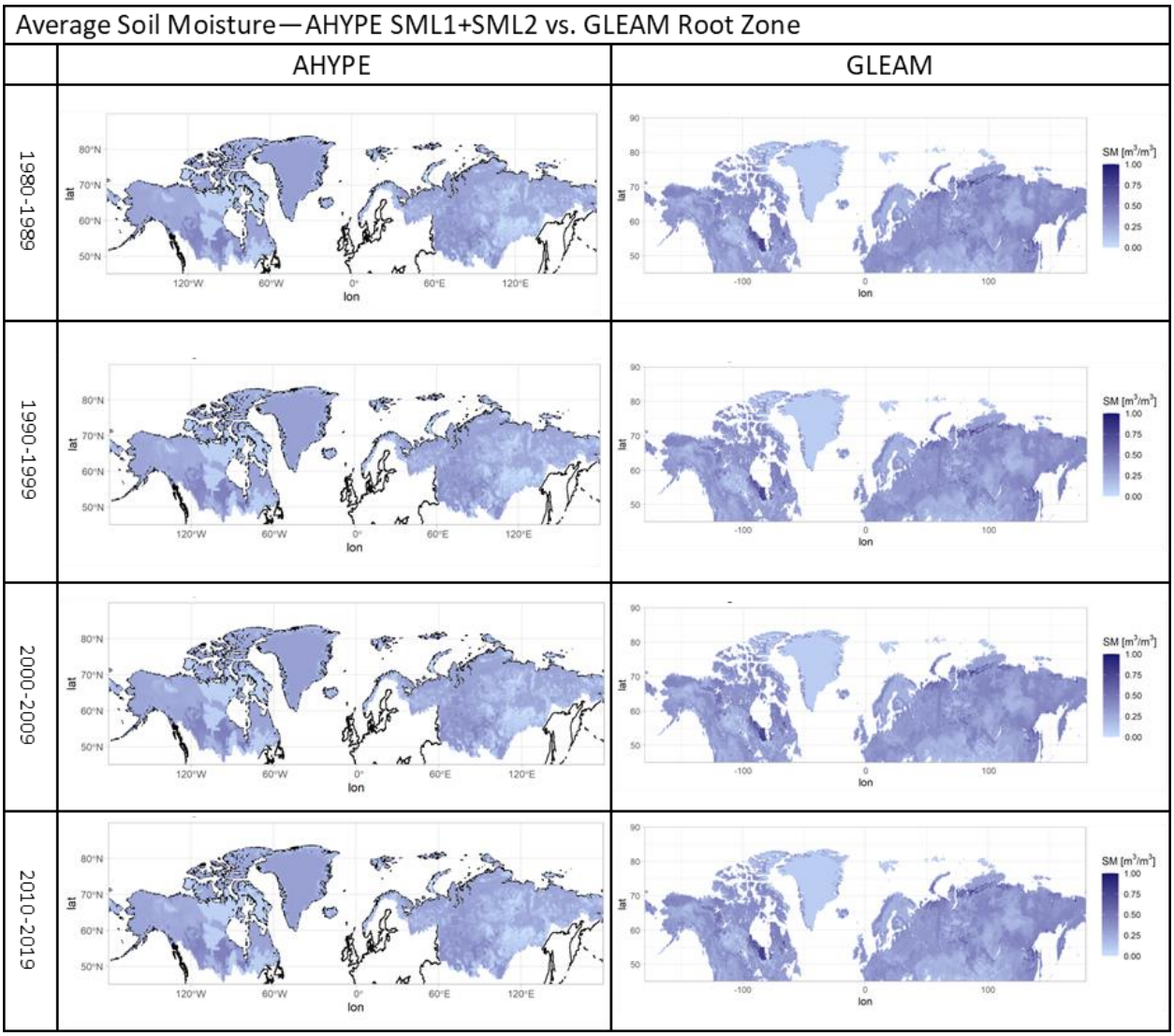

Figure E- 2 AHYPE vs. GLEAM comparison for each decade in the comparison period of the average moisture in the upper two soil layers from AHYPE and the root zone soil moisture from GLEAM.

Appendix F – Future AHYPE trends with Greenland

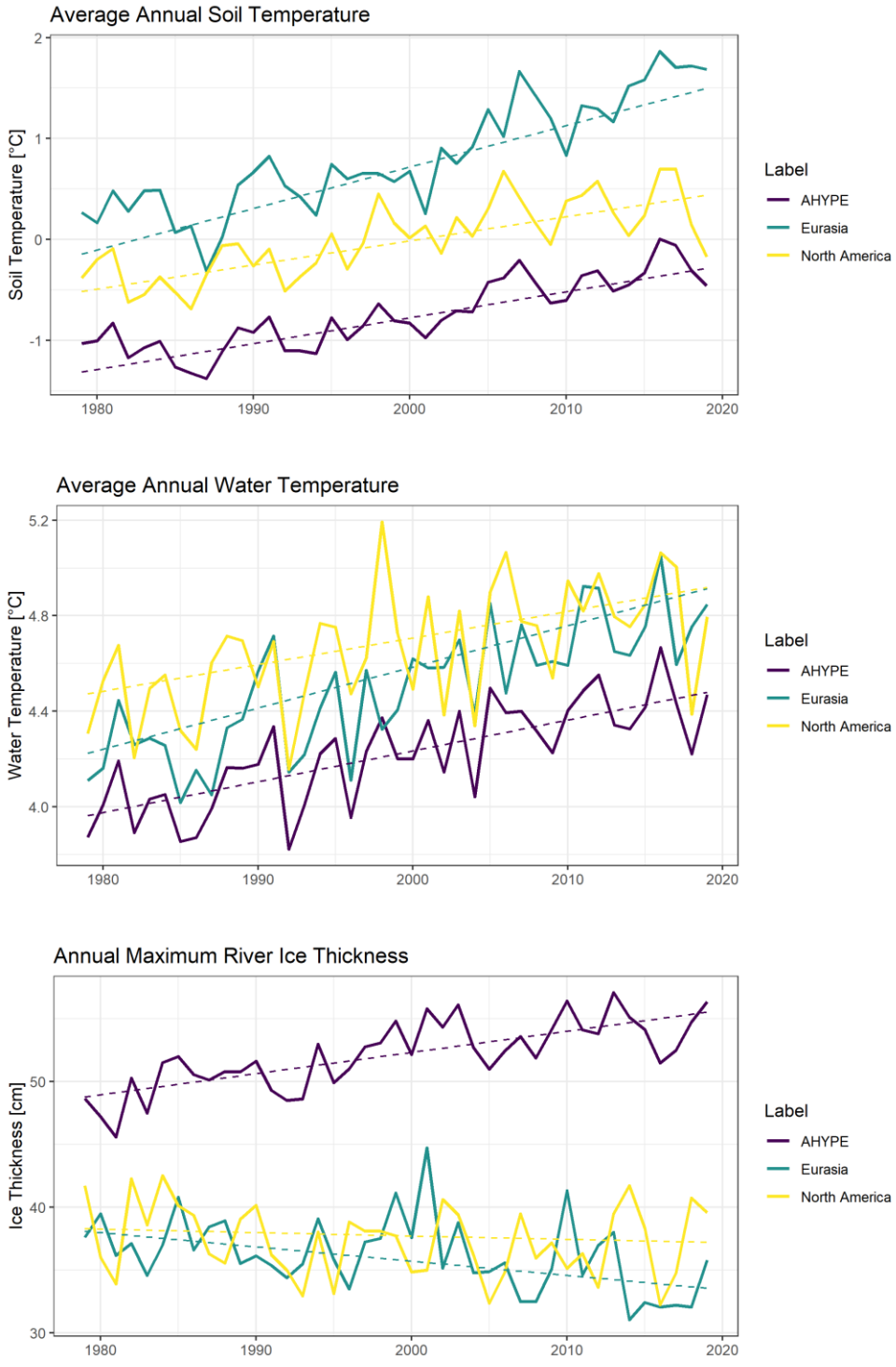

Figure F- 1 Future modeled time series for AHYPE (including Greenland), Eurasia, and North America. Pre-whitened MKT are shown in dashed lines.

Appendix G – Trends Before and After Change Points

Table G- 1 Future trends in annual average fresh water temperature before and after each change point.

CCT2										
		AHYPE*			N.America			Eurasia		
Model	*CP*	*before*	*after*	*% change*	*before*	*after*	*% change*	*before*	*after*	*% change*
CanESM5 ssp126	**2049**	**0.025**	**-0.003**	-114%	**0.019**	-0.001	-107%	**0.031**	**-0.005**	-117%
CanESM5 ssp585	**2059**	**0.052**	**0.087**	66%	**0.052**	**0.084**	60%	**0.052**	**0.091**	74%
MIROC6 ssp126	**2045**	**0.016**	0.002	-86%	0.012	0.003	-77%	**0.021**	0.001	-96%
MIROC6 ssp585	**2062**	**0.030**	**0.058**	91%	**0.031**	**0.054**	73%	**0.030**	**0.063**	110%
MRI-ESM2-0 ssp585	**2065**	**0.021**	**0.023**	10%	**0.024**	**0.022**	-5%	**0.018**	**0.022**	19%

Table G- 2 Future trends in annual maximum river ice thickness before and after each change point.

CMRI										
		AHYPE*			N.America			Eurasia		
Model	*CP*	*before*	*after*	*% change*	*before*	*after*	*% change*	*before*	*after*	*% change*
CanESM5 ssp126	**2049**	**-0.156**	0.007	-105%	**-0.211**	-0.017	-92%	**-0.131**	0.019	-114%
CanESM5 ssp585	**2059**	**-0.203**	**-0.237**	17%	**-0.204**	**-0.268**	31%	**-0.223**	**-0.194**	-13%
MIROC6 ssp126	**2045**	-0.031	0.022	-170%	-0.041	0.020	-148%	-0.018	0.035	-290%
MIROC6 ssp585	**2062**	**-0.114**	**-0.178**	57%	**-0.131**	**-0.168**	29%	-0.070	**-0.156**	124%
MRI-ESM2-0 ssp585	**2065**	**-0.113**	**-0.142**	25%	**-0.120**	**-0.168**	39%	-0.054	**-0.115**	111%

Table G- 3 Future trends in annual average soil temperature before and after each change point.

STMP										
		AHYPE*			N.America			Eurasia		
Model	CP	before	after	% change	before	after	% change	before	after	% change
CanESM5 ssp126	**2049**	**0.056**	**-0.007**	-112%	**0.055**	**-0.005**	-109%	**0.063**	**-0.008**	-113%
CanESM5 ssp585	**2059**	**0.101**	**0.112**	11%	**0.100**	**0.113**	12%	**0.099**	**0.109**	11%
MIROC6 ssp126	**2045**	**0.027**	0.002	-93%	**0.022**	0.001	-94%	**0.030**	0.001	-95%
MIROC6 ssp585	**2062**	**0.060**	**0.094**	56%	**0.068**	**0.091**	34%	**0.055**	**0.099**	79%
MRI-ESM2-0 ssp585	**2065**	**0.051**	**0.050**	-2%	**0.061**	**0.048**	-21%	**0.039**	**0.047**	19%

Appendix H – Mean Air Temperature Rise

Table H- 1 Summary of years that mean temperature rise is achieved by each GCM + SSP combination.

Average Temperature Rise [°C]	*CanESM5 ssp126*	*CanESM5 ssp585*	*miroc6 ssp126*	*miroc6 ssp585*	*Mriesm2 ssp585*
1	1/1/2065	1/1/2027	1/1/2076	1/1/2030	1/1/2035
1.5	1/1/2088	1/1/2031	NA	1/1/2035	1/1/2043
2	NA	1/1/2034	NA	1/1/2040	1/1/2051
2.5	NA	1/1/2038	NA	1/1/2045	1/1/2059
3	NA	1/1/2042	NA	1/1/2050	1/1/2067
3.5	NA	1/1/2045	NA	1/1/2055	1/1/2075
4	NA	1/1/2049	NA	1/1/2060	1/1/2083
4.5	NA	1/1/2053	NA	1/1/2065	1/1/2091
5	NA	1/1/2056	NA	1/1/2070	1/1/2099
5.5	NA	1/1/2060	NA	1/1/2075	NA
6	NA	1/1/2064	NA	1/1/2080	NA
6.5	NA	1/1/2067	NA	1/1/2085	NA
7	NA	1/1/2071	NA	1/1/2090	NA
7.5	NA	1/1/2075	NA	1/1/2095	NA
8	NA	1/1/2078	NA	1/1/2100	NA

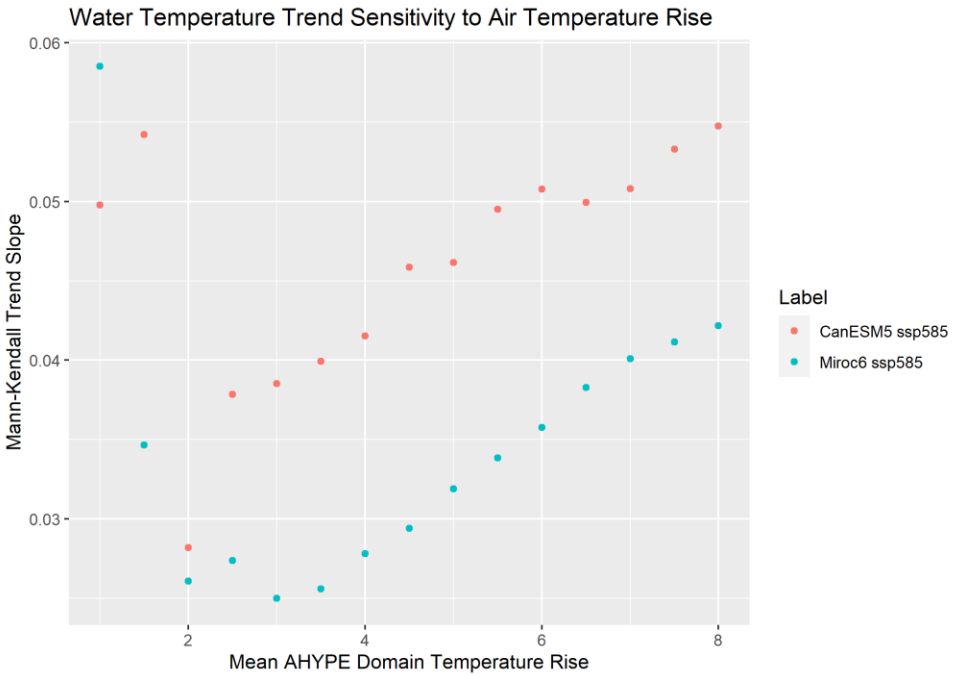

Figure H- 1 Sensitivity of the future water temperature trend (pre-whitened MKT slope) to the mean air temperature rise period chosen for analysis.

Figure H- 2 Future annual average air temperatures for the entire AHYPE domain.

Appendix I - Watershed Change Points

Water Temperature

Mean change points for water temperatures range from 2056-2067. Earlier change points occur in the lower warming scenario GCM+SSP combinations. North American watersheds have later change points compared to those in Eurasia.

Table I- 1 Summary of calculated change points (by year) for average annual water temperature (CCT2) using the single change point pettitt test for each watershed, GCM+SSP combination, ensemble mean over the entire future period. Lighter shading shows later change points and darker shading shows change points which occur earlier in the future period.

Change Points - CCT2

	Watershed											
	Khat.	*Kok.*	*Kol.*	*LaGr.*	*Lena*	*Mack.*	*Nel.*	*Ob*	*Pech.*	*S.Dvi.*	*Yen.*	*Yuk.*
Future Mean	2059	2064	2061	2064	2056	2056	2062	2056	2058	2059	2056	2067
CanESM5 ssp126	2044	2036	2052	2035	2044	2056	2048	2049	2037	2036	2048	2055
CanESM5 ssp585	2060	2057	2059	2056	2057	2056	2059	2054	2058	2060	2055	2056
MIROC6 ssp126	2043	2044	2060	2062	2046	2043	2046	2039	2037	2037	2045	2043
MIROC6 ssp585	2060	2064	2055	2064	2055	2063	2063	2062	2058	2055	2062	2067
MRI-ESM2-0 ssp585	2058	2065	2064	2065	2060	2067	2064	2056	2064	2069	2061	2070

River Ice Thickness

Mean change points for water temperatures range from 2050-2096. Earlier change points occur in the lower warming scenario GCM+SSP combinations.

Table I- 2 Summary of calculated change points (by year) for average annual maximum ice thickness (CMRI) using the single change point pettitt test for each watershed, GCM+SSP combination, ensemble mean over the entire future period. Lighter shading shows later change points and darker shading shows change points which occur earlier in the future period.

Change Points - CMRI

	Watershed											
	Khat.	*Kok.*	*Kol.*	*LaGr.*	*Lena*	*Mack.*	*Nel.*	*Ob*	*Pech.*	*S.Dvi.*	*Yen.*	*Yuk.*
Future Mean	2058	2050	2066	2072	2062	2062	2056	2075	2076	2069	2055	2065
CanESM5 ssp126	2068	2060	2041	2067	2037	2039	2043	2081	2035	2035	2036	2033
CanESM5 ssp585	2080	2073	2066	2073	2054	2065	2057	2062	2069	2069	2057	2066
MIROC6 ssp126	2059	2042	2065	2042	2049	2061	2046	2043	2058	2047	2088	2087
MIROC6 ssp585	2054	2050	2054	2049	2055	2064	2056	2061	2069	2075	2061	2063
MRI-ESM2-0 ssp585	2057	2085	2070	2055	2064	2077	2042	2073	2076	2085	2058	2036

Soil Temperature

Mean change points for water temperatures range from 2056-2062. Earlier change points occur in the lower warming scenario GCM+SSP combinations.

Table I- 3 Summary of calculated change points (by year) for average annual soil temperature (STMP) using the single change point pettitt test for each watershed, GCM+SSP combination, ensemble mean over the entire future period. Lighter shading shows later change points and darker shading shows change points which occur earlier in the future period.

Change Points - STMP

	Watershed											
	Khat.	*Kok.*	*Kol.*	*LaGr.*	*Lena*	*Mack.*	*Nel.*	*Ob*	*Pech.*	*S.Dvi.*	*Yen.*	*Yuk.*
Future Mean	2060	2060	2056	2060	2062	2062	2062	2061	2057	2059	2061	2056
CanESM5 ssp126	2046	2048	2041	2048	2051	2056	2043	2053	2049	2052	2051	2053
CanESM5 ssp585	2060	2059	2059	2059	2057	2059	2059	2056	2057	2059	2058	2056
MIROC6 ssp126	2047	2046	2055	2046	2052	2046	2046	2044	2037	2037	2046	2043
MIROC6 ssp585	2061	2065	2054	2065	2061	2062	2059	2063	2058	2058	2061	2063
MRI-ESM2-0 ssp585	2062	2066	2065	2066	2065	2059	2055	2061	2065	2064	2061	2070